

Lifetime of dielectric elastomer actuators under DC electric fields

Présentée le 3 juin 2022

Faculté des sciences et techniques de l'ingénieur
Laboratoire des Microsystèmes Souples
Programme doctoral en microsystèmes et microélectronique

pour l'obtention du grade de Docteur ès Sciences

par

Fabio BECO ALBUQUERQUE

Acceptée sur proposition du jury

Prof. M. Gijs, président du jury
Prof. H. Shea, directeur de thèse
Prof. F. Carpi, rapporteur
Prof. S. Seelecke, rapporteur
Prof. Y. Leterrier, rapporteur

“These sailors are men who have found a purpose in life and now take simple pleasure in it. [...] Many people make far less out of life”

The Stormlight Archive by Brandon Sanderson

Acknowledgements

I warmly thank Prof. Herbert Shea for the excellent opportunity to work in this stimulating PhD project and in this motivating work environment that constitutes LMTS. Herb's supervision, availability, patience, thoroughness, attention to details, advice and encouragements through the entire project have been important to me and for my development. Thank you for making LMTS such an excellent and enthusiastic work environment, and for your dedication on mentoring each PhD student.

I would like to give a special thanks to Miriam Biedermann, Anne Ladegaard Skov, Andreas Köllnberger, Klaus Eller, Renate Glowacki, Micah Hodgins and Michael Schupp for the successful collaboration, your precious insights and follow-up on the project.

I kindly acknowledge Bürkert Fluid Control Systems for their financial support.

I would like to thank Prof. Stefan Seelecke, Prof. Federico Carpi, Prof. Yves Leterrier, and Prof. Martinus Gijs who kindly accepted to review and evaluate this thesis as jury members.

I would like to thank all the LMTS members for these amazing years that we spent in the lab, in the cleanroom, and in the coffee room, where we could discuss about research, but also about the current state of the world and interesting ideas. Thank you Ronan, Jean-Baptiste, Mehdi, James, Sylvain, Nicolas, Giulio, Mike, Florian, Xiaobin, Samuel, Vito, Ryan, Alexandre, Matthias, Juan, Edouard, Morgan, Krishna, Robert, Amir, Jaemin, Shai, Danick, Min, Rubaiyet, Alexis, Silvia, Ulas, Fatemeh, Brince, Yu. I address a very special thanks to Valentin Py, and to Djen Kühnel for the design and the elaboration of the MAPLE setup, but also on all the excellent conversations we have had over the months. A special thanks for Bekir for the discussions we had around mathematical models. A big thanks also to Myriam for the kindness and for the amazing work you do in making LMTS such a great place. I also want to thank the team of the Danish Polymer Centre in DTU for their welcome during my short stay in Copenhagen.

I am deeply grateful for sharing all these outstanding moments with you and I wish you all the best for your future endeavors.

Finally, I would like to warmly thank my parents for their support and for their kindness. I deeply and wholeheartedly thank Mikaela for her support, her love, her understanding, and her kindness. You are amazing !

Neuchâtel, le 05 Mai 2022



Abstract

Soft actuators have attracted a significant interest in the last decades for emerging fields such as soft robotics and haptic devices. They constitute an interesting alternative to conventional rigid actuators owing to their lightweighness, flexibility, and compliance. Several classes of soft actuators with different actuation strategies have been investigated, from pneumatic actuators to dielectric elastomer actuators (DEAs). DEAs are soft electrically-driven electromechanical transducers composed of a thin ($\approx 10 - 100 \mu\text{m}$ thick) dielectric elastomer membrane in between two soft and compliant electrodes. DEAs can achieve high energy density ($\approx 100 - 3000 \text{ kJ/m}^3$), large actuation strains (5% - 50%), and fast actuation (up to kHz) ¹⁻⁵. These performances have gathered significant attention from the academic community on DEAs for applications in valves, soft robotics, compliant grippers and haptic devices. DEAs also generate interest from the industry, as several companies have proposed DEAs in their product portfolios.

For their commercialization, the reliability and the lifetime of DEAs need to be improved. Although quantifying the DC lifetime of DEAs is an important step toward their commercialization and industrialization, no extensive lifetime study has been conducted in DC fields. DEAs actuated in DC electric fields are interesting for applications such as valves because they maintain an on/off state with low to no power consumption ⁶.

This thesis demonstrate the first extensive studies on the lifetime of silicone-based DEAs under constant (DC) electric fields, and proposes effective approaches to enhance their lifetime under ambient and harsh environmental conditions, without compromising on actuation strain. The comprehensive investigations include the selection of the dielectric elastomers, the selection of the electrode materials, the type of prestretch, the selection of surface area, the encapsulation of the device layers, the influence of electric field, the effect of polarity reversal, the influence of humidity and temperature, and multilayering. The lifetime experiments conducted in this thesis use an automated lifetime test bench designed at LMTS. This setup allows a continuous monitoring of the deformation and the electrical resistance of the electrodes. It also allows to test DEAs under different temperature and humidity conditions. This thesis aims to understand how DEAs fail under DC fields in the long-term scale, i.e. the effects of the failure mechanisms on the lifetime of DEAs and their accelerating factors. The motivations of the thesis are to achieve large actuation strains ($> 5\%$) with high DC lifetimes (> 1 month), to raise the industrial and academic interest toward DEAs, and hence to catalyse future investments in the emerging field of soft DEA technology.

The lifetime of silicone-based DEAs is strongly limited by increasing humidity, temperature, and electrode surface area. I show that there is a significant trade-off between DC lifetime and actuation strain for thin ($\approx 12 \mu\text{m}$) prestretched silicone-based DEAs. All tested DEAs fail exclusively by dielectric breakdown, which cannot be anticipated with sudden strain or electrode resistance changes.

The selection of the dielectric elastomer and of the electrode materials also plays a key role in lifetime at constant strain. Therefore, optimizing these materials and their intrinsic properties to achieve higher lifetime performances at constant strain is promising. Differences in lifetime between different dielectric elastomer materials are not correlated to differences in water vapor permeability or in Young's moduli. The highest lifetimes at constant electric field and at constant actuation strain are obtained by selecting Electro 242-1 silicone as dielectric elastomer. At $20^\circ\text{C} - 90\% \text{ RH}$, DC lifetime decreases in the following order: Electro 242-1 $>$ Sylgard 186 $>$ Elastosil 2030/20 $>$ Sylgard 184.

The dielectric breakdown strength for thin ($\approx 12 \mu\text{m}$) silicone membranes depends on environmental conditions. Humidity has a larger influence than temperature on lowering the breakdown strength of the investigated prestretched silicone elastomers. Under dry conditions (10% RH), increasing the prestretch of the silicone membranes is an effective strategy to improve their dielectric breakdown strength. However, it leads to lower actuation strain due to the stiffening of the membrane (e.g. higher Young's moduli).

The combination of high humidity and high electric field significantly decreases the DC lifetime of equibiaxially prestretched silicone-based DEAs. For Elastosil 2030/20 DEAs at $85^\circ\text{C} - 85\% \text{ RH}$, the mean DC lifetime decreases by a factor of 62x when increasing the electric field from $80 \text{ V}/\mu\text{m}$ (2% actuation strain) to $100 \text{ V}/\mu\text{m}$ (5% actuation strain). At constant temperature, increasing the humidity significantly reduces the DC lifetime. For Elastosil 2030/20 DEAs at $100 \text{ V}/\mu\text{m}$ (4-5% actuation strain), the DC lifetime decreases by a factor of $>125\text{x}$ when the relative humidity is increased from 20% RH to 85% RH at 85°C , and by a factor $>20\text{x}$ when the relative humidity increases from 30% RH to 90% RH at 20°C .

The addition of encapsulation layers is a facile solution to greatly increase the DC lifetime without a significant compromising on the actuation performance and without significantly complexifying the DEA fabrication processes. Adding a soft and thin (4 μm) silicone (LSR 4305) encapsulation layer on both electrodes improves the DC lifetime by a factor of over 6x for both equibiaxially and uniaxially prestretched DEAs. The encapsulation is also effective under dry conditions and minimally affects actuation strain. For equibiaxially prestretched DEAs, I predict 1000 h DC lifetime at 70 V/ μm (1.5% strain) for Elastosil 2030 DEAs, and at 85 V/ μm (2.5% strain) for LSR4305 encapsulated Elastosil 2030 DEAs using an exponential model fit. I show that the lifetime of multilayer uniaxially pre-stretched strip DEAs decreases with increasing number of layers. Adding additional DEA layers increases the output force of DEAs, but at the expense of lower lifetimes, therefore yielding a force – lifetime tradeoff.

Keywords

Dielectric elastomer actuator, lifetime, reliability, DC electric fields, dielectric elastomer actuator failure, breakdown strength

Résumé

Ces dernières décennies, les actionneurs souples ont suscité beaucoup d'intérêt pour des domaines émergents tels que la robotique souple et les dispositifs haptiques. Les actionneurs souples constituent une alternative intéressante aux actionneurs rigides conventionnels grâce à leur légèreté, leur flexibilité et leur conformabilité. Plusieurs classes d'actionneurs souples avec différentes stratégies d'actionnement ont été étudiés, des actionneurs pneumatiques aux actionneurs à membrane diélectrique (DEAs). Les DEAs sont des transducteurs électromécaniques souples, flexibles, légers qui sont actionnés électriquement, et qui sont composés d'une fine ($\approx 10 - 100 \mu\text{m}$ en épaisseur) membrane diélectrique souple logée entre deux électrodes souples et étirables. Les DEAs sont des actionneurs qui peuvent générer des déformations élevées (5% - 50%) et rapides (jusqu'au kHz), ainsi qu'une haute densité en énergie ($\approx 100 - 3000 \text{ kJ/m}^3$)¹⁻⁵. Ces performances ont attiré l'attention de la communauté académique sur les DEAs pour des applications comme des valves, des dispositifs haptiques, ou la robotique souple. Plusieurs entreprises industrielles ont proposé des DEAs dans leurs portfolios.

La prochaine étape pour la commercialisation des DEAs consiste à améliorer la fiabilité et la durée de vie des DEAs. Bien que la quantification de la durée de vie des DEAs dans des champs électriques continus (DC) soit une étape importante pour leur industrialisation et leur commercialisation, il n'existe aucune étude approfondie sur la question. Les DEAs actionnés avec des champs électriques DC sont intéressants pour des valves grâce à leur faible consommation en énergie pour maintenir un état ouvert/fermé⁶.

Cette thèse présente les premières études approfondies sur la durée de vie des DEAs à membrane en silicone en tension continue (DC), et propose des approches techniques pour augmenter significativement leur durée de vie dans des conditions climatiques ambiantes ou rudes, sans compromettre la déformation des DEAs. Les investigations détaillées incluent la sélection du matériau diélectrique, la sélection du matériau pour les électrodes, le type de précontrainte, la sélection de l'aire de l'électrode, l'ajout de couches d'encapsulation, l'influence du champ électrique, d'une alternance de polarité, de l'humidité, de la température et de l'empilement de couches de DEA. Les tests de durée de vie sont effectués avec un banc d'essai automatisé développé au LMTS. Ce banc de test permet de surveiller continuellement la déformation et la résistance électrique des électrodes. Il permet aussi de tester des DEAs dans plusieurs conditions de température et d'humidité. Cette thèse aborde la défaillance des DEAs soumis à des champs électriques DC sur le long-terme, avec pour objectif de trouver quel est le mode de défaillance principal qui limite la durée de vie des DEAs, et quels sont les facteurs majeurs qui accélèrent leur défaillance. La motivation de cette thèse est de concevoir des DEAs aux durées de vie élevées (> 1 mois) à des déplacements significatifs ($> 5\%$), pour augmenter l'intérêt des DEAs auprès de la communauté académique et de l'industrie afin de catalyser des investissements futurs dans le domaine émergent des DEAs.

La durée de vie des DEAs à membrane en silicone diminue significativement avec une augmentation de l'humidité, de la température, et de l'aire de l'électrode. J'observe un compromis significatif entre la durée de vie des DEAs fins ($\approx 12 \mu\text{m}$) à silicone précontraint en DC et la déformation des DEAs. Le mode de défaillance des DEAs testés est exclusivement le claquage diélectrique, qui ne peut être anticipé par des changements de déformation ou de résistance précédant la défaillance.

La sélection du matériau élastomère diélectrique et du matériau pour les électrodes est importante pour optimiser la durée de vie des DEAs à déformation constante. Par conséquent, l'optimisation de ces matériaux et leurs propriétés intrinsèques est prometteur pour améliorer la durée de vie des DEAs. Les différences dans la durée de vie des DEAs entre différents élastomères en silicone ne sont pas corrélés à des différences en perméation de vapeur d'eau ou en module de Young. Les durées de vie les plus élevées à déplacement et à champ électrique constants sont atteints en sélectionnant le silicone Electro 242-1 comme diélectrique. A $20^\circ\text{C} - 90\% \text{ RH}$, la durée de vie en DC diminue dans l'ordre suivant : Electro 242-1 > Sylgard 186 > Elastosil 2030/20 > Sylgard 184.

La tension de claquage diélectrique de fines ($\approx 12 \mu\text{m}$) membranes précontraintes en silicone dépend des conditions climatiques. L'humidité a une plus grande influence que la température dans la diminution du champ électrique de claquage pour les membranes en silicone précontraintes étudiées. A faible humidité (10% RH), augmenter la précontrainte des membranes en silicone est une stratégie efficace pour augmenter le champ électrique de claquage, mais au détriment de déformations réduites à cause du raidissement induit par des modules de Young plus élevés.

La combinaison d'une humidité élevée avec un champ électrique élevé réduit significativement la durée de vie en DC de DEAs en silicone précontraints équi-biaxialement. A 85°C – 85% RH, la durée de vie moyenne en DC des DEAs (Elastosil 2030) diminue d'un facteur 62x en augmentant le champ électrique de 80 V/ μ m (2% déformation) à 100 V/ μ m (5% déformation). A température constante, augmenter l'humidité réduit considérablement la durée de vie des DEAs en DC. A 100 V/ μ m (4-5% déformation), la durée de vie moyenne en DC diminue d'un facteur >125x de 20% RH à 85% RH à 85°C, et d'un facteur >20x de 30% RH à 90% RH à 20°C.

L'application de couches d'encapsulation est une solution technique simple pour augmenter considérablement la durée de vie des DEAs en DC sans compromettre la performance des DEAs en déformation et sans trop complexifier la fabrication des DEAs. L'ajout d'une fine (4 μ m) couche d'encapsulation souple en silicone (LSR 4305) sur les électrodes des DEAs augmente la durée de vie des DEAs précontraints équi-biaxialement et uniaxialement par un facteur >6x. L'encapsulation fonctionne dans des conditions humides et sèches et affecte peu la déformation des DEAs. Pour des DEAs (Elastosil 2030) contraints équi-biaxialement, je prédis une durée de vie de 1000 h en DC à 70 V/ μ m (1.5% déformation) et à 85 V/ μ m (2.5% déformation) pour des DEAs encapsulés avec LSR 4305 en utilisant un modèle d'ajustement exponentiel. La durée de vie des DEAs multicouches précontraints uniaxialement diminue avec une augmentation du nombre de couches. L'ajout de couches de DEA additionnelles augmente la force exercée par les DEAs, mais au détriment de durées de vie plus courtes, révélant ainsi un compromis entre la force et la durée de vie.

Mots-clés

Actionneur à membrane diélectrique, durée de vie, durabilité, champs électriques DC, claquage diélectrique, modes de défaillance

Contents

Acknowledgements	vii
Abstract.....	viii
Résumé	x
List of Figures.....	xv
List of Tables.....	xviii
List of Equations	19
Chapter 1 Introduction	21
1.1 Background of DEA technology	21
1.2 Motivation and objectives of the present thesis	22
1.3 Approach and methodology of the study	22
1.4 Thesis outline.....	23
Chapter 2 Dielectric elastomer actuators	25
2.1 DEA: characteristics	25
2.1.1 DEA applications	27
2.1.2 DEAs vs. other actuation technologies: advantages and limitations.....	29
2.2 Dielectric elastomer and electrode materials for DEAs	31
2.2.1 Dielectric elastomers for DEAs.....	31
2.2.2 Influence of prestretch on dielectric elastomers for DEAs.....	32
2.2.3 Influence of fillers on dielectric elastomers for DEAs	32
2.2.4 Strategies to increase strain of DEAs at constant voltage.....	33
2.2.5 Stretchable electrodes for DEAs	35
2.3 DEA actuation mechanism	36
2.4 Conclusion	39
Chapter 3 State of the art: failure modes and lifetime studies of DEAs under high electric fields	40
3.1 Electrical breakdown and ageing of dielectric elastomers	40
3.1.1 Fundamentals of dielectric breakdown.....	40
3.1.2 Ageing and degradation mechanisms of silicone elastomers	42
3.1.3 Dielectric breakdown strength investigations on dielectric elastomers	46
3.1.3.1 Influence of membrane prestretch and thickness on dielectric breakdown strength	46
3.1.3.2 Influence of Young's modulus and crosslink density on dielectric breakdown strength	48
3.1.3.3 Influence of fillers on the dielectric breakdown strength	49

3.1.3.4	Influence of chemical modifications on the dielectric breakdown strength	51
3.1.3.5	Influence of temperature on the dielectric breakdown strength	53
3.1.3.6	Influence of humidity on the dielectric breakdown strength	54
3.1.3.7	Other factors influencing dielectric breakdown strength	55
3.1.3.8	Monitoring of leakage current and partial discharges	57
3.1.3.9	Influence of space charge accumulation	57
3.2	Electromechanical instability (pull-in instability)	58
3.3	Lifetime studies on DEAs	59
3.4	Conclusion	62
Chapter 4	Experimental characterization.....	64
4.1	DEA devices	64
4.1.1	Fabrication of equibiaxially prestretched DEAs	65
4.1.2	Fabrication of uniaxially prestretched single-layer DEAs	66
4.1.3	Fabrication of uniaxially prestretched multilayer DEAs	68
4.2	Characterization of silicone elastomer membranes	68
4.2.1	Determination of mechanical properties	69
4.2.2	Determination of water vapor permeability	70
4.2.3	Determination of breakdown strength	71
4.3	Automated lifetime setup (MAPLE)	74
4.4	Weibull probability plots	76
4.5	Summary.....	77
Chapter 5	Mechanical properties and dielectric breakdown strength of silicone membranes for DEAs.....	79
5.1	Dielectric breakdown strength of silicone elastomer membranes for DEAs	79
5.1.1	Effect of water vapor content	80
5.1.2	Effect of temperature	81
5.1.3	Effect of membrane prestretch.....	82
5.2	Figures of merit of silicone elastomer membranes for DEAs.....	83
5.3	Water vapor permeability of silicone elastomer membranes for DEAs.....	84
5.4	Mechanical characterization of silicone elastomer membranes for DEAs.....	85
5.5	Summary of key findings	87
Chapter 6	DC lifetime of equibiaxially prestretched single-layer silicone-based DEAs	89
6.1	Actuation: strain and resistance	89
6.2	Effect of elastomer material on DC lifetime	93
6.3	Effect of electric field on DC lifetime	94
6.4	Effect of temperature and humidity on DC lifetime	96
6.5	Effect of encapsulation layer on DC lifetime.....	97
6.6	Effect of electrode material on DC lifetime	101
6.7	Effect of polarity reversal	104
6.8	Conclusion	105

Chapter 7	DC lifetime of uniaxially prestretched strip single-layer and multilayer silicone-based DEAs	107
7.1	Actuation behavior of uniaxially prestretched silicone-based DEAs.....	107
7.1.1	Actuation strain vs. time	107
7.1.2	Actuation strain of single-layer and multilayer strip DEAs: data vs. model.....	112
7.2	Effect of electric field on single-layer strip DEAs	116
7.3	Effect of electrode surface area on single-layer strip DEAs	118
7.4	Effect of elastomer material and of encapsulation layer on single-layer strip DEAs	118
7.5	Effect of number of layers on multilayer DEAs	120
7.6	Conclusion	123
Chapter 8	Conclusion	125
8.1	Achieved results	125
8.2	Future development	127
References.....		129
Curriculum Vitae		143

List of Figures

Figure 2.1 Actuation mechanism of DEAs	25
Figure 2.2 Examples of commonly used DEA design architectures.....	26
Figure 2.3 Examples of reported applications for DEAs	28
Figure 2.4 Current and discontinued commercial products based on DEA technology	29
Figure 2.5 Strain vs. actuation pressure/density and breakdown strength vs. permittivity plots	31
Figure 2.6 Mullins effect, Payne effect, and permanent set	33
Figure 2.7 Decreasing the thickness of a dielectric increases density of defects.....	33
Figure 2.8 Commonly used carbon black based stretchable electrodes	35
Figure 2.9 Commonly used carbon black electrode manufacturing processes.....	36
Figure 2.10 Voltage-stretch curves of unprestretched ideal dielectric elastomer membranes.....	38
Figure 2.11 Influence of prestretch and decreased limiting stretch on voltage-stretch curves.....	38
Figure 3.1 Overview of phenomena leading to ageing and dielectric breakdown	41
Figure 3.2 Overview of the polymer structure of addition-cured silicone elastomers	41
Figure 3.3 Pinholes formed upon electrical breakdown of a silicone membrane.....	42
Figure 3.4 Overview of the factors which contribute to failure and ageing.....	43
Figure 3.5 Mechanisms of chemical degradation in silicone elastomers.....	44
Figure 3.6 Dielectric breakdown strength of silicone films vs. thickness and vs. stretch.....	46
Figure 3.7 Dielectric breakdown strength of VHB films vs. thickness and vs. stretch	47
Figure 3.8 Breakdown strength of silicone films vs. prestretch and vs. thickness	47
Figure 3.9 Influence of stretch on breakdown strength of natural rubber and VHB films.....	48
Figure 3.10 Influence of Young's modulus on breakdown strength of filler-free silicones	48
Figure 3.11 Influence of Young's modulus on breakdown strength of silicones and SEBS	49
Figure 3.12 Influence of filler concentration on breakdown strength of silicone films	50
Figure 3.13 Influence of aromatic groups concentration on breakdown strength of silicones	51
Figure 3.14 Influence of temperature on breakdown strength of silicones and nitrile butyl rubber ..	53
Figure 3.15 Influence of relative humidity on breakdown strength of VHB films.....	54
Figure 3.16 Influence of electrode material on breakdown strength of polyurethane films	55
Figure 3.17 Influence of field type and protective layer on breakdown strength of silicone films.....	56
Figure 3.18 Influence of replacing air by silicone oil/solid on breakdown strength of silicones.....	56
Figure 3.19 Space charge density vs. electric field in filled silicone films	58
Figure 3.20 Theoretical and experimental voltage-stretch curves in VHB and silicone films	59
Figure 3.21 Weibull plot for unprestretched stacked silicone-based DEAs	60
Figure 3.22 1% failure plot for unprestretched and radially prestretched silicone films	61
Figure 4.1 Investigated equibiaxially and uniaxially prestretched silicone DEAs	64
Figure 4.2 Fabrication process of single-layer expanding circle DEAs.....	65

Figure 4.3 Spin-coating of encapsulation layers	66
Figure 4.4 Fabrication process for single-layer uniaxially prestretched strip DEAs.....	67
Figure 4.5 Single-layer strip DEA geometries	67
Figure 4.6 Fabrication process of multilayer uniaxially prestretched strip DEAs	68
Figure 4.7 Mechanical test-bench.....	69
Figure 4.8 Uniaxial pull-testing	69
Figure 4.9 Metal container for water vapor permeability measurements	70
Figure 4.10 Preparation of silicone membranes for dielectric breakdown tests	72
Figure 4.11 Sample for dielectric breakdown tests.....	72
Figure 4.12 Dielectric breakdown test sample photograph	73
Figure 4.13 Pinhole site.....	74
Figure 4.14 Overview of the MAPLE setup for equibiaxially prestretched DEAs	75
Figure 4.15 Modified MAPLE setup for uniaxially prestretched strip DEAs	76
Figure 4.16 Example of Weibull plots for DC lifetime	77
Figure 5.1 Median dielectric breakdown strengths	79
Figure 5.2 Median dielectric breakdown strengths vs. water vapor content	80
Figure 5.3 Effect of temperature, humidity, and elastomer on breakdown strength.....	81
Figure 5.4 Effect of elastomer and prestretch on breakdown strength.....	82
Figure 5.5 DEA stress and strain figures of merit	84
Figure 5.6 Average weight increase owing to water vapor vs. time	84
Figure 5.7 True stress – engineering strain plots at 20°C.....	86
Figure 5.8 True stress – engineering strain plots at 80°C	86
Figure 6.1 Strain, actuation strain, and resistance vs. time	90
Figure 6.2 Strain vs. time for DEAs with different electrode materials	90
Figure 6.3 Pinhole in silicone-based DEAs	91
Figure 6.4 Strain vs. voltage and strain vs. electric field	91
Figure 6.5 Resistance vs. voltage	92
Figure 6.6 Resistance vs. time and vs. voltage for DEAs with different electrode materials	92
Figure 6.7 Effect of elastomer material on DC DEA lifetime	93
Figure 6.8 Effect of electric field on DC DEA lifetime	94
Figure 6.9 MTTF vs. field to breakdown strength ratio	95
Figure 6.10 Time to failure of individual DEAs vs. field to breakdown strength ratio.....	96
Figure 6.11 Effect of temperature and humidity on DC DEA lifetime	96
Figure 6.12 Strain at failure vs. time to failure of DEAs	97
Figure 6.13 Effect of adding encapsulation layers on DC DEA lifetime	98
Figure 6.14 Effect of encapsulation layer coverage and type on DC DEA lifetime	98
Figure 6.15 MTTF vs. electric field	100

Figure 6.16 MTTF vs. actuation strain	100
Figure 6.17 Temperature dependence of MTTF	101
Figure 6.18 Strain vs. voltage and vs. field for DEAs of different electrode materials	102
Figure 6.19 Failure fraction vs. time for DEAs of different electrode materials.....	102
Figure 6.20 Weibull plots of DEA failure probability vs. time	103
Figure 6.21 Strain at failure of individual DEAs with different electrode materials.....	104
Figure 6.22 Effect of polarity reversal on DC DEA lifetime.....	105
Figure 7.1 Actuation strain of uniaxially prestretched DEA strips.....	107
Figure 7.2 Strain vs. time for uniaxially prestretched single-layer DEA strips.....	108
Figure 7.3 Strain vs. time for uniaxially prestretched multilayer DEA strips.....	109
Figure 7.4 Strain vs. voltage and vs. field for uniaxially prestretched single-layer DEA strips	110
Figure 7.5 Strain vs. voltage and vs. field for uniaxially prestretched multilayer DEA strips	111
Figure 7.6 Strain vs. voltage for multilayer DEA strips at varying spring constant.....	111
Figure 7.7 DEA model schematic	112
Figure 7.8 Force vs. stretch for 2-layer DEAs	114
Figure 7.9 Experimental and model strain vs. voltage plot for single-layer and multilayer DEAs.....	114
Figure 7.10 Maxwell force vs. stretch for uniaxially prestretched multilayer DEA strips.....	115
Figure 7.11 Capacitance vs. stretch for uniaxially prestretched multilayer DEA strips.....	116
Figure 7.12 Effect of electric field on DC DEA lifetime	116
Figure 7.13 MTTF vs. field and vs. actuation strain: uniaxial vs. equibiaxial prestretch	117
Figure 7.14 Effect of electrode surface area on DC DEA lifetime.....	118
Figure 7.15 Effect of elastomer material on DC DEA lifetime	119
Figure 7.16 Effect of adding encapsulation layers on DC DEA lifetime	120
Figure 7.17 Effect of number of layers on DC DEA lifetime	121
Figure 7.18 Capacitance vs. time for 2-layer DEAs.....	122
Figure 7.19 Effect of number of layers on DC DEA lifetime at constant strain	123
Figure 8.1 Overview of factors influencing DC DEA lifetime	126

List of Tables

Table 2.1 DEA characteristics vs. other actuation technologies	30
Table 2.2 Strain energy models to describe stress-stretch curves of elastomers	37
Table 3.1 Ageing models for lifetime	45
Table 3.2 Lifetime of silicone-based DEAs under AC ageing	61
Table 3.3 Lifetime of silicone DEAs with stoichiometric imbalances	62
Table 4.1 List of silicone elastomer materials used, and their characteristics	65
Table 5.1 Median breakdown strengths of investigated silicone elastomers	80
Table 5.2 Water vapor permeability of investigated silicone elastomers	85
Table 5.3 Young's moduli of investigated silicone elastomers.....	87
Table 6.1 Properties of investigated silicone elastomers.....	89
Table 6.2 MTTF of silicone-based DEAs vs. different materials	93
Table 6.3 MTTF of silicone-based DEAs vs. temperature, humidity and electric field	95
Table 6.4 Effect of encapsulation layer type and thickness on MTTF of silicone-based DEAs	99
Table 6.5 Effect of electrode material on MTTF of silicone-based DEAs.....	103
Table 6.6 Effect of polarity reversal on MTTF of silicone-based DEAs	105
Table 7.1 DEA stiffness.....	110
Table 7.2 Effect of total spring constant on strain of uniaxially prestretched DEAs	112
Table 7.3 Gent model fit parameters of the experimental force-stretch curves	113
Table 7.4 MTTF of uniaxially prestretched silicone-based DEAs vs. electric field	117
Table 7.5 MTTF of uniaxially prestretched silicone-based DEAs vs. electrode surface area	118
Table 7.6 Effect of elastomer material on MTTF of uniaxially prestretched silicone-based DEAs	119
Table 7.7 Effect of encapsulation layer on MTTF of uniaxially prestretched silicone-based DEAs	120
Table 7.8 Effect of layer numbers on MTTF of uniaxially prestretched silicone-based DEAs.....	121
Table 7.9 Effect of layer numbers on MTTF of uniaxially prestretched silicone-based DEAs (2)	123

List of Equations

Equation 1 – Maxwell stress	25
Equation 2 – Linear actuation strain	25
Equation 3 – Effect of electrode stiffening on linear actuation strain	35
Equation 4 – Internal energy of a capacitor.....	37
Equation 5 – Derivation of Maxwell stress	37
Equation 6 – Derivation of DEA strain.....	37
Equation 7 – Voltage-stretch relationship in elastomers.....	37
Equation 8 – Voltage-stretch relationship in prestretched elastomers	39
Equation 9 – True stress	70
Equation 10 – Water vapor transmission rate (WVTR)	70
Equation 11 – Inaccuracy of dessicant method for WVTR determination	71
Equation 12 – Water vapor permeance.....	71
Equation 13 – Water vapor permeability.....	71
Equation 14 – Dielectric breakdown strength	73
Equation 15 – Standard deviation of individual breakdown strength events	73
Equation 16 – Standard error of median dielectric breakdown strength	73
Equation 17 – Two-parameter Weibull probability density	76
Equation 18 - Unreliability	76
Equation 19 – Mean time to failure (MTTF).....	77
Equation 20 – Failure probability.....	77
Equation 21 – Water vapor content	80
Equation 22 – Strain figure of merit.....	83
Equation 23 – Stress figure of merit	83
Equation 24 – DEA stiffness	110
Equation 25 – Total DEA force for prestretched strip DEAs.....	113
Equation 26 – Gent hyperelastic model mechanical stress	113
Equation 27 – Maxwell force for a N-layer strip DEA.....	113
Equation 28 – Total DEA force for prestretched and actuated strip DEAs.....	113
Equation 29 – Spring force for uniaxial prestretch of strip DEAs	113
Equation 30 – Capacitance as a function of stretch for strip DEAs	115

Chapter 1 Introduction

1.1 Background of DEA technology

Soft actuation technologies hold promising alternatives to more established and reliable rigid actuation technologies where softness, lightweightness and conformability are desired. Soft actuation technologies enable new functionalities that have been extensively investigated for emerging application fields such as soft robotics.

DEAs are soft, noiseless, compliant, lightweight, electrically-driven electromechanical transducers belonging to a class of soft actuators: electroactive polymers (EAPs). DEAs are made of a thin ($\approx 10 - 100 \mu\text{m}$ in thickness) and soft dielectric elastomer membrane (e.g. silicone, VHB, polyurethane) in between two soft and compliant electrodes (ideally of significantly lower thickness vs. dielectric elastomer thickness) ¹. The actuation principle of DEAs is an in-plane expansion and a reduction in thickness of the dielectric membrane induced by the application of an external voltage across the DEA electrodes ⁷. The achievable strain and force performance of DEAs depends on multiple factors such as the magnitude of the electric field (which is limited by the dielectric breakdown strength of the dielectric elastomer), the actuation frequency (in AC electric fields), the selection of the dielectric elastomer material and its properties (e.g. relative permittivity, Young's modulus), the prestretch of the dielectric elastomer, the thickness and Young's modulus of the electrode material (i.e. stiffening on the dielectric membrane), and layer stacking.

In comparison to other soft and rigid actuation technologies, DEAs are attractive owing to its large achievable actuation strains (5% - 50%), high energy density ($\approx 100 - 3000 \text{ kJ/m}^3$), and its fast actuation (up to kHz) ¹⁻⁵. A wide variety of DEA architectures and designs have been reported in the literature, making it a versatile actuation technology that can be adapted to numerous applications. DEAs are interesting for actuation in both AC and in DC fields. Because of its capacitive nature, DEAs actuated in DC fields maintain an on/off state with low to no power consumption, which constitutes a key competitive feature against high power consuming actuation technologies, such as solenoids for e.g. electrically-controlled valves ⁶.

DEAs can be employed in applications such as tunable optics ^{8,9}, compliant grippers ¹⁰⁻¹², pumps ¹³, soft robotics ^{14,15}, loudspeakers ¹⁶, haptic devices ^{17,18} and valves ¹⁹. An extensive overview of applications based on DEAs can be found in reviews ^{2,20}.

The motivations for using DEAs over other rigid actuation technologies are its softness, its compliance, its lightweightness, and its high strains, despite challenges related to lifetime, high voltage and limited output forces. Despite the extensive studies conducted on DEAs, the numerous proof-of-concepts, and the variety of application areas, only few products have been commercialized, such as CT Systems' stack DEAs ($< 9 \text{ N}$) for valves ²¹, the discontinued Vivitouch haptic interfaces and headphones ²², and the e-Rubber from Toyoda Gosei ²³.

A drawback of the DEA technology is the requirement to operate under high electric fields ($50\text{-}120 \text{ V}/\mu\text{m}$) to achieve the strain and force amplitudes needed for industrial applications. This induces a trade-off between performance of DEAs and lifetime, because of the limited dielectric breakdown strength of dielectric elastomers used in DEAs ²⁴, and because high electric fields may accelerate the failure of DEAs. The dielectric breakdown strength of dielectric elastomers is a complex parameter which requires a careful study, since it depends on membrane prestretch, membrane thickness, Young's modulus, the chemistry and the filler composition of the dielectric membrane, the electrode material, temperature and humidity. Understanding the dependence of dielectric breakdown strength on these factors allows to find safe operation ranges for long-term actuation, and to better understand the failure mechanisms of DEAs.

Investigating the long-term DC reliability of DEAs, identifying failure mechanisms and accelerating factors, as well as improving DEA lifetime without compromising on actuation performance are needed for industrial and commercial applications. Reliable DEAs with stable, temperature and time independent actuation are achieved with silicone elastomers under AC actuation. A previous study demonstrated that silicone-based DEAs can reliably actuate over millions of cycles under AC actuation at room temperature and

humidity²⁵. Existing investigations on the reliability of DEAs are however scarce: only few research papers investigate the lifetime of DEAs under AC actuation, and none for DC actuation.

This thesis specifically addresses the lack of quantitative data on DC lifetime of prestretched silicone-based DEAs and the challenge of understanding how DEAs fail under DC electric fields. The next subsections present the objectives of the thesis and the approach taken to conduct comprehensive DC lifetime studies on silicone-based DEAs.

1.2 Motivation and objectives of the present thesis

The motivation of this thesis is to present the first comprehensive DC lifetime studies on DEAs to advance the field and its prospective commercial applications. The research objective of the thesis is to gain a better understanding of how silicone-based DEAs fail under DC electric fields by quantifying their lifetime under different environmental conditions and electric field conditions, using different elastomer and electrode materials, and to find straightforward technical solutions to significantly increase the lifetime of DEAs at a constant actuation strain performance.

Conducting long-term reliability studies for DEAs under DC electric fields and proposing solutions to enhance their lifetime is important for the scientific community as well as for the industry, to enable industrial projects where reliable soft, lightweight and low power consumption actuators could constitute a competitive advantage.

The main goals for this research thesis are to:

1. Quantify the DC lifetime of DEAs for different dielectric elastomer and electrode materials, and for different electric field, temperature and humidity conditions using an automated lifetime setup (MAPLE) which monitors actuation strain and electrode resistance.
2. Investigate what failure mode(s) are dominant in DEAs and which accelerating factors are the most important.
3. Find effective mitigation solutions and strategies that significantly increase the DC lifetime of DEAs, and to patent them.
4. Provide plots to predict DC lifetime for any temperature, field, and humidity condition, based on accelerated aging models.
5. Evaluate under which operation ranges more than 1-year DC lifetimes are expected.

The work of this thesis was conducted at EPFL from November 2018 until February 2022, with the collaboration of Valentin Py and Djen Kühnel for the elaboration, the design, and the software interface of the MAPLE lifetime test setup.

The project was funded by Bürkert Fluid Control Systems.

1.3 Approach and methodology of the study

The approach of the present experimental study is to investigate the influence of humidity, electric field, temperature, elastomer material, electrode material, and the addition of encapsulation layers on DC lifetime of prestretched silicone-based DEAs.

I use 12 μm thick equibiaxially and uniaxially prestretched silicone elastomers as dielectric, and a carbon black-PDMS composite as electrodes for DEAs. The selection of elastomer membrane, electrode material and DEA design geometry are extensively discussed in Chapter 4.

I address the following scientific questions:

- How is DC lifetime affected by temperature (T), relative humidity (RH), electric field, as well as the selection of dielectric and electrode materials? What is the most important factor influencing DC lifetime?
- What are the main failure mechanisms for DEAs under DC fields? Can DEA failure be predicted by monitoring strain or electrode degradation?
- How can DC lifetime be significantly improved without compromising on actuation strain?

To address those questions, I use an automated lifetime (MAPLE) setup developed at LMTS-EPFL by Djen Kühnel and Valentin Py (partially in the scope of this thesis) to conduct the lifetime studies on 6 DEAs in parallel inside an environmental chamber up to 85°C – 85% RH. The setup is designed to monitor (every 10s) actuation strain, electrode resistance (by 4-point resistance measurement using a multiplexer onto a multimeter) and DEA lifetime by detecting short-circuits within 5 ms and disconnecting the failed samples by using a high voltage power supply connected to six individual relays. Further details on the automated lifetime (MAPLE) setup are provided in Chapter 4, and detailed in ²⁶.

The DEAs are tested under constant DC actuation, i.e. DEAs are subjected to a constant applied voltage. I typically use electric fields ranging from 80 V/ μm (\approx 60% of breakdown strength, 2% actuation strain) to 110 V/ μm (\approx 90% of breakdown strength, 7% actuation strain) that yield reasonable actuation strains and measurable lifetime ranges (from seconds to 200 h) to gather enough data for predictive lifetime plots (i.e. accelerating ageing).

I test the following environmental conditions: 85°C – 85% RH, 85°C – 20% RH, 20°C – 90% RH, 20°C – 30% RH, as well as other intermediate conditions.

Finally, as discussed in Chapter 5, I investigate the dielectric breakdown strength of silicone elastomers under static conditions, their mechanical properties, and their permeability to water vapor with the objective to correlate those material properties to DC lifetime.

1.4 Thesis outline

In this thesis, I show that the DC lifetime of silicone-based DEAs is significantly affected by the selection of elastomer and electrode materials, by the magnitude of the electric field, and by environmental conditions using an automated lifetime (MAPLE) setup.

The thesis is structured as following:

State of the art:

Chapter 2: Dielectric elastomer actuators

Chapter 2 introduces the state of the art of dielectric elastomer actuator technology. The section discusses its working mechanism, its advantages and limitations, its applications, as well as an overview of the materials used for DEAs, and the effects of the structural materials on the actuation performance.

Chapter 3: State of the art on failure modes and lifetime studies of dielectric elastomer actuators (DEAs) under high electric fields

Chapter 3 presents the state of the art of the failure modes of DEAs under high electric fields, as well as a state of the art on lifetime studies conducted on DEAs, with a focus on silicone elastomers. I show that no extensive DC lifetime study has been conducted on DEAs.

Experimental characterization:

Chapter 4: Experimental characterization

Chapter 4 introduces the thin silicone-based prestretched DEA devices tested (and their manufacturing), and the experimental methods used in the thesis to characterize DC DEA lifetime (i.e. automated MAPLE lifetime setup), the mechanical properties, the breakdown strength, and the water vapor permeability of thin silicone elastomer membranes.

Results and data:

Chapter 5: Mechanical properties and dielectric breakdown strength of silicone membranes for DEAs under different temperature and humidity conditions

Chapter 5 presents how temperature and humidity influence the DEA stress and strain figures of merit, mechanical properties, water vapor permeability, and breakdown strength of silicone elastomer membranes. The investigated silicone elastomer films (20-25 μm thick) show dielectric breakdown strengths in the range of 110 V μm^{-1} to 210 V μm^{-1} , except LSR 4305 with values from 50 V μm^{-1} to 80 V μm^{-1} . Humidity significantly decreases the breakdown strength of prestretched silicone membranes, with up to 43% reductions under moderate (PR 1.3) and larger (PR 1.5) prestretch, and limited (2%-10%) reductions under lower prestretch (PR 1.1). Higher prestretch generally enhances the stress figure of merit because of higher dielectric breakdown strengths, and reduces the strain figure of merit of silicone elastomers owing to increased Young's moduli at high prestretch. The stress figure of merit falls by 10%-

30% when increasing temperature from 20°C to 80°C and by 20%-70% when increasing relative humidity from 10% RH to 90% RH. The strain figure of merit falls by 10%-60% when increasing temperature from 20°C to 80°C and by 20%-70% when increasing relative humidity from 10% RH to 90% RH. For silicone elastomers, Sylgard 184 shows the highest stress figures of merit and LSR 4305 the highest strain figures of merit under all investigated conditions.

Chapter 6: DC Lifetime of equibiaxially prestretched single-layer silicone-based DEAs

Chapter 6 presents how temperature, humidity, electric field, elastomer material selection, polarity reversal, and the application of encapsulation layers influences the DC lifetime of equibiaxially prestretched silicone-based DEAs (single-layer) with expanding circle electrodes. The DEAs are actuated at electric fields ranging between 50% and 90% of the breakdown strength. The DEAs fail exclusively by dielectric breakdown, which cannot be anticipated with changes in strain or in electrode resistance right before breakdown. The combination of electric field and humidity significantly influences the DC lifetime of DEAs of prestretched silicone membranes coated with pad-printed carbon black-PDMS electrodes. For Elastosil 2030/20 DEAs at 85°C – 85% RH, the mean DC lifetime decreases by a 62x factor by increasing electric field from 80 V/μm (2% actuation strain) to 100 V/μm (5% actuation strain), and by a factor of 1000x from 80 V/μm (2% actuation strain) to 110 V/μm (7% actuation strain). At 100 V/μm (4-5% actuation strain), the DC lifetime decreases by a factor of >125x from 85°C – 20% RH to 85°C – 85% RH, and by a factor >20x from 20°C – 30% RH to 20°C – 90% RH. Adding a soft and thin (4 μm) silicone (LSR 4305) encapsulation layer on both electrodes increases lifetime by a factors up to 75x under both dry and humid conditions, and minimally affects actuation strain.

Chapter 7: DC lifetime of uniaxially prestretched strip single-layer and multilayer silicone-based DEAs

Chapter 7 presents how electric field, electrode surface area, elastomer material selection, layer stacking, and the application of encapsulation layers influences the DC lifetime of uniaxially prestretched silicone-based strip DEAs with spring bias. The DEAs fail exclusively by dielectric breakdown, which cannot be anticipated with changes in strain right before breakdown. I demonstrate that the DC lifetime of uniaxially prestretched strip DEAs with spring bias increases significantly by decreasing the electrode surface area, by operating under lower fields, by replacing Elastosil 2030/20 by Electro 242-1, and by adding thin and soft silicone encapsulation layers. Increasing the electric field decreases the mean time to failure (MTTF) of single-layer Elastosil 2030/20 DEAs by 2x (9.1 h vs. 4 h) from 60 V/μm to 75 V/μm with actuation strain increasing from 0.9% to 1.8%, and by 15x (9.1 h vs. 0.6 h) from 60 V/μm to 90 V/μm with actuation strain increasing from 0.9% to 3.5% at 85°C – 85% RH. Increasing the number of layers in multilayer DEAs decreases DC lifetime. At constant actuation strain of 2%, the DC lifetime decreases by a factor 0.55x (from 38 h to 21 h) at 85°C – 85% RH, and by a factor 0.6x (from 72 h to 43 h) at 20°C – 90% RH from 2-layer DEAs to 4-layer DEAs. From 4-layer DEAs to 16-layer DEAs, the DC lifetime further decreases by a factor 0.27x (from 21 h to 5.6 h) at 85°C – 85% RH, and by a factor 0.21x (from 43 h to 9 h) at 20°C – 90% RH.

Chapter 8: Conclusion

Chapter 8 draws a conclusion based on the main findings of the thesis and gives an outlook with possible pathways for further investigations on understanding how DEAs fail, and on potential improvements on the lifetime of DEAs.

Chapter 2 Dielectric elastomer actuators

This section presents a summary of the state of the art for dielectric elastomer actuators (DEAs). I first present the DEA technology: its characteristics, its applications, and its advantages and limitations. I then present what materials are typically used as dielectric layer and electrode and how they can influence the actuation performance of DEAs. Finally, I show how the actuation mechanism of DEAs works by introducing the models that have been used to characterize their actuation.

2.1 DEA: characteristics

Dielectric elastomer actuators (DEAs) are soft transducers composed of a dielectric elastomer membrane ($\approx 10\text{--}100\ \mu\text{m}$ thick) in between two compliant electrodes ¹. The actuation mechanism of DEAs has been first described by Röntgen in 1880 ²⁷, and then by Pelrine et al. in 1998 ⁷.

The DEA technology is attractive because of its large achievable actuation strains (typically $> 5\%$ linear strain, and up to well over 100% ^{1,28,29} up to a record 1692% area strain ³⁰ for VHB-based DEAs), high energy density ($100 - 3000\ \text{kJ/m}^3$), silent actuation, fast actuation (from $\approx \text{s}$ for VHB-based DEAs down to $< 1\ \text{ms}$ for silicone-based DEAs ⁹) and low power ($\approx \text{mW}$ under low frequency regimes ⁶) consumption ¹⁻⁵.

However, because DEAs need to be operated under high electric fields ($50 - 200\ \text{V}/\mu\text{m}$) to achieve the required strain and force ranges for industrial applications, a trade-off between performance and lifetime exists, owing to the limited breakdown strength of elastomers used in DEAs ²⁴.

The actuation mechanism of DEAs is governed by an in-plane expansion associated with a thickness reduction of the dielectric layer induced by a Maxwell pressure (c.f. Eq.1) generated by an applied voltage across it (yielding electric fields typically of $\approx 50 - 200\ \text{V}/\mu\text{m}$), as shown in Figure 2.1. The driving forces for the actuation are the electrostatic attraction between charges in opposite electrodes and the minimization of electrode charge density through the expansion of the active electrode area.

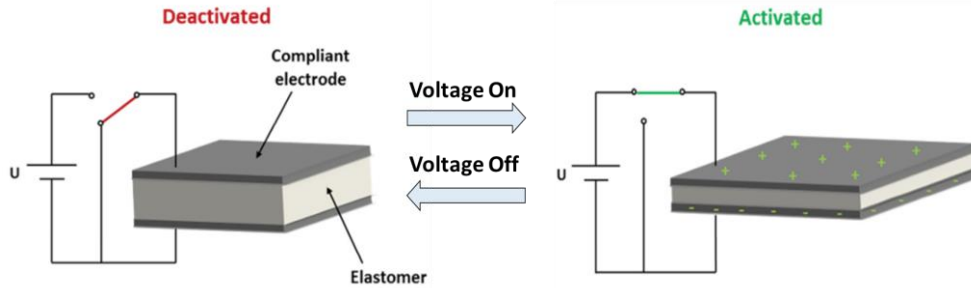


Figure 2.1: Actuation mechanism of DEAs. Reproduced from ²⁴. Upon the application of an external voltage between the compliant electrodes, the dielectric elastomer membrane reduces in thickness (out of plane direction) with an expansion in surface area (in-plane direction).

The Maxwell internal stress (σ) induced by an applied external voltage V is given by ^{1,7}:

$$\sigma = \epsilon_0 \epsilon_r \frac{V^2}{\delta^2} = \epsilon_0 \epsilon_r E^2 \quad (\text{Eq. 1})$$

with ϵ_0 the permittivity of vacuum, ϵ_r the relative permittivity, δ the thickness of the dielectric elastomer membrane, E the field across the dielectric elastomer membrane.

The linear actuation strain (s_z) achieved by DEAs is given by ^{1,7}:

$$s_z = -\epsilon_0 \epsilon_r \frac{V^2}{Y \delta^2} = -\frac{\epsilon_0 \epsilon_r}{Y} E^2 \quad (\text{Eq. 2})$$

with Y is the Young's modulus of the dielectric elastomer. Eq. 2 is valid for strains below 20% where the Young's modulus is independent from strain and assuming that the electrodes do not induce any stiffening effect on the dielectric membrane ⁷. The derivations of Eq. 1 and 2 are detailed in section 2.3.

At constant electric field, both the force and strain performance of DEAs can technically be enhanced with an increase in relative permittivity (ϵ_r) for the dielectric membrane. However, the current strategies to increase the relative permittivity generally negatively affect breakdown strength, as discussed in Chapter 4. Therefore, if higher forces are desired, multilayer DEAs are generally used. At constant electric field, a Young's modulus decrease is also technically increasing the strain performance of DEAs. However, as discussed in Section 2.2 and in Chapter 4, decreasing Young's modulus generally decreases breakdown strength and weakens the mechanical stability of the DEA. As DEAs are typically actuated in a prestretched state, the magnitude and the type of prestretch influence the elastomer's Young's modulus and hence the actuation strain. Finally, the achievable strain range is dependent on the dielectric and the electrode materials selected for the DEA (c.f. Section 2.2). In the literature, many research works have focused on large strain DEAs^{31,32} with VHB-based DEAs.

A wide variety of DEA architectures have been reported^{2,20,33–36}, as shown in Figure 2.2. Widely studied architectures are multilayer DEA stacks^{36–48} (employed as thickness compression DEAs), and uniaxially prestretched strip DEAs^{49–51} (employed as surface expansion DEAs) with spring bias.

The interest for multilayer DEA stacks arises from the limited force range (\approx mN range) generated by single-layer DEAs. Multilayer stacks are interesting for applications requiring significant forces (0.5–10 N, and up to 90 N for DEAs coupled with biased springs⁴⁶), such as valves.

Uniaxially prestretched strip DEAs with spring bias are typically used for applications where large displacements (>1 mm) are needed, such as in pumps and valves^{49,52–54}. The displacement is dependent on the spring constant of the spring bias, and negative spring bias yield the highest actuation strokes^{55,56}. A recent overview of DEA architectures and their actuation performance is found in³⁴.

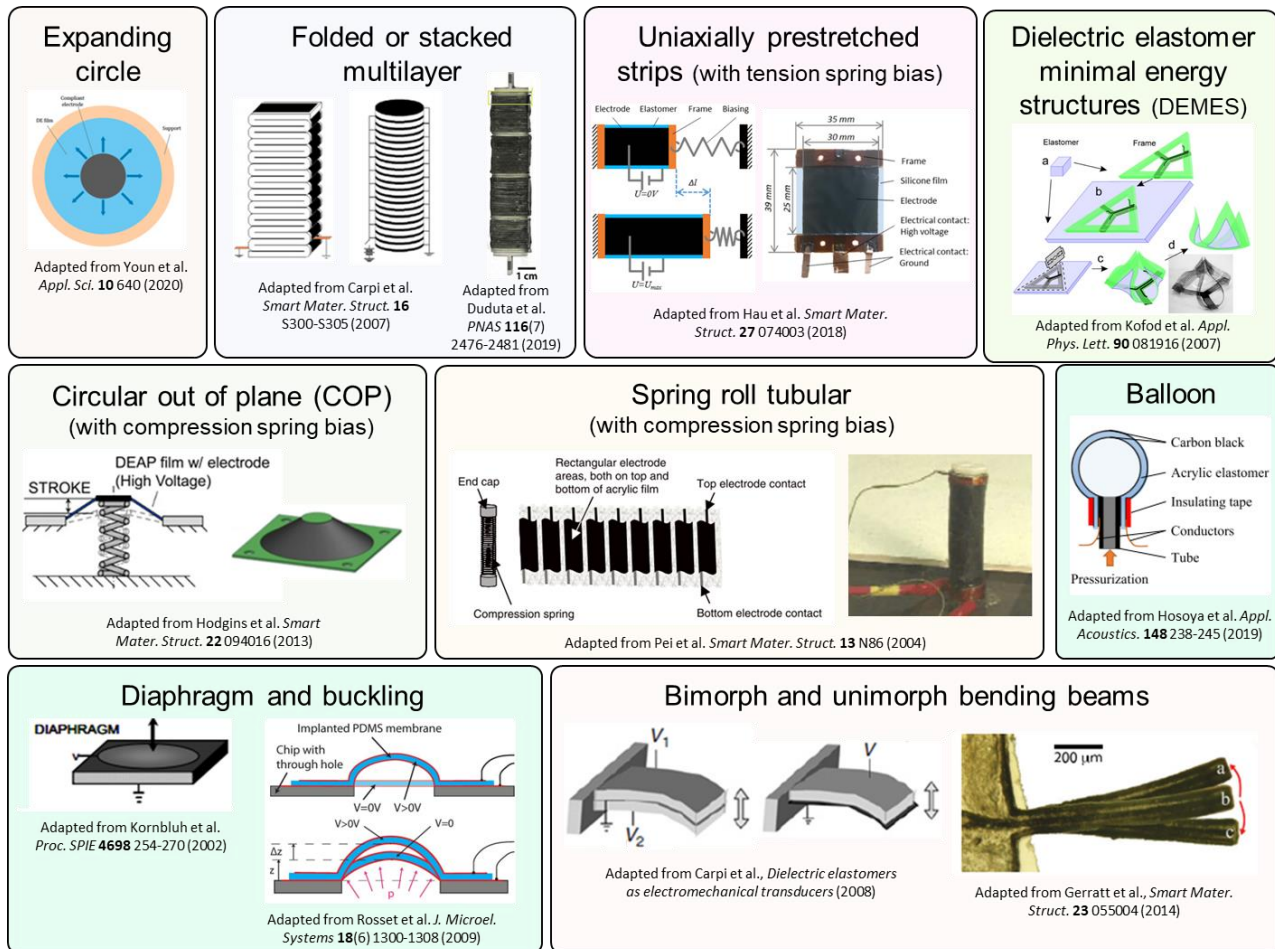


Figure 2.2: Examples of commonly used DEA design architectures: expanding circle^{25,57}, folded⁴³ and stacked^{37–42,44–48} multilayers, uniaxially prestretched strips^{49,58}, minimal energy (DEMES) structures^{59–62}, circular out-of-plane^{6,46,56}, tubular spring rolls^{35,63}, balloon⁶⁴, diaphragm⁶⁵, buckling^{66–69}, and bending beams^{36,65,70}.

In this thesis, I select two DEA design architectures (c.f. Chapter 5): equibiaxially prestretched expanding circle DEAs (single-layer), and uniaxially prestretched strip DEAs with linear spring bias (both single-layer and multilayer). The first design architecture constitutes an excellent model for conducting reproducible reliability studies, while the second design architecture is closer to a DEA geometry that would be used in industrial and commercial applications (e.g. DEA valves).

2.1.1 DEA applications

The motivation for using DEAs highly depends on the application and its associated currently used technologies against which it competes. In most applications listed below, there are already well-established technologies (e.g. electromagnetics, piezoelectrics, etc.) which are reliable, produced at industrial scale (therefore with the capability of being cost-effective owing to economies of scale) and with superior performance (vs. DEAs). Also, a fraction of those applications (e.g. cell stretchers, soft robotics, compliant grippers) are niche fields of high potential which are still at their infancy, and where competing technologies often offer better performances than DEAs.

DEAs can be used in the following applications (sorting from most interesting to least interesting):

- Valves^{6,19}: for compact miniature valves, DEAs constitute an interesting alternative to solenoid electromechanic valves because of its capacitive nature, as there is no power consumption when holding a on/off position. DEAs ($\approx \text{mW}$ ⁶) exhibit up to 1000x lower power consumption at low frequencies vs. solenoid valves ($\approx \text{W}$ ⁶) for comparable valve opening times of 6 ms⁶. Furthermore, DEAs are silent, and multilayer stacks can generate acceptable force ($\approx 1 \text{ N}$) and stroke ranges (1-10 mm)¹⁹. However, in contrast to DEAs, solenoid valves are industrially produced at large-scale, are reliable, and affordable¹⁹. Multilayer DEA stacks¹⁹ and circular out of plane DEAs with spring bias⁶ are typically used as design architectures for valves.
- Haptic devices^{17,18,71,72}: the skin is receptive to shear and normal forces down to the μN from frequency ranges between DC and 500 Hz⁷¹. Because of its soft, thin and lightweight nature, DEAs can also be used for haptic applications (vibration feedback), and it can generate $\approx 10 \text{ mN}$ forces and $> 5 \mu\text{m}$ displacements at least in a fraction of the receptive frequency range^{17,71,72} (in contrast with conventional piezoelectric actuators or single vibrating motors which can only output one given vibration frequency and amplitude⁷¹). If the DEAs are very thin, low voltage ($< 450\text{V}$) actuation is allowed without any bulky electronics⁷³. Multilayer DEA stacks are typically used as design architecture for haptic devices^{17,18,71,72}.
- Compliant grippers^{10–12}: Because of their soft and compliant nature, DEA grippers allow the manipulation and grasping of soft and deformable fragile objects and/or lightweight ($< 1 \text{ kg}$) objects with many complex shapes^{10,74}. The versatility of the gripping direction can be tuned by adding stiffening directional fibers¹¹ and the holding force performance (typically $\approx \text{mN}$ for single-layer DEAs) can be increased by exploiting out-of-plane fringe fields with interdigitated electrode design (i.e. electroadhesion) up to 3.5 N shear force per cm^2 ¹⁰. Multilayer DEAs and DEMES^{60,75} DEAs are used as design architectures for grippers. Competing technologies for grippers include e.g. pneumatic actuators, and shape memory alloys^{12,76}.
- Soft robotics^{14,15,77}: the compliant, lightweightness, and fast actuation of DEAs is interesting for soft robotics. The versatility of DEA design architectures allows for versatile robots and applications^{2,78}. Recent examples of soft robots made of DEAs include autonomous untethered insects⁷⁹, and flying robots⁸⁰.
- Tunable optics^{8,9}: adaptive lenses made of DEAs exploit its fast response time (as low as $< 1 \text{ ms}$ with silicones as dielectric, allowing $> 1 \text{ kHz}$ actuation⁹). Annular-shaped DEA is used as design architecture for tunable optics⁹. However, the optical quality of DEA lenses is relatively limited (especially vs. fixed focal length lenses) and dependent on the elastomer material⁹. Alternative technologies such as piezoelectric and electromagnetic devices are used for electrically driven tunable lenses, as detailed in a recent review⁸¹.
- Pumps¹³: For microfluidic pumps ($< 2 \text{ l/min}$ flow rate), DEAs yield a silent alternative to pneumatic actuators which need an external motor¹³, especially under low flow rates where conventional pneumatic pumps are limited¹³. Flow rate is controlled by the voltage amplitude¹³. The fast response time, silent operation and actuation reproducibility of DEAs allow it to be an interesting alternative for applications such as in blood pressure testers¹³.
- Cell stretchers^{82,83}: owing to the transparency of elastomer membranes, and fast actuation, DEAs constitute a unique technology as miniaturized cell stretchers for mechanobiological studies on cell deformation and stimulation under high strain rates (up to 870 s^{-1}) while enabling the optical monitoring of the cells under a microscope⁸³. Studying how cells react to mechanical stimuli has the potential to increase our understanding of cardiac diseases and cancer⁸³.
- Loudspeakers¹⁶: loudspeakers made of thin film membranes can yield good sound pressures and large vibration amplitudes when vibrating under operation in a DC bias and a AC drive voltage^{16,64,84}. Prestretched single-layer films and balloon

architectures are used for loudspeakers. Potential applications could extend to active noise control (e.g. automotive industry)¹⁶, but conventional technologies (e.g. electromagnetics) have better performances.

An extensive overview of applications based on DEAs can be found in reviews^{2,3,33,85–87}. Examples from the literature are demonstrated in Figure 2.3.



Figure 2.3: Examples of reported applications for dielectric elastomer actuators (DEAs).

The academic interest for investigating DEA-based proof of concepts in those applications relies on the potential of DEAs to be a soft, compliant, lightweight technology which contrasts from rigid actuation technologies. However, from a technical standpoint, if softness and high strains are not a requirement and if high power consumption is not a concern, rigid actuation technologies are preferred over DEAs for commercial applications. Most DEA applications stay at the proof of concept stage because of the superior performance of competing actuation technologies, and because taking the DEA technology to industrial scale would require significant investments (e.g. establishing a production line), and that such investments need to be justified not only by a superior performance of the devices, but also by an established market demand for DEA-based devices (vs. other alternative actuator technologies), which does not exist yet.

Therefore, only few DEA commercial products exist, such as CT Systems' stack DEAs (< 9 N) for valves ²¹, the discontinued Vivitouch haptic interfaces and headphones ²², and the e-Rubber from Toyoda Gosei for e.g. haptic devices ²³ as shown in Figure 2.4.

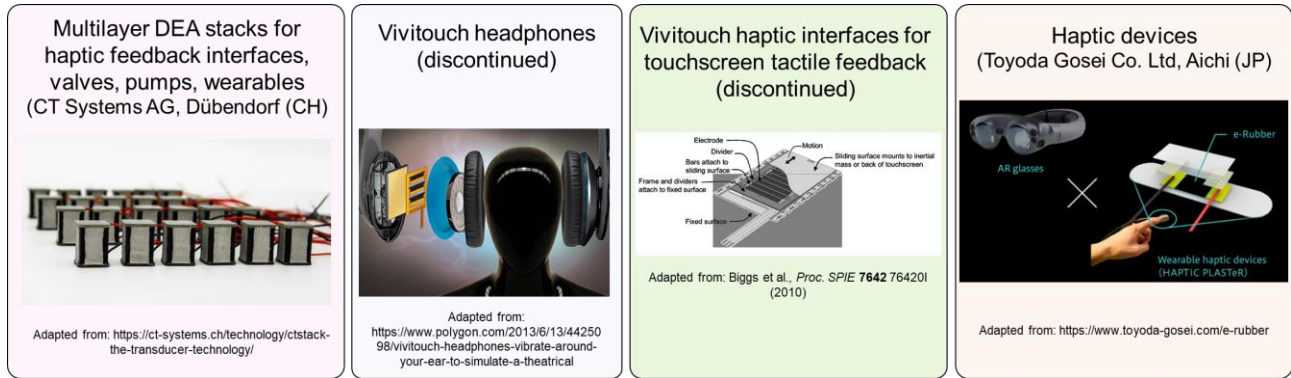


Figure 2.4: Current and discontinued commercial products based on DEA technology: multilayer DEA stacks from CT Systems AG ⁸⁸, discontinued headphones and haptic interface products from Vivitouch ²², and e-Rubber (for e.g. haptic feedback devices) from Toyoda Gosei ²³.

2.1.2 DEAs vs. other actuation technologies: advantages and limitations

DEAs are in the soft electroactive polymer actuators category, along with ionic polymer – metal composites (IPMCs, e.g. PVDF-based polymers such as NafionTM coated with thin metallic (Pt or Au) nanoparticle layers ⁸⁹ ⁹⁰, ferroelectric polymers (e.g. PVDF and copolymers, Nylon-11) ^{4,89,91}, liquid crystal elastomers ⁹², and electrostrictive graft elastomers ^{93,94}. A more detailed overview of these alternative technologies can be found in ^{4,89,95,96}.

Table 2.1 provides an overview of DEA characteristics in comparison to competing soft and rigid actuation technologies. In comparison to those actuation technologies, DEAs display several advantages, such as the ability to deliver relatively high strains (10-400% linear strains, although < 80% strain is preferred for long-term actuation ⁷⁴) ⁴, fast actuation speed (\approx ms–s response time for silicone-based DEAs ⁹) ^{9,97}, and high energy density, as shown in Table 2.1. Furthermore, DEAs are soft and compliant, light-weight, use low cost materials, can operate silently with an effective electromechanical conversion, and versatile device architectures and designs are possible, as discussed in the previous section ^{14,2}. Finally, owing to its capacitive nature, DEAs actuated in DC fields allow an on/off state to be maintained with no power consumption in the actuator (if we assume there is no leakage current), which constitutes an interesting feature for e.g. valves ⁶. However, for applications where softness, low weight, low power consumption or large strains are not important, conventional and more established actuator technologies are preferred.

The actuation performance (i.e. range of achievable strain and stress) and the specifications given in Table 2.1 for DEAs are highly dependent on the selection of materials, as discussed in section 2.2, but also on other factors such as e.g. actuation frequency ^{71,98}. The values shown in Table 2.1 cannot be simultaneously reached, e.g. high strain amplitudes cannot be reached at high strain rates or high actuation frequencies for DEAs. Finally, operating DEAs for long lifetimes (> 1 week) requires a compromise on actuation strain, because of a trade-off between lifetime and actuation strain owing to the operating voltages being close to dielectric breakdown strength.

Table 2.1: DEA characteristics in comparison to other soft and rigid actuation technologies ^{4,77,96,99–106}.

Actuation technology	Strain (%)	Actuation stress (MPa)	Young's modulus (MPa)	Work density (kJ/m ³)	Power density (kW/m ³)	Strain rate (%/s)	Maximal efficiency (%)	Actuation frequency (Hz)
Dielectric elastomer actuators (DEAs)	1 - 1000 ⁷⁷	0.5 ¹⁰¹	0.1 - 3 ⁷⁷	100 - 3000 * 80 - 750** ^{77,103}	10 ³ - 10 ⁵ ^{77,79}	10 ² - 10 ⁵ ⁷⁷	30 - 80* 80 - 90** ^{4,103}	1 - 10000 ^{9,77}
Ionic polymer – metal composites	0.5 - 10 ⁷⁷	15 ¹⁰¹	25-2500 ⁷⁷	1-10 ⁷⁷	0.01-1 ⁷⁷	1-3 ⁷⁷	-	0.1 - 2 ⁷⁷
Shape memory alloy (NiTi)	4 - 8 ^{77,100}	200 ¹⁰⁴ - 800 ¹⁰¹	28 - 75 ¹⁰³ ⁷⁷	10 ⁴ - 10 ⁵ ⁷⁷	10 ³ -10 ⁵ ⁷⁷	10-50 ⁷⁷	3 ¹⁰⁴	0.5 - 5 ⁷⁷
Shape memory polymer (PU)	50 - 800 ^{100,96}	0.4 ¹⁰¹ - 3 ¹⁰⁰	10 - 3000# ¹⁰⁰ 0.1 - 10 ## ¹⁰⁰	< 50 - 2000 ⁹⁶	-	-	< 10 ^{4,103}	0.1 ⁷⁷
Skeletal muscle	20 - 40 ⁷⁷	0.35 ⁴	10 - 60 ⁷⁷	8 - 40 ⁷⁷	50 - 300 ⁷⁷	10 - 50 ⁷⁷	35 - 40 ^{4,103}	1 - 10 ⁷⁷
Solenoids	10 - 40 ¹⁰²	0.04 - 0.1 ¹⁰²	0.3 - 1 ¹⁰²	-	10 - 40 ¹⁰²	-	50 - 80 ¹⁰²	< 80 ¹⁰²
Piezoelectric polymers (PVDF)	0.1 ⁴	< 4.8 ⁴	2 - 10 x 10 ³ ¹⁰²	2.4 ⁴	3 x 10 ⁵ ¹⁰²	-	> 90 ⁴	< 10 ⁷ ¹⁰²
Piezoelectric ceramics (PZT)	0.2 ^{4,104}	< 110 ^{4,104}	50 - 300 x 10 ³ ¹⁰²	100 ¹⁰³	< 120 ¹⁰⁴	2 ¹⁰⁶	90 ⁴	< 3 x 10 ⁷ ¹⁰²
Electromagnetic (voice coil)	50 ^{4,105}	0.1 ⁴	-	5 ¹⁰⁵	100 ¹⁰⁵	10 ¹⁰⁶	>90 ^{4,105}	< 20 ¹⁰⁵
Hydraulic	50 ^{104,105}	20 ^{104,105}	2 - 3 x 10 ³ ⁹⁹	5 x 10 ³ ¹⁰⁵	2 x 10 ⁴ ¹⁰⁵	2 ¹⁰⁶	80 ^{104,105}	4 ¹⁰⁵
Pneumatic	10 - 40 ⁷⁷	0.7 ^{104,105}	0.1 - 100 ⁷⁷	1 - 200 ^{77,105}	10 - 1000 ⁷⁷	10 - 70 ⁷⁷	90 ¹⁰⁴	< 20 ^{77,105}
Electrostrictive P(VDF-TrFE)	4.3 ⁴	< 43 ⁴	-	50 ⁴	2.5 x 10 ⁵ ¹⁰⁵	-	80 ⁴	5000 ¹⁰⁵

* For VHB elastomers ** For silicone elastomers # For temperatures below T_{transition} ## For temperatures above T_{transition}

The DEA technology has some limitations which hinder its technology readiness and affect its competitive advantage against other technologies:

- a. DEAs very often need a bulky high voltage power supply to drive them.

High electric fields (50-150 V/μm) are needed to reach sufficient actuation ranges (>5%) for DEAs, therefore requiring a bulky high voltage power supply (>1 kV) to drive the actuator, given typical film thicknesses (10-100 μm). Size is a major limitation for some applications (tunable optics for smartphones, compact valve arrays or wearable haptic devices). A thickness reduction of the dielectric elastomer ^{73,107,108} or an increase in dielectric permittivity of the dielectric elastomer ^{109,110} are promising solutions for DEAs, but no long-term (>1h) lifetime studies have been conducted. These solutions and their associated tradeoffs are discussed in Section 2.2.4.

- b. Lifetime of DEAs is limited by dielectric breakdown, and few reliability studies are reported.

In DEAs, an electrical breakdown can lead to a complete failure, resulting in either a short-circuiting pinhole ¹¹¹ or an open-circuit membrane tearing ¹¹². There is currently a limited understanding on mechanisms of DEA failure and very few reliability studies ^{113–117} have been reported, as discussed in Chapter 4. Dielectric breakdown of the dielectric elastomer is stochastic (defect-dependent) and time-dependent, as ageing and degradation processes occur during actuation, which reduces dielectric breakdown strength over time ¹¹⁸ and hence limits DEA lifetime. Given the wide range of possible elastomer materials, electrode materials (and electrode designs) and DEA architectures, there is still room for numerous lifetime investigations which would allow a better understanding of trade-offs of DEA lifetime vs. strain and force performance ¹¹⁹.

- c. There is a need for better materials and more reliability studies for DEAs.

Long-term operational stability and reliability studies need to be conducted to establish concrete metrics for DEAs ⁵, but also to understand how and why DEAs fail fast (especially under large strains), in order to find better elastomer and electrode materials to achieve reliable DEAs. A motivation for this thesis is to carry out some of these studies and develop reliable DEAs to increase interest from research groups and industrial companies toward DEAs and catalyze future investments in the field that would drive the technology costs down.

- d. Expensive dedicated production line needs to be built and a market needs to be found.

The DEA technology competes with existing actuation technologies which are reliable, and which are produced at large scale with well established production lines allowing economies of scale. The industrial production of DEAs would require a dedicated production line with reliable and reproducible manufacturing processes for elastomers. Such an investment is costly and needs to be justified by a market demand. Currently, there is no established market niche where DEAs constitute a unique and attractive technology owing to its softness, high strains and low power consumption. If the field of haptic devices (for consumer electronics or for gaming/metaverse purposes) develops in the future, DEAs would constitute an interesting technology to consider.

2.2 Dielectric elastomer and electrode materials for DEAs

2.2.1 Dielectric elastomers for DEAs

The choice of dielectric elastomer membrane (0.1-100 μm) is important to the actuation performance of DEAs. Ideal dielectric elastomer material candidates for DEAs should exhibit ^{20,24,33,120}: a) a high breakdown strength ($> 60 \text{ V}/\mu\text{m}$), b) low Young's modulus (0.1 – 1 MPa), c) low viscoelasticity (i.e. low creep, permanent set, hysteresis), d) low dielectric losses, e) low electrical conductivity (i.e. little leakage current $< \text{pA}$), f) good resistance to tearing, g) chemical and thermal stability over the service temperature ranges, h) low thickness (10-50 μm) with good homogeneity, and i) high stretchability and elongation at break ($>200\%$).

Common elastomer materials used for DEAs are acrylics (e.g. VHB), silicones, polyurethane, and natural rubber ^{2,4,24}. DEAs made of, SEBS ¹²¹, polybutadiene ⁹⁵, interpenetrating polymer networks (IPNs) ^{122–125}, fluorosilicones ^{95,126}, fluoroelastomers ¹²⁶, and polyisoprene ⁹⁵ have also been reported. Tailored elastomers can also be used as dielectric elastomer actuators for DEAs, such as multiblock polymers ¹²⁷, azobenzene-grafted silicones ¹²⁸, alkyl-thiol grafted silicones ¹²⁹, nitroaniline-modified silicones ¹³⁰, nitrile modified silicones ¹³¹, phenyl-grafted silicones ¹³², and recently, poly-n-butyl acrylate polymers crosslinked with oligomer crosslinkers, which exhibits low Young's modulus (0.08 MPa), high ultimate strength to Young's modulus ratio, high toughness (allowing elongations above 2400%), and high actuation strains (118% at $70 \text{ V}/\mu\text{m}$) ¹³³. An extensive overview of the different elastomer materials used for DEAs are found in ^{4,5,24,89,95,134–136}.

Important DEA actuation performance parameters such the range of achievable strains, actuation pressure, dielectric permittivity, and dielectric breakdown strength are intrinsically dependent on the choice of the dielectric elastomer material, as presented in Figure 2.5.

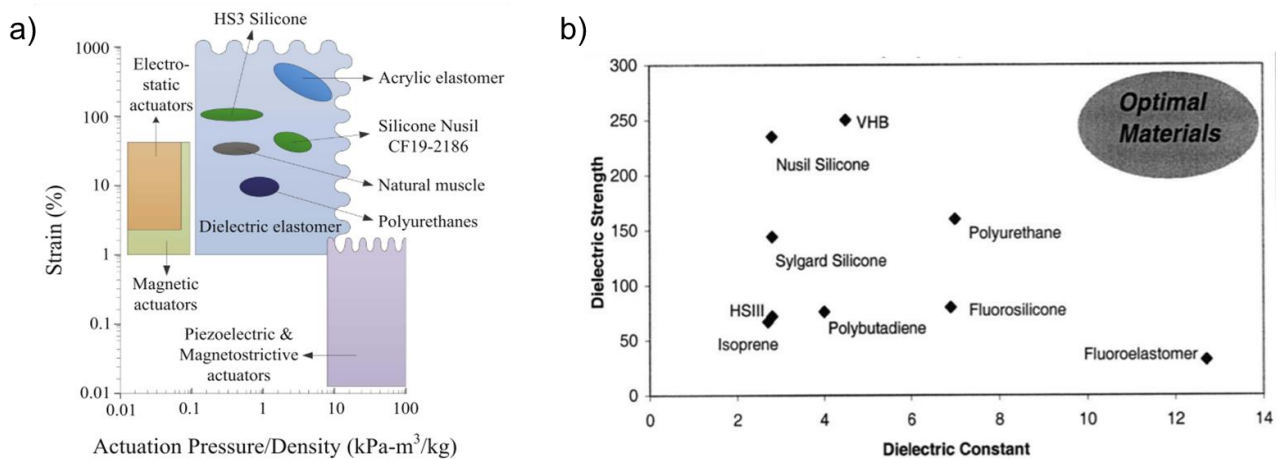


Figure 2.5: a) Strain vs. actuation pressure to density ratio for DEAs with some typical dielectric elastomer materials. Reproduced from ³³. b) Dielectric breakdown strength vs. dielectric permittivity of some typical dielectric elastomer materials. Reproduced from ¹³⁷.

Acrylic elastomers (VHB) have been the most investigated elastomers in the literature because of its large achievable strains (up to 1692% area strain ³⁰), large theoretical energy density (up to $3.4 \text{ J}/\text{cm}^3$) and commercial availability ¹³⁸. However, VHB exhibits time and temperature-dependent mechanical properties, has high viscous losses (i.e. large creep, hysteresis, permanent set), displays a limited bandwidth (i.e. VHB DEA performance significantly decreases above 1 Hz actuation ⁹), and its electromechanical response is history, temperature and frequency dependent ^{24,97,139}.

Despite having a lower dielectric permittivity ($\epsilon_r \approx 2.8$ vs. 4.4 for VHB) and having a reduced strain range, silicone elastomers constitute a better solution than VHB for reliable DEAs as they show relatively low viscous losses, low Mullins effect, fast electromechanical response (allowing bandwidths up to the kHz⁹) and do not exhibit time and temperature dependent mechanical properties^{24,97}. A further advantage of silicone elastomers is the commercial availability of numerous hardness ranges, allowing tailored mechanical properties and different DEA strain/force ranges to be achieved¹³⁹. Stable and reproducible actuation performances over millions of AC cycles have been achieved with prestretched silicone-based DEAs^{25,57,115}.

Compared to silicones, polyurethanes have a higher relative permittivity, but exhibit limited strains, and have an increased sensitivity toward higher humidity owing to their increased polarity¹²⁰. Natural rubber is used for energy generation¹⁴⁰, but they exhibit limited dielectric breakdown strengths (50 – 90 V/ μm), especially under high humidity¹⁴¹.

2.2.2 Influence of prestretch on dielectric elastomers for DEAs

Membrane prestretch (typically 300% equibiaxial prestretch for VHB and usually maintained by a peripheral rigid frame) is used to suppress electromechanical instability in VHB elastomers to achieve very large strains^{31,32,142} and to attenuate loss of tension (i.e. membrane wrinkling owing to compressive stresses either in passive areas or from rigid frame or fibers^{32,143,144,145}) in DEAs with large electrode areas^{142,144}. For silicone elastomers, prestretch is also used to attenuate loss of tension, but it requires a lower prestretch magnitude (typically 30% equibiaxial prestretch), which reduces the likelihood of mechanical rupture¹³⁹ (microcracks and tearing) over its lifetime. Also, the prestretch magnitude is significantly lower for silicone DEAs than for VHB DEAs to avoid stiffening. For castable silicone-based DEAs of a given thickness after prestretch, Akbari et al. found that increasing the prestretch value above 1.5 significantly increases the voltage needed to achieve a given strain, which implies that there is an optimal value of prestretch beyond which no improvement in the DEA actuation performance can be attained owing to stiffening¹⁴⁴. An important interpretation from that analysis is that a lower initial dielectric membrane thickness is preferred over an excessive prestretch to operate at relatively low voltages for a given actuation stretch.

Prestretch also increases the dielectric breakdown strength^{146–149}, as discussed in Chapter 4. Despite the numerous theoretical and practical investigations on the effect of prestretch on the actuation performance of DEAs⁴, little is known on the mechanisms of breakdown strength increase with higher prestretch^{4,150,151}. On a molecular scale, prestretching silicone elastomers allows trapped volatile short cyclic silicones to diffuse out from the elastomers¹⁵⁰ and it also leads to perpendicularly aligned polymer chains with respect to electric field, which would hinder charge carriers to freely move in along the electric field¹⁵¹.

Prestretching decreases the mechanical loss (i.e. $\tan(\delta)$) factor¹⁵², and can be exploited to allow actuation along a given preferred direction¹⁴⁴. Achieving large strain (>30%) DEAs is dependent on prestretch direction, as uniaxial prestretch (2.75 uniaxial prestretch to avoid electromechanical instability) leads to higher actuation strains (up to 138% in the transverse direction of prestretch) than equibiaxially-prestretched (1.45 equibiaxial prestretch) DEAs (actuation strains only up to 30%) for Sylgard 184 (silicone) DEAs¹⁴⁴. Usually, prestretch is maintained with a rigid frame¹⁵³, which can be limiting for some applications.

2.2.3 Influence of fillers on dielectric elastomers for DEAs

Elastomers incorporate significant fractions of fillers to ensure stable mechanical properties of the material^{24,154–156}, as discussed in Chapter 4. Elastomers with significant filler concentrations yield undesired mechanical phenomena, such as Mullins effect, Payne effect, and permanent set^{24,157}, as shown in Figure 2.6.

The Mullins effect is an elastomer softening phenomenon resulting from the reorganization of the polymer chains upon stretching, which lead to irreversible changes in the polymer structure and hence onto the stress-stretch curve of the elastomer over increasing number of stretching cycles^{158,159}. The Mullins effect occurs each time the membrane is stretched beyond its historical highest value²⁴.

The Payne effect is observed when an elastomer is cyclically loaded at little strain amplitude ranges, and refers to the dependence of the storage modulus (i.e. shear modulus) on shear strain, owing to elastomer deformations induced by the interactions between filler particles with themselves or with the elastomer network²⁴.

The permanent set is an irreversible deformation that occurs when stretching an elastomer for a certain time. The stretching leads to a shift in initial stretch owing to a reorganization of the elastomer network upon stretching.

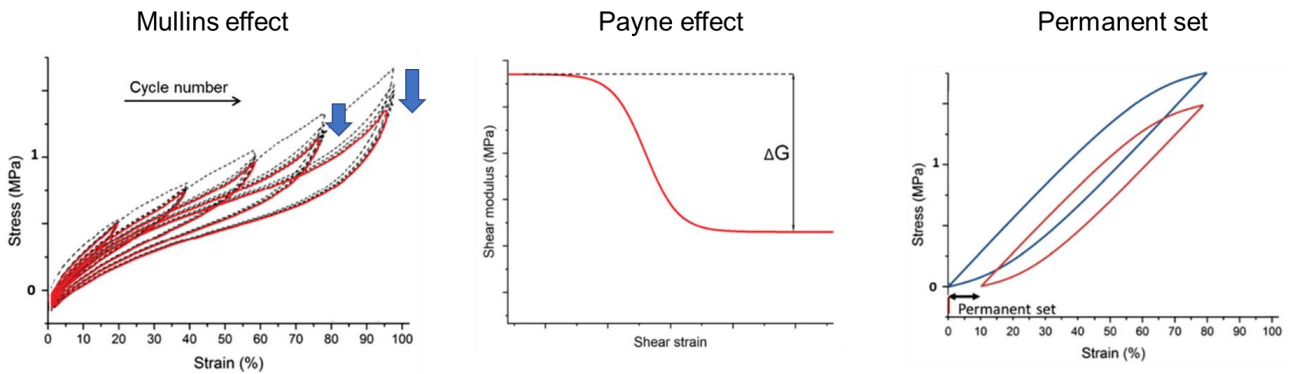


Figure 2.6: a) Mullins effect: softening induced by the reorganization of the polymer molecular chains induced during the stretching history on the polymer. b) Payne effect: elastomer deformations yield a shear strain dependent storage modulus. c) Permanent set: the elastomer does not get back to initial stretch in the absence of stress after being stretched for at least one cycle. Figures are reproduced from ¹⁵⁷.

Alternatives to adding fillers are elastomers composed of polymer blends of varying dielectric permittivity, elastomer networks with grafted polar groups, or copolymers are a promising field for investigating new elastomer systems of increased dielectric permittivity ^{134,160,161}.

2.2.4 Strategies to increase strain of DEAs at constant voltage

DEAs are attractive because of their potential to reach significant strains, and the strain performance of DEAs can be tuned by changing the dielectric membrane's properties. To reach higher actuation strains at constant voltage, one can a) reduce the dielectric membrane thickness, or b) decrease its Young's modulus, or c) increase its dielectric permittivity. All those methods present limitations ¹⁶²:

a) Reducing dielectric membrane thickness

Silicone elastomers (unlike VHB which is only commercially available as 0.5 mm and 1 mm thick cured rolls) are commercially available as uncured two-part formulations (or alternatively as cured films of various fixed thicknesses, e.g. Wacker Elastosil® 2030/20 and 2030/50), allowing for the membrane thickness to be tuned during its fabrication by blade-casting ¹⁵³, spray-coating ⁴⁸, spin-coating ³⁸, pad-printing ¹⁰⁸ or molecular beam deposition ¹⁶³. Decreasing the thickness of silicone membranes is therefore straightforward, but reduces the force generated by the DEA (stacking multiple layers is a solution to compensate), yields important scaling issues (e.g. thickness homogeneity, defects, dust, and electrode stiffening ³) and complicates the handling of the membranes for further manufacturing and for use.

As shown in Figure 2.7, the density of defects (e.g. dust, contaminants, microcavities, free volume) increases with lower thickness ³, therefore reducing the breakdown strength, and affecting the reliability of the membranes. Furthermore, the variations in thickness (i.e. thickness inhomogeneities) become increasingly important relative to the membrane thickness as it decreases, which exacerbates inhomogeneities in electric field ³, therefore affecting DEA reliability. Reducing membrane thickness does not involve changes in Young's modulus or permittivity of the elastomer ³. However, there is a limit on the extent to which thickness can be decreased, as elastomers typically incorporate fillers (e.g. SiO₂, TiO₂) of 20 to 200 nm diameter ^{155,156,164} which can form aggregates (up to 2 μm range scale for metal oxide fillers ¹³⁴).

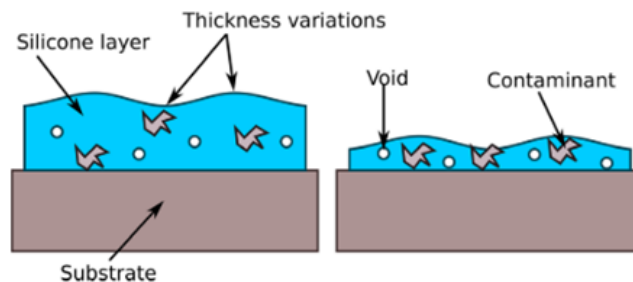


Figure 2.7: Decreasing the thickness of the dielectric leads to an increased density of defects (e.g. dust, contaminants, microcavities, free volume) and exacerbated thickness inhomogeneity vs. total membrane thickness. Schematic is reproduced from ³.

When reducing the membrane thickness below 10 μm , thin ($\ll 10 \mu\text{m}$) and low Young's modulus ($Y_{\text{electrode}} \ll Y_{\text{dielectric}}$) electrodes need to be selected to avoid stiffening^{107,108,165}, since electrode stiffening becomes increasingly important as the dielectric membrane thickness decreases. Electrode stiffening is further discussed in section 2.2.5.

One of the key issues for DEAs is their operation at high voltages ($>1 \text{ kV}$), which requires a high voltage power supply. Small (6.4 mm x 11.4 mm x 33.8 mm) DC:HVDC converters (EMCO XP Power A series) of 9 g yield up to 6 kV output voltage^{86,166}, and can be integrated in 5 cm x 4 cm x 0.8 cm circuit boards¹⁶⁶. However, for applications where size and/or weight of the integrated device is a concern, operating the DEAs at low ($< 300 \text{ V}$) voltages by decreasing the membrane thickness would allow for more compact cost-effective driving electronics⁷¹ and compatibility with CMOS circuits in consumer electronics¹⁰⁸.

There are several examples of DEAs operating at low voltage in the literature. Poulin et al. demonstrated a 3 μm thick silicone (Sylgard 184, 1.1 equibiaxial prestretch) DEA with pad-printed electrodes which can achieve strains of 7.5% at 245 V^{107,108}. Ji et al. demonstrated a 3 DEA stack of 6 μm thick silicone membrane with 2 nm thick single-walled carbon nanotube (SWCNT) electrodes that exhibit 25% area strain at 450 V⁷¹. 1 μm -thick silicone with 30 nm thick SWCNT electrodes yielded 4% strain at 100 V^{79,167}. 200 nm-thick molecular beam deposited silicone membranes coated with gold electrodes yielded with 6% strains at 12 V¹⁶³.

b) Decrease Young's modulus

Reducing the Young's modulus is a solution to increase the strain of DEAs (c.f. Eq.2), but it decreases output force. The Young's modulus of elastomers is dependent on the crosslinking density (i.e. the chain length separating two crosslinks), on the temperature, and on the concentration of fillers¹⁵⁷. Reducing the Young's modulus of elastomers either requires the selection or the synthesis of a low crosslink density elastomer, adding plasticizers, or decreasing the filler concentration²⁴. Reducing crosslink density influences the mechanical properties of elastomers such as its elongation at break, creep, relaxation, permanent set, cracking and tear strength¹⁶⁸. The addition of plasticizers can lead to phase separation over time within the elastomer¹³⁴ or evaporation leading to microcavities¹⁶⁹. Because of their low T_g , commercial silicone formulations generally do not intrinsically possess plasticizers which may cause such issues¹⁶⁹. Silicones intrinsically possess a significant fraction of fillers (e.g. mostly silica fillers for compatibility, typically forming aggregates^{159,170}) to strengthen the mechanical stability (e.g. increase Young's modulus, tensile strength and tear resistance¹⁵⁶) of silicone elastomer networks^{24,134,155,156}. Decreasing the filler concentration would therefore weaken the elastomer network and potentially lead to premature cracking or electromechanical instability. Overall, reducing the Young's modulus affects the elastomer's mechanical stability by increasing viscoelastic effects, and yields significant decreases in dielectric breakdown strengths, as discussed in Chapter 4.

c) Increase relative permittivity

The relative permittivity of elastomers can be increased by adding or increasing the concentration of high permittivity fillers (e.g. metal oxides such as TiO_2 , Al_2O_3 , BaTiO_3) in the elastomer, by using an interpenetrating polymer network (IPN), by adding high permittivity liquids or soft fillers, by incorporating functional copolymers to the elastomer network, or by using modified elastomers with covalently grafted dipoles^{24,111,134,171}.

Adding fillers (e.g. metal oxides) significantly increases the Young's modulus of elastomers, but highly increases the viscosity of the uncured formulations, and often decreases dielectric breakdown strength¹³⁴, as discussed in Chapter 4. Furthermore, if the filler concentration reaches a critical threshold, percolation between fillers occurs, which may induce the formation of additional conductive paths across the dielectric film^{157,171}. Higher Young's modulus is interesting for designing DEAs with high output force, but counterproductive for reliably achieving higher strains, especially if lower dielectric breakdown strengths are achieved.

Elastomers with significant filler concentrations can also be difficult to process because of their elevated viscosity¹³⁴, and are prone to undesired time, history, and strain dependent mechanical phenomena such as Mullins effect, Payne effect and permanent set^{24,157}.

The dielectric membrane thickness, the Young's modulus, the crosslinking density as well as the concentration and type of fillers influence the dielectric breakdown strength and hence the reliability of DEAs, as discussed in Chapter 4.

In this thesis, I select thin ($\approx 20 \mu\text{m}$ before prestretch, $\approx 12 \mu\text{m}$ after prestretch) prestretched silicone-based elastomers as dielectric layer because of its wide use in the DEA community, and its reported high reliability under AC actuation ($>$ millions of AC cycles)²⁵.

2.2.5 Stretchable electrodes for DEAs

The choice of electrode is also important for the actuation performance of DEAs, as it should be soft ($Y \leq 1$ MPa, ideally as low as possible), thin ($< 5 \mu\text{m}$ ideally), highly (Ω -k Ω range) conductive (especially for high AC frequency where low RC time constant is needed) upon stretching (giving homogeneous conductivity up to 100% strain), not penetrating the dielectric (i.e. no presence of liquid or particles which could migrate through the dielectric), having low viscoelasticity, and completely adhering to the dielectric substrate¹⁶². To increase strain, electrode stiffening needs to be low, by decreasing the electrode thickness and/or the Young's modulus of the electrode. The effect of electrode stiffening on the linear strain of a single-layer DEA is given by:

$$s_z = s_{z,0} \frac{\delta_{DE} Y_{DE}}{\delta_{DE} Y_{DE} + 2 * \delta_{EL} Y_{EL}} \quad (\text{Eq. 3})$$

where $s_{z,0}$ is the strain where the electrode stiffening is neglected, δ_{DE} the dielectric membrane thickness, Y_{DE} the dielectric membrane's Young's modulus, Y_{EL} the electrode material's Young's modulus, δ_{EL} the thickness of the electrode.

From Eq.3, the impact of electrode stiffening on the strain performance of single-layer DEAs becomes increasingly important as δ_{DE} decreases. To decrease the stiffening, the thickness of the electrode and/or the modulus of the electrode need to be significantly reduced.

In the literature¹⁶², commonly used electrodes on DEAs include pad-printed^{25,172} or inkjet-printed¹⁷³ carbon black-PDMS composite, carbon grease²⁵, dry carbon powder²⁵, self-clearing single-walled carbon nanotubes^{174,175}, silver nanowires^{176,177}, liquid metals (e.g. Ga)^{178,179}, ionic hydrogels¹⁸⁰, and metallic thin films (manufactured by electron beam evaporation, electroplating, cathodic sputtering, or photolithography⁸⁹)¹⁸¹.

Carbon black-based electrodes (shown in Figure 2.8) are generally used as stretchable electrodes for silicone-based DEAs¹⁶². Dry (loose) carbon powder has a low stiffening on the dielectric membrane, but is hard to manipulate during manufacturing, is not appropriate for cleanroom manufacturing, has a poor adhesion to the surface and can easily be scratched⁸⁹. Carbon grease has a better adhesion to the elastomer surface and also exhibits a low stiffening impact on the membrane, but is highly viscous and can diffuse into the dielectric membrane⁸⁹. A cured carbon black – PDMS composite (i.e. carbon black particles in a soft cured elastomer network) as an electrode provides a high mechanical resilience, no diffusion to the membrane, an excellent adhesion to the membrane and is stable over time, but it exerts an important stiffening on the dielectric membrane¹⁶².

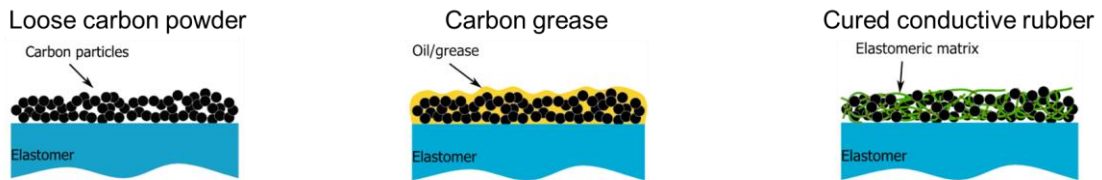


Figure 2.8: Commonly used carbon black based stretchable electrodes¹⁶². Reproduced from¹⁶².

Various manufacturing methods for carbon black-based electrodes can be used, such as pad-printing (stamping), inkjet-printing (drop on demand DoD), screen-printing and spray coating (shadow masking)¹⁶², as shown in Figure 2.9.

Spray-coating with a shadow mask enables thin and uniform layers, with good resolution (if the mask is in contact with the membrane), but if there is a contact between the membrane and the mask, the mask removal may induce damage on membranes, especially for low thickness membranes¹⁶². Screen-printing is a fast method to apply a grease or conductive rubber, but the mesh is in contact with the membrane, and mesh clogging is a frequent issue. Inkjet-printing is a non-contact patterning method that allows relatively high resolution ($100 \mu\text{m}$) patterns, which can be easily changed using a software (less expensive for testing numerous electrode pattern designs than screen-printing where a new mesh is needed for each new pattern design)¹⁶². By using a multi-nozzle system, inkjet printing can also be adapted for large scale production of DEAs¹⁶². However, nozzle clogging is frequent owing to particle sedimentation or excessive solvent evaporation, and the development and the optimization of the ink formulation is time-consuming, because the jetability of the ink is dependent on viscosity, vapor pressure, surface tension, and temperature, and because the interactions between the substrate and the ink have to be carefully studied to avoid coffee ring effects (resulting from fast evaporation rates), and to ensure a wetting contact angle ($< 90^\circ$) to avoid resolution loss by droplet bulging¹⁶².

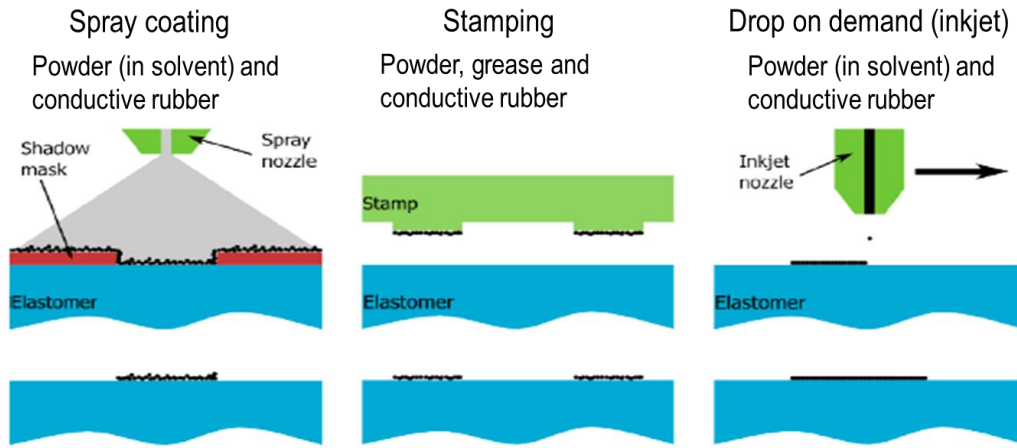


Figure 2.9: Commonly used manufacturing processes used for carbon black based stretchable electrodes ¹⁶². Reproduced from ¹⁶².

Pad printing (stamping) yields $\approx 2\text{--}5\text{ }\mu\text{m}$ thick electrodes (e.g. carbon powder, carbon grease or carbon black-rubber composites) with relatively high resolution ($500\text{ }\mu\text{m}$) patterns ¹⁵³. However, unlike inkjet-printing, pad printing implies a mechanical contact between the membrane and the ink-coated stamp, which may damage the membrane, especially if its thickness is low ($< 10\text{ }\mu\text{m}$) ¹⁵³. Finally, each pattern requires either a mask or a dedicated laser-engraved cliché.

Metal-based electrodes exhibit significantly higher conductivity ($\approx \Omega$ resistance) vs. carbon black-based electrodes ($1\text{--}100\text{ k}\Omega$ resistance), but are not stretchable (cracking above $2\text{--}3\%$) and induce a significant stiffening on the dielectric membrane owing to their elevated Young's modulus ($> \text{GPa}$) ¹⁶². Techniques to improve stretchability of metal-based electrodes include using liquid (e.g. Gallium-based) metal electrodes ^{178,179,182}, using zig-zag ¹²⁶ patterned electrodes, using out-of-plane metal electrodes on corrugated membranes ^{183,184}, or out-of-plane buckled electrodes ¹⁶², or using metal particles blended in an elastomer matrix (e.g. by using ion implantation) ^{185,186}.

Electrodes made of silver nanowires ^{176,177,187,188,189} have been reported, with satisfactory electrical conductivity ($R_s = 0.1\text{--}1\text{ k}\Omega/\text{square}$) for linear strains up to 140% ¹⁷⁶. Electrodes made of thin ($< 0.1\text{ }\mu\text{m}$) conductive ($R_s \approx 20\text{ k}\Omega/\text{square}$) single-walled carbon nanotubes are also commonly used for DEAs, and are interesting owing to its self-clearability, which allows DEAs to survive multiple breakdown events, albeit at reduced strain performance ^{174,175,189–193}. However, the adhesion of carbon nanotubes to the dielectric membrane is challenging ¹⁶². The sharp edges of the nanotubes generate field concentrations and corona discharges (which can be mitigated by blending the nanotubes in a aqueous matrix, e.g. water based polyurethane) ¹⁹². Finally, carbon nanotubes are not easy to handle and pattern on elastomer membranes ¹⁶².

Hydrogels can also be used as transparent electrodes, whose conductivity ($R_s = 0.1\text{--}1\text{ k}\Omega/\text{square}$ up to 600% strain) arises from the mobility of ions across its structure ¹⁸⁰. However, water evaporation limits the lifetime of hydrogel electrodes, and encapsulation is needed for increasing its lifetime ¹⁸⁰. Furthermore, diffusion of ionic moieties and water molecules toward the dielectric are problematic for lifetime, as discussed in Chapter 3.

The electrode nature also affects DEA lifetime, as discussed extensively in Chapter 4. Extensive reviews on flexible and stretchable electrodes for DEAs is found in ^{162,165}.

In this thesis, I mostly use pad-printing (stamping) for the patterning of electrodes on our silicone DEAs, and I use an ink composed of carbon black particles in a soft cured elastomer network is used as a standard ink, following the preparation and manufacturing recipe in Rosset et al. ¹⁵³, as discussed in Chapter 5. Both the ink and the manufacturing process yield excellent lifetimes for silicone-based DEAs under AC actuation ²⁵, and hence constitute a suitable selection for the investigations on DC lifetime which need to be long enough to conduct statistical analysis on lifetime at $\approx 5\%$ strain. A scheme of the pad-printing process on thin membranes is detailed in ¹³⁹.

2.3 DEA actuation mechanism

As introduced in Section 2.1, the actuation mechanism of DEAs is driven by an external voltage generating a Maxwell stress which yields a thinning and a in-plane surface expansion ⁷. The driving forces for that motion are the attractive forces between charges of

opposite polarity in opposite electrodes which squeeze the dielectric elastomer, and the repulsion between charges of similar polarity within the same electrode that yield an in-plane expansion to minimize the energy.

This section follows the work and the derivations from Pelrine et al.⁷. Assuming a DEA with ideal electrodes (i.e. no stiffening effect on actuation) of surface A and ideal dielectric elastomer membrane (isotropic, flat, incompressible, no defects or thickness inhomogeneities) of relative permittivity ϵ_r and thickness δ , which behaves as a capacitor (of capacitance C), Pelrine et al. derives the internal energy U at voltage V ⁷:

$$U = \frac{CV^2}{2} = \frac{\epsilon_0 \epsilon_r AV^2}{2\delta} \quad (Eq. 4)$$

Assuming incompressibility (i.e. Poisson ratio of 0.5) for the dielectric elastomer membrane, the Maxwell stress (σ) is defined in Pelrine et al. by the derivative of internal energy as a function of thickness ($\frac{dU}{d\delta}$), divided by surface area (A), yielding the equation Eq.1 shown in section 2.1⁷:

$$\sigma = \frac{1}{A} \frac{dU}{d\delta} = \frac{1}{A} \left(\frac{-\epsilon_0 \epsilon_r AV^2}{\delta^2} \right) = \frac{\epsilon_0 \epsilon_r V^2}{\delta^2} = \epsilon_0 \epsilon_r E^2 \quad (Eq. 5)$$

For DEAs under strains below 20% with dielectric membrane of constant Young's modulus (Y) and ideal electrodes (i.e. no stiffening), the DEA strain is directly given by⁷:

$$s_z = \frac{-P}{Y} = \frac{-\epsilon_0 \epsilon_r}{Y} E^2 \quad (Eq. 6)$$

Because dielectric elastomers used in DEAs are hyperelastic materials, the stress-stretch curve $\sigma(\lambda)$ is non-linear and stretch-dependent. Hence, Hooke's law cannot be applied to describe how stress increases as a function of the material's deformation. Several hyperelastic models are used instead to describe the stress-strain curve of DEAs, for instance Gent, Neo-Hookean, Yeoh models among others, as shown in Table 2.2³⁴. The Gent model is frequently selected owing to its consideration of a limiting stretch λ_{lim} , i.e. stretch where the stress exponentially increases to infinity as the polymer network reaches its maximal stretchability limit before mechanical chain rupture.

Table 2.2: Strain energy hyperelastic model functions for the description of the non-linear stress – stretch curves of elastomers^{34,194}.

Model	Energy function
Gent	$W_s = -\frac{GJ_{lim}}{2} \log\left(1 - \frac{\lambda_1^2 + \lambda_2^2 + \lambda_1^{-2}\lambda_2^{-2} - 3}{J_{lim}}\right)$
Neo-Hookean	$W_s = \frac{G}{2} (\lambda_1^2 + \lambda_2^2 + \lambda_1^{-2}\lambda_2^{-2} - 3)$
Yeoh	$W_s = \frac{c_1}{2} (I_1 - 3) + \frac{c_2}{2} (I_1 - 3)^2 + \frac{c_3}{2} (I_1 - 3)^3$ with $I_1 = \lambda_1^2 + \lambda_2^2 + \lambda_3^2$
Ogden	$W_s = \sum_{p=1}^N \frac{\mu_p}{\alpha_p} (\lambda_1^{\alpha_p} + \lambda_2^{\alpha_p} + \lambda_1^{-\alpha_p} \lambda_2^{-\alpha_p} - 3)$
Mooney-Rivlin	$W_s = C_1 (I_1 - 3) + C_2 (I_2 - 3)$ with $I_1 = \lambda_1^2 + \lambda_2^2 + \lambda_3^2$ and $I_2 = \lambda_1^2 \lambda_2^2 + \lambda_2^2 \lambda_3^2 + \lambda_3^2 \lambda_1^2$

Zhao and Suo have developed a model to explain the high actuation strains observed in VHB DEAs^{142,195}. Zhao and Suo consider an ideal (e.g. incompressible, isotropic, homogeneous thickness) dielectric membrane of initial thickness δ_0 and unit square surface (e.g. $x = y = 1$) without any electrodes and without any external load (or prestretch) which expands in-plane, and shrinks in the thickness reduction when submitted to a voltage V ¹⁴². Zhao and Suo derive the following expression for voltage – stretch ($V - \lambda$) relationship for elastomers with a stress-stretch curve $\sigma(\lambda)$ ^{142,195}:

$$V = \frac{\delta_0}{\lambda^2} \sqrt{\frac{\sigma(\lambda)}{\epsilon_0 \epsilon_r}} \quad (Eq. 7)$$

Eq.7 is represented in Figure 2.10 as the blue curve ¹⁴². According to Zhao and Suo, as the voltage increases with stretch, it reaches a critical limit at the theoretical value of $\lambda = 1.26$ (limit of electromechanical instability) beyond which a spontaneous transition from a low stretch stable state to a high stretch stable state is allowed at no extra voltage. The high stretch stable state can be beyond the dielectric breakdown strength of the elastomer (c.f. Type II). The electromechanical instability is dependent on the elastomer's mechanical properties, as it depends on its non-linear stress – stretch curve and on the elastomer network's limiting stretch.

Three types of elastomer membranes can be distinguished according to Zhao and Suo, as seen in Figure 2.10 ¹⁴²:

- Type I elastomers which undergo dielectric breakdown (red curve in Figure 2.10) before electromechanical instability occurs. Such dielectric elastomers are generally stiff (e.g. high Young's modulus at low stretch) and do not exhibit high actuation strains ¹⁴². Silicones are Type I elastomers.
- Type II elastomers which undergo electromechanical instability at constant voltage, thereby failing as a result of spontaneous thinning. VHB-based elastomers are Type II elastomers ¹⁴².
- Type III elastomers which undergo electromechanical instability, and survive the operation as the dielectric breakdown strength (red curve in Figure 2.10) has not been crossed. Such DEAs can generate large strains without early breakdown failure. VHB elastomers modified with interpenetrating networks behave as Type III elastomers ¹⁴².

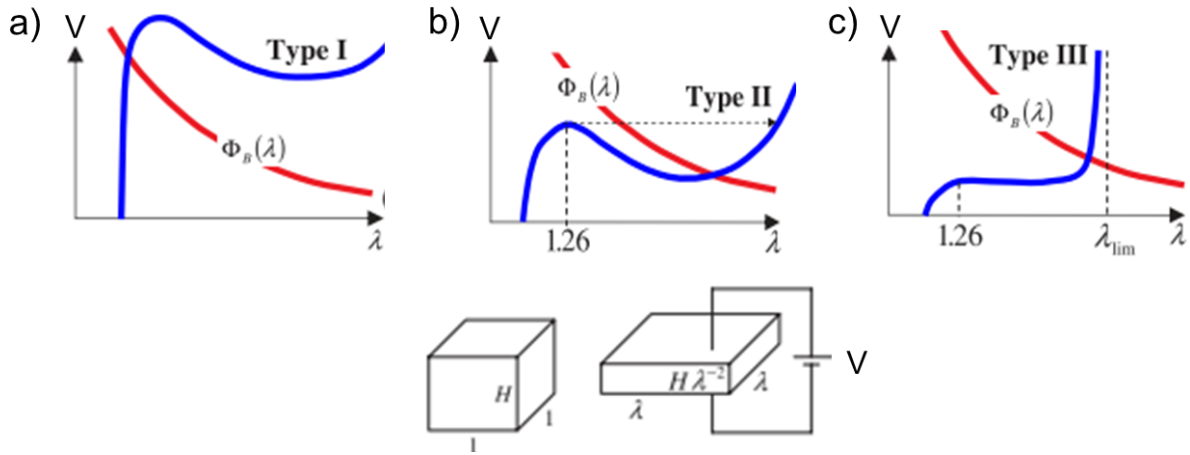


Figure 2.10: Voltage – stretch curve (Eq.7 – blue curve) for unprestretched unloaded ideal dielectric elastomer membranes subject to thickness reduction and area expansion, and breakdown voltage – stretch curve (red curve) ^{142,195} for a) Type I, b) Type II, and c) Type III elastomers. Type I elastomers fail by dielectric breakdown at low strain. Type II elastomers undergo dielectric breakdown upon electromechanical instability whereby the membrane thins spontaneously at constant voltage. Type III elastomers survive the electromechanical instability by jumping to a state of stable actuation at high strains without undergoing dielectric breakdown. Reproduced from Zhao and Suo ¹⁴².

Koh et al. identified strategies to modify the shape of the stress – stretch curve $\sigma(\lambda)$ of Type II elastomers in order to reduce or even eliminate electromechanical instability, as shown in Figure 2.11 ³²: applying a prestretch to a membrane ^{32,144,196}, reducing the limiting stretch λ_{lim} by using interpenetrating networks ¹²⁴, increasing crosslinking density (and tuning the Young's modulus by adding a plasticizer) ¹⁹⁷, or adding a swelling solvent to the elastomer network ¹⁹⁸.

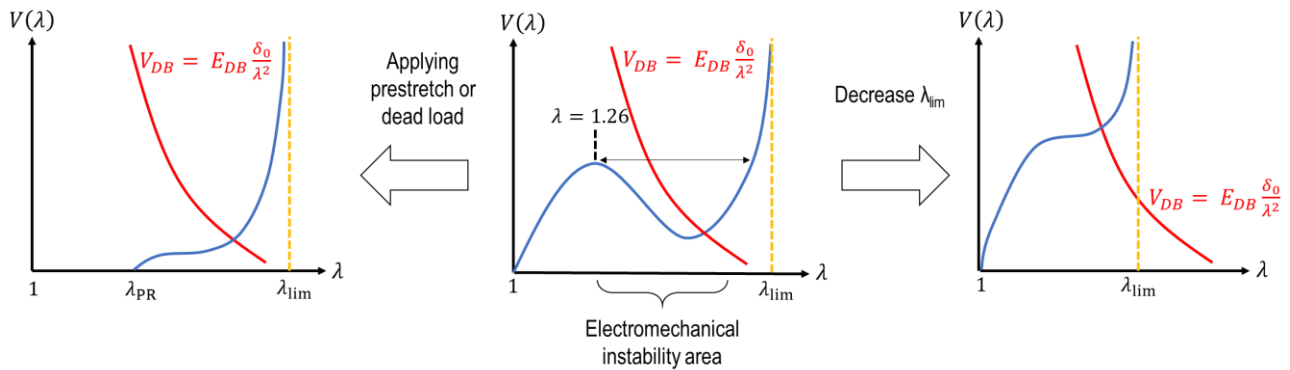


Figure 2.11: Influence of addition of prestretch (or dead load), and decreased limiting stretch λ_{lim} to dielectric elastomers under an applied voltage. Inspired from Koh et al. ³².

Koh et al. extended Eq. 7 to account for the addition of membrane prestretch or a dead load (represented as an additional force F_{ext} applied on the elastomer), thereby yielding ³²:

$$V = \frac{\delta_0}{\lambda^2} \sqrt{\frac{\sigma(\lambda) - \frac{F_{ext}}{\delta_0} \lambda}{\epsilon_0 \epsilon_r}} \quad (Eq. 8)$$

According to Koh et al., adding a prestretch or a dead load on Type II elastomers shifts the onset of the voltage – stretch curve closer to the limiting stretch λ_{lim} and hence leads to the same outcome as if one would use interpenetrating networks or elastomers with higher crosslinking density ³². As suggested from Eq. 8, adding a prestretch reduces the voltage needed for actuation because the thickness of the elastomer is reduced by the prestretch ³². If the prestretch is high enough, the voltage – stretch curve can be sufficiently reduced such that it becomes monotonic, hence suppressing electromechanical instability.

This thesis focuses on silicone DEAs (behaving as Type I elastomers) under limited actuation strain ranges (< 10%), and electromechanical instability is hence not a critical issue. Further details about theoretical models, electromechanical instability, and high strain DEAs using Type II and Type III dielectric materials are found in ^{29–32,142,199}.

2.4 Conclusion

DEAs are interesting soft actuators with low power consumption when holding a constant (DC) position, and their potential to deliver high strains. Because the strain of DEAs scales with the squared electric field, dielectric breakdown is a major failure pathway for DEAs, and therefore yields a significant tradeoff between strain and lifetime. Silicone-based DEAs yield significantly lower strains than VHB-based DEAs, but exhibit a reproducible, stable, and time and temperature independent strain behavior.

In this thesis, I study the lifetime of prestretched silicone-based DEAs with carbon black-PDMS electrodes operating at strains of ≈ 5 %. In this strain regime, silicone-based DEAs fail predominantly by dielectric breakdown, leading to an irreversible short-circuiting pinhole.

Chapter 3 introduces the state of the art of the failure modes and the reported lifetime studies on DEAs. Chapter 4 shows how the lifetime of silicone-based DEAs is measured using an automated setup, and how the mechanical properties, dielectric breakdown strength and water vapor permeability of thin silicone elastomer films are measured. Chapter 5 presents the data of dielectric breakdown strength, water vapor permeability, and stress – strain curves of silicone elastomer membranes. Chapters 6 and 7 present the DC lifetime data for equibiaxially prestretched single-layer silicone-based DEAs, and uniaxially-prestretched single-layer and multi-layer silicone-based DEAs.

Chapter 3 State of the art: failure modes and lifetime studies of dielectric elastomer actuators (DEAs) under high electric fields

Reported failure mechanisms of dielectric elastomers embedded in DEAs under the presence of an external electric field are dielectric breakdown, electromechanical instability, mechanical breakdown (or stretch-induced rupture) and loss of mechanical tension ^{4,7,24,112,143,148,151,177,196,200–205}. In this chapter, I present those failure mechanisms, and the literature associated with it, with an enhanced focus on silicone elastomers, as they are specifically investigated in this thesis.

Section 3.1 discusses electrical breakdown which is an important mechanism under high electric fields, where the breakdown strength is highly dependent on elastomer mechanical and chemical properties, as well as environmental conditions. Section 3.2 discusses electromechanical breakdown which is a concern if large actuation strains ($> 25\%$ ^{32,142}) are to be achieved. Section 3.3 gives an overview of the lifetime studies that have been conducted on DEAs.

3.1 Electrical breakdown and ageing of dielectric elastomers

3.1.1 Fundamentals of dielectric breakdown

The electrical breakdown failure of polymer films sandwiched by two electrodes is an irreversible process which leads to the destruction of the insulator (or at least a localized part of it) by the formation of a conductive path bridging the electrodes ¹¹⁸. Under high electric fields, polymer dielectric films are prone to fail on different timescales through numerous dielectric breakdown failure mechanisms that are highly dependent on ^{118,206–211}:

- a) The properties of the dielectric insulator (e.g. electrical conductivity, bond energy, intrinsic mechanical/thermal/physical properties).
- b) The structural homogeneity of the dielectric insulator (e.g. presence of free volumes, impurities, defects, nanocavities, and microcavities).
- c) External parameters such as the applied (AC/DC) voltage, exposure to UV light or radiation, temperature, and humidity.

These factors influence how charges migrate and accumulate (space charge accumulation, c.f. section 3.1.3.9) within the dielectric and influence the degradation processes (c.f. section 3.1.2) leading to dielectric breakdown failure of polymer dielectric insulators under high electric fields ^{118,206–211}. Literature on dielectric breakdown and degradation mechanisms occurring in rigid polymer dielectric insulators (e.g. intrinsic breakdown, thermal breakdown, electromechanical breakdown, erosion breakdown) is extensively discussed in ^{118,206,209,212–218} and is summarized in Figure 3.1. An overview of temperature and voltage-dependent charge injection and charge conduction processes across polymer dielectrics is given in references ^{118,206,219–222}. There is limited knowledge on which mechanisms are dominant in silicone elastomers, but there is evidence of space charge accumulation (c.f. section 3.1.3.9), and leakage currents owing to partial discharges and degradation mechanisms (c.f. section 3.1.3.8) prior to dielectric breakdown.

Dielectric breakdown is the result of cumulative damage where the dielectric membrane undergoes progressive chemical and/or thermal degradation (erosion) of the walls of microcavities and low-density regions due to partial discharges ^{118,209,215,223}. Section 3.2 presents the chemical degradation processes that occur specifically in silicone elastomers. Detailed information about the nature and mechanism of formation of partial discharges as well as about breakdown in gases has been extensively described in ^{118,206,212,213}.

The presence of free volumes, nano/microcavities, and defects within the insulator, as well as localized regions with enhanced electric fields (owing to e.g. space charge clusters and solvated ions) increase conduction within the insulating material, thereby enhancing leakage current, decreasing breakdown strength and leading to ageing or premature electrical breakdown ¹¹⁸.

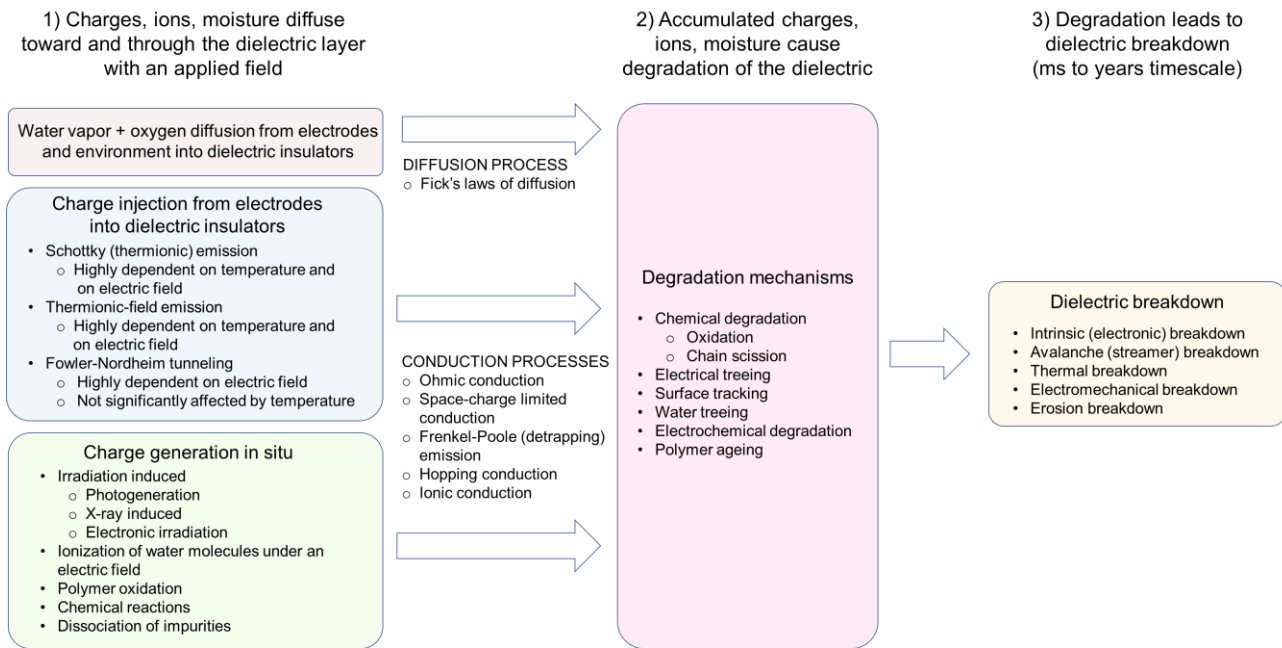


Figure 3.1: Overview of phenomena leading to ageing and dielectric breakdown of polymer dielectric insulators^{118,206}. Charges, ions, and moisture diffuse through the dielectric insulator and accumulate in microcavities and defects within the dielectric, leading to degradation processes and conductive tree propagation which ultimately lead to a short-circuit of the dielectric insulator from timescales of ns to years^{118,206,209,212}.

Given the high voltages required for actuation of DEAs, the most evident type of failure of DEAs is the dielectric breakdown of the dielectric elastomer membrane²⁴, whose investigations are presented in Section 3.1.3. In comparison to rigid dielectric insulators, dielectric elastomers such as silicone elastomers undergo a thickness decrease when a voltage is applied, which implies that the electrical breakdown voltage is not solely dependent on the intrinsic breakdown strength of the elastomer but also on actuation strain^{32,148}, membrane thickness^{116,148,151,204,224,225} and prestretch^{116,147–151}, temperature^{147,226}, type of voltage supply (AC/DC)²²⁶, relative humidity¹⁴⁷, water vapor content¹⁴⁷, and the addition of silicone oil or silicone solid²²⁷. Weibull statistical analysis is usually used to account for the stochastic nature of the breakdown and provide an effective evaluation of a thin elastomer's quality²²⁸. An overview of the polymer structure of silicone elastomers is given in Figure 3.2.

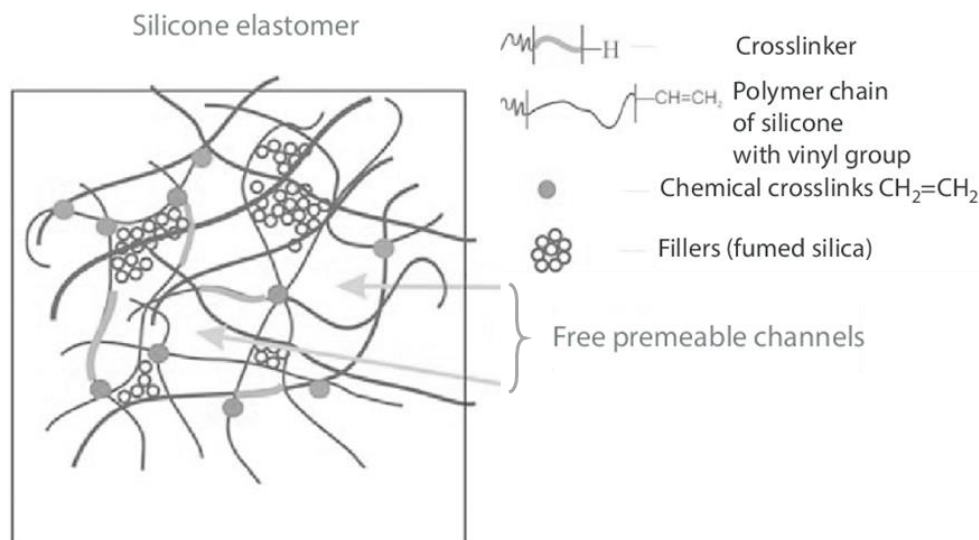


Figure 3.2: Overview of the polymer structure of crosslinked addition-curing silicone elastomers. Cured silicone elastomers are composed of silicone chains, aggregates of silica (or titania) reinforcing fillers, and free volume where humidity and gases can freely permeate through the network^{24,134,229}. Reproduced from²²⁹.

Mateiu et al. showed that dielectric breakdown of silicone-based elastomers results in the formation of a microscopic pinhole ($\approx 200 \mu\text{m}$ diameter scale) with the presence of solid aggregates within the walls and at the vicinity of the pinhole, with outward ridges at

the surface and in the bulk (suspected to generate significant stress inhomogeneities that can lead to complete tearing of the dielectric membrane (if a prestretch is initially applied))¹¹¹, as observed in Figure 3.3. Ghilardi et al. also observed similar low-resistivity pinholes, which lead to short-circuited DEAs¹¹².

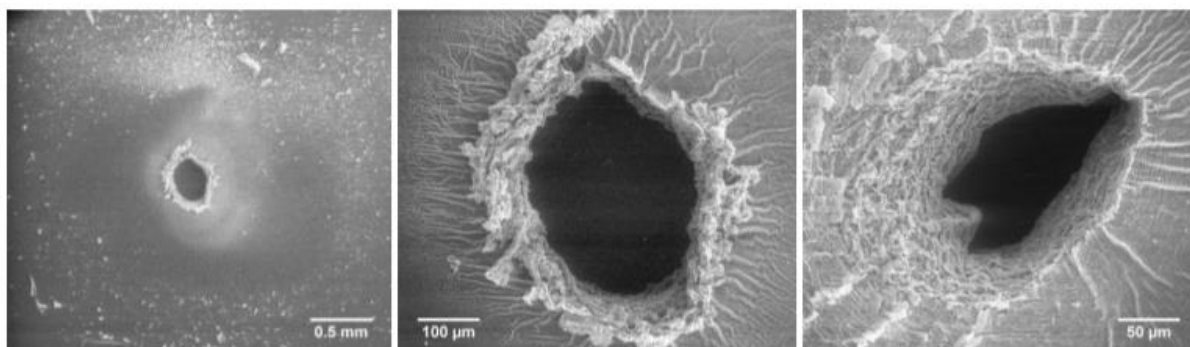


Figure 3.3: Pinholes formed upon electrical breakdown of a silicone membrane¹¹¹. Reproduced from^{111,171}.

By changing the chemical nature of the silicone elastomer (e.g. by incorporating alkyl chloride side groups into the silicone), pinholes without any ridges are witnessed, which implies that tear propagation is significantly less likely to be initiated^{111,171}.

Using carbon nanotubes as self-clearable electrodes, Yuan et al.^{4,230} have witnessed pinholes of different patterns which were recovered by carbon nanotubes and which still allowed a normal DEA operation²³⁰, as discussed later in this chapter.

However, for some DEAs, tearing after the pinhole formation (≈ 10 ms - 1 s interval) could also be observed, leading to open-circuited DEAs¹¹². The tearing is suspected to originate from the elastic energy that is stored in prestretched elastomers and that enhances tear propagation from the pinhole outwards¹¹².

There is a limited understanding on the fundamental mechanisms preceding dielectric breakdown in thin dielectric elastomer films²³¹. Vaicekauskaitė et al. have studied the stage preceding dielectric breakdown on thin unprestretched silicone (50 μ m thick Elastosil 2030/50, and 60 μ m thick LR 3043/50) films enclosed by round metal pin electrodes (of varying sizes) using a high speed camera, showing that²³¹:

- Right before breakdown, elastomers undergo local membrane thinning (visible only via high speed camera), and form wrinkled ring-shaped bulged patterns around rigid electrodes (owing to electrostatic forces) as well as bubbles of 0.7-3 mm size (depending on electrode type).
- Similar structures are observed for post-cured silicone elastomers, indicating that these structures are not induced by the evaporation of any absorbed water molecules in silica fillers or any trapped solvents or low molecular weight moieties.
- The breakdown spot for unprestretched films is located at a random location at the weakest spot of the elastomer, whereas, for prestretched samples, the breakdown spot is located at the center (i.e. location of highest field) suggesting that the influence of defects is less important if a prestretch is applied.
- Prestretched films exhibit higher breakdown strengths than unprestretched membranes, and thinning, wrinkling and bubbling phenomena do not occur in equibiaxially (100%) prestretched membranes even in (mechanically aged) membranes tested 14 days of prestretching.

3.1.2 Ageing and degradation mechanisms of silicone elastomers

Ageing of dielectric membranes is complex, hard to investigate at the molecular level, dependent on numerous factors (c.f. Figure 3.4²³²), and there are still many questions that need to be addressed²¹⁸, especially in silicone elastomers, where limited research has been conducted on ageing under external fields.

Silicone elastomers exhibit a high stability toward environmental conditions (e.g. heat, moisture, pollutants, UV light, electrical discharges) and keep their hydrophobicity over extended periods of time in comparison to other polymer materials²³³, owing to its strong $\sim\text{Si}-\text{O}-\text{Si}\sim$ bonds. However, silicone elastomers have a high permeability for gases (e.g. oxygen, water vapor), even if solvated ionic clusters in condensed water (typically formed in nano/microcavities during ageing) have a slow diffusion in PDMS in the absence of any electric field¹⁶⁹.

Ageing of rigid and thick (> 0.1 mm) silicone rubber insulators has been studied in the high voltage insulation industry²³⁴, but these studies are still relevant for soft, thin (< 0.1 mm) silicone elastomer films (because of similar chemistry), where ageing and degradation have not been thoroughly studied (c.f. section 3.1.3). The degradation and ageing processes in silicone elastomers occurs at the molecular scale, and involve polymer oxidation (which can be self-sustained), polymer (covalent bond) chain scission, hydrolysis, and crosslinking^{233,235} (as shown in Figure 3.5), and the formation of nano-scale free volumes or air gaps²¹⁸.

When exposed to heat, moisture, UV light and oxidizing agents for long periods of time, side reactions such as oxidative degradation, photocatalytic degradation and hydrolysis can occur²³³, which yield the ageing of the silicone rubber. Since the Si-CH₃ bond is weaker (318 kJ/mol, i.e. 3.3 eV) than the Si-O (452 kJ/mol, i.e. 4.7 eV) bond¹⁶⁹, it is believed that Si-C bonds are cleaved first^{169,233,235}. Oxidation reactions, backbone chain scissions and crosslinking of the radical products originating from homolytic bond cleavages lead to the degradation of silicone polymer chains^{233,235}. Upon PDMS chain scission, PDMS chains of low molecular weight are formed²³⁶. The progressive diffusion of small PDMS chains from bulk toward the insulator's surface can allow silicone rubber insulators to maintain surface hydrophobicity²³⁶, but exposing the bulk to a higher risk of erosion path formation (i.e. formation of nanocavities)^{233,237}.

In rigid insulator films, the degradation processes are generally originating from defects and air-filled nanocavities/free volumes (owing to its lower permittivity vs. polymer and higher electron mean free path^{118,206,238–241}) sustained by partial discharges, free radical species (monitored with electron paramagnetic resonance²⁴²)^{118,208,223,241}, space charges^{210,242,243} and solvated ions^{118,225,232,235,239,241,244–246}. Over time under DC fields, the progressive chemical and thermal erosion of the walls of nanocavities and low-density regions subject to partial discharges (coupled with trapped accumulated space charge clusters) initiate their expansion to ultimately become microcavities (>1 μm), and can trigger the inception of electrical and/or water treeing leading to a conductive channel path across the dielectric which in turn further increases leakage currents and promotes the migration of aqueous and solvated ion species^{118,213,241,244,247,248}. Under a constant DC electric field, all degradation and ageing processes carry on, and sustain positive feedback processes to eventually yield a complete electrical breakdown. No extensive investigation has been conducted on soft thin (< 100 μm) silicone elastomers to confirm that such mechanisms for breakdown failure are dominant.

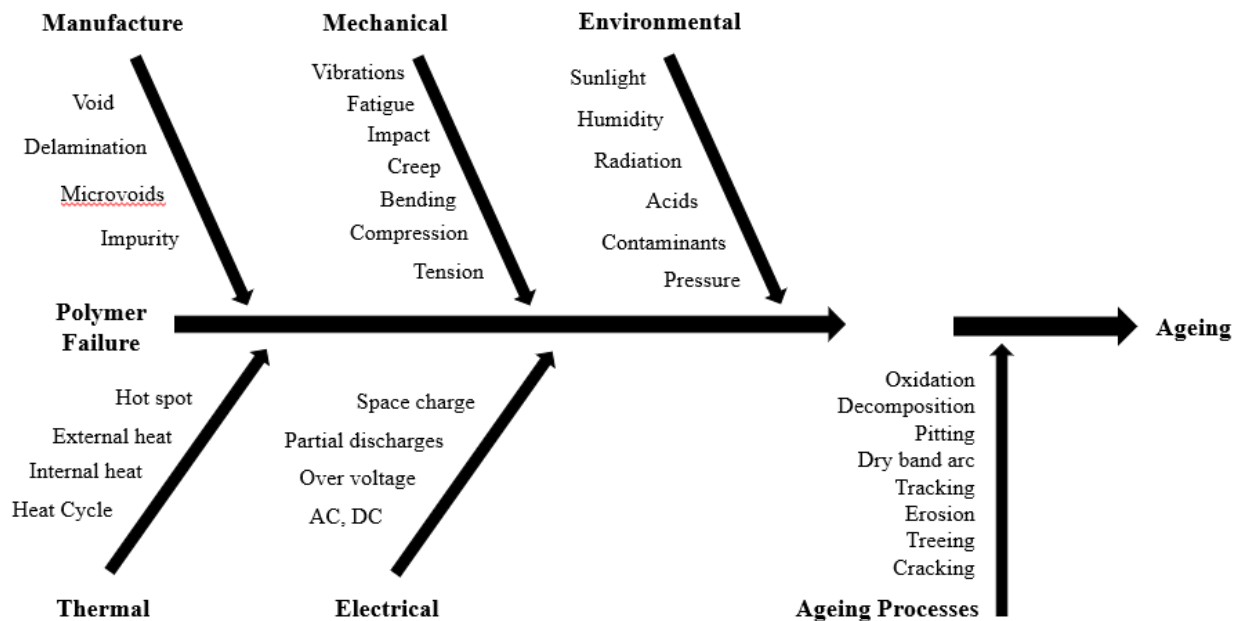


Figure 3.4: Overview of the factors which contribute to the failure and the ageing of the polymer insulators²³². Reproduced from²³².

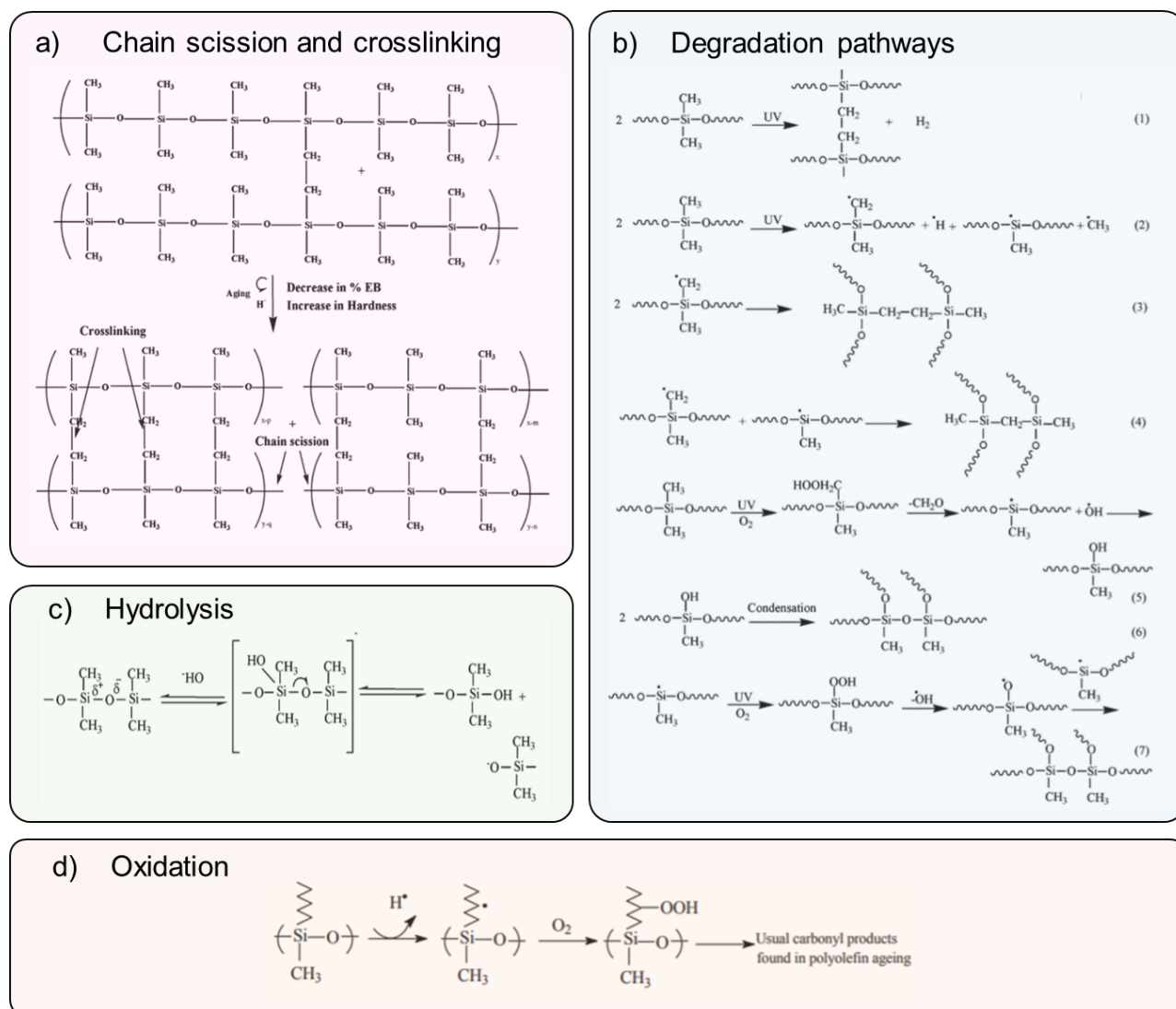


Figure 3.5: Mechanisms of a) chain scission and crosslinking, b) degradation pathways, c) hydrolysis, and d) oxidation in silicone elastomers ^{233,235}. Figure 3.5a) b) c) are reproduced from ²³³. Figure 3.5d) is reproduced from ²³⁵.

Increasing concentrations of ionic impurities have been shown to decrease the dielectric strength of silicone rubber ²⁴⁹. The presence of salt contaminants is known to enhance the surface hydrophilicity and corona arcing/discharges in silicone rubbers and induce chain scission in silicone rubbers ²³⁶.

Bleszynski and Kumosa ²³⁶ proposed a model for the degradation of silicone rubber insulators submitted to high voltages involving the formation of hypochlorous acid (HOCl) from the hydrolysis of water in a NaCl (3%) aqueous solution ²³⁶, which yields both hydrolysis and oxidation reactions ²³⁶.

According to Harley et al. ²⁵⁰, the silica fillers of the silicone rubber act as “host” surfaces where adsorption of water or other species (e.g. ions forming solvated ion clusters) occurs and ultimately leads to aggregates ²⁵⁰. Bleszynski and Kumosa suggested that the silica fillers could potentially enhance the local diffusion and concentration of hypochlorous acid in such multilayer aggregates which would lead to the formation of significant concentrations of localized microcavities ²³⁶.

The siloxane chain backbone is flexible and the activation energies for conformational rotations are very low, typically around 3 – 14 kJ/mol (i.e. 0.03 – 0.15 eV) ¹⁶⁹, and intermolecular interactions between polymer chains are low (since the Si–O dipole-dipole interactions between adjacent chains are hindered by the methyl groups of the backbone), which implies that significant free volumes are inherently present within silicones ^{169,251}. Ion mobility through silicone rubber (PDMS) is facilitated owing to the presence of free volumes ^{169,249}.

Crosslinking can generate free volumes and voids inside the dielectric during manufacturing. Silicone elastomer networks prepared through platinum-catalyzed hydrosilylation (i.e. addition-curing silicones, where the curing reaction involves vinyl-terminated PDMS chains and hydride-terminated PDMS chains, catalyzed by a platinum catalyst) yield elastomers with a very low number of voids since almost no byproducts are formed during the crosslinking process²⁴, whereas networks prepared through condensation curing (i.e. curing reaction involving hydroxyl-terminated polymers which release one water molecule per catalyzed condensation) are slower, humidity-dependent, and generally yield lower dielectric strength materials, possibly owing to low molecular weight PDMS byproducts and voids²⁴.

Short unreacted linear or cyclic PDMS chains can also be produced if the crosslinking occurs via the nucleophilic substitution of chlorosilanes²⁴. Removing these residual low molecular weight silicones by evaporation requires a post-curing for several hours, that yields higher modulus silicone elastomers with increased tensile strength and reduced extensibility^{150,252}.

Several ageing models have been developed in the literature for rigid dielectric insulators, as shown in Table 3.1. Few of these models have been applied to silicone elastomers because of scarce ageing investigations. An extensive overview of ageing models is found in²⁵³.

Table 3.1: Overview of the main ageing models used for lifetime (mean time to failure - MTTF) modelling of polymer dielectric insulators. T is the temperature [K], E the electric field [V/ μ m], E_a the activation energy [J], E_t the electric field threshold of partial discharge inception [J], n, k_3, k_1 are power law factors [-], $R = 8.31 \frac{J}{mol \cdot K}$ the ideal gas constant, $k_B = 1.38 * 10^{-23} \frac{m^2 kg}{s^2 K}$ is Boltzmann constant, $h = 6.63 * 10^{-34} \frac{m^2 kg}{s}$ is Planck's constant, m the voltage endurance coefficient [-], ΔG the free energy of activation [J], ΔH the activation enthalpy [J], ΔS the activation entropy [J/K], B a material-dependent constant [-], $A_{eq}(E)$ is the fraction of degraded moieties at equilibrium between forward degradation and reverse reactions [-], A^* is the critical fraction of degraded moieties that induces cavities large enough for partial discharges to occur [-], w is the trap width [-], N_c the critical trap density, N_0 the initial trap density, σ a mechanical stress [Pa], Δv a stress activation volume, γ a molecular factor [m³], A_0 is a pre-exponential factor. Details about the models and derivations can be found in the respective references.

Ageing Model	Lifetime (MTTF)
Arrhenius (Dakin) model ^{210,212,254,255}	$MTTF = A_0 e^{\frac{E_a}{RT}}$
Dakin-Studniarz model ^{210,256}	$MTTF = A_0 e^{\frac{-mE}{(E-E_t)}}$
Inverse power model ²¹⁰	$MTTF = A_0 E^{-n}$
Eyring model ^{212,253}	$MTTF = A_0 T^{-n} e^{\frac{-\Delta G}{k_B T}}$ $MTTF = A_0 V^{-n} e^{\frac{-\Delta G}{k_B T}}$
Peck model ^{253,257}	$MTTF = A_0 R H^n e^{\frac{E_a}{RT}}$
Zakrevskii and Sudar model ^{239,246}	$MTTF = A_0 e^{\frac{E_{a,trap} - wqE}{RT}}$
Space charge DC DMM model ^{208,210}	$MTTF = \frac{h}{2k_B T} e^{\left(\frac{\Delta H / k_B - B E^{2n} / 2}{T} \frac{\Delta S}{k_B} \right)}$ $\ln \left(\frac{A_{eq}(E)}{A_{eq}(E) - A^*} \right) \left[\cosh \left(\frac{\Delta G / k_B - B E^{2n}}{2T} \right) \right]^{-1}$
Parpal and Crine electrical ageing model ^{241,248}	$MTTF = \frac{h}{2k_B T} e^{\left(\frac{\Delta G_0}{k_B T} \right)} \text{csch} \left(\frac{e \lambda E}{k_B T} \right)$
Lewis kinetic model ^{255,258,259}	$MTTF = \frac{h}{k_B T} \left(e^{\frac{-\Delta G_1}{k_B T}} + e^{\frac{-\Delta G_2}{k_B T}} \right)^{-1}$
Chen model ²⁵⁵	$MTTF = \frac{N_c - N_0}{A_0} E^{-\frac{k_3}{k_1}}$
Zhurkov mechanical ageing model ²⁴¹⁻²⁴³	$MTTF = A_0 * \exp \left(\frac{(E_{a,bond} - \gamma \sigma)}{k_B T} \right)$
Crine mechanical model ²⁴¹	$MTTF = \frac{h}{2k_B T} e^{\left(\frac{\Delta G_0}{k_B T} \right)} \text{csch} \left(\frac{\Delta v \sigma}{k_B T} \right)$

3.1.3 Dielectric breakdown strength investigations on dielectric elastomers

The following subsections summarize the dielectric breakdown strength studies conducted on dielectric elastomers for DEAs.

3.1.3.1 Influence of membrane prestretch and thickness on the dielectric breakdown strength

As presented in Section 2.2.2, prestretch of the dielectric membrane is an important parameter that influences the actuation performance of DEAs. Prestretching dielectric elastomer membranes generates stiffened elastomers along the prestretching direction and thereby yields thinner membranes of enhanced dielectric breakdown strength^{4,24,144,151}.

On a molecular scale, prestretching silicone elastomers allows trapped volatile short cyclic silicones to diffuse out from the elastomers^{24,150} and it also leads to the alignment of polymer chains (perpendicularly to electric field) and of defects¹⁵¹. The enhanced electrical breakdown strength upon membrane prestretching could be due to the aligned polymer chains which would hinder charge carriers to freely move along the direction of the electric field¹⁵¹. However, the positive impact of prestretch on enhancing electrical breakdown strength and its underlying mechanisms are still a mystery and subject to debate²⁰³.

As shown in Figure 3.6, Gatti et al. have experimentally investigated the electrical breakdown of Wacker Elastosil P7670 silicone elastomer films of various thicknesses, sandwiched with rigid copper electrodes, and highlighted an increase of electrical breakdown strength with a decrease in membrane thickness ($E_B \approx \delta^{-0.23}$) and with an increase in prestretch ($E_B \approx \lambda^{0.77}$)¹⁴⁸.

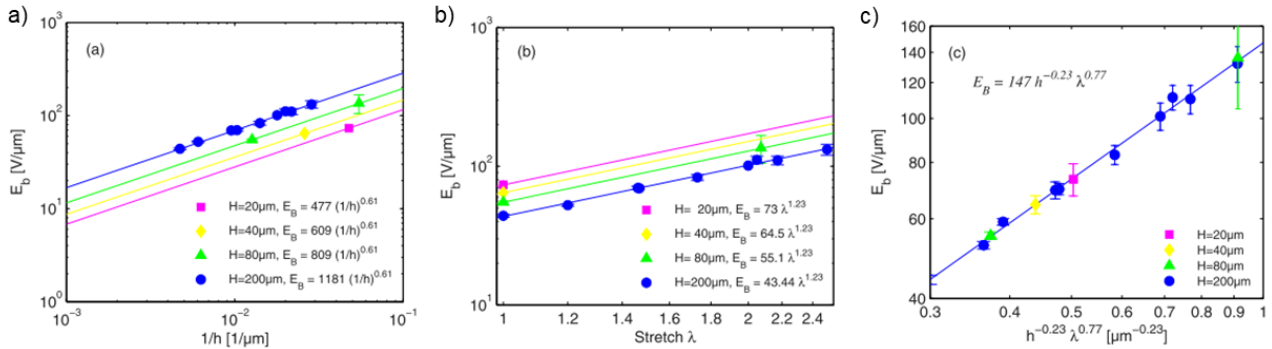


Figure 3.6: Dielectric breakdown strength (E_B) of silicone (Elastosil P7670) elastomer films of varying initial thickness (H) as a function of a) thickness after prestretch (h), b) stretch (λ), and c) scaling parameter ($h^{-0.23} \lambda^{0.77}$)¹⁴⁸. Dielectric breakdown strength increases with decreasing membrane thickness and increasing membrane prestretch. Reproduced from¹⁴⁸.

Their empirical analysis concluded that enhancing the prestretch is more effective than lowering the elastomer thickness to increase the electrical breakdown strength, that the need for eliminating electromechanical instability is not always necessary, and that silicone membranes with high prestretch and initial thickness could be preferred over low thickness and low prestretch membranes to achieve high dielectric strength elastomers¹⁴⁸. These conclusions contrast from Akbari et al.¹⁴⁴ findings for biaxially prestretched castable silicone elastomers (e.g. Sylgard 186) where a thinner dielectric membrane thickness and a moderate prestretch value are preferred over a highly prestretched thicker membrane since high prestretch values significantly stiffen the dielectric membrane (i.e. the membranes become strain-stiffening) without any positive improvement on electromechanical properties (i.e. the voltage required to achieve a given actuation increases)^{24,144}, as discussed in Section 3.2.

As shown in Figure 3.7, a very similar power law was also found by Huang et al. for the relationship of dielectric breakdown strength vs. membrane thickness and prestretch for VHB elastomers (with 18 μm diameter copper wire as electrodes)²⁶⁰. The dielectric breakdown strength of VHB elastomers increases with a decrease in membrane thickness after stretch^{260,261}, and with an increase in membrane prestretch²⁶⁰. Kofod et al. showed that a 500% area prestretch increases dielectric breakdown strength by a factor 12 x (218 V/μm vs. 18 V/μm) vs. unprestretched VHB 4910 films²⁶¹.

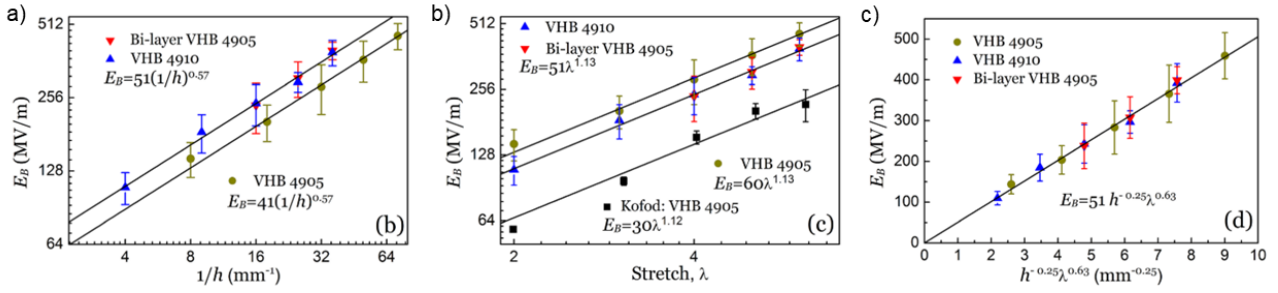


Figure 3.7: Dielectric breakdown strength (E_B) of VHB (4905 and 4910) elastomer films as a function of a) thickness after prestretch (h), b) stretch (λ), and c) scaling parameter ($h^{0.25} \lambda^{0.63}$)²⁶⁰. Dielectric breakdown strength increases with decreasing membrane thickness and increasing membrane prestretch^{260,261}. Reproduced from²⁶⁰.

Tröls et al. found similar findings for VHB 4910 (1 μm thick before prestretch) and natural rubber (ZruElast A1040, 300 μm before prestretch) DEAs with both circular compliant electrodes and rigid plate (brass) electrodes, where an increase in radial prestretch yields an increase in dielectric breakdown strength²⁶². VHB 4910 and ZruElast A1040 DEAs with compliant electrodes exhibit lower dielectric breakdown strengths than equivalent DEAs with rigid electrodes at similar prestretch²⁶². Also, higher electrode surface areas and slower voltage ramp sweep rate yield lower dielectric breakdown strengths²⁶¹.

Iannarelli et al. studied the dielectric breakdown strength of prestretched Elastosil 2030 (100 μm thickness before thickness) silicone films with carbon black – PDMS composite spray-painted electrodes, revealing that higher prestretch and lower membrane thickness increases dielectric breakdown strength¹¹⁶, as shown in Figure 3.8.

Förster-Zügel et al. also highlighted a factor 2x increase in breakdown strength (195 $\text{V}/\mu\text{m}$ vs. 98 $\text{V}/\mu\text{m}$) by applying a prestretch (from $\lambda=1$ to $\lambda=0.5$ along the thickness direction) on Elastosil 2030/30 films (30 μm thick)¹⁴⁹.

Zakaria et al. showed that the breakdown strength of silicone elastomer films increases by factors ≈ 1.5 -2 x by prestretching Elastosil RT625 and POWERSIL LR 3043/30 membranes (40-100 μm thick) to 60% and 120% uniaxial prestretch¹⁵⁰, and by a factor 2.5x (250 $\text{V}/\mu\text{m}$ vs. 100 $\text{V}/\mu\text{m}$ at no prestretch) with a 200% equibiaxial prestretch for Elastosil RT 625 membranes, and a factor 3x (320 $\text{V}/\mu\text{m}$ vs. 120 $\text{V}/\mu\text{m}$ at no prestretch) with a 200% equibiaxial prestretch for POWERSIL XLR 630 membranes¹⁵¹. Also, decreasing the membrane thickness from 100 μm to 20 μm yields a > 2 x factor increase in dielectric breakdown strength (100 $\text{V}/\mu\text{m}$ to over 200 $\text{V}/\mu\text{m}$) for unprestretched Elastosil RT 625 and POWERSIL XLR 630 membranes¹⁵¹.

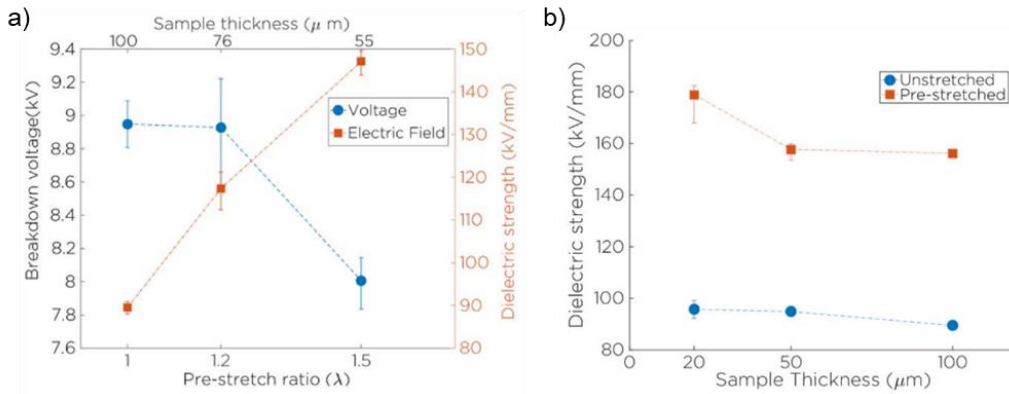


Figure 3.8: Breakdown strength of 100 μm -thick Elastosil 2030/100 silicone elastomer films as a function of a) prestretch magnitude, and b) thickness¹¹⁶. Dielectric breakdown strength increases with decreasing membrane thickness and increasing membrane prestretch¹¹⁶. Reproduced from¹¹⁶.

From a thermal perspective (i.e. using a model where thermal effects only are considered), Zakaria et al. have found that, theoretically, higher breakdown strengths are obtained with thin film thicknesses (with effective heat dissipation) in comparison to thicker membranes where Joule heating and conductivity can be more significant^{151,205}. According to Zakaria et al., thin (i.e. $< 100 \mu\text{m}$) silicone dielectric membranes do not fail through thermal breakdown under a constant external electric field since the required electric field for thermal breakdown was found to be significantly higher ($\approx 400 - 1000 \text{ V}/\mu\text{m}$) in comparison to the dielectric strength of the common silicone elastomers ($\approx 50 - 150 \text{ V}/\mu\text{m}$)²⁰⁵.

Chen et al. showed that the dielectric breakdown strength of $293 \pm 5 \mu\text{m}$ thick natural (Oppo Band Green 8003) rubber, of $224 \pm 4 \mu\text{m}$ thick styrenic (Theraband Yellow 11726) rubber and of $1492 \pm 16 \mu\text{m}$ 3-layer stack of VHB 4905 with rigid cylinder brass electrodes (25 mm diameter for HV electrode, and 150 mm diameter for ground electrode²⁶³) significantly increases with increasing stretch, as shown in Figure 3.9¹⁴¹.

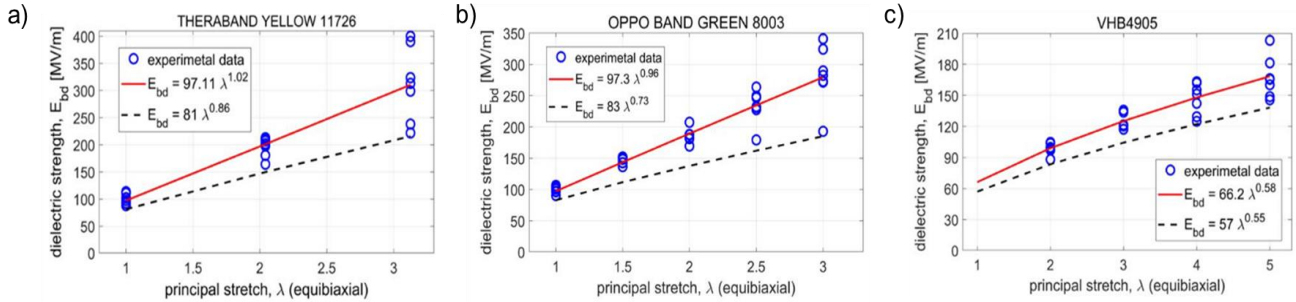


Figure 3.9: Influence of equibiaxial stretch on the dielectric breakdown strength of a) styrenic rubber, b) natural rubber, and c) VHB 4905 3-layer stack with rigid cylinder brass electrodes¹⁴¹. Reproduced from¹⁴¹.

In summary, lower membrane thickness and higher prestretch increase the breakdown strength of soft elastomers for DEAs.

3.1.3.2 Influence of Young's modulus and crosslink density on dielectric breakdown strength

From the studies of Yu and Skov²⁰³, Banet et al.¹³⁶ and Vaicekauskaitė et al.²⁶⁴, there is a general trend that increasing Young's modulus generally increases the dielectric breakdown strength for silicone elastomers (but not systematically).

Yu and Skov showed a relationship between the Young's modulus and the electrical breakdown strength, derived for an elastomer without any fillers or entanglements, from a molecular model involving Kuhn step lengths²⁰³. At a given temperature, the electrical breakdown strength of PDMS scales as: $E_B \approx Y^{0.588}$ shown as the red curve in Figure 3.10a, but this equation does not apply for filled elastomers or high molecular weight elastomers where entanglements are significant²⁰³.

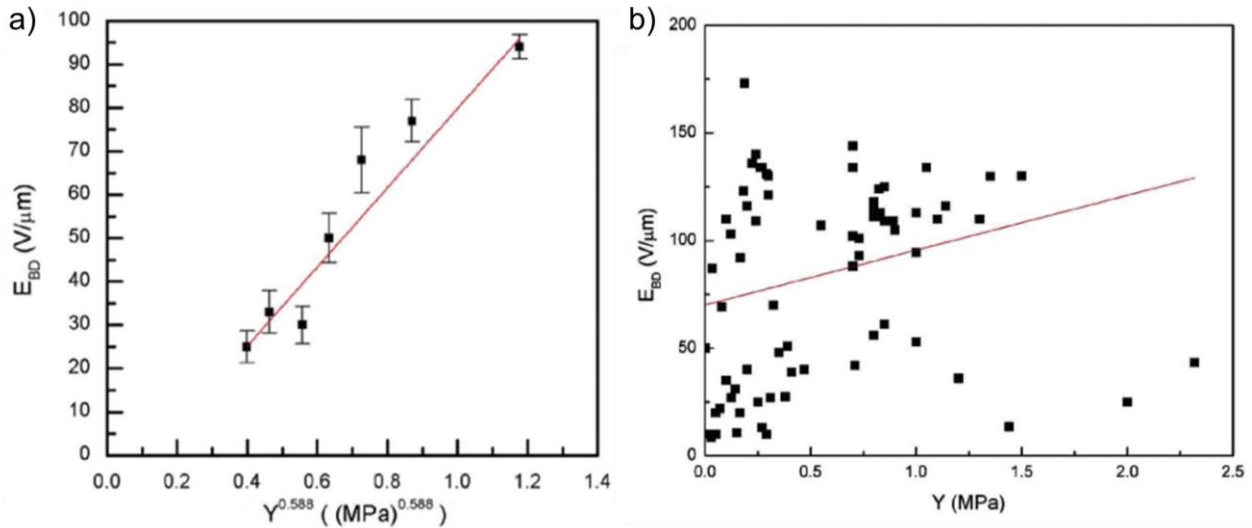


Figure 3.10: a) Influence of Young's modulus on the breakdown strength of filler-free bottlebrush elastomers of varying crosslink density²⁰³. b) Influence of Young's modulus on breakdown strength of unprestretched silicone elastomer formulations²⁰³. Dielectric breakdown strength increases with higher Young's modulus. Reproduced from²⁰³.

Kollosche et al. demonstrated that unprestretched styrene-ethylene-butylene-styrene (SEBS) thermoplastic elastomers exhibit an increasing dielectric breakdown strength with increasing Young's modulus²⁶⁵, as shown in Figure 3.11b.

Zakaria et al. showed that the relationship between Young's modulus and breakdown strength is not straightforward if prestretching is involved, because of the nonlinear mechanical properties of the elastomer¹⁵¹. Therefore, as seen in Figure 3.11a, breakdown

strength increases monotonically with an increase in membrane prestretch, albeit the Young's modulus being lower at prestretch of 1.5 than at prestretch of 1, and therefore, having no monotonic trend between Young's modulus and dielectric breakdown strength¹⁵¹.

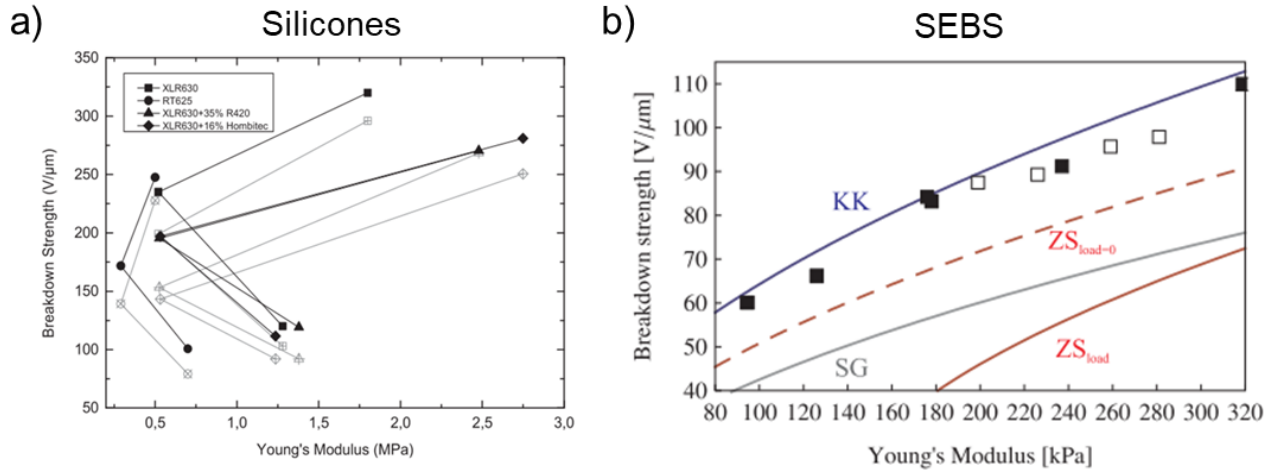


Figure 3.11: a) Dependence of breakdown strength on Young's modulus of unprestretched and equibiaxially prestretched (1.5, 2) silicone elastomers¹⁵¹. Reproduced from¹⁵¹. b) Dependence of breakdown strength on Young's modulus in unprestretched SEBS elastomer films ($70 \pm 5 \mu\text{m}$)²⁶⁵. Datapoints correspond to experimental data, and lines to models discussed in²⁶⁵. Reproduced from²⁶⁵.

3.1.3.3 Influence of fillers on the dielectric breakdown strength

Increasing filler concentration and/or selecting fillers with higher permittivity typically increases the Young's modulus of elastomer formulations and dielectric losses^{24,266,267}. Furthermore, it influences the breakdown strength^{24,111}, as adding fillers introduces impurities that may lead to lower breakdown strength²⁶⁸. The size and nature (e.g. polarity, permittivity) of fillers influences partial discharge and leakage current behaviors^{216,269}, and affects space charge accumulation (for conductive fillers)²⁷⁰.

There is general tradeoff between relative permittivity (ϵ_r) and dielectric breakdown strength for polymer and ceramic insulators, with a theoretical limit of around $\epsilon_r E_{DB}^2 = 400 \text{ V}^2/\mu\text{m}^2$ ^{271,272}. When tailoring thin elastomer membranes ($< 20 \mu\text{m}$) of varying filler concentrations, filler particle size (typically from 20 nm to 200 nm diameter^{155,156}) is a concern because the size of filler aggregates need to be significantly lower than the membrane thickness²⁶⁸.

Lotz et al. showed that adding aluminium oxide (Al_2O_3 – Evonik AEROXIDE® Alu C 805), titanium dioxide (TiO_2 – Evonik AEROXIDE® T 805) or barium titanate (BaTiO_3 – Alfa Aesar 41633) fillers decreases the breakdown strength (under 50 Hz AC at 5 V/s step-increasing ramp rate following DIN EN 60243-1 norm) of spin-coated 10-20 μm thick Wacker Elastosil P7670 films²⁶⁸. Formulations with added 3 wt% concentrations of Al_2O_3 or TiO_2 yielded a breakdown strength reduction from 30 V/μm to 15 V/μm, and from 30 V/μm to 20 V/μm with added 3 wt% concentrations of BaTiO_3 in comparison to pristine elastomer films²⁶⁸, as shown in Figure 3.12.

Vudayagari et al. showed that the addition of titanium dioxide (TiO_2) nanoparticle fillers (3 wt%) yields a slight increase in permittivity (from 2.8 to 3.4 at 1 MHz) and a breakdown strength decrease from 123 V/μm to 90 V/μm on Elastosil® LR 3043/30 (30 μm thick) and from 145 V/μm to 129 V/μm on Elastosil® LR 3043/50 (50 μm thick) silicone films (tested with 20 mm spherical electrodes at 10 V/s step-increasing ramp rate)²⁷³. They also showed that adding hydrophobic fillers consisting of fumed SiO_2 - TiO_2 core and a silica outer shell (Evonik AEROXIDE® STX 801, 9 wt%) yields a breakdown strength increase from 123 V/μm to 133 V/μm on Elastosil® LR 3043/30 and from 123 V/μm to 133 V/μm on Elastosil® LR 3043/50 films²⁷³.

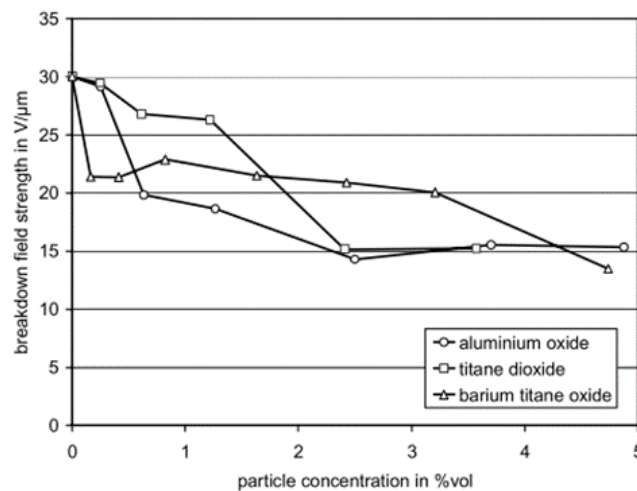


Figure 3.12: Influence of the concentration of aluminium oxide (Al_2O_3), titanium dioxide (TiO_2) and barium titanate (BaTiO_3) on the dielectric breakdown strength (at 50 Hz AC fields) of silicone (Wacker Elastosil P7670) elastomer films ²⁶⁸. Reproduced from ²⁶⁸.

Szabo et al. demonstrated that the addition of TiO_2 (50% w/w) fillers yields a decrease in breakdown strength from 40 V/μm to 25 V/μm and that the addition of BaTiO_3 (50 % w/w) fillers yields a decrease in breakdown strength from 40 V/μm to 26 V/μm for Elastosil RT601 silicone films ²⁷⁴. Huang et al. also reported significant breakdown strength decreases for BaTiO_3 filled ethylene vinyl acetate elastomers (15 V/μm for filled 50% vol BaTiO_3 elastomers vs. 43 V/μm for pristine elastomers) for a relative permittivity increase from 4 to 12 at 10^3 Hz ²⁷⁵.

Böse et al. reported 250 μm thick silicone elastomers with added undried BaTiO_3 fillers of higher permittivity (7.3 for elastomers with 20% vol in BaTiO_3 concentration vs. 3.0 for reference silicone elastomer Wacker RT 625, at 10^3 Hz), but with lower breakdown strengths under DC (18 V/μm vs. 45 V/μm for Wacker RT 625) and under 50 Hz AC (22 V/μm vs. 32 V/μm for Wacker RT 625) ²⁷⁶. By adding dried < 2 μm diameter BaTiO_3 fillers, breakdown strengths of Elastosil P 7670 elastomers are not significantly affected under DC (38 V/μm vs. 36 V/μm for elastomer without particles) and under 50 Hz AC (28 V/μm vs. 29 V/μm for elastomer without particles), and higher actuation strain at constant field (7% vs. 3.5% at 20 V/μm) could be achieved ²⁷⁶.

Hu et al. showed that the addition of (4 %vol) surface passivated aluminium nanoparticles in a 50 μm thick poly(n-butyl acrylate) elastomer increases the relative permittivity from 5 to 8.4 (at 400 Hz), but decreases breakdown strength from 179 V/μm to 140 V/μm and decreases actuation strain at 140 V/μm from 101% to 56% ²⁷⁷.

Yao et al. demonstrated that the addition of conductive carbon nanospheres (5 wt%) in polyurethane yields a significant increase in dielectric permittivity (137 vs. 7.1 for pristine polyurethane) and in strain at 6 V/μm (2.4 % vs. 0.05% for pristine polyurethane), albeit at a significantly decreased breakdown strength (6 V/μm vs. 25 V/μm) ²⁷⁸.

Molberg et al. demonstrated that the addition of conductive polyaniline particles encapsulated in poly(divinyl benzene) does not significantly decrease the breakdown strength of silicone elastomers (62 V/μm with 14% vol polyaniline particles vs. 66 V/μm for pristine silicone). By tuning the crosslink density and curing chemistry and the concentration of polyaniline fillers, breakdown strengths vary with a general trend that softer elastomer formulations exhibit lower breakdown strengths ²⁷⁹.

Tian et al. showed that adding 2 wt% graphene nanoplates on a 500 μm thick silicone (Dow Silastic™ 3481) significantly increases the dielectric permittivity to 90 vs. 3 for pristine elastomer (at 10^3 Hz), but at the detriment of higher dielectric loss (1.4 vs. < 0.2 for < 2 wt% concentrations), higher conductivity and a significant decrease in breakdown strength (15 V/μm vs. 45 V/μm for pristine Silastic™ 3481) ²⁸⁰.

Formulating a silicone elastomers with filler particles is complex, as a sufficient filler concentration is needed to ensure mechanical stability of the elastomer, yet above a certain critical filler concentration, conductive paths may also arise within the dielectric as a result of filler particle percolation (i.e. a conductive path is generated when fillers of enhanced permittivity are aligned along the electric field direction) ¹⁷¹, and phenomena such as Payne and Mullins effects as well as permanent set become important ^{24,281}.

The conclusion of this subsection is that formulating an elastomer with a tailored filler concentration is complex, with tradeoffs between permittivity, Young's modulus, breakdown strength and actuation strain at constant electric field.

3.1.3.4 Influence of chemical modifications on the dielectric breakdown strength

Several strategies can be used to tailor the relative permittivity of an elastomer or its Young's modulus, such as modifying the filler concentration^{24,268}, using polymer blends^{161,282,283}, using interpenetrating networks^{122,124,125,284}, or chemically-modified elastomer networks^{24,110,285}. The chemical grafting into silicones (PDMS) of dipolar functional groups such as aromatic groups or alkyl chloride groups in small quantities enhance the electrical breakdown strength^{111,132,171,286} without the undesired viscous loss that is typically observed when adding plasticizers or solvents²⁸⁵, and the lower breakdown strengths and higher Young's moduli typical of filler addition²⁴.

The incorporation of alkyl chloride groups in significant amounts was shown to electromechanically stabilize the dielectric membrane and enhance its electrical properties, partly because of its enhanced breakdown strength, low Young's modulus, higher electrical stability and better microscopic morphology^{111,171}.

Madsen et al. showed that alkyl-chloride (25 mol%) functionalized silicone (DMS-V31, 28000 g/mol) elastomers yield an increase of relative permittivity from 3.3 to 3.9, with a 25% increase in dielectric breakdown (from 82 V/ μ m to 101 V/ μ m)^{110,285}. Madsen et al. showed that the addition of 20 phr (parts per hundred rubber) chloropropyl-functionalized silicone oil to a Elastosil LR3043/50 silicone films increases relative permittivity from 2.7 to 3.9, and increases dielectric breakdown strength from 121 ± 4 V/ μ m to 151 ± 4 V/ μ m, but for higher oil concentrations, dielectric breakdown decreases down to 85-92 V/ μ m for 100 phr (per hundred rubber) oil concentrations, probably owing to lower Young's modulus^{110,287,288}.

The incorporation of aromatic groups within the elastomer matrix (e.g. through copolymers) is motivated by the ability of delocalized π electrons of the aromatic moieties to trap high kinetic energy electrons (i.e. hot electrons) and form trapped anion radicals¹³² which behave like negative space charges near the cathode¹³². As a result, the electric field near the cathode is reduced, which decreases electron injection from the cathode and thus "postpones" electrical breakdown of the elastomer¹³².

As shown in Figure 3.13, silicone-PPMS (polyphenylmethylsiloxane) copolymers with low concentrations of phenyl groups ($\approx 0.8 \cdot 10^{-3}$ mol/g of elastomer) show a 30% higher electrical breakdown strength (72 V/ μ m vs. 54 V/ μ m for pristine silicone) with respect to pristine silicone for a slight increase in relative permittivity (3.3 vs. 3.1 for pristine silicone), while still conserving a low conductivity, low dielectric losses and a reasonable mechanical stability, albeit at the cost of a higher Young's modulus^{132,286}. The molecular design of the elastomer is important since high concentrations of phenyl groups can lead to micro-scale phase separation between aromatic domains and silicone domains and thereby yield undesired defects within the polymer matrix^{132,286}. The addition of non-covalently grafted low molecular-weight aromatic compounds into pure silicone elastomers is difficult since phase separation occurs over time, thereby leading to conductive regions which can gather space charges and enhance electrical conduction instead of electrically stabilize the elastomer¹⁷¹.

PDMS-PPMS copolymer elastomers

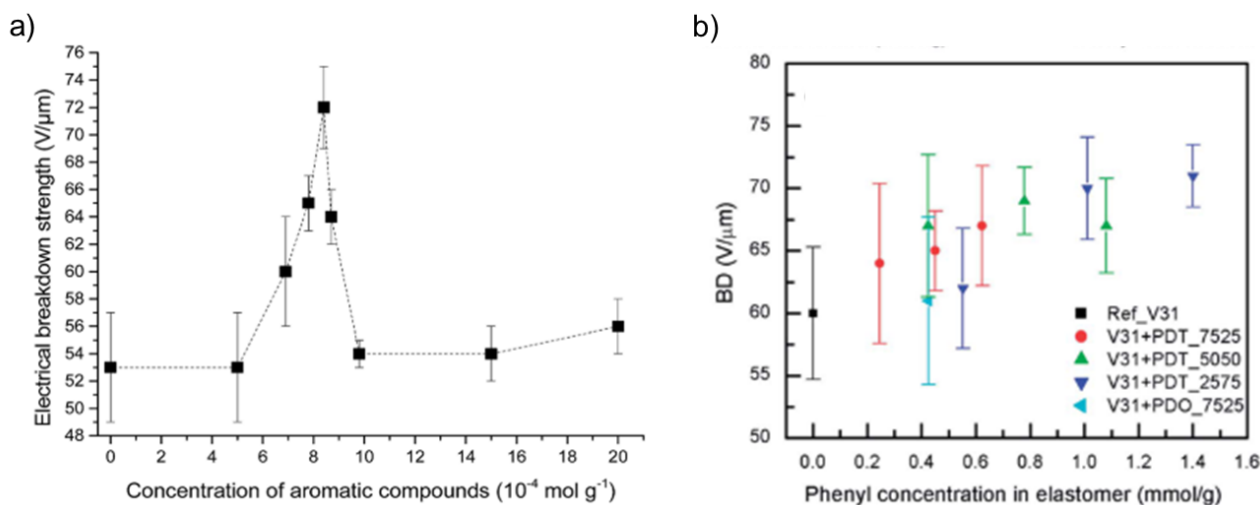


Figure 3.13: Influence of the concentration of aromatic (phenyl) groups in breakdown strength of PDMS-co-PPMS elastomers^{132,286}. Reproduced from¹³² and²⁸⁶.

Most of chemical modifications on elastomers involve grafting of polar groups to enhance dielectric permittivity in order to decrease the operation voltage required to reach a given strain ²⁴, albeit affecting the dielectric breakdown strength of the elastomer formulation.

Stoyanov et al. demonstrated a SEBS-*g*-MA (polystyrene-*co*-ethylene-*co*-butadiene-*co*-styrene-*g*-maleic anhydride) elastomer with chemically-grafted conductive polyaniline groups that exhibit a breakdown strength decrease (120 V/ μ m vs. 140 V/ μ m for SEBS-*g*-MA) for polyaniline volume concentrations of 2% (but yielding a dielectric permittivity of 9 vs. 2 for SEBS-*g*-MA, at 1 Hz), whereas above that threshold, breakdown strength drops significantly to 30 V/ μ m at 2.2 % polyaniline volume concentration ²⁸⁹.

Kussmaul et al. showed that the addition of grafted para-nitroaniline-based dipolar groups to silicone elastomers (11 wt%) yields a breakdown strength decrease from 130 V/ μ m to 50 V/ μ m (for a permittivity increase from 3.0 to 5.9), which they attribute to Young's modulus decrease ²⁹⁰. Perju et al. showed that the grafting of nitroaniline groups to silicone elastomers (62-93 μ m thick) yielded DEAs of high relative permittivity (10.6 – 18.8) capable of reaching up to 8% strain at 900 V (7.5 V/ μ m) ¹³⁰, but exhibiting low breakdown strength (9-29 V/ μ m) ^{130,291}.

Madsen et al. reported a tailored silicone elastomer with nitrobenzene side chains groups with higher relative permittivity (3.6-59.3 vs. 3.0 for pristine silicone at 1 Hz) and higher breakdown strength (61-81 V/ μ m vs. 55 V/ μ m for pristine silicone) ²⁶⁶.

Böse et al. reported a silicone elastomer with grafted trifluoropropyl groups and added fluorinated silicone oil (as plasticizer) of higher permittivity (5.4 for actuators with 40% w/w fluorinated silicone oil concentration vs. 2.9 for reference silicone elastomer Wacker RT 625, at 10³ Hz), but with lower breakdown strengths under DC (24 V/ μ m vs. 35 V/ μ m for Wacker RT 625) and under 50 Hz AC (23 V/ μ m vs. 29 V/ μ m for Wacker RT 625) ²⁹².

Zhang et al. showed that grafting a silicone elastomer with 4 wt% azobenzene groups yields an increase in breakdown strength from 66 V/ μ m to 89 V/ μ m along with an increase in permittivity from 2.7 to 3.95 at 10³ Hz (and 17% actuation strain at 65 V/ μ m), albeit lower breakdown strengths are achieved below and above 4 wt% concentrations ¹²⁸. Increasing the fraction of azobenzene groups up to 4 wt% increases the cohesive Van der Waals interactions (i.e. increases activation energy of free volume formation), but further increasing the fraction of azobenzene groups above 4 wt% increases the polarity of the elastomer (yielding a decrease its breakdown strength) ¹²⁸.

Racles et al. demonstrated that silicone copolymers with grafted polar cyanopropyl groups (10 mol%) exhibit higher breakdown strength (59 V/ μ m vs. 49 V/ μ m for pristine silicone) and higher maximal actuation strain (5.6% vs. 0.6%), albeit at a limited relative permittivity increase (3 vs. 2.6). Increasing the concentration of polar cyanopropyl groups beyond 10 mol% yields higher relative permittivity (4-4.9), but decrease dielectric breakdown strength (down to 19 V/ μ m) and maximal actuation strain (down to 1.7%) ²⁹³.

Sun et al. reported a tailored network made of carboxylated polymethylvinylsiloxane and a hydroxyl-terminated linear silicone chain precursors, where increasing the concentration of carboxylated precursor yields a significant increase of relative permittivity (23 for a 2:1 carboxyl precursor to linear chain precursor ratio vs. 3.2 for silicone reference without any carboxylated compounds at 100 Hz), and a significant increase of actuation strain from 1.4% to 11.2% (at 15 V/ μ m), albeit at a decreased Young's modulus (0.2 MPa vs. 0.4 MPa), and a decrease in breakdown strength from 23.5 V/ μ m to 15.7 V/ μ m ²⁹⁴.

Caspari et al. ¹²⁹ showed that silicone formulations grafted with alkyl thiols yielded elastomers with enhanced dielectric permittivity (3.4–7 vs. 2.9 at 10⁶ Hz) and actuation strain at constant field (of 0.2-3% vs. 0%) in comparison to Elastosil film as a reference, while maintaining low dielectric losses (< 0.05) and displaying low leakage current density (0.5 μ A/cm² at 27 V/ μ m and at 10% lateral actuation strain), albeit at reduced Young's moduli (0.2-0.7 MPa vs. 1.2 MPa for Elastosil) ¹²⁹. The elastomers have also shown a strain-stiffening behavior and it was claimed that electromechanical instability could be suppressed even in the absence of prestretch ¹²⁹.

Yu et al. showed that interpenetrating silicone (Gelest DMS-V35) networks with grafted ionic moieties (positively charged amine groups and negatively charged acid groups) exhibit higher breakdown strengths (45-98 V/ μ m vs. 40 V/ μ m) and significantly higher relative permittivity (6.7-2100 vs. 2.5 at 0.1 Hz) than pristine DMS-V35 elastomers, but with 1000x higher dielectric loss (tan δ of 2.3-11.6 vs. 0.13 at 0.1 Hz) ²⁹⁵. Some interpenetrating ionic silicone formulations are capable of self-healing (after heating at 120°C for 6h) after dielectric breakdown, albeit at altered mechanical properties and reduced achievable strains ²⁹⁶.

Dünki et al. reported a tailored self-healing polymethylvinylsiloxane elastomer with grafted nitrile (-CN) end groups and 5 wt% of hexamethyldisilazane-treated silica particles (to keep low viscoelastic losses) that exhibits high relative permittivity (10.1 vs. 3 for Elastosil RT 745, at 10⁴ Hz) and reaching actuation strains of 18% at 10 V/ μ m, but showing a low breakdown strength of 10.8 V/ μ m

vs. 25 V/ μm for Elastosil RT 745 (tested at a voltage step rate of 25 V/s), higher conductivity ($\approx 10^{-11}$ vs. $\approx 10^{-15}$ for Elastosil RT 745) ²⁹⁷.

Many tailored elastomers with different self-healing strategies have been developed, with different relative permittivity, breakdown strength, Young's moduli and dielectric loss ranges, which are summarized in Tables 1 from references ^{298,299}.

Other recent chemically tailored elastomers include a polyurethane acrylate elastomer copolymerized with polyethylene glycol diacrylate (PUA-PEGDA) which reach breakdown strengths of 15-25 V/ μm increasing with an increase in the wt% of PEGDA ³⁰⁰, and a poly(*n*-butyl acrylate) whose breakdown strength is above 70 V/ μm (120% area strain) for 400% equibiaxially-prestretched DEAs ¹³³.

The conclusion for this subsection is that tailoring a chemically grafted silicone elastomer is complex, because of trade-offs between mechanical properties, breakdown strength, dielectric loss, and DEA performance.

3.1.3.5 Influence of temperature on the dielectric breakdown strength

Increasing the temperature accelerates ageing processes, and phenomena such as diffusion processes and electrical conductivity are enhanced ¹¹⁸. Increasing the temperature generally decreases the dielectric breakdown strength of thick ²²⁶ elastomer films, as presented in Figure 4.11b.

However, as shown in Figure 3.14a, Fasolt et al. demonstrated that increasing the temperature from 10°C to 50°C under humid conditions (85% RH) for unprestretched thin (50 μm) silicone (Elastosil 2030/50) elastomer films with rigid electrodes yields a slight increase in breakdown voltage, potentially owing to an increased elastomer chain mobility leading to dipole rearrangement under higher temperatures ¹⁴⁷.

Increasing the temperature increases the probability of thermal breakdown (i.e. thermal runaway). Thermal stresses depend on material properties and on the frequency of AC voltage, since they originate from Ohmic losses in the electrodes, and dielectric losses in the dielectric elastomer ²⁴⁰, which lead to local temperatures which can be significantly higher than the operation temperature ³⁰¹.

Zakaria et al. have demonstrated using a model for electrothermal breakdown that single layer silicone (e.g. Elastosil® LR 3043/30, POWERSIL® XLR® 630, POWERSIL® RT® 625) films (of thickness between 20 μm and 150 μm) typically undergo dielectric breakdown (e.g. dielectric breakdown strength < 200 V/ μm) before electrothermal breakdown by thermal runaway (which required electric fields between 300 V/ μm to over 1000 V/ μm , in an increasing trend with lower thickness) ²⁰⁵.

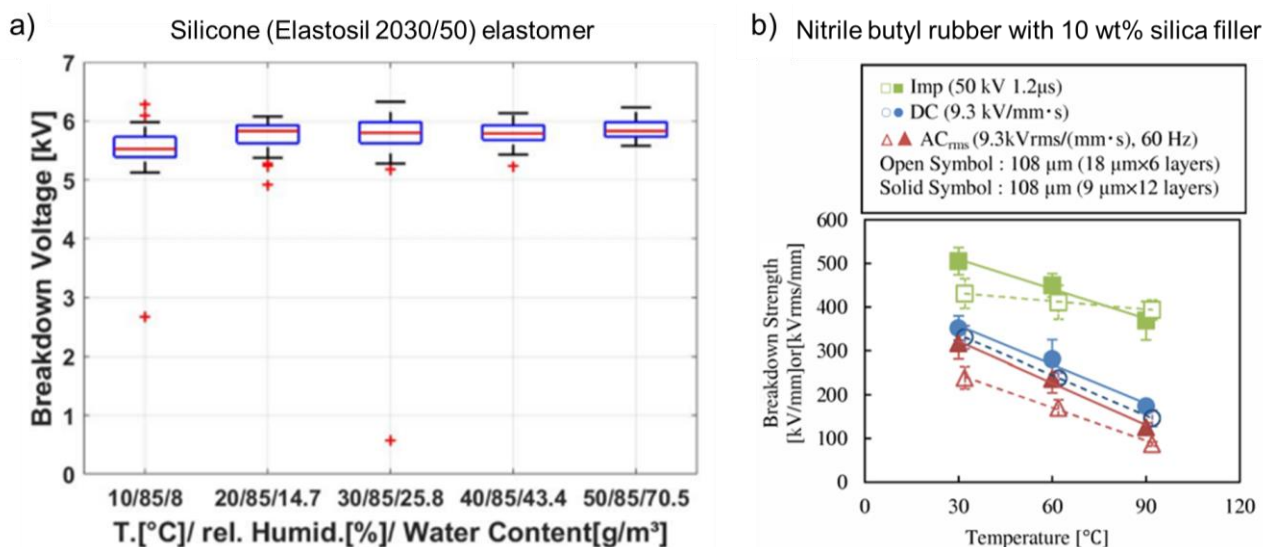


Figure 3.14: a) Effect of temperature on the dielectric breakdown strength of unprestretched Elastosil 2030/50 (50 μm thick) elastomers under humid conditions (85% RH) ¹⁴⁷. Reproduced from ¹⁴⁷. b) Influence of temperature on the breakdown strength of 10 mm thick nitrile butyl rubber (NBR) with 10 wt% silica fillers ²²⁶. Reproduced from ²²⁶.

However, thermal runaway can become significant for stacked multilayer DEAs operated under high AC fields and frequencies. Christensen et al. have showed using a theoretical model on a silicone elastomer (Elastosil® RT® 625) that the maximal number of layers to reliably operate a DEA stack before thermal breakdown is dependent on the operation temperature and the electric field ³⁰². Higher temperature and higher electric field during operation require the use of DEA stacks with lower number of layers to avoid thermal runaway, but the number of stacks is still significant (>1000 layers at 150 V/ μ m and 320 K) before thermal breakdown ³⁰².

Using a 49-layer silicone (Elastosil® P7670) DEA stack, and a thermo-electro-mechanical model, Kleo et al. demonstrated that silicone DEA stacks submitted to 1000 V AC fields of frequencies between 10 Hz and 1000 Hz lead to significant temperature increases in the DEA between +20°C and +50°C amplitude in the bulk elastomer, and up to +80°C amplitude near the electrical contacts (connected with wires) after 30 minutes ³⁰¹. The amplitude of temperature increase significantly increases from 100 Hz to 1000 Hz AC operation ³⁰¹.

3.1.3.6 Influence of humidity on the dielectric breakdown strength

Fasolt et al. showed that the breakdown voltage in 50 μ m thick unprestretched silicone (Elastosil 2030/50) films is not significantly affected by water vapor content (i.e. absolute humidity) from the environment surrounding the DEA ⁵².

Chen et al. showed that the dielectric breakdown strength of equibiaxially prestretched (300% x 300%) VHB 4905 films under an external load of 0.5 N is affected by relative humidity, decreasing from 200 ± 15 V/ μ m at 0% RH down to 167 ± 15 V/ μ m at 80% RH ³⁰³, as shown in Figure 4.12b. This is further supported by Liu et al. that reported that the dielectric breakdown strength decreases from 160 V/ μ m to 140 V/ μ m by changing the humidity from 20% RH to 80% RH in equibiaxially prestretched (300% x 300%) VHB 4910 films ³⁰⁴. The higher the prestretch, and the higher the relative dielectric breakdown decrease with increasing humidity, as shown in Figure 3.15a ³⁰⁴.

Chen et al. reported that the dielectric breakdown strength in 293 ± 5 μ m thick natural rubber (Oppo Band Green 8003), and in 224 ± 4 μ m thick styrenic rubber (Theraband Yellow 11726) with rigid cylinder brass electrodes (25 mm diameter for HV electrode, and in 150 mm diameter for ground electrode ²⁶³) decreases after being immersed in water, with a more enhanced reduction observed on natural rubber (from 97 V/ μ m to 50-90 V/ μ m range) than on styrenic rubber (from 97 V/ μ m to 75-90 V/ μ m range) owing to its higher water permeability ^{141,263}. They observed that drying the elastomer films for 2 hours at 40°C increases the dielectric breakdown strength almost to values obtained for dry samples which have not been immersed in water ¹⁴¹.

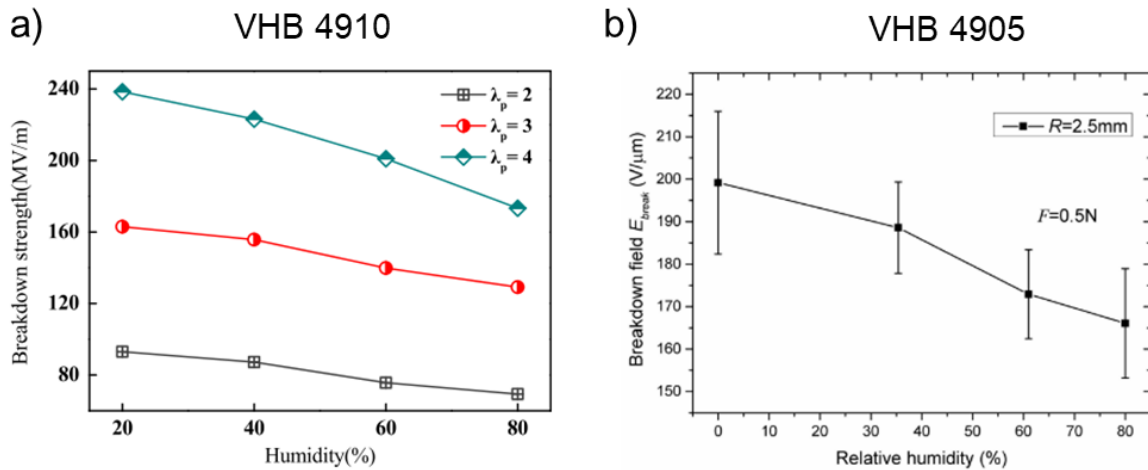


Figure 3.15: Effect of relative humidity on the breakdown strength of a) equibiaxially prestretched VHB 4910 membranes coated with circular (12 mm diameter) gold electrodes at room temperature ³⁰⁴ (reproduced from ³⁰⁴) and of b) equibiaxially prestretched (300% x 300%) VHB 4905 membranes with a hemispherical electrode of 2.5 mm radius of curvature and 0.5 N compressive force at 24°C ³⁰³ (reproduced from ³⁰³).

3.1.3.7 Other factors influencing dielectric breakdown strength

Other factors such as the curvature of the external electrode (used for breakdown strength characterization) and its applied compressive force onto the dielectric membrane can influence the dielectric breakdown strength^{151,303,305}.

Chen et al. showed that a lower radius of curvature of a hemispherical aluminium electrode pin yields higher dielectric breakdown strengths for prestretched (300% x 300%) VHB 4905 films, and that higher compressive forces up to 0.5 N generally increase breakdown strength^{303,305}. According to Chen et al., the reduction of electrode size and the increase in applied compressive force lead to higher local compression stresses which stiffen the elastomer (i.e. increase Young's modulus) and hence increase dielectric breakdown strength^{303,305}. Zakaria et al. did not find a clear trend between electrode radius and dielectric breakdown strength for unprestretched and equibiaxially prestretched (1.5) POWERSIL XLR630 silicone elastomers with 50-60 nm thick silver deposited electrodes¹⁵¹.

Kochetov et al. showed that the type of electrode material and its effective surface area also influences the dielectric breakdown strength of polyurethane elastomers³⁰⁶, as presented in Figure 3.16. The highest dielectric breakdown strength is observed for films (A) without any coated electrodes (a 4 mm diameter rigid semi-spherical shaped electrode is used for the tests at a ramp voltage of 33 V/s) with a characteristic breakdown strength of 97 V/ μ m, which decreases to 89 V/ μ m for films (B) with gold electrodes, and decreases further to 79 V/ μ m for films (C) with gold electrodes coated with a semiconductor layer (for the gold electrode to remain conductive even after cracking), and finally decreases to 71 V/ μ m for films (D) with compliant electrodes (with low adhesion forces)³⁰⁶.

The high breakdown strength values obtained for polyurethane films without any electrodes was attributed to the electrode size and contact surface of the semi-spherical electrode used vs. the electrode surface of the gold and compliant electrodes³⁰⁶. The reduction of breakdown strength with the addition of a semiconductor layer above the gold electrodes is attributed to a volume effect and potentially to the increased active surface area vs. gold electrodes which suffered from local cracking, whereas the reduction of breakdown strength for the compliant electrode could originate from the manufacturing method of the compliant electrodes and the migration of conductive particles toward the polyurethane film which would generate local electric field enhancement regions that accelerate degradation processes³⁰⁶.

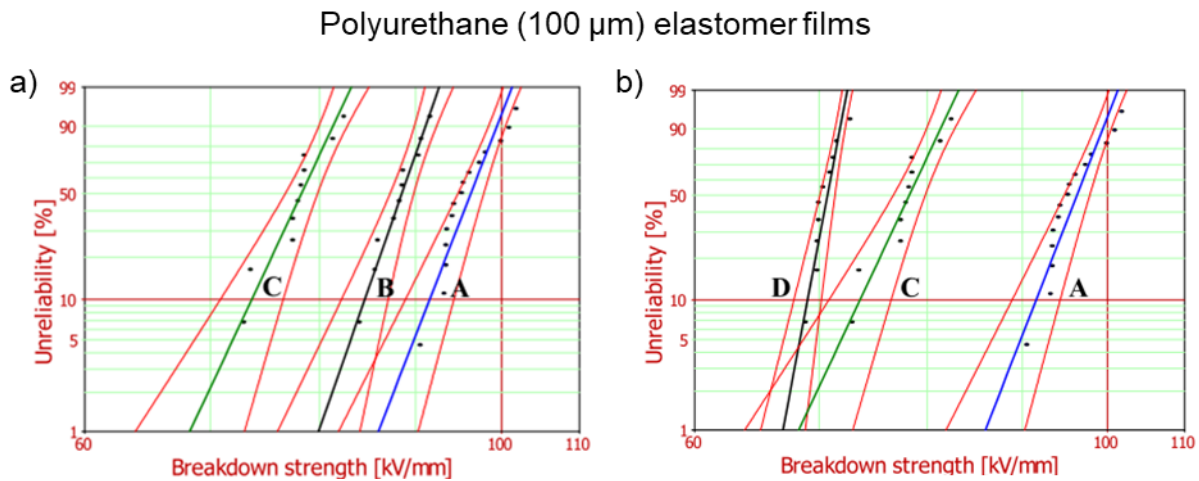


Figure 3.16: Influence of electrode material on the breakdown strength of 100 μ m thick polyurethane elastomer films³⁰⁶. Dataset A corresponds to films without electrodes, dataset B to films coated with rigid gold electrodes (by sputtering), dataset C to films coated with rigid gold electrodes covered with a semiconductor layer, and dataset D to films coated with compliant electrodes (conductive particles in a conductive paste, composition not reported)³⁰⁶. Reproduced from³⁰⁶.

Förster-Zügel et al. reported that the type of electric field and the addition of a protective encapsulating layer also influences the dielectric breakdown strength (defined in their work as the scale parameter of the Weibull fit, i.e. at the breakdown probability of 63.2%) of unprestretched Elastosil 2030 (30 μ m thick) DEAs with expanding circle graphite powder electrodes (of 6 mm diameter), as presented in Figure 3.17¹⁴⁹.

The characteristic breakdown strength does not increase between unprestretched DEAs under DC fields (98 V/ μ m) and under AC fields at 125 Hz (98 V/ μ m), but however increases significantly under AC fields at 500 Hz (125 V/ μ m) because of time-dependent

material properties (e.g. RC time constant) as lower deformations are reached at higher frequency ¹⁴⁹. Under DC fields, the characteristic breakdown strength of unprestretched DEAs is not influenced by the addition of a protective silicone layer (97 V/ μ m vs. 98 V/ μ m), but under AC fields at 500 Hz, the addition of a protective silicone layer is detrimental to its breakdown strength as it decreases by 22% (from 125 V/ μ m to 98 V/ μ m) possibly owing to thermal effects, as the addition of encapsulation layers reduce heat conduction from the DEA to the external environment which leads to local temperatures and thermal runaway ¹⁴⁹.

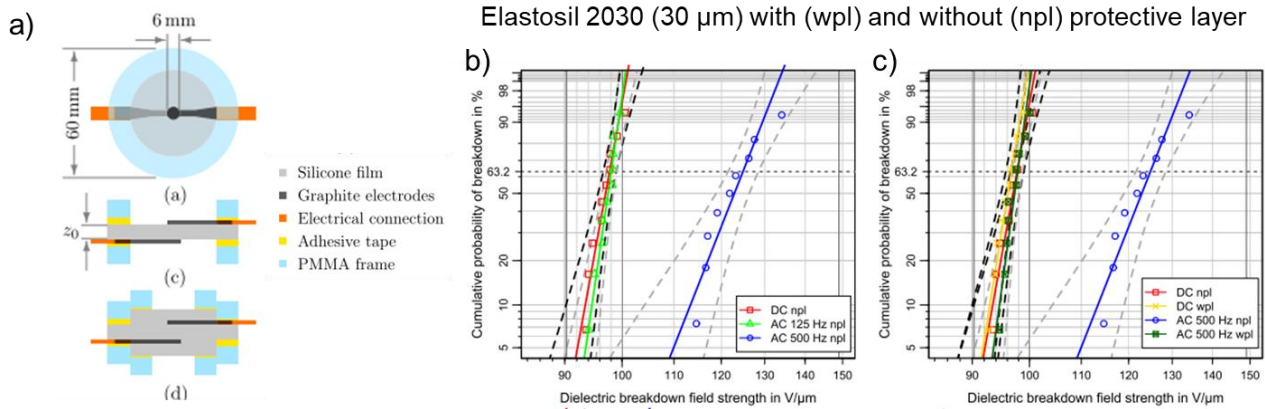


Figure 3.17: a) DEA specimen used to evaluate the effect of b) type of applied electric field (DC vs. AC) and of c) the addition of a protective layer (wpl) on unprestretched Elastosil 2030 DEAs with expanding circle 6 mm diameter graphite powder electrodes (applied by shadow masking) ¹⁴⁹. Reproduced from ¹⁴⁹.

Förster-Zügel et al. showed that the substitution of air as ambient media by silicone oil (Wacker® AP 1000) or a solid silicone influences the dielectric breakdown strength of 50 μ m thick Elastosil 2030/50 silicone films with rigid brass electrodes (8 mm diameter for top electrode and 100 mm x 100 mm ground electrode), as shown in Figure 3.18 ²²⁷. Both the addition of silicone oil and of solid silicone increase the dielectric breakdown strength. Adding silicone oil increases the dielectric breakdown strength (defined in their work as the scale parameter of the Weibull fit, i.e. at the characteristic breakdown probability of 63.2% ²⁰⁴) from 128 V/ μ m to 139 V/ μ m, while adding silicone solid increases the dielectric breakdown strength from 128 V/ μ m to 141 V/ μ m ²²⁷.

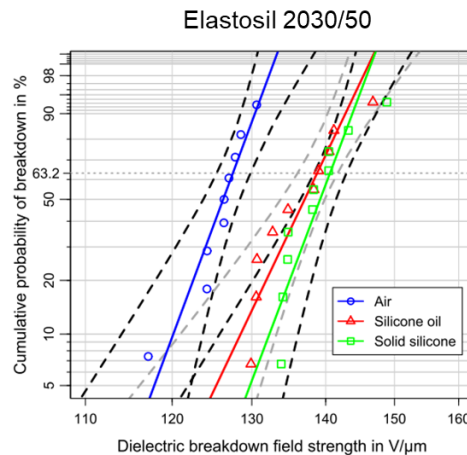


Figure 3.18: Effect of substitution of air (in blue) by silicone oil (in red) or solid silicone (in green) environments ²²⁷. Reproduced from ²²⁷.

An interpretation for their observations could be the significantly higher dielectric permittivity of silicone (2.8) vs. air (1) that yields no electric field enhancement in the edges of the brass electrodes between the electrodes and the silicone elastomer, and therefore a lower partial discharge activity at constant electric field, but partial discharge and leakage current have not been monitored ²²⁷.

Yu and Skov demonstrated that adding silicone oil (TR 50) or chloropropyl oil (LMS 152) to a silicone (Elastosil LR 3043/30) elastomer yields 10% to 40% decrease of dielectric breakdown strength ²⁰³, therefore contrasting from the findings of Förster-Zügel et al. They also highlight that bimodal elastomers typically possess lower dielectric breakdown strength than filled elastomers, yet higher breakdown strengths than unfilled bottlebrush elastomers ²⁰³.

3.1.3.8 Monitoring of leakage current and partial discharges

A focus on detecting electrical breakdown events within silicone dielectric elastomers through the monitoring of partial discharges^{200,201,307,308} or through voltage drop measurement¹¹² has been carried out on DEAs using custom detection methods^{112,200,201,307}.

Leakage current and partial discharges could be predictors for DEA failure since the breakdown of a DEA stems from thermal runaway or the damage related to the accumulation of partial discharges over time²⁰⁰.

Gisby et al.²⁰⁰ observed that VHB based DEAs which display higher leakage currents at a constant electric field and higher frequency of partial discharges failed at electric fields lower than $200 \text{ V}/\mu\text{m}$ ²⁰⁰. However, the exact mechanism of failure was not determined, a limited set of DEAs was used²⁰⁰. However, this observation made for VHB-based DEAs could also be interesting for silicone-based DEAs as partial discharges are observed for both materials^{112,200,201,307}. No correlations between the DEA lifetime and the leakage current or the frequency of partial discharges was carried out and the impact of the leakage current and the frequency of partial discharges on long-term reliability and performance of the DEAs has not been studied²⁰⁰.

Iannarelli et al.³⁰⁷ demonstrated that mechanically aged (by cyclic stretching) silicone elastomers show higher partial discharge magnitudes in comparison to unaged samples, although neither electrical ageing nor DEA operating conditions were considered³⁰⁷.

3.1.3.9 Influence of space charge accumulation

Under DC actuation at high electric fields, space charge accumulation occurs within the dielectric membrane and negatively affects the reliability and the performance of the DEA over time²⁴.

In silicone elastomers, space charge accumulation can arise from several phenomena²⁴, such as:

- a) Charge injection from electrodes and from conductive defects which locally enhance the electric field.
- b) Combination of current density and spatial resistance inhomogeneity.
- c) Ionization-induced hetero-charge formation within the dielectric.
- d) Localized polarization due to presence of water or to water trees structures.

Space charges at the vicinity of air gaps and nano/microcavities can be detrapped in high electric fields and induce significant electron injection and acceleration within free volumes or air gaps (i.e. voids) to trigger partial discharges (due to their ability to store electro-mechanical energy, exert local compressive mechanical stresses and enhance electric fields locally)^{309,208,210}. Furthermore, space charges can promote ageing mechanisms by lowering the activation energy of a particular ageing process or by forming cavities and free volumes through mechanical deformations, physicochemical degradation, chemical reactions and morphological modifications within the dielectric as a result of the electromechanical energy stored within space charge clusters^{118,208,309}. Such ageing mechanisms are known to enhance charge injection and conduction mechanisms over time^{118,208,210,310}.

According to Francis et al.³¹¹, the accumulation of space charges on the electrode-dielectric interface under high DC voltages contributes to the partial discharge activity of dielectric elastomers, based on modelling and experiments on a VHB elastomer sandwiched by two round steel electrodes and submitted to a constant (1 min) DC voltage followed by a voltage increase which led to sudden bursts of partial discharge activity³¹¹. However, no measurement of space charges (e.g. by pulsed electroacoustic methods³¹²) was carried out to validate their theory and thereby correlate the space charge accumulation with the partial discharge activity³¹¹.

Charge injection, charge mobility and space charge accumulation within an insulator are highly dependent on the electric field^{118,309}. Space charge accumulation occurs typically above a given electric field threshold in polymer dielectric insulators^{118,212,220,247,313,314,315} and in silicone elastomers³¹³. A concise description of conduction mechanisms and space charge accumulation is given in^{206,220,316}.

As seen in Figure 3.19, Kochetov et al. demonstrated that space charge accumulation in TiO_2 -filled silicone elastomers becomes significant above a given electric field threshold around $20 \text{ V}/\mu\text{m}$ ³¹³. Above this threshold, degradation and ageing processes are triggered^{309,313} resulting from enhanced electric fields induced by the build-up of space charges over time³⁰⁹. Measurements on $125 \mu\text{m}$ thick films from Danfoss Polypower with and without additional titania (TiO_2) fillers revealed that space charges accumulated at poling magnitudes up to $43 \text{ V}/\mu\text{m}$ for 2 hours showed that the space charge accumulation depletion time after poling is of 10 minutes, indicating that the detrapping is rapid owing to shallow traps (i.e. indicating no deep traps with high energy barrier^{118,206})³¹³. They have not observed an increase in detrapping time with higher titania filler concentrations, implying that titania fillers do not form deep traps of high energy barrier³¹³.

In the literature, traps (e.g. defects, degraded polymer chains by oxidation or chain scission, free volumes) hinder the mobility of electrons and ions (free charges) because of their energy levels which are found in between conduction band and valence band energy levels of the insulating membrane^{206,317,318}. The higher the depth of the energy level (difference between band energy and trap energy), the higher the residence time of an electron/ion in a trap^{206,314}. Over time, shallow (i.e. low depth) traps are formed within the insulator, and older traps deepen, which implies that increased charge concentrations can be accumulated within the traps²⁰⁶. Traps are partly responsible for the initiation of electrical and thermal degradation of polymer insulators³¹⁴ because of their ability to “catch” charge carriers which leads to space charge accumulation^{208,210,239,241,309,319}.

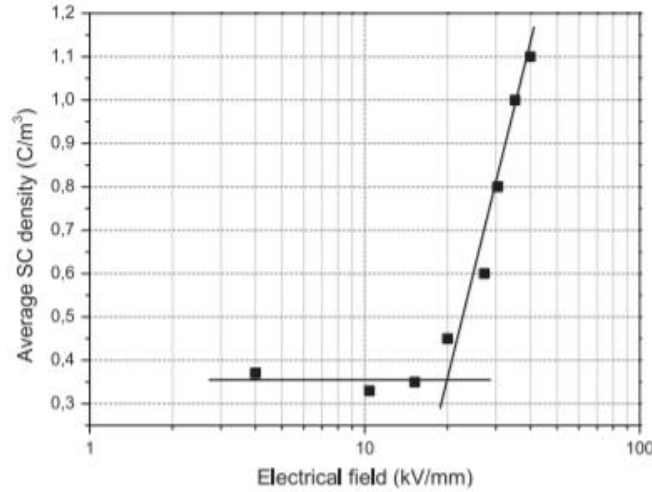


Figure 3.19: Average space charge density vs. electric field for a TiO_2 -filled silicone elastomer³¹³. Space charge accumulation occurs above 20 V/ μm . DEA actuation usually occurs at electric fields around 70-100 V/ μm , which is 4-5x higher than the onset of space charge accumulation. Reproduced from³¹³.

3.2 Electromechanical instability (pull-in instability)

As discussed in Section 2.3, electromechanical instability is a common phenomenon in elastomers (which exhibit relatively low Young's moduli) where, above a given actuation strain threshold, a spontaneous membrane thinning occurs, which induces a higher electric field through the membrane which in turn further supports thinning and electric field enhancement until a catastrophic electrical breakdown is reached because of locally excessive electrical fields^{31,32,199}. The actuation strain threshold above which electromechanical instability occurs depends on the shape of its stress-strain curve ($\sigma(\lambda)$), which is typically non-linear (i.e. Young's modulus is stiff at initial stretch, then softens, and finally increases near the limiting stretch of the elastomer) and which directly impacts the voltage – stretch curve's local maximum value (c.f. equation 7 in Section 2.3). The electromechanical instability typically occurs in VHB-based DEAs^{32,142}, and originates from excessive field-induced pressures that the dielectric membrane cannot compensate with its own elasticity along the out-of-plane direction⁷, thereby driving membrane thickness to thin progressively as long as the electric-field induced pressure exceeds the restoring elastic force of the elastomer.

An extensive and detailed overview of the theory and the mathematical analysis of electromechanical instability and of large actuation of elastomers is provided in^{31,32,142,199}.

The Suo model assumes a thermodynamic system composed of an elastic dielectric with a free energy function submitted to two dead loads (i.e. mechanical stresses) and coated with two compliant electrodes with a given accumulated charge and no stiffness¹⁹⁹. The electromechanical instability is defined by Suo et al. as when the determinant of the Hessian matrix (of the system's free energy function) reaches a positive value, thereby allowing the derivation of the voltage magnitude above which electromechanical instability occurs^{32,142,199}. The Suo model can therefore give the voltage-stretch curves for a given prestretch value and estimate which maximal strain value can be achieved (which in absence of prestretch assuming an elastomer with a monotonically-increasing stress-stretch curve $\sigma(\lambda)$ was found to be 26% (for a $\sigma(\lambda)$ curve following a neo-Hooke's model)^{31,199}) without the membrane undergoing electromechanical instability^{32,142,199}, as presented in Figure 2.10 in Section 2.3. However, the model does not consider the stiffening effect and the shear stress of the electrodes and it uses dead loads and not rigid frames which are often used to maintain a given prestretch.

For VHB-based DEAs which are prone to electromechanical instability, a high prestretch ($> 100\%$ biaxial, typically $300\% \times 300\%$) is applied to eliminate this instability phenomenon to reach actuation strains above 100% ^{28,142,196}, as shown in Figure 3.20a.

According to Zurlo et al., it is an incorrect interpretation of Suo's theory to consider that high prestretch values can fully eliminate electromechanical instability, since the catastrophic thinning of the dielectric elastomers cannot be suppressed ³²⁰.

Silicone elastomers have significantly smaller limiting stretches than VHB elastomers ³², which influences the shape of the voltage – stretch ($V(\lambda) - \lambda$) curve, as discussed in Section 2.3 in and as experimentally shown in Figure 3.20b ¹⁹⁶. This implies that silicone elastomers display a strain-stiffening behavior which makes them less prone to reach electromechanical instability before electrical breakdown ¹⁹⁶, but also unable to reach very high actuation strains.

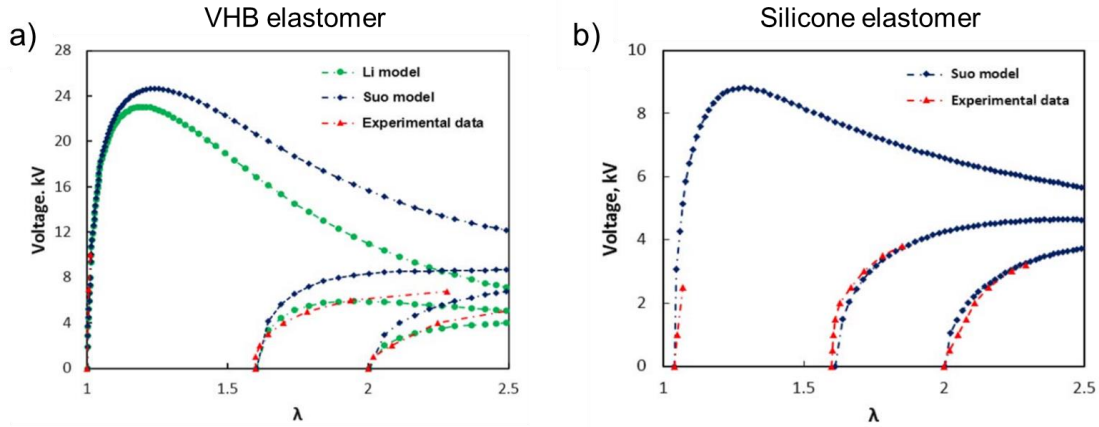


Figure 3.20: a) Theoretical and experimental voltage-stretch curves for VHB 4910 ¹⁹⁶. b) Theoretical and experimental voltage-stretch curves for $300\mu\text{m}$ thick LSR 4305 DEV silicone rubber ¹⁹⁶. Reproduced from ¹⁹⁶.

Silicone membranes require lower magnitudes (vs. VHB elastomers) of equibiaxial prestretch to reduce (or eliminate) electromechanical instability, typically equibiaxial prestretch of >1.5 for e.g. Sylgard 186 of $30\mu\text{m}$ after prestretch ^{144,196}. As discussed in Section 2.2.2, because an equibiaxial prestretch of 1.5 is generally sufficient for silicone DEAs to overcome electromechanical instability and loss of tension, higher prestretch values are not necessary, as it would significantly enhance Young's modulus ¹⁴⁴, and thus decrease the actuation performance of DEAs (i.e. increase voltage needed for a given actuation strain) ^{144,196}.

The ratio between the active region (i.e. the DEA electrode surface area) and the passive region (i.e. the entire DEA surface except the electrode area) is also determinant since it can impact whether the dielectric membrane would undergo electrical breakdown, electromechanical instability or loss of tension first ³². It has been found that small ratios between the active and the passive regions ($<1:5$) are more prone to undergo loss of tension before electrical breakdown or electromechanical breakdown, whereas electrical breakdown and electromechanical breakdown dominate over loss of tension at higher ratios between the active and passive regions ($>1:5$) ³², given that the applied prestretch is moderate ($\lambda_{\text{pre}} < 4$). The results, although not specific for silicone elastomer membranes since they depend on the strain behavior and the dielectric strength of the elastomer, constitute nonetheless an interesting insight for a suitable electrode design of expanding circle silicone-based DEAs.

Given the focus of this thesis on understanding failure of silicone dielectric elastomers operating under low strains ($<20\%$), the electromechanical instability is not relevant since silicone elastomers under this condition undergo direct electrical breakdown before electromechanical instability ¹⁹⁶, as discussed in Section 2.3.

Dielectric elastomers can tear (tensile rupture) as a result of excessive straightening of polymer chains beyond their maximal unfolded chain length ^{143,321}. For silicone elastomers, mechanical breakdown is not a major breakdown pathway for mildly prestretched (1.3 equibiaxial) silicone-based DEAs actuated at low ($<20\%$) actuation strains ²⁴. However, upon electrical breakdown, tearing of the membrane may occur due to inhomogeneous stress concentrations in areas at the vicinity of pinholes ²⁴.

3.3 Lifetime studies on DEAs

The lifetime of DEAs has not been thoroughly studied in the literature. This section presents the few reported lifetime investigations and summarizes their findings.

Kornbluh et al.¹¹⁷ reported lifetimes of prestretched (3x3) VHB4910 DEAs over 1 million AC (5 Hz) cycles for 40% surface strains and 20x lifetime enhancement from wet (100% RH) to dry (50% RH) conditions. Biggs et al.¹²⁰ have also highlighted the effect of humidity at 25°C on the AC lifetime of acrylic-based DEAs, with 25000 cycles lifetime at 20%RH and only 100 cycles at 90% RH. Chen et al.⁵⁷ have shown that silicone (Elastosil 2030 250/150) DEAs possesses AC (1 Hz) lifetimes above 1 million cycles for electric fields between 65 and 80 V/ μm .

Lotz, Matysek and Schlaak^{42,322} investigated the lifetime of unprestretched stacked silicone-based DEAs under AC actuation with multiple electrode materials (as shown in Figure 3.21), finding that stacked DEAs probably degraded due to the interconnections between the electrode layers, as they observed significantly lower lifetimes with higher AC frequencies¹¹⁵, suggesting that stacking of DEAs is detrimental to its lifetime. In their work, failure is defined as when the DEA charging current drops below 75% of its original value at constant voltage, i.e. when the impedance of the DEA has increased such that the current falls below 75% of its original value¹¹⁵. They have also identified that stacked DEAs could also possibly fail by a localized thermal degradation occurring at the vicinity of the highly resistive electrode-electrical connection transition where large currents (>mA) are dissipated (thereby leading to thermal runaway)¹¹⁴. The separation of graphite particles in graphite electrodes during the stretching process could also damage the electrode over time and hinder the actuation¹¹⁴. Electrodes composed of a combination of graphite and silver grease has shown higher lifetimes (lasting 10^9 cycles) than electrodes composed of the individual materials (lasting $\approx 10^8$ cycles – 1270 hours)¹¹⁵.

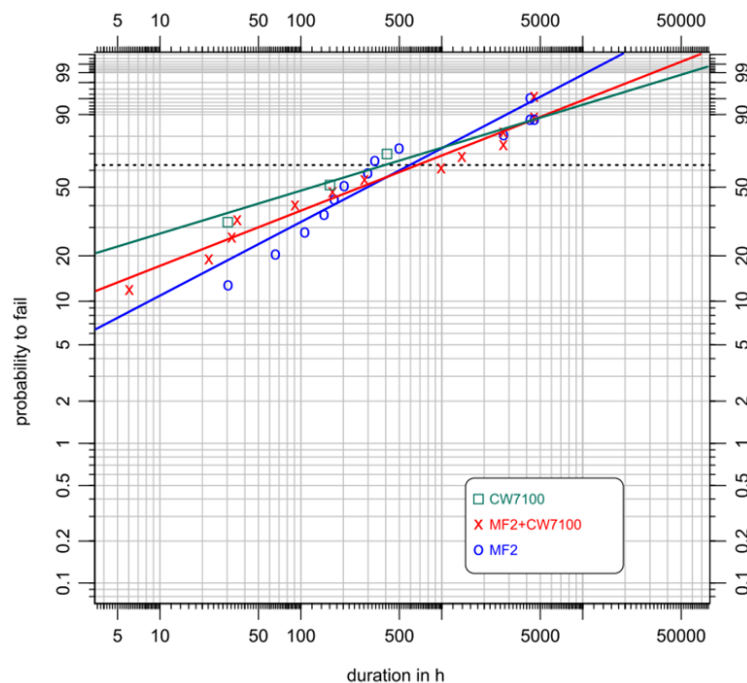


Figure 3.21: Weibull failure probability plots for unprestretched stacked silicone-based DEAs with electrodes made of silver grease (Chemtronics CW7100) electrodes, graphite powder electrodes (NGS GmbH MF2), and a combination of silver grease and graphite powder (MF2 + CW7100)¹¹⁴. Reproduced from¹¹⁴.

Iannarelli et al. have studied the lifetime of silicone (Wacker Elastosil 2030/50) membranes submitted to a DC voltage, with an accelerating ageing method using a gradual multi-step voltage ramp^{146,323}. As shown in Figure 3.22, higher prestretch values are detrimental to the DEA lifetime for a given applied electric field, i.e. higher prestretch values enhance ageing and lead to faster failure³²³. However, the testing was not carried out at constant DC voltages and no compliant electrodes were applied on the dielectric membrane. Furthermore, their analysis relies on the assumptions that the ageing mechanism is monotonically increasing with the stress magnitude (i.e. electric field), and that the failure time follows a Weibull distribution with a constant β parameter for all stress steps)³²³.

To investigate how the electrode material can influence the lifetime of DEAs and degrade over time under fast (50 Hz) AC actuation, Rosset et al. developed an electrode ageing setup to monitor both the electrode resistance (4-point) and actuation strain over time: the Novel Electrode Resistance Degradation (NERD) setup^{25,172,173}.

The NERD setup allows fast ageing experiments on silicone-based DEAs under AC actuation to be carried out, because of the low viscoelastic losses of the silicone elastomer¹⁷². The ageing of DEAs is induced by a series of multiple AC cycles (2000 cycles at 50Hz

for each step) and, in between each cycle, the electrode resistance as well as the actuation stretch and strain at rest are recorded^{113,172,173}.

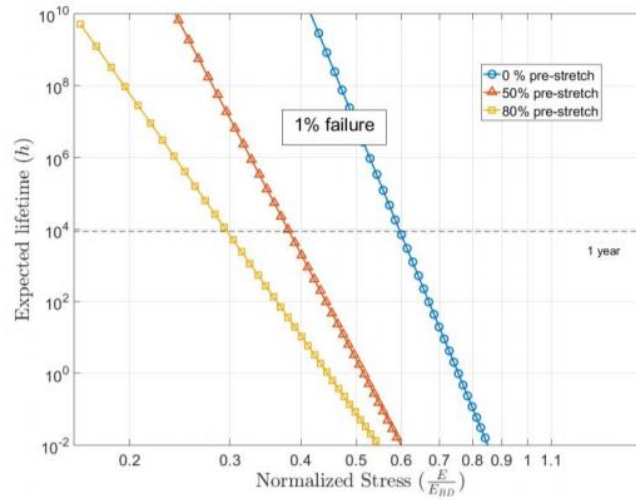


Figure 3.22: 1% failure plot for unprestretched and radially prestretched Wacker Elastosil 2030/50 silicone elastomer membranes³²³. Reproduced from³²³.

Investigations with the NERD setup on silicone-based DEAs revealed that pad-printed carbon black-PDMS electrodes survive over 41 million AC cycles with 70% resistance increase, inkjet-printed carbon-black electrodes over 14 million AC cycles with 160% resistance increase, and carbon grease between 6000 and over 11 million AC cycles with only 3% resistance increase²⁵, as shown in Table 3.2. The actuation stretch decreases over time, and the permanent set (i.e. the strain in absence of any applied voltage) slightly increased for most formulations in the first 200000 cycles²⁵.

They postulate that the ageing of the elastomers is not likely to be due to an increasing membrane stiffness, but rather from a decrease of the elastomer's dielectric permittivity or from resistivity changes, and that higher frequencies for AC actuation do not significantly enhance ageing if the viscoelastic nature of the elastomer is very small²⁵.

Table 3.2: Lifetime and performance of silicone-based DEAs with different electrode compositions and application methods by high-cycle AC ageing with the NERD setup^{25,172}. Reproduced from²⁵.

Electrode type	Number of DEAs that failed before 10 ⁶ cycles	Change in R at 0 V after 10 ⁶ cycles (%)	Change in R at V _{test} after 10 ⁶ cycles (%)	Linear strain at V _{test} after 10 ⁶ cycles (%)	Lifetime (# of cycles)
Grease/Manual					
5% (930 V)	2 of 2		DEA failure		62000 and 88000
Grease/Stamping					
5% (980 V)	5 of 11	+6%	+3%	5.5	6,000 to >11.10 ⁶
Powder/Manual					
5% (970 V)	0 of 2	+330%	+280%	4	>14.10 ⁶
Powder/Inkjet					
5% (940 V)	0 of 4	+340%	+160%	4	>14.10 ⁶
Rubber/Stamping					
5% (990 V)	0 of 7	+76%	+70%	4	>41.10 ⁶

Generally, a dielectric breakdown failure leads to a permanent short-circuit which leads to the complete failure of a DEA. However, self-clearing single-walled carbon nanotubes can be used as electrodes to increase lifetime as they can survive multiple breakdown events with negligible strain decrease after the breakdown events^{162,165,324}.

Stoyanov et al. achieved DEAs that can survive multiple breakdowns at 25% strain for more than 25000 AC cycles without any dramatic impact on the actuation performance on the DEAs¹⁷⁴. Because of its high stiffness, increasing thickness of SWCNT electrodes leads to lower strains³²⁴.

The mechanism of self-clearing is explained by the degradation of SWCNTs by arcing and thermal degradation which lead to conductivity loss ³²⁴. During the breakdown event (i.e. the short-circuit event), the SWCNTs vaporize, allowing a small layer of electrode to be expelled out from the discharge site to allow the formation of non-conductive SWCNT-covered areas ¹⁶⁵.

The density of carbon nanotubes in the electrodes can be important factor that affects the dielectric breakdown strength of a DEA device ¹⁹⁰. Duduta et al. have shown that lower areal densities of carbon nanotubes yield higher dielectric breakdown strength for the DEA devices, whereas the acrylic elastomer's Young's modulus does not have an important influence ¹⁹⁰, but no lifetime study was conducted.

Lau et al. reported VHB-based DEAs with 3 μm thick charcoal powder electrodes which also exhibit a self-clearing behavior ³²⁵, but no lifetime study was conducted.

Caspari et al. demonstrated that 60–180 μm thick DEAs made of prestretched (30% biaxial) tailored silicone formulations with grafted alkyl thiols yielded elastomers which exhibit AC (for frequencies between 0.5 Hz to 8 Hz, higher frequencies have not been tested) lifetimes over 50000 cycles with low (0.5 $\mu\text{A}/\text{cm}^2$) leakage currents for 10% lateral strain (at 27 V/ μm) ¹²⁹.

Zhang et al. showed that the stoichiometric imbalance of addition-cured silicone networks (produced by hydrosilylation of vinyl-terminated PDMS chains and hydrosilane multi-functional crosslinkers) influences the properties of the network, its electromechanical ageing in AC fields, and the AC lifetime of silicone-based DEAs ^{177,326}. Their results highlighted that higher stoichiometric imbalances (defined as the ratio between hydrosilane (Si-H) groups over vinyl groups) lead to higher crosslink density (determined through swelling studies), higher Young's modulus, lower dielectric permittivity and, more importantly, higher lifetime under AC ageing ³²⁶, as shown in Table 3.3. A stoichiometric excess in hydride groups over vinyl groups yields higher AC (0.5 Hz) lifetimes, from 7755 cycles at a 30% hydride group excess to 108324 cycles at 200% hydride group excess ³²⁶. Over time, all aged formulations experienced an increase in crosslinking density and Young's modulus along with a decrease of permittivity and actuation strain, but the effects were enhanced by the stoichiometric imbalance, suggesting that the electromechanical ageing process is driven by the crosslinking of excessive hydrosilane (Si-H) groups under the influence of the applied electric field ³²⁶. However, their studies have only covered their own custom formulation which included silica reinforcers and silicone oil ^{177,326}, and they conducted no study in DC conditions.

Table 3.3: Characteristic lifetime (t_0), Young's modulus (Y) and crosslink density (d) obtained for silicone formulations with different stoichiometric imbalances (r) ³²⁶. Reproduced from ³²⁶.

#	r	d [mol mm^{-3}]	Y [MPa]	t_0 [cycles]
E1	1.3	47.0	0.10	7755
E2	1.7	52.9	0.13	80 211
E3	3	55.9	0.15	10 8324

To conclude, there is no extensive DEA lifetime investigation in DC fields. The few AC investigations show that the choice of membrane prestretch, electrode and dielectric elastomer materials, and humidity are important factors that influence the AC lifetime of DEAs, and hence likely to be important factors in DC conditions as well.

3.4 Conclusion

Dielectric elastomer actuators can fail through dielectric breakdown, electromechanical breakdown, and mechanical breakdown. For prestretched (1.3 equibiaxial) silicone elastomer membranes actuated at low strains (i.e. < 20%), dielectric breakdown is dominant.

Dielectric breakdown is the outcome of cumulative damage of the elastomer membrane owing to chemical degradation (oxidation, hydrolysis, chain scission) processes, space charge accumulation and partial discharges in weak localized regions of the elastomer (e.g. nanocavities, defects, low density regions) which progressively reduce its insulative properties until a complete breakdown.

The breakdown strength of dielectric elastomer membranes generally increases with increasing membrane prestretch, decreasing membrane thickness, increasing Young's modulus, decreasing temperature, and decreasing humidity. The selection of fillers and their concentration in the dielectric membrane is an important parameter that significantly affects its breakdown strength. Similarly, the selection and concentration of chemically grafted end groups to an elastomer matrix influences its breakdown strength.

No literature exists on the DC lifetime of silicone-based DEAs. The few DEA lifetime investigations in AC fields show that environmental conditions (e.g. relative humidity, temperature), the nature of the electrode material, the nature and the prestretch of the elastomer membrane, and electric field are important parameters that influence DEA lifetime, but no systematic large-scale lifetime study has been conducted.

This thesis addresses the lack of investigations on DC lifetime of DEAs by exploring how DC lifetime of prestretched silicone-based DEAs is affected by environmental conditions, electric field, and by the choice of dielectric material and electrode materials, with the objective to understand how DEAs fail under DC fields and to find an engineering solution to significantly increase the lifetime of DEAs without compromising its actuation strain performance.

Chapters 5 to 7 study the influence of temperature, humidity, electric field, as well as the type of elastomer and electrode materials on breakdown strength (Chapter 5) and on DC lifetime of DEAs (Chapters 6 and 7), since all those parameters generally influence how fast dielectric breakdown occurs. The next chapter (4) presents an overview of the experimental characterization methods used (e.g. DEA devices, mechanical characterization, electrical characterization, lifetime assessment and strain monitoring).

Chapter 4 Experimental characterization

This chapter presents the investigated DEA devices, and an overview of the characterization methods used in this thesis. Section 4.1 presents the selection and the fabrication of DEA devices. Section 4.2 shows how mechanical properties (e.g. Young's modulus, stress-strain curves), water vapor permeability, and dielectric breakdown strength of soft silicone elastomer membranes are measured in this thesis. Section 4.3 introduces the automated lifetime setups (MAPLE) which determine DC lifetime data of DEAs presented in Chapters 6 and 7. Section 4.4 introduces the Weibull statistics used for dielectric breakdown strength and DC lifetime data of DEAs. The results, text and figures presented in this chapter were published in *Smart Materials and Structures* ^{26,327,328} and in *SPIE Proceedings* ^{329,330} ⁽¹⁾.

4.1 DEA devices

For our lifetime tests, I select commercially available silicone (PDMS) elastomer materials with different mechanical properties. The choice of silicone (PDMS) over other candidates (e.g. VHB, polyurethanes, natural rubber, SEBS) is due to its wide variety of commercially-available hardness ranges, low viscous losses, fast actuation, and mechanical properties which are independent from time and temperature ^{24,97}, as discussed in Section 2.2.1. Previous studies also demonstrate that prestretched silicone-based DEAs achieve a stable and reproducible over millions of AC cycles without failure ^{25,115,331}.

The geometries of the DEA specimens used in this thesis are shown in Figure 4.1.

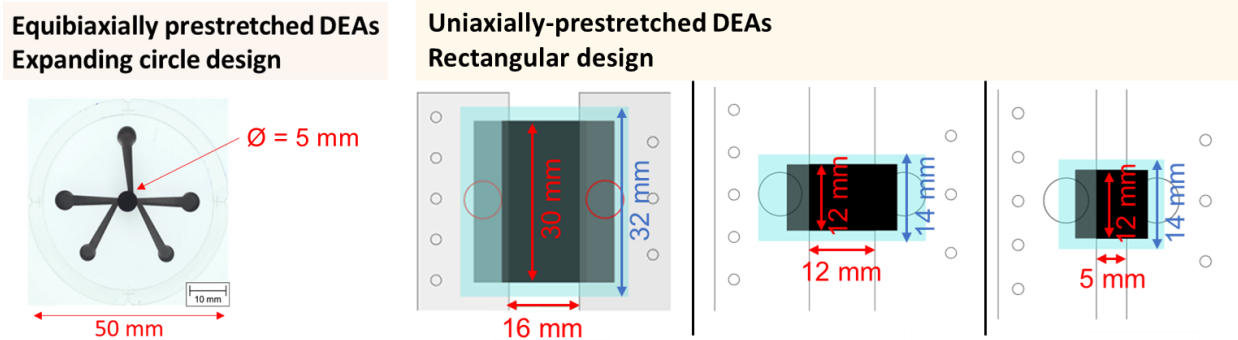


Figure 4.1: Investigated DEAs with equibiaxially (PR = 1.3) and uniaxially (PR = 1.7) prestretched silicone membranes coated with 4 μm thick carbon black-based electrodes.

I select an equibiaxial prestretch of 1.3 for the investigations on single-layer expanding circle (of diameter $\varphi = 5$ mm) DEAs in Chapter 6, and a uniaxial prestretch of 1.7 (i.e. 1.7 uniaxial prestretch $\approx 1.3^2$ equibiaxial prestretch, assuming an incompressible elastomer) for the investigations on single-layer and multilayer rectangular strip DEAs in Chapter 7. An equibiaxial prestretch of 1.3 is selected

⁽¹⁾ Reference list for data, figures and text of Chapter 4:

26 : Kühnel, D., B. Albuquerque, F., Py, V. and Shea, H., "Automated test setup to quantify the lifetime of dielectric elastomer actuators under a wide range of operating conditions," *Smart Mater. Struct.* **30**, 065020 (2021).

326: Beco Albuquerque, F. and Shea, H., "Influence of electric field, temperature, humidity, elastomer material, and encapsulation on the lifetime of dielectric elastomer actuators (DEAs) under DC actuation," *Smart Mater. Struct.* **30**, 125022 (2021).

327: Beco Albuquerque, F. and Shea, H., "Influence of humidity, temperature and prestretch on the dielectric breakdown strength of silicone elastomer membranes for DEAs," *Smart Mater. Struct.* **29** (10), 105024 (2020).

328: Beco Albuquerque, F. and Shea, H. R., "Effect of electrode composition and patterning method on the lifetime of silicone-based dielectric elastomer actuators (DEA) under different environmental conditions," *Proc. SPIE XXIII* **11587**, 115871B (2021).

329: Beco Albuquerque, F. and Shea, H., "Factors influencing the mean-time-to-failure of single-layer uniaxially prestretched silicone-based DEAs," *Proc. SPIE In Press* (2022).

because it is high enough to avoid membrane wrinkling during actuation, and because higher prestretch values increase the effective Young's modulus and lead to lower actuation strain.

I investigate equibiaxially prestretched DEAs with expanding circle design (c.f. Figure 4.1) for the electrode as it is a commonly-used standard design for the study of the influence of numerous parameters (humidity, temperature, prestretch, field, etc.) on lifetime.

I investigate uniaxially prestretched DEAs with rectangular carbon black – PDMS electrode design (c.f. Figure 4.1), as this design has been previously investigated by Hau et al. ⁴⁹ and because the design can be potentially used in applications such as e.g. valves.

As discussed in Section 2.2.5, the electrode material and thickness influence the actuation performance of DEAs. In this thesis, I use a carbon black – PDMS composite ink previously developed at LMTS which is pad-printed onto our DEAs to yield a $4 \pm 1 \mu\text{m}$ thick electrode (of estimated $\approx 0.2 \text{ MPa}$ stiffness ³²⁷) of $10 \text{ k}\Omega/\text{square}$ sheet resistance ²⁶. The electrode composition is 0.8 g of carbon black particles (Akzo Nobel Ketjenblack EC-600JD) and 8 g of silicone matrix (Silbione LSR 4305) in 22 g of isooctane and 22 g of isopropanol. The equibiaxial prestretching of membranes and the pad-printing process are detailed in ¹⁵³.

In section 6.6, I use two additional electrode materials: an inkjet-printed carbon black suspension (with Akzo Nobel Ketjenblack EC-300J carbon black powder, Wacker Belsil SPG 128 VP dispersant and OS2 silicone solvent, following the formulation in reference ³³²), and a dry carbon black powder (of grinded Akzo Nobel Ketjenblack EC-600JD) applied with a paint brush through a mask.

4.1.1 Fabrication of equibiaxially prestretched DEAs

I prepare the equibiaxially prestretched DEAs following the process described in ¹⁵³, as shown in Figure 4.2. I investigate the following elastomer membranes:

- A) Wacker Elastosil® 2030/20 film, supplied as already casted and cured films on a removable backing.
- B) Dow Corning Sylgard™ 186 (A:B 10:1), blade-casted in lab following Rosset et al. recipe ¹⁵³.
- C) Dow Corning Sylgard™ 184 (A:B 10:1), blade-casted in lab following Rosset et al. recipe ¹⁵³.
- D) Momentive Silopren® Electro 242-1 (A:B 1:1), blade-casted in lab following Rosset et al. recipe ¹⁵³.

Table 4.1 shows the list of investigated silicone elastomer materials, their mixing ratios, and their properties. Data on the dielectric breakdown strength and the Young's moduli of these elastomer membranes under different prestretch and environmental conditions are presented in Chapter 5.

Table 4.1: List of investigated silicone elastomer materials and the measured film thickness before prestretch. Reproduced from ³²⁸.

Elastomer material	Type	Relative permittivity (ϵ_r) [-]	Measured ³²⁷ Young's modulus (Y) @ 20°C - 90% RH [MPa]	Measured film thickness [μm]
Elastosil 2030/20	Commercial film	2.8 ²²⁷	1.3 ± 0.1	20 ± 1
Sylgard 186 (A:B 10:1)	Blade-casted (in a cleanroom)	2.8 (1 Hz) ³³³	1.4 ± 0.1	22 ± 2
Sylgard 184 (A:B 10:1)		3.0 (1 Hz) ³³³	3.9 ± 0.2	24 ± 2
Electro 242-1 (A:B 1:1)		2.7 *	1.5 ± 0.1	25 ± 2
LSR 4305 (A:B 1:1)		2.9 ¹⁹⁶	0.18 ± 0.01	22 ± 2

* According to the manufacturer

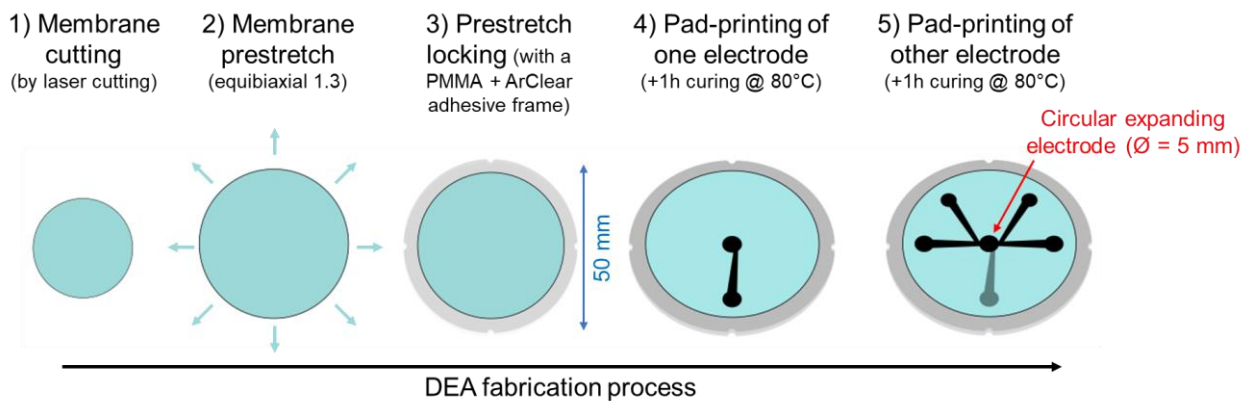


Figure 4.2: Fabrication process of single-layer expanding circle DEAs made of equibiaxially ($\text{PR}=1.3$) prestretched silicone membranes coated with $4 \mu\text{m}$ thick carbon black-based electrodes, following the process described by Rosset et al. ¹⁵³. Details on the fabrication process are given in reference ¹⁵³.

The elastomer membranes are equibiaxially prestretched to 1.3x (i.e. to $\approx 12 \mu\text{m}$ thickness after prestretch). The electrode is a $4 \pm 1 \mu\text{m}$ thick pad-printed carbon black-PDMS material¹⁵³. I observe no swelling or wrinkling after pad-printing and/or curing of the ink. The thickness of the final prestretched membranes is systematically measured with a white light transmission interferometer, as described in¹⁵³.

In section 6.5, I investigate the influence of soft (SEBS or LSR 4305 silicone) encapsulation layers on DC lifetime. I postulate that the addition of hydrophobic encapsulation layers would delay water vapor migration toward the dielectric membrane, thereby increasing its lifetime. The encapsulation layer is fabricated by spin-coating a solution of LSR 4305:OS2 (1:4 ratio) or of SEBS (Hexpol Dryflex 500040):toluene (1:4 ratio) on both sides of the DEA above the electrodes, as shown in Figure 4.3. The encapsulation layer (of thickness ranging from $2 \mu\text{m}$ to $7 \mu\text{m}$, measured with a white light transmission interferometer) covers the entire electrode surface and its vicinity up to 20 mm radius.

The DC electric fields used for our tests with equibiaxially prestretched DEAs in Chapter 6 are 80, 90, 100 and $110 \text{ V}/\mu\text{m}$, which correspond to 67%, 75%, 83% and 92% of the dielectric breakdown strength of Elastosil 2030/20 at 1.3 equibiaxial prestretch and at $85^\circ\text{C} - 85\% \text{ RH}$. I test the following environmental conditions: $20^\circ\text{C} - 30\% \text{ RH}$, $20^\circ\text{C} - 90\% \text{ RH}$, $85^\circ\text{C} - 20\% \text{ RH}$ and $85^\circ\text{C} - 85\% \text{ RH}$ for lifetime tests, using an automated lifetime setup (MAPLE²⁶) detailed in Section 4.3 and shown in Figure 4.14.

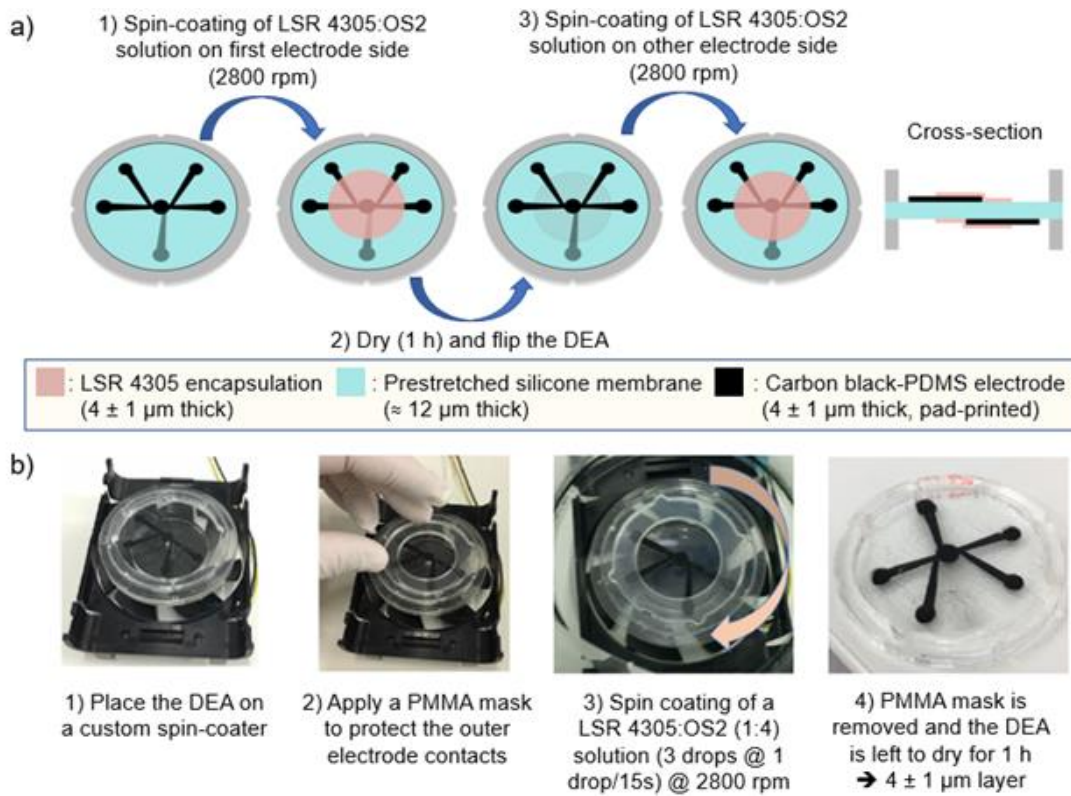


Figure 4.3: a) Schematic overview of spin-coating of encapsulation layers (SEBS or LSR 4305 silicone) on silicone-based DEAs with expanding circle pad-printed carbon black-PDMS electrodes. b) Spin-coating experimental process: a DEA is placed on a custom spin-coater, and a mask is applied to avoid the coverage of the outer electrical contacts by the encapsulation during spin coating (at 2800 rpm).

4.1.2 Fabrication of uniaxially prestretched single-layer DEAs

Uniaxially prestretched strip DEAs made of silicone (Elastosil 2030/20 or Electro 242-1) as dielectric membranes with a rectangular carbon black – PDMS electrode design (c.f. Figure 4.5) are investigated, with the fabrication process detailed in Figure 4.4. DC lifetime investigations on uniaxially prestretched single-layer strip DEAs are shown in Chapter 7, and reported in³³⁰.

I test three different electrode geometries:

- A) 60 mm^2 , i.e. $12 \text{ mm} \times 5 \text{ mm}$ active electrode area (for a $14 \text{ mm} \times 5 \text{ mm}$ total size)

- B) 150 mm², i.e. 12 mm x 12 mm active electrode area (for a 14 mm x 12 mm total size)
- C) 480 mm², i.e. 30 mm x 16 mm active electrode area (for a 32 mm x 16 mm total size).

For the three geometries, a passive region of 1 mm width around the DEAs prevent arcing from the sides.

The prestretching of the DEAs is done by applying a linear spring bias, inspired from the works of Hau et al. and Hodgins et al.^{49,334}. The DEAs are uniaxially prestretched to 1.7x (i.e. to $12.2 \pm 0.2 \mu\text{m}$ thickness after prestretch) using three springs of 10 mN/mm spring constant to match the stiffness of the DEAs ($\approx 33 \text{ mN/mm}$ for 14 mm x 12 mm DEAs).

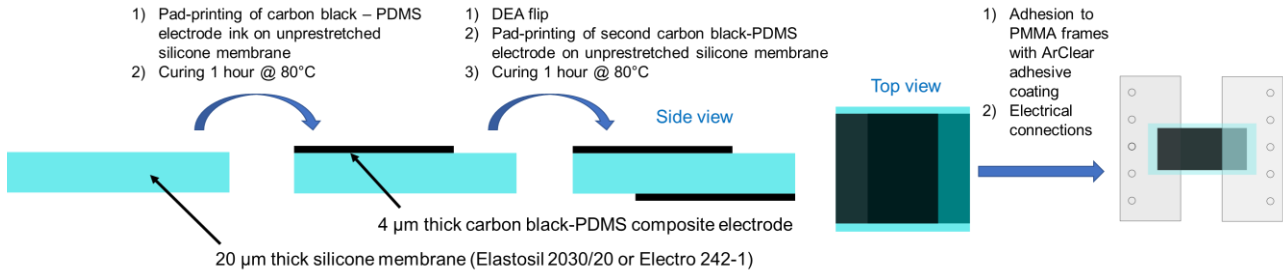


Figure 4.4: Detailed fabrication process for single-layer uniaxially prestretched strip DEAs (c.f. Chapter 7). The carbon black-PDMS electrode ink is pad-printed on silicone membranes before prestretch.

The DC electric fields used for our tests with uniaxially prestretched DEAs in Chapter 7 are 60, 75 and 90 V/ μm . I test the following environmental conditions: 20°C – 90% RH, and 85°C – 85% RH. using an automated lifetime setup adapted from the automated lifetime MAPLE setup used for equibiaxially prestretched expanding circle DEAs, shown in Figure 4.15.

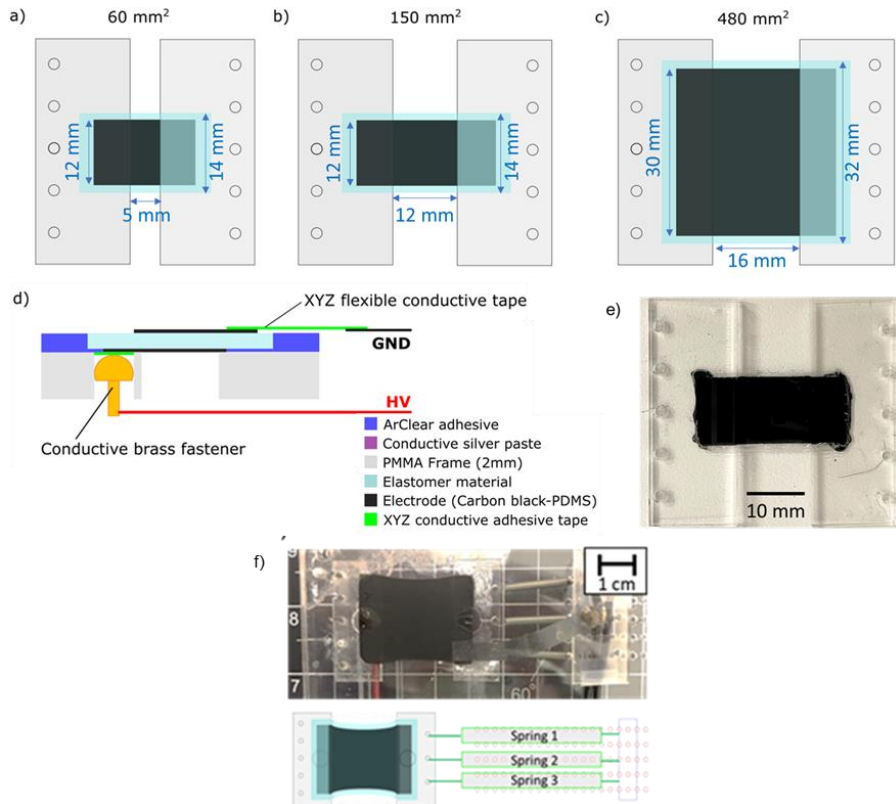


Figure 4.5: a) Single-layer DEA with rectangular a) 12 mm x 5 mm (60 mm²) b) 12 mm x 12 mm (150 mm²), and c) 30 mm x 16 mm (480 mm²) width x length carbon black-PDMS composite electrodes. d) The DEAs are attached to PMMA frames with ARclear® 8932EE (Adhesives Research) silicone adhesive layers, and connected to a high voltage power supply with a brass fastener pin (on the HV side) and a flexible XYZ conductive tape (on the GND side). e) A picture of a 150 mm² DEA attached to its PMMA frames. f) An example of a uniaxially prestretched rectangular DEA specimen. The prestretch can be adjusted by pulling or pushing the spring's holding frame where the GND connection is conducted. A insulative gap of 1 mm per side is left to avoid breakdown by arcing from the sides.

4.1.3 Fabrication of uniaxially prestretched multilayer DEAs

DC lifetime investigations on uniaxially-prestretched multilayer strip DEAs made of silicone Elastosil 2030/20 membranes with a rectangular carbon black – PDMS electrode design (14 mm x 12 mm DEAs, c.f. Figure 4.6) are presented in Chapter 7, with the fabrication process detailed in Figure 4.6.

I first pad-print a carbon black – PDMS ink onto a unprestretched Elastosil 2030/20 membrane (1) and I cure the ink at 80°C for 1 h (Step 1). The ink formulation is the same as for equibiaxially prestretched DEAs. Wrinkled samples are discarded. The second step is the plasma bonding (2 x 1 minute @ 90% power using a Diener Zepto 2.6L plasma surface cleaning system) of an Elastosil 2030/20 membrane with a membrane coated with the pad-printed cured ink (Step 2). The two layers are slowly and carefully layered right after plasma treatment (Step 2). The next step (Step 3) is to remove one of the backings of the stack, plasma treat it along with an additional Elastosil 2030/20 membrane to then carefully layer them, yielding a 1-layer DEA.

Step 3 is repeated several times to yield 2, 4, and 16-layer DEAs. Challenges during the manufacturing process are loss of adhesion between the electrode surface and the dielectric membrane, wrinkling of the membrane during pad-printing, and the presence of air bubbles that arises when layering the layers.

Once the number of layers is reached, the DEA stack is laser-cut (Trotec Speedy 300 – 60 W CO₂ laser) to yield the final DEA dimensions, and the top and bottom backings are removed. The bottom side of the DEA stack is then attached to a ARclear® 8932EE silicone adhesive-coated PMMA frame (Step 4). The carbon black – PDMS ink is then applied (≈ 0.3 mL with a pipette) to the sides of the DEA stack as electrical contacts and the ink is cured at 80°C for 1 hour. Finally, a flexible XYZ conductive tape is applied to the contacts to make the connection to GND. The connection to HV is ensured with a direct contact to a brass metal pin. The quality of the electrical connections is checked with a capacitance measurement for all DEAs before the lifetime tests. DEAs exhibiting low capacitances are discarded. The entire manufacturing process has a yield of $\approx 60\%$.

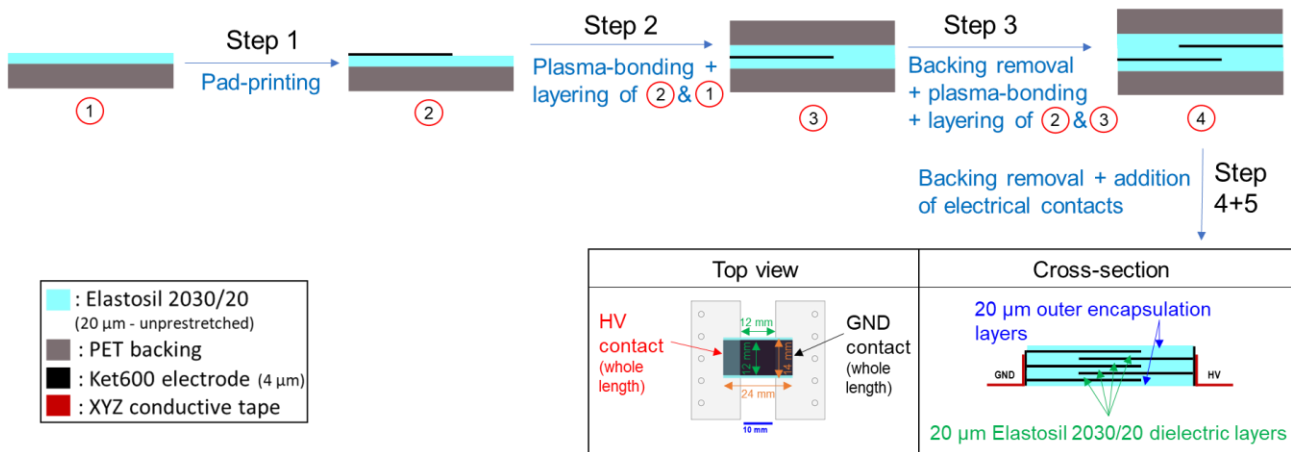


Figure 4.6: Detailed fabrication process for multilayer uniaxially prestretched strip DEAs. The carbon black-PDMS electrode ink is pad-printed on silicone membranes before prestretch.

4.2 Characterization of silicone elastomer membranes

This subsection presents how mechanical properties, water vapor permeability and dielectric breakdown strength of silicones are characterized.

I investigate the Young's modulus of the silicone elastomers used as dielectric elastomers for DC lifetime studies to evaluate whether DC lifetime is significantly affected by the mechanical properties of the dielectric membrane. I investigate the water vapor permeability to evaluate if lower DC lifetimes are correlated to higher water vapor permeability, since increasing the relative humidity lead to significantly lower lifetime for silicone-based DEAs as shown in Chapters 6 and 7. I investigate the dielectric breakdown strength to demonstrate how it is affected by temperature, humidity, and membrane prestretch, and to estimate how lifetime is correlated to the ratio of field to breakdown strength E/E_{DB} , as discussed in Section 6.3.

4.2.1 Determination of mechanical properties

The Young's moduli of the investigated elastomers with a pure shear configuration at 20°C and 80°C are obtained using a custom mechanical test-bench, designed and developed by the Intelligent Materials Systems Lab at the Universität des Saarlandes (Prof. Seelecke)³³⁴, as seen in Figure 4.7. The mechanical test bench is equipped with a 10 N force sensor and a linear motor with an embedded displacement sensor.

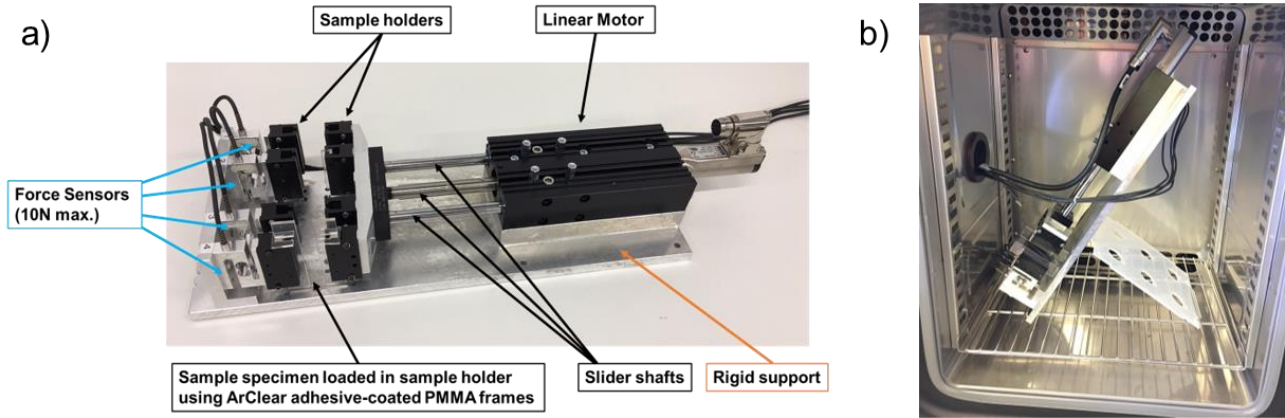


Figure 4.7: a) Mechanical test-bench used for the quantification of true stress – engineering strain curves and Young's moduli for the investigated elastomers. b) The mechanical test-bench can be placed inside an environmental chamber and sustain elevated temperatures (up to 80°C) and humidity levels (up to 90%RH).

The membrane samples used for mechanical characterization are pure shear configuration specimens, as shown in Figure 4.8. Following the recommendations in Carpi et al.³³⁵, the pure shear configuration specimen possesses a sample length which is at least 5x larger than its width: specimen sizes of 12 mm width, 70 mm length and of $\approx 20 \mu\text{m}$ thickness for silicone films, and of 4 mm width, 70 mm length and of $\approx 500 \mu\text{m}$ thickness for VHB 4905 films are pulled uniaxially in a pure shear configuration along the width direction at a linear speed of 0.5 mm s^{-1} (3 mm s^{-1} for VHB 4905) up to a maximal displacement of 15.6 mm, i.e. a uniaxial strain of $\epsilon_x = 130\%$ for silicones (and 40 mm, i.e. $\epsilon_x = 1000\%$ uniaxial strain for VHB 4905).

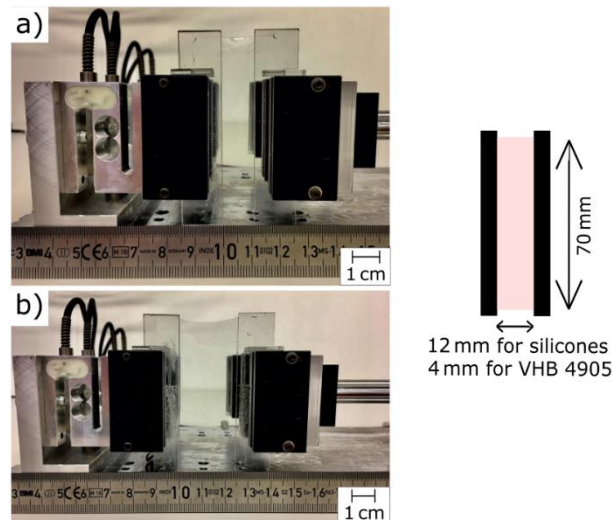


Figure 4.8: Uniaxial pull-testing of a specimen sample (70 mm length x 12 mm width for silicones and 70 mm length x 4 mm width for VHB 4905) with a pure shear configuration. a) Specimen at 0% engineering strain. b) Specimen at 100% engineering strain with visible necking.

Each specimen undergoes four extension cycles and yields force vs. displacement data that can be used to draw stress-strain curves. The three last cycles are averaged to yield a single true stress-engineering strain curve. The first cycle is discarded because of significant Mullins effect. The true stress (σ_{True}) is calculated by:

$$\sigma_{True} = \frac{F}{\delta_0 L(\varepsilon_Z)} (1 + \varepsilon_Z) = \frac{F}{\delta_0 L(\varepsilon_Z)} \left(1 + \frac{\Delta x}{w_0}\right) \quad (Eq. 9)$$

where F is the force recorded by the force sensor, δ_0 and w_0 respectively the initial specimen thickness and width, ε_Z the engineering strain, Δx the linear displacement along the width direction and $L(\varepsilon_Z)$ the specimen length as a function of engineering strain (i.e. necking).

4.2.2 Determination of water vapor permeability

The water vapor permeability of silicone membranes is determined using a ASTM E96/E96M – 16 procedure: the desiccant method³³⁶ at 23°C – 50% RH, a test condition used in Trifol et al³³⁷.

The desiccant method consists in adding a water-absorbing dry silica gel (25g - predried in an oven at 120°C for 12 h) into a metal cup, which is then covered with a thin pre-conditioned membrane, thereby sealing the volume inside the metal cup, as shown in Figure 4.9.

The experimental procedure occurs as followed:

- Silicone membranes (30-60 μm thick for casted membranes or 3 x 20 μm stacked membranes for Elastosil 2030/20 film) of diameter $\varnothing = 80$ mm and the metal containers are conditioned in an environmental chamber at 23°C – 50%RH for 12h. The desiccant (silica gel) is pre-dried in an oven for 12h at 120°C.
- The metal containers (of $\varnothing = 75$ mm outer diameter and $\varnothing = 60$ mm inner diameter) are each filled with 25 g of dry silica gel desiccant.
- The conditioned silicone membranes are applied above the metal containers containing the desiccant without any pre-stretch, and are tightly sealed. The containers are then weighed and transferred to a controlled environmental chamber at 23°C – 50%RH.
- The elastomer-sealed metal cup is maintained at 23°C – 50% RH and the mass increase of each sample owing to water absorption (Δm) by the silica gel desiccant (moisture originating from diffusion across the silicone membrane) through the elastomer membrane (of $\varnothing = 60$ mm diameter, i.e. a test surface area of $A = 28.27\text{cm}^2$, i.e. 0.002827m^2) is monitored every 2 hours over 8 hours. For each elastomer material, three samples are tested (c.f. Section 5.3).

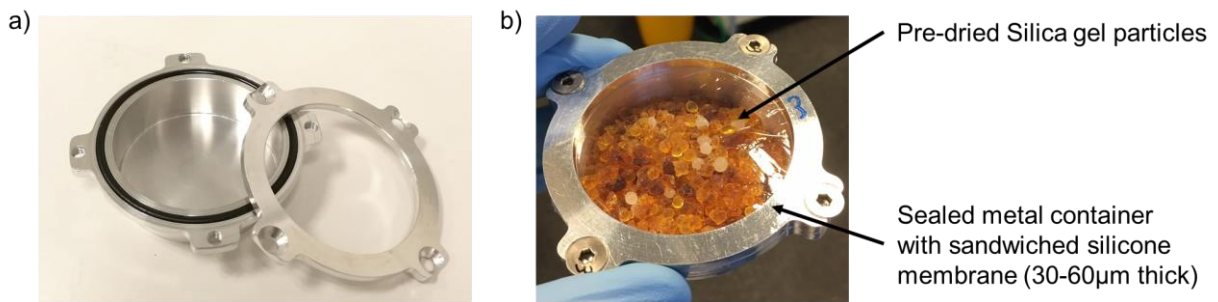


Figure 4.9: a) Metal container used for the water vapor permeability measurements. b) Assembled metal container with sandwiched silicone elastomer membrane, and containing pre-dried silica gel particles.

The water vapor transmission rate (WVTR [$\text{g}/\text{m}^2\text{day}$], i.e. the water vapor flow per unit of time through a surface area) for each elastomer material is calculated from the average of the mass increase over the 3 tested specimens, with the following equation³³⁶:

$$WVTR = \frac{\Delta m}{t * A} = \left(\frac{dm}{dt}\right) / A \quad \left[\frac{\text{g}}{\text{day m}^2}\right] \quad (Eq. 10)$$

A linear regression on average weight change – time plots is computed for each elastomer material (3 samples per elastomer material). For each material, the slope of the curve is then divided by the surface area of the specimen ($A = 28.27\text{cm}^2$, i.e. 0.002827m^2).

The inaccuracy of the desiccant method was estimated with a simple reproducibility study on 2x3 Elastosil 2030 ($60 \pm 1 \mu\text{m}$) specimens over 8h, yielding:

$$\% \text{ Inaccuracy} = \frac{\sum_{i=1}^N \left(\frac{\sigma(\Delta m_i)}{\Delta m_i} \right)}{N} \cong 2\% \quad (\text{Eq. 11})$$

where $\sigma(\Delta m_i)$ is the standard deviation of the average measured weight increases Δm_i at time i for the N (6) specimens. Elastosil 2030 has been selected for this calculation because of the reproducible thickness across the 6 specimens.

Water vapor permeance (WVP) is directly calculated from the WVTR using the following equation ³³⁶:

$$WVP = \frac{WVTR}{\Delta p} = \frac{WVTR}{P_{\text{sat},H_2O(23^\circ\text{C})} * (RH_1 - RH_2)} \left[\frac{g}{Pa \text{ day } m^2} \right] \quad (\text{Eq. 12})$$

where $P_{\text{sat},H_2O(23^\circ\text{C})} = 2.8 \text{ kPa}$ is the water vapor saturation pressure (over liquid water), calculated with the Goff-Gratch equation ³³⁸, RH_1 is the relative humidity of the outer environment (50% RH) and RH_2 is the relative humidity inside the cup (assumed to be 0% RH owing to the desiccant).

The water vapor permeability (P) is defined as the product of water vapor permeance (WVP) with membrane thickness (δ) as shown in Equation Eq.13 and is used for individual specimens, as each specimen possesses a specific membrane thickness.

$$P = D * S = \frac{WVTR}{\Delta p} \delta = WVP * \delta \left[\frac{g \text{ mm}}{Pa \text{ day } m^2} \right] \quad (\text{Eq. 13})$$

The water vapor permeability reported in Section 5.3 is the average value of the three permeabilities of each specimen. The number of tested samples (3 specimens per elastomer material) is relatively limited. In the future, more test samples are required to establish water vapor permeability data with increased precision.

As shown in Equation 13, the water vapor permeability can be written as the product of a kinetic factor (diffusivity D in $\text{cm}^2 \text{ s}^{-1}$) and a thermodynamic factor (water solubility S in $\text{g cm}^{-3} \text{ Pa}^{-1}$), assuming a planar membrane where the diffusivity is independent from water concentration, and assuming a steady state with a linear relationship (sorption isotherm) between equilibrium concentration (of dissolved water molecules within the membrane) and the environmental vapor pressure ³³⁹. The solubility factor is a relevant factor to consider and to correlate to lifetime studies, but it has not been determined in the scope of this thesis.

According to ASTM E96/E96M ³³⁶, the permeability shall only be calculated if the specimen's thickness is above 12.5 mm. The calculation of permeability is nonetheless carried out for thin (30-60 μm thick) silicone films for comparison purposes at normalized thickness. Water vapor transmission increases exponentially with decreasing specimen thickness in thick (2-6 mm) silicone rubber ³⁴⁰.

In Section 5.3, I provide the data on water vapor transmission rate (WVTR), water vapor permeance (WVP), and permeability on silicone membranes (used in this thesis for DC lifetime investigations), averaged on three samples per elastomer membrane.

4.2.3 Determination of breakdown strength

The dielectric breakdown strength of prestretched silicone elastomers has been calculated at constant membrane thickness using patterned rigid gold electrodes, as presented in reference ³²⁷.

The preparation of prestretched silicone membranes for dielectric breakdown studies is shown in Figure 4.10. Silicone membranes are equibiaxially prestretched following the method of Rosset et al ¹⁵³. The equibiaxially prestretched elastomer membrane is placed on a gold-patterned (20 nm thick) glass slide (will serve as the ground electrode). The patterning of the glass slide's ground electrode is carried out using a mask and the Jeol JFC-1200 fine coater at a pressure of 8 Pa under an Argon atmosphere for a duration of 140s at 20mA, yielding $\approx 20 \text{ nm}$ thick rigid gold electrode. Six gold electrodes (that serve as the high voltage electrodes) are patterned by sputtering through a mask on top of the elastomer membrane, leading to a 1 mm x 1 mm overlapped surface area between both electrodes, as shown in Figures 4.11a and 4.11b.

The choice of rigid gold electrodes and the constraint of the glass slide yields no mechanical strain during the dielectric breakdown strength test, allowing a characterization at constant membrane thickness.

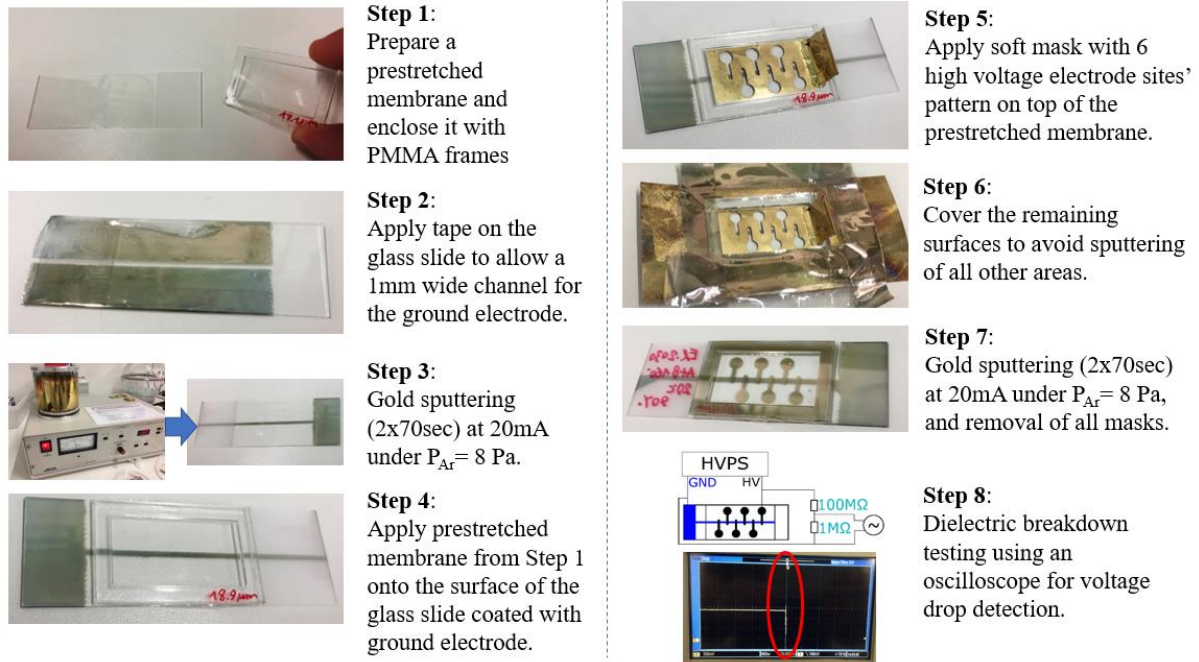


Figure 4.10: Preparation steps of equibiaxially prestretched silicone membranes coated with rigid gold electrodes for dielectric breakdown tests ³²⁷.

The geometry and dimensions of the high voltage electrode sites was designed to ensure a sufficient distance (>2.8 mm) between two adjacent sites to avoid arcing in air between them.

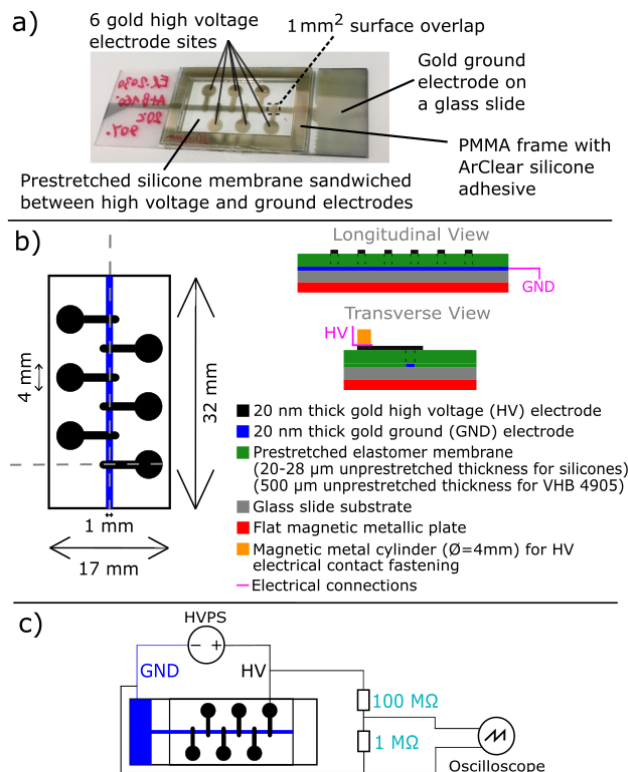


Figure 4.11: a) Photograph of a sample for dielectric breakdown testing, consisting of a prestretched elastomer membrane attached to a glass slide and sandwiched between gold electrodes. b) Schematic diagram of the samples c) Circuit used for the dielectric breakdown measurement.

The determination of the dielectric breakdown strength under controlled humidity and temperature environment is carried out inside a ESPEC SH-661 environmental chamber by applying an initial voltage (corresponding to $\approx 30\%$ of the expected breakdown strength) and increasing the voltage at a rate of 10 V s^{-1} until the breakdown occurs. A Peta-pico-voltron high voltage power supply ³⁴¹ is used. Generally, 12 datapoints (i.e. testing 2 samples each with 6 sites) are obtained for each condition. The dielectric breakdown is

detected on an oscilloscope (Tektronix DPO 2014 – 100 MHz – 1GS s⁻¹) as a rapid (sub μ s) voltage drop below a trigger threshold set slightly below the initial voltage.

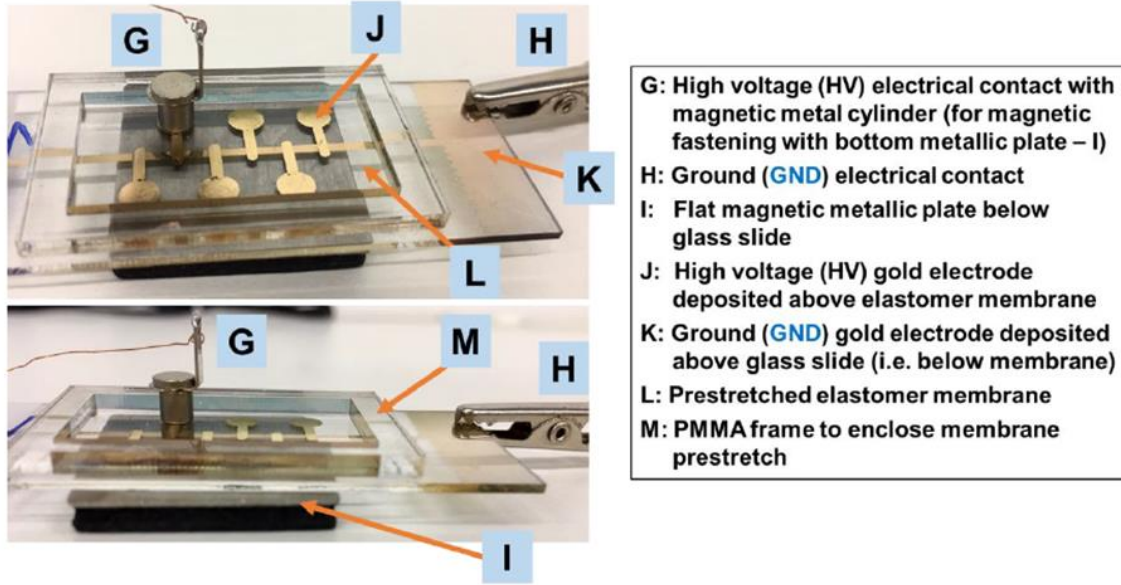


Figure 4.12: Dielectric breakdown test sample. A glass slide with a deposited thin (≈ 20 nm) gold ground electrode and a prestretched elastomer membrane with six deposited thin (≈ 20 nm) gold high voltage electrode sites on top stands on a flat magnetic plate. The high voltage connections are ensured with a magnetic cylinder without damaging the sample and can be easily switched from one electrode site to another during the test.

The dielectric breakdown strength on a membrane of thickness δ (measured using a white-light transmission interferometer¹⁵³, calibrated accordingly to silicones' refractive index) is determined with:

$$E_{DB} = \frac{V_{DB}}{\delta} \left[\frac{V}{\mu m} \right] \quad (Eq. 14)$$

The error (i.e. standard deviation) $s_{E_{DB,i}}$ for each breakdown strength $E_{DB,i}$ datapoint is given by:

$$s_{E_{DB,i}} = E_{DB,i} * \sqrt{\left(\frac{s_{\delta}}{\delta}\right)^2 + \left(\frac{s_{V_{DB,i}}}{V_{DB,i}}\right)^2} \quad (Eq. 15)$$

where s_{δ} is the standard deviation for the sample's thickness (δ in μm) over N measurements defined as $s_{\delta} = \sqrt{\frac{1}{N-1} \sum_{i=1}^N (\delta_i - \bar{\delta})^2}$, $s_{V_{DB,i}} = \pm 10V$ is related to the experimental uncertainty of the 10V/s voltage ramp, and $V_{DB,i}$ is the dielectric breakdown voltage of a given datapoint.

In section 5.1, I provide data on median dielectric breakdown strengths (\bar{E}_{DB} , in V/ μm), and their respective standard error ($s_{\bar{E}_{DB}}$) for N datapoints under fixed elastomer material, prestretch, relative humidity and temperature conditions is given by³²⁷:

$$s_{\bar{E}_{DB}} = 1.253 * \frac{1}{\sqrt{N}} * \sqrt{\frac{1}{N} \sum_{i=1}^N (E_{DB,i} - \bar{E}_{DB})^2} \quad (Eq. 16)$$

where $E_{DB,i}$ is a given dielectric breakdown strength datapoint and \bar{E}_{DB} the mean dielectric breakdown strength value for N datapoints. The 1.253 factor is a correcting factor to quantify the standard error of the median value instead of the standard error of the mean value.

The presence of a visible pinhole defect faster testing confirms the occurrence of a dielectric breakdown, as observed in Figure 4.13. The temperature and humidity inside the environmental chamber are monitored with an external sensor (Sensirion EK-H4) during the tests.

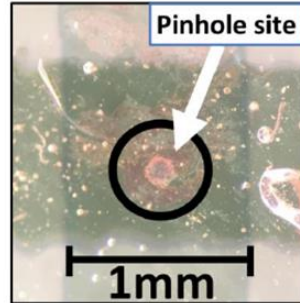


Figure 4.13: Typical pinhole site in the electrode overlap area. The typical diameter of a pinhole is 20-250 μm .

4.3 Automated lifetime setup (MAPLE) for expanding circle equibiaxially pre-stretched DEAs and rectangular electrode uniaxially prestretched DEAs.

The MAPLE lifetime setup shown in Figure 4.14 is designed to continuously monitor strain, and electrode resistance every 10 seconds on 6 DEAs in parallel for long test durations (> 1 -month lifetime studies). The setup is designed to be placed in an environmental chamber and can sustain environmental conditions up to $85^\circ\text{C} - 85\% \text{ RH}$.

The MAPLE automated lifetime setup was developed by Dr. Djen Kühnel and Valentin Py, and a detailed description is found in Kühnel et al. ²⁶. My own contribution to the MAPLE automated lifetime setup is solely on the validation of the setup to ensure that the measured strain and electrode resistance are correct and consistent.

Figure 4.14a and 4.14b provide an overview of the MAPLE setup test stand, where each DEA is mounted with a camera (resilient up to $85^\circ\text{C} - 85\% \text{ RH}$), as shown in Figure 4.14.c. Figure 4.14.d presents a diagram with all components needed for the setup: a DEA holder test stand with cameras (for visual monitoring), an interface board to connect each DEA to a digital multimeter (for resistance monitoring), and a 6-channel power supply driving the DEAs. The data is recorded in a PC which coordinates the testing. The sample holder dimensions have been selected such that two setups fit inside an environmental chamber, as shown in Figure 4.14.e. Figure 4.14.f shows the typical measurement cycle for our lifetime tests, divided in cycles of 1 hour of DC actuation followed with a voltage ramp, repeated until all DEAs break or until 300 h of actuation.

I monitor strain to verify how stable actuation strain is over the lifetime of DEAs, and to evaluate whether strain increases/decreases right before breakdown. The electrode strain is calculated using an ellipse fitting of the outline of the dark electrode surface area, using a Python interface. I monitor electrode resistance (4-point) to evaluate whether any significant degradation of the electrode material occurs over actuation time. Electrode resistance was monitored in silicone-based DEAs under AC fields with the NERD setup previously developed at LMTS presented in Rosset et al. ¹⁷³.

If a DEA fails by dielectric breakdown, the system disconnects all DEAs and then reconnects them one by one to detect the short-circuited DEA and permanently disconnect the relay associated to it to avoid test interruptions. Every hour, the voltage is set to 0V, and a voltage ramp is applied to monitor permanent set (i.e. strain at 0V) and to observe how strain and electrode resistance evolve over voltage. Further details about the MAPLE setup can be found in reference ²⁶.

I obtain the results from Chapter 6 on expanding circle DEAs using the automated MAPLE lifetime setup, presented in ²⁶ and detailed in Figure 4.14.

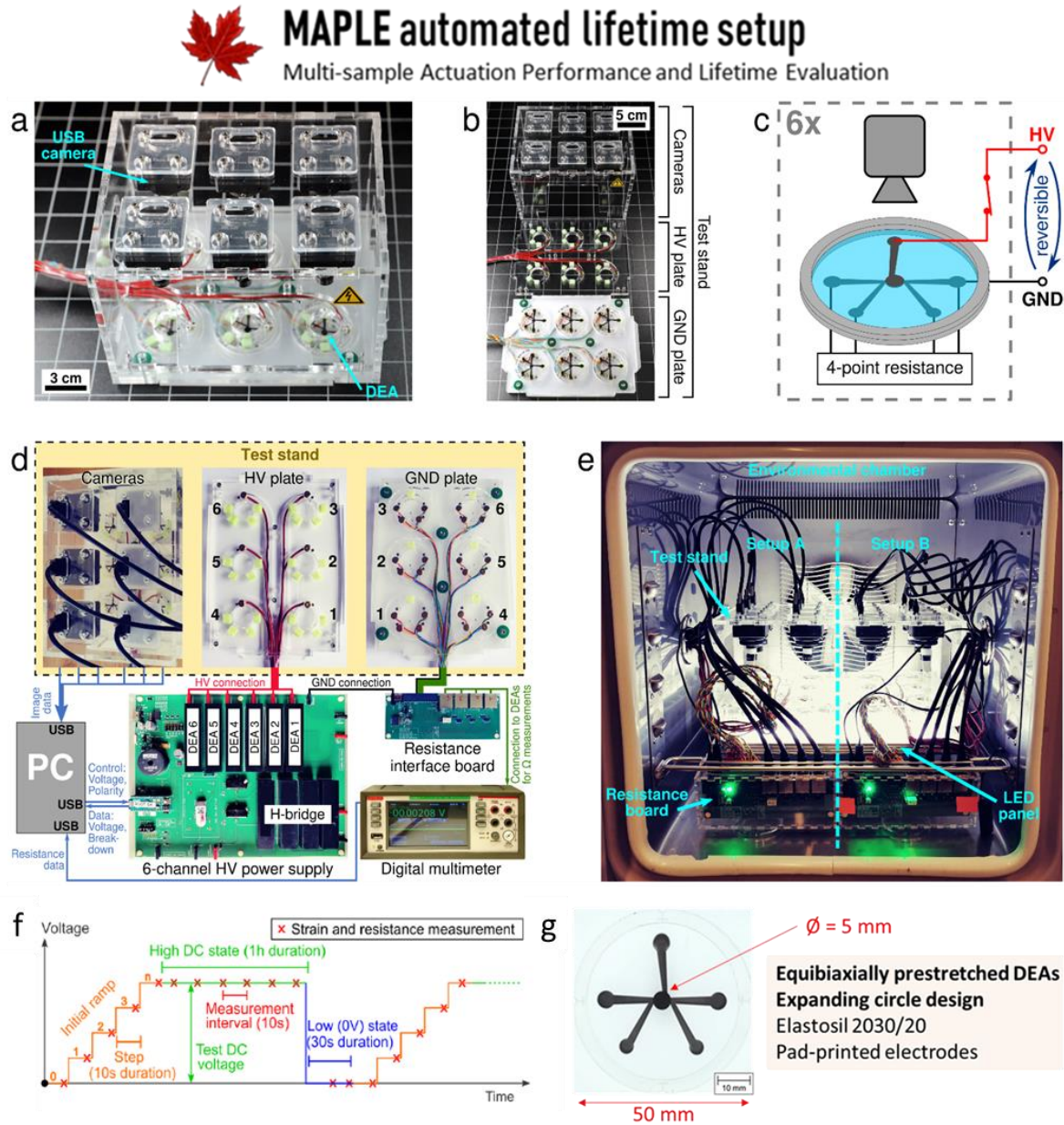


Figure 4.14: Overview of the MAPLE setup of 200 x 125 x 130 mm size. a) Up to six expanding circle DEAs can be tested, with one camera per DEA. b) DEAs can be easily loaded and removed by disassembling. c) A camera is mounted above each DEA for strain measurement. Each DEA is connected to four feed lines on the bottom electrode to allow in-situ electrode resistance measurements. Each DEA is connected to the power supply (through a relay) to disconnect each individual DEA in case of failure. d) Connection diagram showing the components of the setup. e) For each environmental chamber, two MAPLE setups (test stand and resistance interface board) can fit side by side, yielding operation up to 85 °C and 85% humidity. f) Measurement cycle for DC actuation lifetime tests. g) Typical equibiaxially prestretched single-layer DEA device tested in this work, with a circular 5 mm diameter electrode.

I obtain the results from Chapter 7 on uniaxially prestretched rectangular strip DEAs using a modified MAPLE setup shown in Figure 4.15 which does not monitor electrode resistance, and which has a modified strain recognition. The same high voltage power supply is used, and the same cameras. The sample holder is however modified to accommodate the size of the samples and its prestretching springs.

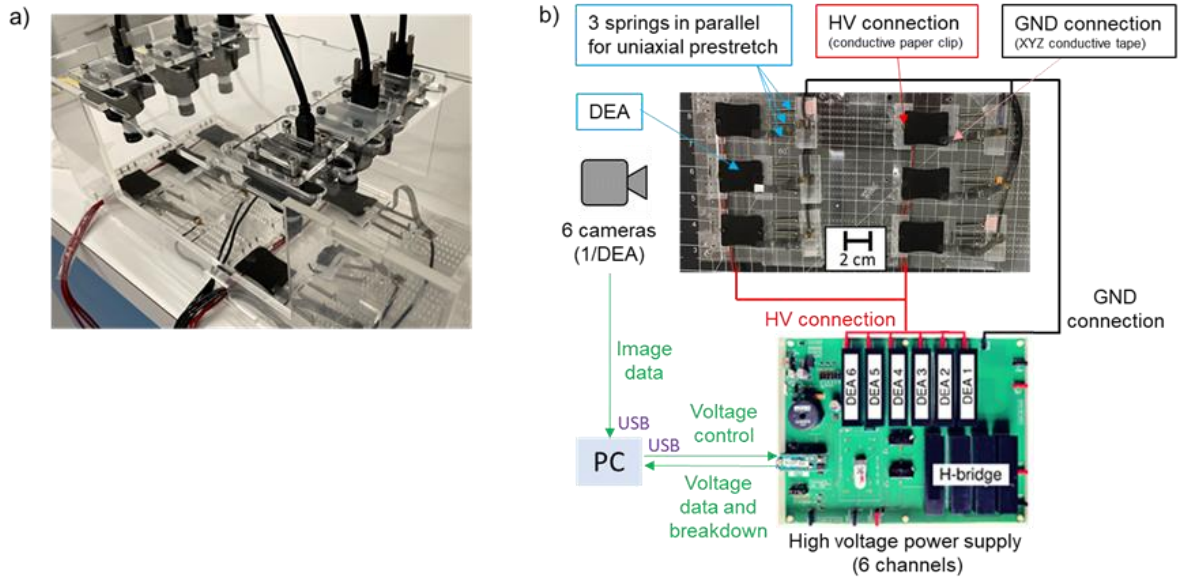


Figure 4.15: a) Modified MAPLE setup for uniaxially prestretched rectangular strip DEAs with continuous strain monitoring of 6 DEAs in parallel and dielectric breakdown detection. b) Schematic diagram of the modified MAPLE setup. Each DEA is prestretched using several springs in parallel.

For our tests, uniaxial strip DEAs are prestretched with > 2 springs (which are attached to the main frame with a spring holder) in parallel and not by a holding frame with adhesive as it is the case for equibiaxial DEAs. The prestretch can be adjusted in the modified MAPLE setup by varying the spring distance between the spring holder and the DEA. The DEAs are prestretched to 1.7, which is approximately equivalent to 1.3 equibiaxial prestretch. I use conductive fastener clips for the high voltage connection and an XYZ conductive tape (which adheres to the DEA surface) for the ground connection. The adapted MAPLE setup for uniaxial DEAs does not monitor electrode resistance, but only strain. The same Python script can be used, but with a modified strain recognition algorithm.

Both MAPLE lifetime setups presented here allow a high versatility of DEA devices to be tested, with varying elastomer membrane materials (of different mechanical properties) and prestretch, varying electrode materials and sizes.

Output data obtained for the MAPLE lifetime setup are failure fraction vs. time plots (from breakdown detection of individual DEAs), strain vs. time, strain vs. voltage, resistance vs. time, and resistance vs. voltage plots, as demonstrated in Chapters 6 and 7.

4.4 Weibull probability plots

Weibull analysis is frequently used as a statistical tool to describe dielectric breakdown strength²²⁸ and to evaluate the lifetime distribution of a device³⁴². An extensive overview of Weibull probability plots for dielectric breakdown strength (c.f. Chapter 5)³²⁷ and for DC lifetime distributions (c.f. Chapter 6)³²⁸ of equibiaxially-prestretched DEAs is provided in the Supplementary materials of my reported articles.

For lifetime investigations, the two-parameter Weibull probability density function is given by³⁴²:

$$f(t) = \frac{\beta}{\eta} \left(\frac{t}{\eta}\right)^{\beta-1} e^{-\left(\frac{t}{\eta}\right)^{\beta}} \quad (\text{Eq. 17})$$

where η is the scale parameter (i.e. characteristic lifetime at which 63.2 % of the devices fail³⁴²), β is the shape parameter (i.e. slope of the Weibull fit). The unreliability (i.e. the cumulative failure probability) is then defined by³⁴²:

$$F(t) = \int_0^t f(t) dt = 1 - e^{-\left(\frac{t}{\eta}\right)^{\beta}} \quad (\text{Eq. 18})$$

A Python script³⁴³ is used for a Weibull fitting on a population of n DEAs, which can include suspensions (i.e. unfailed DEAs at the end of the lifetime test), to yield the parameters β and η , as well as 90% confidence intervals. From those parameters, I obtain the mean time to failure ($MTTF$)³⁴⁴:

$$MTTF = \eta * \Gamma\left(\frac{1}{\beta} + 1\right) \quad (Eq. 19)$$

where Γ is the gamma function. Values for MTTF are given in Tables in Chapters 6 and 7.

The failure probability (i.e. unreliability – c.f. equation Eq.18) for each lifetime datapoint is estimated by Benard's approximation (median ranks method) which corresponds to Equation Eq.20³⁴⁵:

$$y_i \approx \frac{i - 0.3}{n + 0.4} \quad (Eq. 20)$$

where y_i is the median rank (i.e. the estimated failure probability) for the i^{th} failure ($i = [1, \dots, n]$) among a total number of samples n (both failed and unfailed). Weibull probability plots of unreliability (estimated by Eq.20) vs. time (on a logarithmic scale) for datasets comprising at least 3 failure datapoints are shown in Supplementary materials of reference³²⁸. An example of Weibull probability plot of DC lifetime distribution for Elastosil 2030/20 (silicone) DEAs is given in Figure 4.16.

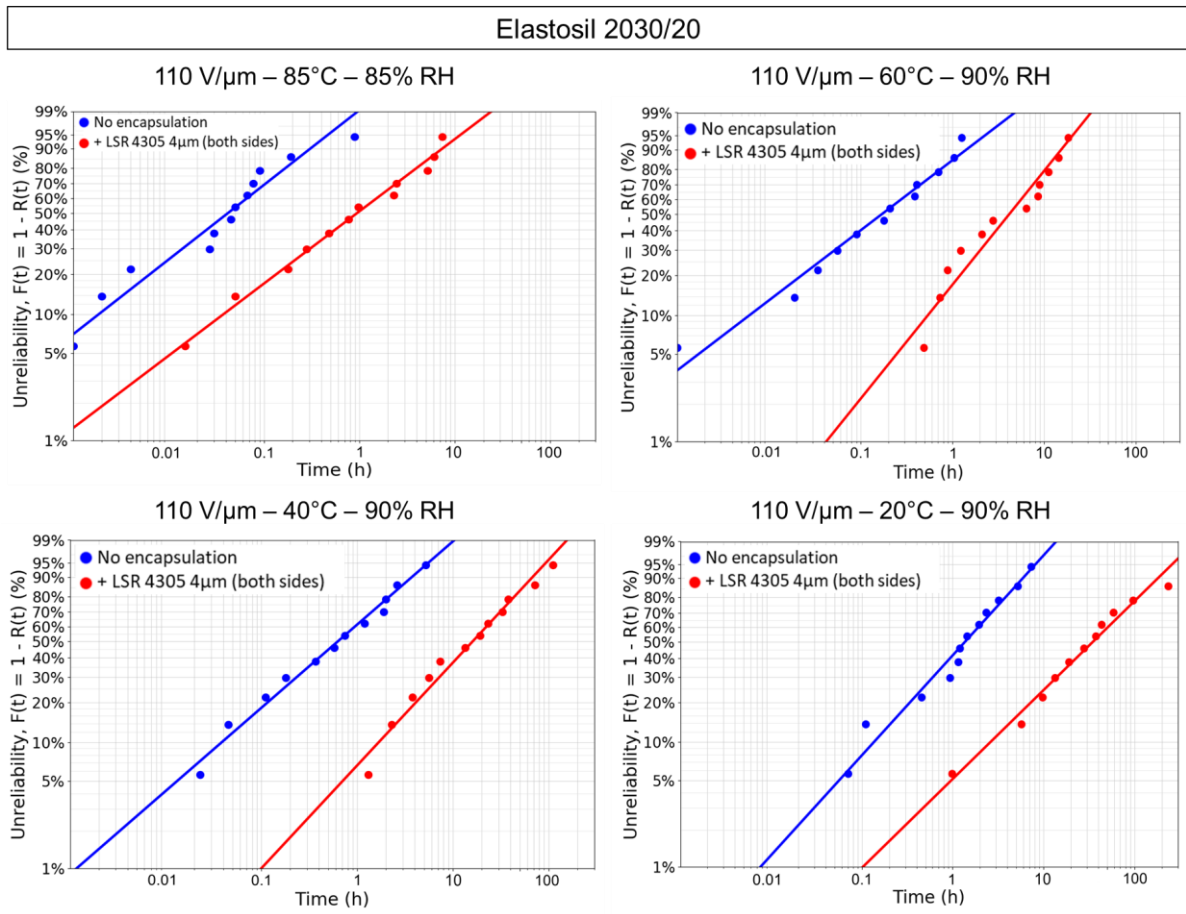


Figure 4.16: Example of Weibull plots for DC lifetime of Elastosil 2030/20 DEAs: effect of the encapsulation layer on DC DEA lifetime at constant electric field of 110 V/μm under different environmental conditions. Only the datasets with three or more failure datapoints are shown in Weibull plots, and solid lines correspond to the Weibull fits for each dataset.

4.5 Summary

This chapter presents the manufacturing of DEA devices and the experimental methods used in this thesis.

For the DC lifetime studies (c.f. Chapters 6 and 7), I manufacture equibiaxially prestretched and uniaxially prestretched silicone-based DEAs following the recipes developed at LMTS¹⁵³.

I characterize the DC lifetime of DEAs using an automated lifetime setup (MAPLE) developed by Djen Kühnel and Valentin Py²⁶ which monitors electrode resistance and strain over time and which disconnects failed DEAs (by short-circuit detection). The DC lifetime results are described with Weibull statistics.

I characterize the mechanical properties (e.g. Young's modulus, stress-strain curves) of pure shear configuration elastomer specimens using a custom mechanical test-bench designed by the Intelligent Materials Systems Lab at Universität des Saarlandes³³⁴, and assembled at LMTS by Valentin Py. The dielectric breakdown strength of prestretched elastomer membranes with rigid gold electrodes and the water vapor permeability of silicone membranes are characterized following the procedures detailed here.

Chapter 5 presents the results of mechanical properties, dielectric breakdown strength and water vapor permeability of silicone elastomer membranes, following the experimental methods and setups presented here. Chapters 6 and 7 present the DC lifetime data of equibiaxially and uniaxially prestretched silicone-based DEAs using the automated lifetime setup (MAPLE) presented here.

Chapter 5 Mechanical properties and dielectric breakdown strength of silicone membranes for DEAs under different temperature and humidity conditions

This chapter presents data on dielectric breakdown strength, mechanical properties, and water vapor permeability of silicone elastomer membranes, with the objective to correlate those properties to the DC lifetime data presented in Chapters 6 and 7. Section 5.1 presents an overview of the breakdown strength data of prestretched silicone elastomer membranes under numerous environmental conditions. Section 5.2 presents the DEA figures of merit for silicone elastomer membranes. Section 5.3. shows the water vapor permeability data of silicone elastomer membranes. Section 5.4 presents the stress-strain curves and the mechanical properties of silicone elastomer membranes. The results, text and figures presented in this chapter were published in Smart Materials and Structures ³²⁷ (2).

5.1 Dielectric breakdown strength of silicone elastomer membranes for DEAs

This section presents the results on the median dielectric breakdown strengths (and their respective errors) of prestretched silicone elastomer membranes (and prestretched 3 x 3 VHB 4905 membrane because it is commonly used in DEAs), as summarized in Table 5.1 and in Figure 5.1.

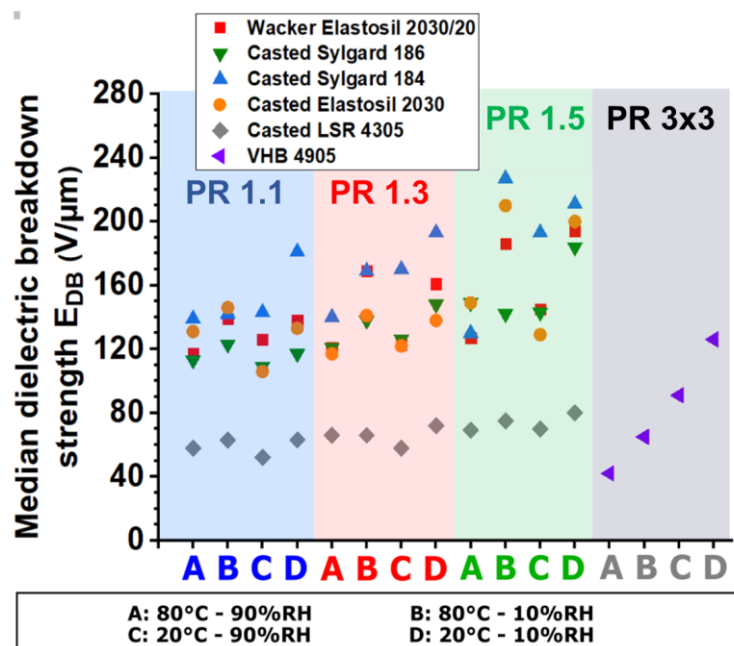


Figure 5.1: Median dielectric breakdown strengths for each investigated set of prestretch values, temperature and relative humidity ranges for Wacker Elastosil 2030/20, casted Elastosil 2030, casted Sylgard 186, casted Sylgard 184, casted LSR 4305 and VHB 4905. For corresponding data, c.f. Table 5.1. For readability considerations, error bars are not shown. Standard errors are found in Table 5.1.

Figure 5.1 and Table 5.1 show that the dielectric breakdown strength of silicone elastomers generally decreases with decreasing membrane prestretch, and with increasing relative humidity at constant temperature. The effect of temperature on the dielectric breakdown strength of silicone elastomers is not straightforward. The next subsections address the effect of water vapor content (5.1.1), temperature (5.1.2), and of membrane prestretch (5.1.3) in detail.

⁽²⁾ Albuquerque, F. B. and Shea, H., "Influence of humidity, temperature and prestretch on the dielectric breakdown strength of silicone elastomer membranes for DEAs," Smart Mater. Struct. **29** (10), 105024 (2020).

Table 5.1: Median dielectric breakdown strengths for the investigated elastomers under fixed equibiaxial prestretch, temperature, and relative humidity conditions. The standard errors for the median dielectric breakdown strength calculations are given by Eq. 16 from section 4.2.3. and in ³²⁷.

Material	Condition	Water vapor content (g/m ³)	Median dielectric breakdown strength E_{DB} (V/ μ m)			
			PR 1.1	PR 1.3	PR 1.5	PR 3 x 3
Wacker Elastosil 2030/20	80°C - 90%RH	261.5	117 \pm 5	121 \pm 8	127 \pm 5	
	80°C - 10%RH	29.1	139 \pm 6	169 \pm 9	186 \pm 10	
	20°C - 90%RH	15.5	126 \pm 6	123 \pm 4	145 \pm 8	
	20°C - 10%RH	1.7	138 \pm 4	161 \pm 12	194 \pm 6	
Sylgard 186	80°C - 90%RH	261.5	113 \pm 4	121 \pm 6	149 \pm 7	
	80°C - 10%RH	29.1	123 \pm 4	138 \pm 8	142 \pm 8	
	20°C - 90%RH	15.5	109 \pm 2	126 \pm 4	143 \pm 9	
	20°C - 10%RH	1.7	117 \pm 5	148 \pm 4	184 \pm 8	
Sylgard 184	80°C - 90%RH	261.5	139 \pm 7	140 \pm 8	130 \pm 8	
	80°C - 10%RH	29.1	142 \pm 4	169 \pm 9	227 \pm 7	
	20°C - 90%RH	15.5	143 \pm 10	170 \pm 8	193 \pm 9	
	20°C - 10%RH	1.7	181 \pm 10	193 \pm 7	211 \pm 22	
Casted Elastosil 2030	80°C - 90%RH	261.5	131 \pm 5	117 \pm 5	149 \pm 10	
	80°C - 10%RH	29.1	146 \pm 5	141 \pm 7	210 \pm 13	
	20°C - 90%RH	15.5	106 \pm 3	122 \pm 6	129 \pm 6	
	20°C - 10%RH	1.7	133 \pm 5	138 \pm 6	200 \pm 7	
LSR 4305	80°C - 90%RH	261.5	58 \pm 2	66 \pm 2	69 \pm 2	
	80°C - 10%RH	29.1	63 \pm 1	66 \pm 2	75 \pm 3	
	20°C - 90%RH	15.5	52 \pm 2	58 \pm 2	70 \pm 2	
	20°C - 10%RH	1.7	63 \pm 2	72 \pm 2	80 \pm 4	
VHB 4905	80°C - 90%RH	261.5				42 \pm 4
	80°C - 10%RH	29.1				65 \pm 4
	20°C - 90%RH	15.5				91 \pm 4
	20°C - 10%RH	1.7				126 \pm 2

5.1.1 Effect of water vapor content

The water vapor content (c.f. Table 5.1) for our 4 test conditions is determined using Eq.21 ^{346,338}:

$$W \left(\frac{g}{m^3} \right) = \frac{m_{\text{water vapor}}}{V_{\text{air}}} = \frac{P_{\text{water, sat}}(T) * RH}{R_w * T} \quad (\text{Eq. 21})$$

where T is the temperature, $R_w = 0.00461 \text{ hPa m}^3 \text{ K}^{-1} \text{ g}^{-1}$, RH (%) is the relative humidity, $P_{\text{water, sat}}(T) = 473.5 \text{ hPa}$ and 23 hPa under 80°C and 20°C respectively, calculated with the Goff-Gratch equation ³³⁸.

Figure 5.2 plots the median dielectric breakdown strength against water vapor content (i.e. for different temperature and humidity conditions) for three prestretch values, for all tested materials. Increasing water vapor content leads to significant reductions in median dielectric breakdown strengths, especially under moderate and large prestretch conditions (PR 1.3 and PR 1.5 for silicone films, as well as PR 3x3 for VHB 4905 films).

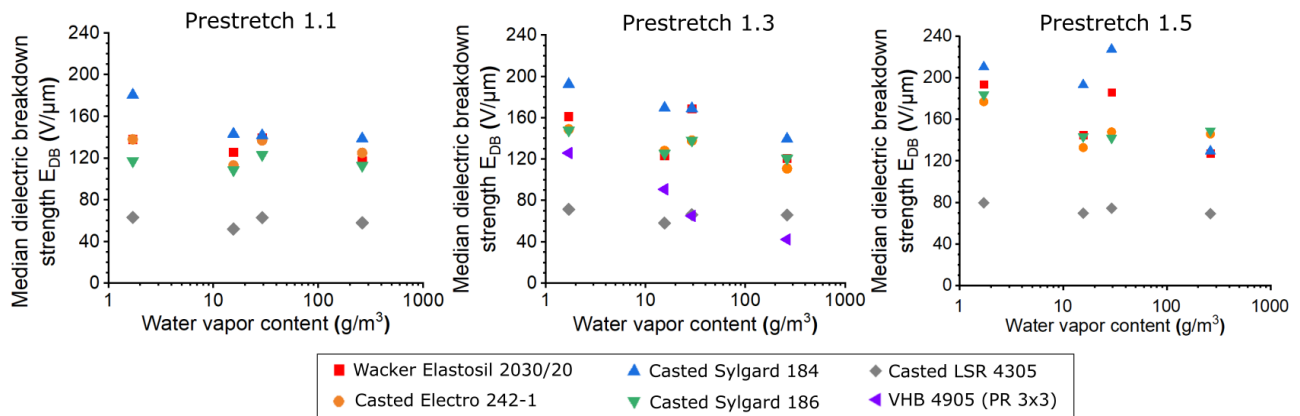


Figure 5.2: Median dielectric breakdown strengths of the investigated elastomers as a function of water vapor content (g/m³). For readability, the error bars are not displayed. For readability considerations, error bars are not shown. Standard errors are found in Table 5.1.

I observe up to 38% reduction in dielectric breakdown strength for casted Sylgard 184 (under prestretch 1.5) from our driest conditions (1.7 g m^{-3} water vapor content, i.e. 20°C -10% RH) to wettest conditions (261.7 g m^{-3} water vapor content, i.e. 80°C -90% RH). For VHB 4905 (PR 3x3), a 65% reduction dielectric breakdown strength is observed from driest to wettest conditions.

Under low prestretch (PR 1.1), dielectric breakdown strength reductions are smaller and less affected by water vapor content, as the median values of breakdown strength at low water vapor contents often overlap with the standard error of breakdown strengths at high water vapor contents (c.f. Table 5.1). The highest observed dielectric breakdown strength reduction at PR 1.1 is 25% for casted Sylgard 184 films from 20°C - 10% RH to 80°C - 90% RH.

Of the investigated silicone elastomers, Sylgard 184 has the largest decrease in dielectric breakdown strengths with increasing water vapor content: 22%, 27% and 38% decrease from 20°C -10% RH to 80°C -90% RH under PR 1.1, PR 1.3 and PR 1.5. For the same conditions, Wacker Elastosil 2030/20 exhibits breakdown field decrease of 15%, 25% and 35%, and Electro 242-1 shows decreases of 9%, 25% and 18%. Sylgard 186 shows reductions of 3%, 18% and 19%, significantly less than Sylgard 184.

The dielectric breakdown strength of LSR 4305 is the least affected by water vapor content among the investigated elastomers, with 8%, 8% and 13% reductions for the same conditions exposed above. Compared to silicones, prestretched (PR 3x3) VHB 4905's dielectric breakdown strength is more affected by water vapor content.

Figure 5.3 plots the dielectric breakdown strengths grouped by prestretch, for all 4 tested environmental conditions and for all materials.

5.1.2 Effect of temperature

The effect of temperature on the dielectric breakdown strength of silicone elastomers is less straightforward to interpret than the effect of humidity, as lower temperatures do not systematically yield higher dielectric breakdown strengths. For Sylgard 184, increasing the temperature from 20°C to 80°C decreases the median dielectric breakdown strength under most prestretch and humidity values, up to 31% for PR 1.5 and 90% RH. However, for Electro 242-1, Sylgard 186, LSR 4305 and Elastosil 2030/20, the effect of a temperature change does not lead to a clear trend in breakdown field.

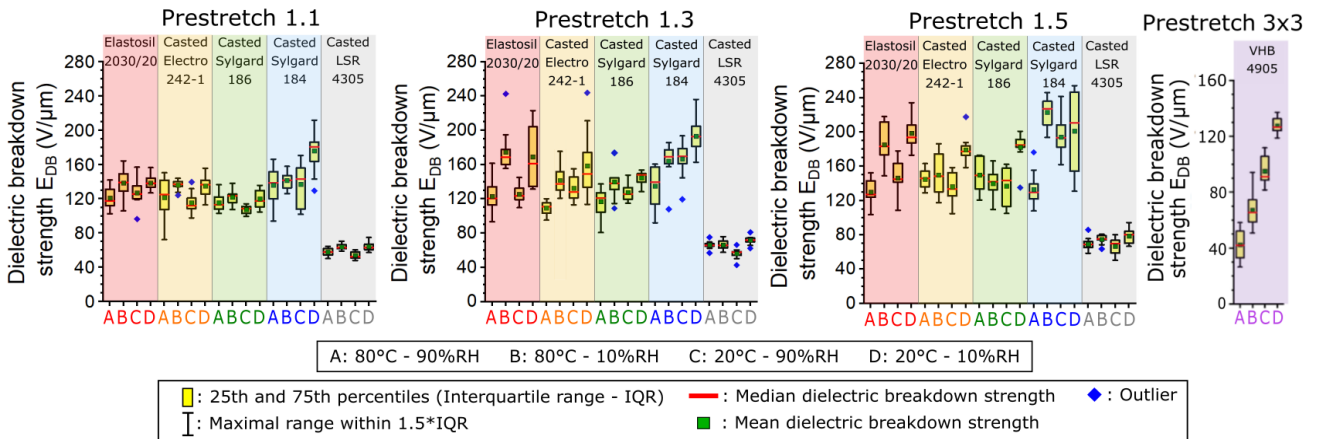


Figure 5.3: Effect of temperature, humidity and elastomer type on the dielectric breakdown strength of silicone elastomer membranes at constant equibiaxial prestretch. Dielectric breakdown strengths for VHB 4905 (Prestretch PR: 3x3) are exposed for comparison. Outliers correspond to datapoints beyond the maximal range of the whiskers defined by the lowest and highest datapoints within $1.5 \times$ of the interquartile range (IQR).

For most materials and prestretches, the interquartile ranges overlap between high (80°C) and low (20°C) temperatures. I cannot conclude that temperature induces significant changes in dielectric breakdown strength of the investigated silicone elastomers. Furthermore, the effect of temperature is material-dependent.

For VHB 4905, higher temperatures lead to significant decreases in median dielectric breakdown strength (roughly 50% drop from 20°C to 80°C). Liu et al. have previously reported that prestretched (PR 3x3) VHB 4910 films exhibit dielectric breakdown strengths of $\approx 150 \text{ V } \mu\text{m}^{-1}$ and $\approx 50 \text{ V } \mu\text{m}^{-1}$ at 20°C and 80°C respectively³⁴⁷, close to the values obtained in this work. VHB 4905 is the only material in our study for which temperature plays a larger role than humidity on dielectric breakdown strength.

Our results for commercial Elastosil 2030/20 films differ from findings by Fasolt et al.¹⁴⁷ who observed that temperature affects the dielectric breakdown strength more significantly than humidity for unstretched samples and that humidity does not change the dielectric breakdown strength.

The reduction of dielectric breakdown strength at high humidity and high temperatures, as observed in Figure 5.3, could be related to enhanced water vapor permeation and diffusion or to enhanced charge injection and migration from the electrode toward the insulating silicone elastomer under such harsh conditions, as previously reported for silicone elastomers used in high voltage insulation applications^{348–352}.

Both water vapor diffusion and charge migration would result in enhanced space charge accumulation within the silicone elastomer and a higher concentration of ionic and conductive species within the silicone elastomer as the voltage increases, thereby leading to higher local electric fields. This could locally initiate partial discharges in air-filled microcavities, triggering a dielectric breakdown event^{118,303,308}.

5.1.3 Effect of membrane prestretch

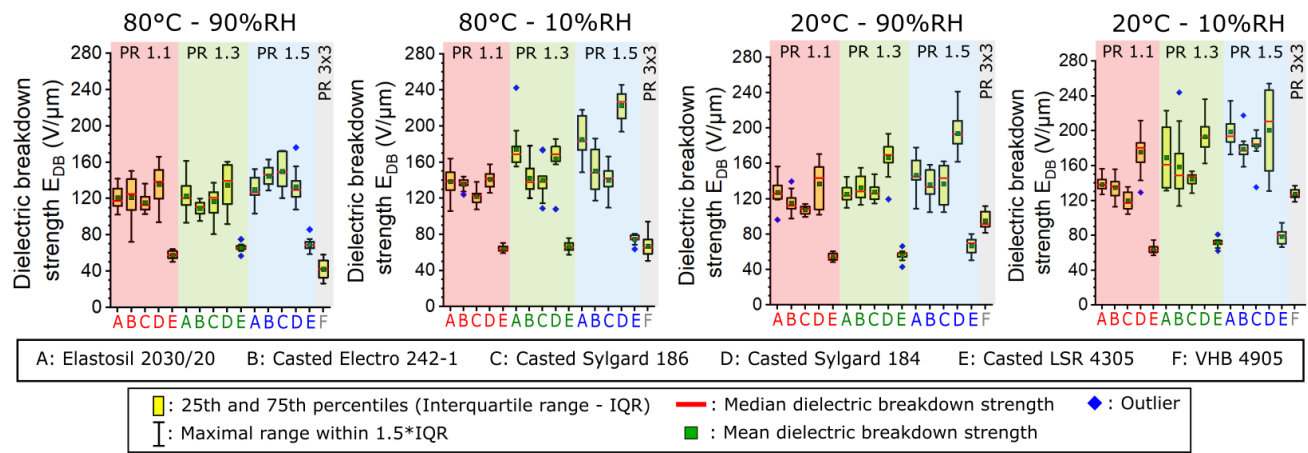


Figure 5.4: Influence of different silicone elastomer materials and membrane prestretch on the dielectric breakdown strength at constant temperature and humidity. Dielectric breakdown strengths for VHB 4905 (Prestretch PR: 3x3) are exposed for comparison. Outliers correspond to datapoints beyond the maximal range of the whiskers defined by the lowest and highest datapoints within 1.5x of the interquartile range (IQR).

Figure 5.4 plots the dielectric breakdown strengths grouped by environmental condition, for all materials and prestretches.

As shown in Figure 5.4, higher elastomer prestretch yields higher dielectric breakdown strengths in dry conditions (10% RH) for Elastosil 2030/20, Sylgard 186 and Sylgard 184. From low (PR 1.1) to moderate (PR 1.3) prestretch, the median dielectric breakdown strength of these elastomers increases between 6% to 21%. From moderate (PR 1.3) to high (PR 1.5) prestretch, the median dielectric breakdown strength increases between 13% to 37%.

For the same elastomers, I observe smaller increases in breakdown strength due to prestretch under 90% RH. From low (PR 1.1) to moderate (PR 1.3) prestretch, the median dielectric breakdown strength of these elastomers increases between -2% to 16%. From moderate (PR 1.3) to high (PR 1.5) prestretch, the median dielectric breakdown strength increases between -7% to 26%.

For LSR 4305 and casted Electro 242-1 elastomers, the median dielectric breakdown strength of these elastomers increases between 7% to 30% from low (PR 1.1) to high (PR 1.5) prestretch, but there is little increase from low (PR 1.1) to moderate (PR 1.3) prestretch.

In the literature, enhanced prestretch values on silicone elastomer membranes systematically yield higher dielectric breakdown strengths^{116,147–151}. For 30μm-thick Elastosil 2030 films, Förster-Zügel et al. reported that prestretched (PR≈1.4) films showed higher (150-190 V μm⁻¹) dielectric breakdown strengths than unstretched films (90-100 V μm⁻¹)¹⁴⁹. Similar values are found in this work for prestretched 20μm-thick Elastosil 2030/20 films.

Under low prestretch (PR 1.1) and high prestretch (PR 1.5), all silicone elastomers present similar dielectric breakdown strengths, except LSR 4305 which has lower dielectric breakdown strengths. At PR 1.3, casted Sylgard 184 has the highest dielectric breakdown strengths except at 80°C – 90% RH.

VHB has similar dielectric breakdown strengths as silicone elastomers at prestretch 1.1 at 20°C – 10% RH. However, the breakdown strength decreases strongly at 20°C-90% RH and decreases yet further at 80°C-10% RH and 80°C-90% RH, where it has a lower dielectric breakdown strength than LSR 4305. This notable decrease with larger humidity and temperatures reveals that VHB 4905 is not an ideal elastomer for DEAs which should operate under high temperature and/or high humidity environments. Silicones are better suited for such conditions.

Here, higher prestretch values are also associated with decreased elastomer membrane thickness, because all membranes are pre-stretched from similar initial thickness (c.f. Table 4.1 in section 4.1.1). The observed increase in dielectric breakdown strength with higher prestretch could hence also be due to a decrease in film thickness. To distinguish the effect of membrane thickness from the effect of prestretch on dielectric breakdown strength, further tests with different prestretches for a given final elastomer film thickness would be needed.

5.2 Figures of merit of silicone elastomer membranes for DEAs

To compare the strain performance of different elastomers, the following figure of merit was introduced by P. Sommer-Larsen and A.L. Larsen ³⁵³:

$$Fom_{strain} = \frac{3\varepsilon_0\varepsilon_r E_{DB}^2}{Y} \quad (Eq. 22)$$

where E_{DB} is the median dielectric breakdown strength. This figure of merit is the maximal strain that could theoretically be obtained for a dielectric material with a given Young's modulus (Y), relative permittivity (ε_r) and dielectric breakdown strength (E_{DB}), ignoring non-linear effects.

To compare the maximal force per unit area for different DEAs, the maximal theoretical Maxwell pressure can be used as a figure of merit:

$$Fom_{stress} = \sigma_{max} = 3\varepsilon_0\varepsilon_r E_{DB}^2 \quad (Eq. 23)$$

Although both figures of merit allow different elastomers to be compared in terms of strain and force performance, factors such as dielectric losses, non-linear mechanical properties, operational lifetime, time-dependent fatigue and creep behavior as well as manufacturing-related aspects are not considered.

The stress (Fom_{stress}) and strain (Fom_{strain}) DEA figures of merit are dependent on the dielectric breakdown strength, permittivity, and for Fom_{strain} also on Young's modulus of the elastomer. Therefore, humidity, temperature and prestretch directly impact the figures of merit. This section presents how Fom_{stress} and Fom_{strain} are affected by these parameters. Dielectric breakdown strength data is shown in Section 5.1, and Young's moduli data is shown in Section 5.4.

As shown in Figure 5.5, an increase in equibiaxial prestretch generally increases the stress figure of merit (Fom_{stress}) for casted Sylgard 184, and Elastosil 2030/20, whereas casted Sylgard 186, casted Electro 242-1 and casted LSR4305 only display slight increases. However, increasing the equibiaxial prestretch is detrimental for the strain figures of merit (Fom_{strain}) of the investigated silicone elastomers, because of the increase in Young's modulus with increasing prestretch (c.f. Section 5.4).

Higher humidity levels at constant temperature decrease both stress (Fom_{stress}) and strain (Fom_{strain}) figures of merit, especially under PR 1.3 and PR 1.5. Changing from dry (10% RH) environments to wet (90% RH) environments generally leads to 20-60% decrease in stress (Fom_{stress}) and strain (Fom_{strain}) figures of merit, up to 70% decrease depending on the type of elastomer and its prestretch, owing to the reduction in dielectric breakdown strength with increasing relative humidity. However, in some conditions, no decrease in figures of merit with increasing humidity is observed.

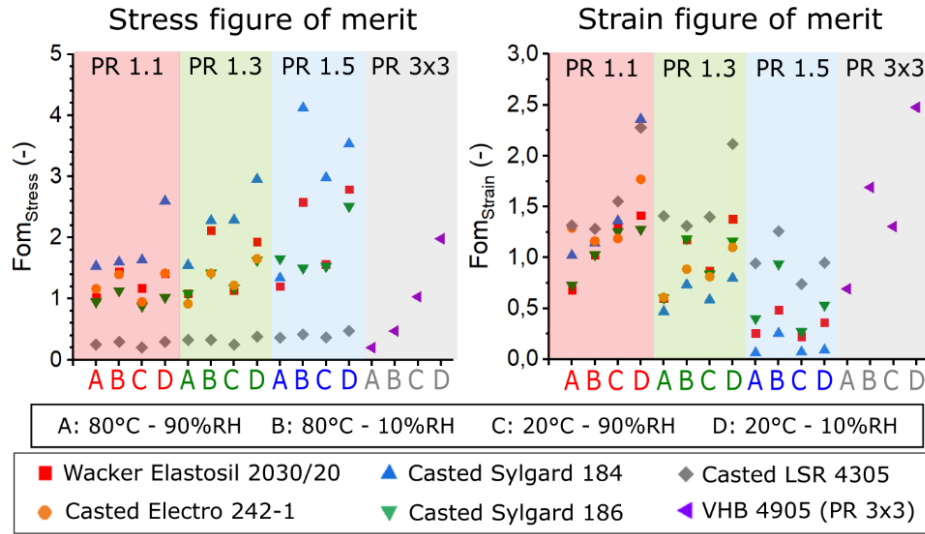


Figure 5.5: DEA figures of merit for stress (left) and for strain (right) of silicone elastomer membranes under different equibiaxial prestretch, temperature and humidity levels. Figures of merit for VHB 4905 (Prestretch PR: 3x3) are exposed for comparison. For readability concerns, the error bars are not displayed. For readability considerations, error bars are not shown.

Higher temperatures at constant humidity can also affect the Fom_{stress} , although their effect is generally less pronounced, with only 10-30% decreases. However, temperature becomes an important factor for the Fom_{strain} , where 10-60% reductions are often encountered, owing to the differences in elastomer stiffness.

Overall, Sylgard 184 presents the highest Fom_{stress} among the investigated elastomers, i.e. DEAs made of Sylgard 184 membranes could theoretically deliver the largest actuation pressures and forces. LSR 4305 has the lowest stiffness, and the highest Fom_{strain} , i.e. LSR 4305 DEAs could theoretically deliver the largest actuation strains.

At 20°C, comparable Fom_{strain} of approximately 2 are computed for VHB 4905 (PR 3x3), LSR 4305 (PR 1.1) and Sylgard 184 (PR 1.1). However, the Fom_{strain} equation does not hold for non-linear behavior in highly prestretched elastomers³⁵³ such as VHB 4905 (PR 3x3). VHB 4905 can in practice reach significantly higher strains than silicone elastomers⁴. However, VHB exhibits drawbacks such as high viscous losses, slow actuation response, crack growth and a creep over time⁹⁷.

5.3 Water vapor permeability of silicone elastomer membranes for DEAs

This section presents the results on the water vapor permeability of prestretched silicone elastomer membranes which are summarized in Table 5.2. In water vapor permeability experiments (c.f. section 4.2.2), the weight increase owing to water vapor permeating through unprestretched silicone membranes (30-60 μm thick) is monitored over time, yielding the plots on Figure 5.6.

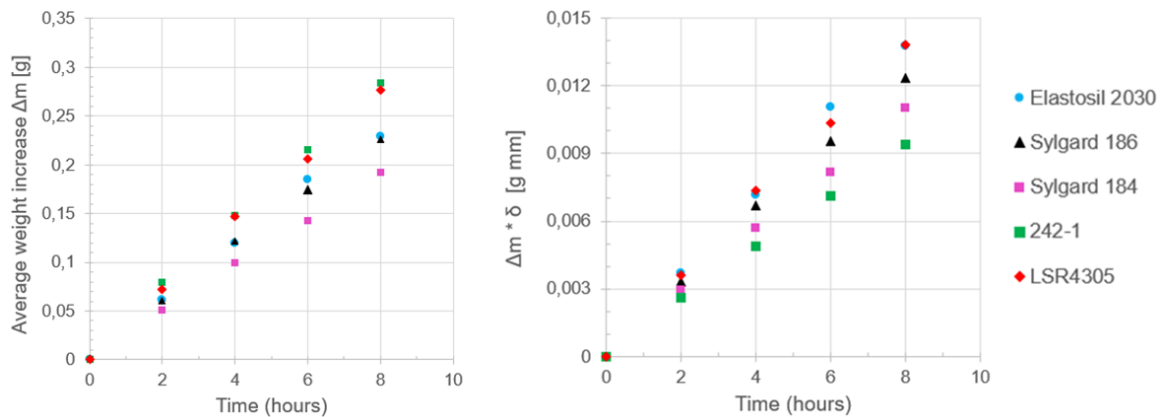


Figure 5.6: a) Average weight increase (on 3 specimens) vs. time owing to water vapor that permeates through the unprestretched silicone membranes at 23°C – 50% RH. b) Average thickness-normalized weight increase (on 3 specimens) vs. time for unprestretched membranes at 23°C – 50% RH. For readability considerations, error bars are not shown.

Figure 5.6 shows that the average weight increase (without (a) and with (b) thickness normalization) does not significantly vary among the investigated silicone elastomer materials. After thickness normalization, Elastosil 2030/20 and LSR 4305 show the highest permeated water vapor weight increase (with 0.014 g mm after 8 hours under 23°C-50% RH), whereas Electro 242-1 shows the lowest thickness normalized weight increase (with 0.009 g mm after 8 hours under 23°C-50% RH, i.e. a factor 0.6x vs. Elastosil 2030/20).

Table 5.2: Water vapor transmission rate (WVTR), water vapor permeance and water vapor permeability for silicone elastomer membranes. WVTR is calculated with equation Eq. 10, water vapor permeance with equation Eq. 12, and water vapor permeability with equation Eq. 13 in section 4.2.2.

Elastomer material	Measured specimen thicknesses [μm]	WVTR [$\text{g day}^{-1} \text{m}^{-2}$]	Water vapor permeance [$\text{g Pa}^{-1} \text{day}^{-1} \text{m}^{-2}$]	Water vapor permeability [$\text{g mm Pa}^{-1} \text{day}^{-1} \text{m}^{-2}$]
Elastosil 2030/20 film	60, 60, 60	250 ± 5	0.179 ± 0.006	$(10.7 \pm 0.4) 10^{-3}$
Sylgard 186 (lab-casted A:B 10:1)	47, 53, 64	245 ± 4	0.175 ± 0.004	$(9.6 \pm 0.4) 10^{-3}$
Sylgard 184 (lab-casted A:B 10:1)	59, 57, 56	205 ± 3	0.146 ± 0.004	$(8.4 \pm 0.3) 10^{-3}$
Electro 242-1 (lab-casted A:B 1:1)	36, 29, 33	305 ± 5	0.218 ± 0.006	$(7.2 \pm 0.3) 10^{-3}$
LSR 4305 (lab-casted A:B 1:1)	53, 47, 50	296 ± 3	0.211 ± 0.006	$(10.6 \pm 0.4) 10^{-3}$

Table 5.2 shows that the water vapor permeability is lowest for Electro 242-1, with $(7.2 \pm 0.3) \cdot 10^{-3} \text{ g mm Pa}^{-1} \text{ day}^{-1} \text{ m}^{-2}$, a factor 0.7x of Elastosil 2030/20's water vapor permeability with $(10.7 \pm 0.4) \cdot 10^{-3} \text{ g mm Pa}^{-1} \text{ day}^{-1} \text{ m}^{-2}$. The higher water vapor permeance and water vapor transmission rates (WVTR) observed in Electro 242-1 with respect to Elastosil 2030/20 are owing to the lower elastomer thickness used for Electro 242-1 samples vs. Elastosil 2030/20 samples. The difference in water vapor permeability between Electro 242-1 and Elastosil 2030/20 membranes could be due to differences within the elastomer formulation and its intrinsic properties, but there is no extensive investigation to demonstrate what fundamentally influences water vapor permeability.

The water vapor permeability of LSR 4305 ($\approx 0.15 \text{ MPa}$ at low strain) is similar to Elastosil 2030/20 ($\approx 1 \text{ MPa}$ at low strain), even though they have significantly different Young's moduli (c.f. Section 5.4). Both Sylgard 186 and Sylgard 184 show lower water vapor permeability vs. Elastosil 2030/20, yet higher permeability than for Electro 242-1 membranes.

The conclusion of this section is that changing the type of silicone elastomer material does not significantly change water vapor transmission rates and water vapor permeability. The highest difference in water vapor permeability vs. Elastosil 2030/20 is for Electro 242-1, with a factor 0.7x.

5.4 Mechanical characterization of silicone elastomer membranes for DEAs

This section presents the stress-strain curves and the calculated Young's moduli of silicone elastomer membranes, determined with 70 mm x 12 mm x 20 μm (length x width x thickness) pure shear specimens with a mechanical test bench presented in Section 4.2.1.

Figure 5.7 shows the true stress – engineering strain curves of silicone elastomers at 20°C. Figure 5.8 shows the true stress – engineering strain curves of silicone elastomers at 80°C. True stress is calculated from the measured force (via a 10 N force sensor in the mechanical test bench) using Equation Eq.9 from section 4.2.1.

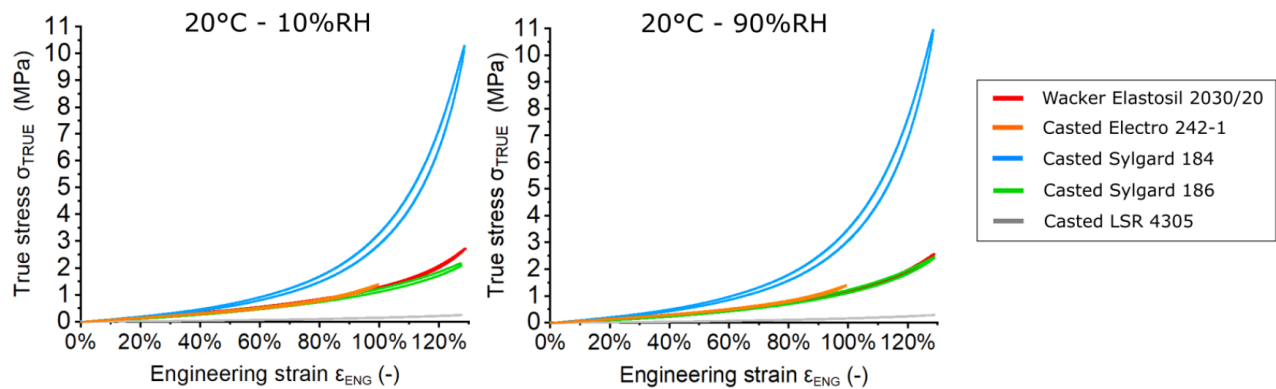


Figure 5.7: True stress – engineering strain plots for the investigated silicone elastomers at 20°C. Only the second cycle is shown here. Young's moduli from Table 5.3 are calculated as the slope of the curves around the engineering strain values using Origin.

Figures 5.7 and 5.8 show that Sylgard 184 membranes are significantly stiffer than Elastosil 2030/20, casted Electro 242-1, and casted Sylgard 186 membranes. LSR 4305 is the least stiff elastomer, with significantly lower true stress at high engineering strains (reaching < 0.5 MPa at most).

Increasing the relative humidity at constant temperature generally does not significantly affect the true stress – engineering strain curves for the studied silicone elastomer membranes or Young's modulus. Increasing the temperature from 20°C to 80°C generally stiffens silicone elastomers up to $\approx 70\%$ engineering strains (c.f. Table 5.3), and yields a significant softening at high engineering strains ($> 100\%$ engineering strains) which affects the true stress – engineering strain curves.

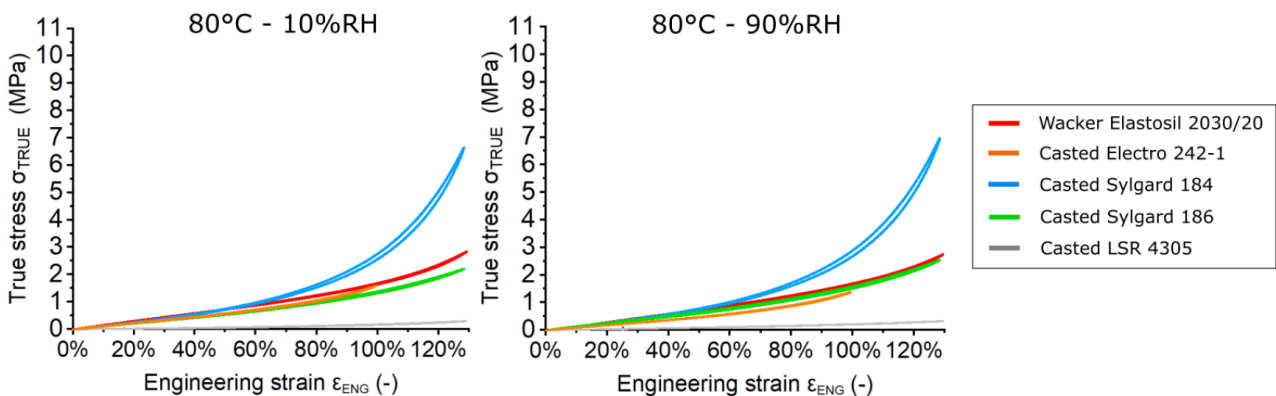


Figure 5.8: True stress – engineering strain plots for the investigated silicone elastomers at 80°C. Only the second cycle is shown here. Young's moduli from Table 5.3 are calculated as the slope of the curves around the engineering strain values using Origin.

Table 5.3 shows the values of Young's moduli calculated from the true stress – engineering strain curves. Used values of engineering strain in Table 5.3 correspond to equibiaxial prestretch of 1.1 (i.e. 21% uniaxial), equibiaxial prestretch of 1.3 (i.e. 69% uniaxial), equibiaxial prestretch of 1.5 (i.e. 125% uniaxial), which are selected to characterize dielectric breakdown strength (c.f. Section 5.1) and DEA figures of merit (c.f. Section 5.2).

Table 5.3 shows that the Young's modulus (at constant engineering strain) is generally not significantly affected by relative humidity at constant temperature. However, increasing temperature from 20°C to 80°C at constant humidity slightly increases the Young's modulus at constant engineering strain of 5%, 21%, and 69%, whereas it slightly decreases Young's modulus at high engineering strain (125%) for Elastosil 2030/20, Sylgard 186, and LSR 4305. For Sylgard 184, the decrease in Young's modulus with higher temperature occurs also at 69% engineering strain.

Table 5.3: Young's moduli of the investigated silicone elastomers at 5%, 21%, 69%, and 125% engineering strain. Young's moduli are calculated from Figures 5.7 and 5.8 from the slope of the true stress – engineering strain curves around the respective engineering strain values, using Origin software.

Material	Condition	Thickness δ	$Y_{\epsilon=5\%}$ [MPa]	$Y_{\epsilon=21\%}$ [MPa]	$Y_{\epsilon=69\%}$ [MPa]	$Y_{\epsilon=125\%}$ [MPa]
Wacker Elastosil 2030/20	80°C - 90%RH	20 ± 1 μm	1.4 ± 0.1	1.5 ± 0.1	1.8 ± 0.1	4.7 ± 0.2
	80°C - 10%RH	20 ± 1 μm	1.5 ± 0.1	1.4 ± 0.1	1.8 ± 0.1	5.3 ± 0.2
	20°C - 90%RH	20 ± 1 μm	1.0 ± 0.1	0.9 ± 0.1	1.3 ± 0.1	7.0 ± 0.3
	20°C - 10%RH	20 ± 1 μm	1.1 ± 0.1	1.0 ± 0.1	1.4 ± 0.1	7.7 ± 0.4
Casted Sylgard 186	80°C - 90%RH	22 ± 1 μm	1.4 ± 0.1	1.3 ± 0.1	1.8 ± 0.1	4.1 ± 0.2
	80°C - 10%RH	23 ± 1 μm	1.2 ± 0.1	1.1 ± 0.1	1.2 ± 0.1	1.6 ± 0.1
	20°C - 90%RH	23 ± 1 μm	0.7 ± 0.1	0.7 ± 0.1	1.4 ± 0.1	5.6 ± 0.2
	20°C - 10%RH	22 ± 2 μm	0.8 ± 0.1	0.8 ± 0.1	1.4 ± 0.1	4.7 ± 0.2
Casted Sylgard 184	80°C - 90%RH	22 ± 2 μm	1.4 ± 0.1	1.5 ± 0.1	3.3 ± 0.2	21 ± 1
	80°C - 10%RH	22 ± 1 μm	1.3 ± 0.1	1.4 ± 0.1	3.1 ± 0.2	16 ± 1
	20°C - 90%RH	23 ± 1 μm	1.0 ± 0.1	1.2 ± 0.1	3.9 ± 0.2	41 ± 1
	20°C - 10%RH	22 ± 1 μm	1.0 ± 0.1	1.1 ± 0.1	3.7 ± 0.2	39 ± 2
Casted Electro 242-1	80°C - 90%RH	24 ± 2 μm	0.9 ± 0.1	0.9 ± 0.1	1.5 ± 0.1	
	80°C - 10%RH	23 ± 1 μm	1.3 ± 0.1	1.2 ± 0.1	1.6 ± 0.1	
	20°C - 90%RH	22 ± 1 μm	0.8 ± 0.1	0.8 ± 0.1	1.5 ± 0.1	
	20°C - 10%RH	23 ± 1 μm	0.9 ± 0.1	0.8 ± 0.1	1.5 ± 0.1	
Casted LSR 4305	80°C - 90%RH	24 ± 2 μm	0.19 ± 0.01	0.19 ± 0.01	0.23 ± 0.01	0.38 ± 0.02
	80°C - 10%RH	25 ± 1 μm	0.27 ± 0.01	0.23 ± 0.01	0.25 ± 0.01	0.33 ± 0.01
	20°C - 90%RH	25 ± 1 μm	0.13 ± 0.01	0.13 ± 0.01	0.18 ± 0.01	0.49 ± 0.02
	20°C - 10%RH	25 ± 2 μm	0.15 ± 0.01	0.13 ± 0.01	0.18 ± 0.01	0.50 ± 0.02

Increases in Young's modulus with temperature are typical for elastomers because of entropic spring behavior³⁵⁴. Observed differences in Young's modulus and in stress-strain curves between materials is more complex because it is dependent of fillers (e.g. type, concentration), on molecular structure (e.g. molecular chain length, crosslink density) and on crosslinking conditions (e.g. curing temperature, curing time, post-curing). I did not conduct in-depth characterization studies on these silicone elastomer formulations to correlate the observed Young's moduli variations with the intrinsic properties of the elastomers.

5.5 Summary of key findings

This chapter presents how humidity, temperature and prestretch influence the dielectric breakdowns strength, Young's modulus, water vapor permeability, and DEA figures of merit (i.e. maximum force and strain that DEAs can generate) for several commercial silicone elastomers.

The investigated silicone elastomer films (20-25 μm thick) show dielectric breakdown strengths in the range of 110 V μm^{-1} to 210 V μm^{-1} , except LSR 4305 with values from 50 V μm^{-1} to 80 V μm^{-1} . Thin (30-60 μm) silicone elastomers show similar water vapor transmission rates (between 200 and 310 g day⁻¹ m⁻²) and similar water vapor permeability (from 7 to 11 * 10⁻³ g mm Pa⁻¹ day⁻¹ m⁻²). At uniaxial stretch of 69% (equivalent to equibiaxial prestretch of 1.3), the investigated silicone elastomer films exhibit Young's moduli between 1.2 to 1.8 MPa, except LSR 4305 with Young's moduli around 0.2 MPa, and Sylgard 184 with Young's moduli between 3.1 and 3.9 MPa.

Increasing the prestretch of the silicone membrane is an effective strategy to increase the dielectric breakdown strength of silicone elastomers under dry conditions, but leads to lower strain due to higher Young's moduli. Under humid conditions, only limited breakdown strength increases are observed by prestretching.

Prestretched silicone elastomers exhibit 2%-38% reductions in dielectric breakdown strengths with water vapor content increase from 1.7g m⁻³ (20°C – 10% RH) to 261.7 g m⁻³ (80°C – 90% RH). Higher humidity leads to decreased dielectric breakdown strengths in

silicone elastomers, with up to 43% reductions under moderate (PR 1.3) and larger (PR 1.5) prestretch, and limited (2%-10%) reductions under lower prestretch (PR 1.1).

Humidity has a larger influence than temperature on lowering the dielectric breakdown strength of the investigated silicone elastomers. Increasing the temperature from 20°C to 80°C leads up to 30% lower breakdown strengths for prestretched silicone membranes.

Higher prestretch generally enhances the stress figure of merit because of higher dielectric breakdown strengths, and reduces the strain figure of merit of silicone elastomers owing to increased Young's moduli at high prestretch. The stress figure of merit falls by 10%-30% when enhancing temperature from 20°C to 80°C and by 20%-70% when enhancing relative humidity from 10% RH to 90% RH. The strain figure of merit falls by 10%-60% when enhancing temperature from 20°C to 80°C and by 20%-70% when enhancing relative humidity from 10% RH to 90% RH. For silicone elastomers, casted Sylgard 184 shows the highest stress figures of merit and casted LSR 4305 the highest strain figures of merit under all investigated conditions.

The next chapter presents the DC lifetime investigations conducted in equibiaxially prestretched (PR=1.3) silicone-based expanding circle DEAs. The operation voltages are selected such that the operation electric field is between 50% to 90% of dielectric breakdown strength for lifetime studies within reasonable timeframes (from minutes to weeks).

Chapter 6 DC Lifetime of equibiaxially pre-stretched single-layer silicone-based DEAs

In this chapter, I present data on DC lifetime of equibiaxially prestretched single-layer silicone-based DEAs with expanding circle electrodes. Section 6.1 presents an overview of the evolution of strain and electrode resistance over time and voltage (in Elastosil 2030/20 DEAs). Section 6.2 shows the influence of elastomer material selection on DC DEA lifetime. Section 6.3 shows the effect of electric field on DC DEA lifetime. Section 6.4 presents the effect of temperature and relative humidity on DC DEA lifetime. Section 6.5 presents the effect of encapsulation layer on DC DEA lifetime, with an extended discussion on DC lifetime – actuation strain tradeoff. Section 6.6 shows the influence of the electrode material selection on DC DEA lifetime. Section 6.7 presents the influence of applying DC polarity reversal on DC DEA lifetime. The data, text and figures of Sections 6.1, 6.2, 6.3. and 6.5 were published in ³²⁸ (3), data, text and figures of Section 6.1, and 6.6 were published in ³²⁹ (4), whereas data and figures of Section 6.7 were published in ²⁶ (5).

The list of investigated silicone elastomer materials, their mixing ratios, and their properties (c.f. Chapter 5) are summarized in Table 6.1.

Table 6.1: List of investigated silicone elastomer materials with measured film thickness before prestretch and properties ^{142,196,327,333}.

Elastomer material	Type	Specificity	Relative permittivity (ϵ_r) [-]	Young's modulus (Y) @ 20°C - 90% RH [MPa]	Water vapor transmission WVTR [$\text{g day}^{-1} \text{m}^{-2}$]	Breakdown strength @ 20°C – 90% RH	Measured film thickness [μm]
Elastosil 2030/20	Commercial film	Standard film of homogeneous thickness	2.8 ¹⁴²	1.3 ± 0.1 ³²⁷	250 ± 5	123 ± 4	20 ± 1
Elastosil 2030/20 (A:B 1:1)	Blade-casted (in a clean-room)	Casted formulation of Elastosil 2030/20	N.D.	N.D.	259 ± 5	N.D.	21 ± 1
Sylgard 186 (A:B 10:1)		Casted formulation of similar modulus	2.8 (1 Hz) ³³³	1.4 ± 0.1 ³²⁷	245 ± 4	126 ± 4	22 ± 2
Sylgard 184 (A:B 10:1)		Casted formulation of high modulus	3.0 (1 Hz) ³³³	3.9 ± 0.1 ³²⁷	205 ± 4	170 ± 8	24 ± 2
Electro 242-1 (A:B 1:1)		Casted formulation of higher lifetimes	2.7 *	1.5 ± 0.1 ³²⁷	305 ± 5	128 ± 5	25 ± 2
LSR 4305 (A:B 1:1)		Casted formulation of low modulus	2.9 ¹⁹⁶	0.18 ± 0.01 ³²⁷	296 ± 3	58 ± 2	22 ± 2

* According to the manufacturer

6.1 Actuation : strain and resistance

This section discusses the evolution of DEA actuation strain and electrode resistance over time and over voltage for silicone-based DEAs (equibiaxially prestretched, 1.3) tested under DC fields using the MAPLE automated setup ²⁶ (c.f. Section 4.3). The DEAs are maintained under constant DC fields, and, every hour, a ramp from 0 V to the high voltage set DC field is carried out to extract strain and electrode resistance vs. voltage plots ^{26,328}. All DEAs are preconditioned for 1 hour under fixed environmental conditions before the launch of the DC lifetime tests.

(3) Beco Albuquerque, F. and Shea, H., "Influence of electric field, temperature, humidity, elastomer material, and encapsulation on the lifetime of dielectric elastomer actuators (DEAs) under DC actuation," *Smart Mater. Struct.* **30**, 125022 (2021).

(4) Beco Albuquerque, F. and Shea, H. R., "Effect of electrode composition and patterning method on the lifetime of silicone-based dielectric elastomer actuators (DEA) under different environmental conditions," *Electroact. Polym. Actuators Devices XXIII* **11587**(115871B), 115871B (2021).

(5) Kühnel, D., Beco Albuquerque, F., Py, V. and Shea, H., "Automated test setup to quantify the lifetime of dielectric elastomer actuators under a wide range of operating conditions," *Smart Mater. Struct.* **30**(065020) (2021).

Figure 6.1 shows the change of DEA strain (Figure 6.1a), actuation strain (Figure 6.1b), and electrode resistance (Figure 6.1c) over time for Elastosil 2030/20 DEAs with pad-printed electrodes at $100 \text{ V}/\mu\text{m}$ under four environmental conditions ($85^\circ\text{C} - 85\% \text{ RH}$, $85^\circ\text{C} - 20\% \text{ RH}$, $20^\circ\text{C} - 90\% \text{ RH}$, and $20^\circ\text{C} - 30\% \text{ RH}$). Yellow crosses indicate DEA failures, which occur by dielectric breakdown, not by membrane tearing.

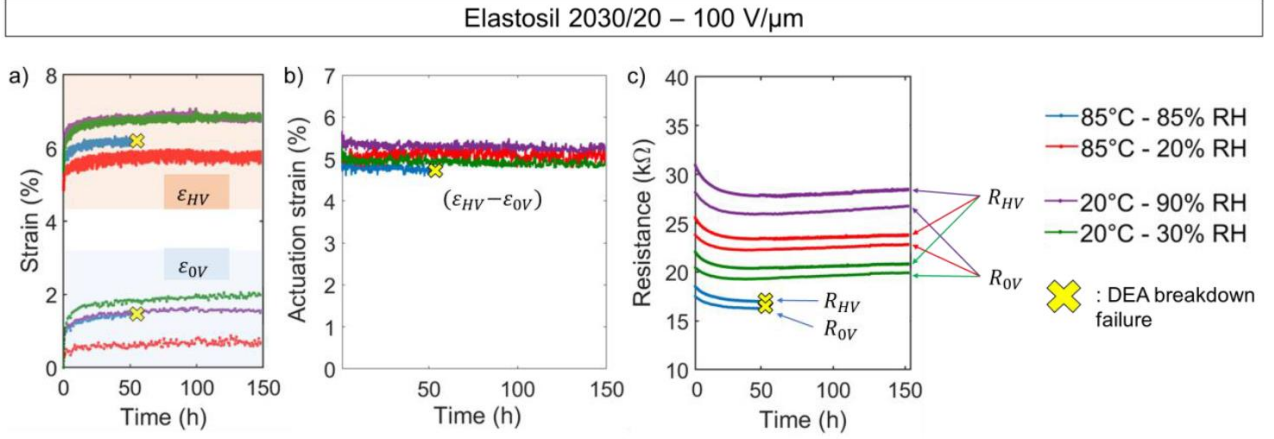


Figure 6.1: Elastosil 2030/20 DEAs with pad-printed electrodes at $100 \text{ V}/\mu\text{m}$. a) Linear strain of DEAs at $0 \text{ V}/\mu\text{m}$ (ϵ_{0V} , i.e. permanent set) and at $100 \text{ V}/\mu\text{m}$ (ϵ_{HV}), b) actuation strain, and c) electrode resistance (at $0 \text{ V}/\mu\text{m}$ and at $100 \text{ V}/\mu\text{m}$) vs. time under four environmental conditions. A yellow cross indicates a DEA failure.

The strain (ϵ_{HV}) of DEAs remains stable over time, except during the first hours of DC actuation, where the strain slightly increases, owing to the permanent set (ϵ_{0V}), well known for elastomers^{158,159}. The permanent set stabilizes below 2% and is not found to depend on environmental conditions. I observe that the actuation strain ($\epsilon_{HV} - \epsilon_{0V}$) is relatively stable over time. In the next subsections, the actuation strain is reported in tables for each tested condition.

The electrode resistance of the pad-printed DEAs slightly decreases over the first hours of actuation, then stabilizes at around 15 – 30 kΩ for hundreds of hours, indicating that no significant electrode degradation takes place in our DC-actuated DEAs. The electrode resistance at 0 V decreases over the initial hours, while the permanent set (ϵ_{0V}) increases. There is no explanation for this behavior. No significant change in resistance or strain was observed in the seconds preceding dielectric breakdown for all studied DEAs.

Figure 6.2 shows how strain evolves over time for silicone-based DEAs made with pad-printed, inkjet-printed and dry carbon powder electrodes (c.f. Section 6.6). DEAs exhibit a stable strain after the initial first hours of actuation, regardless of the electrode material used. During the first hours of actuation, the increase of the strain at high voltage (HV) is tightly correlated to the increase in strain at 0 V for all DEAs, and I observe between 0.5% and 1.7% permanent set. There is no observable dependence of permanent set on the type of electrode material.

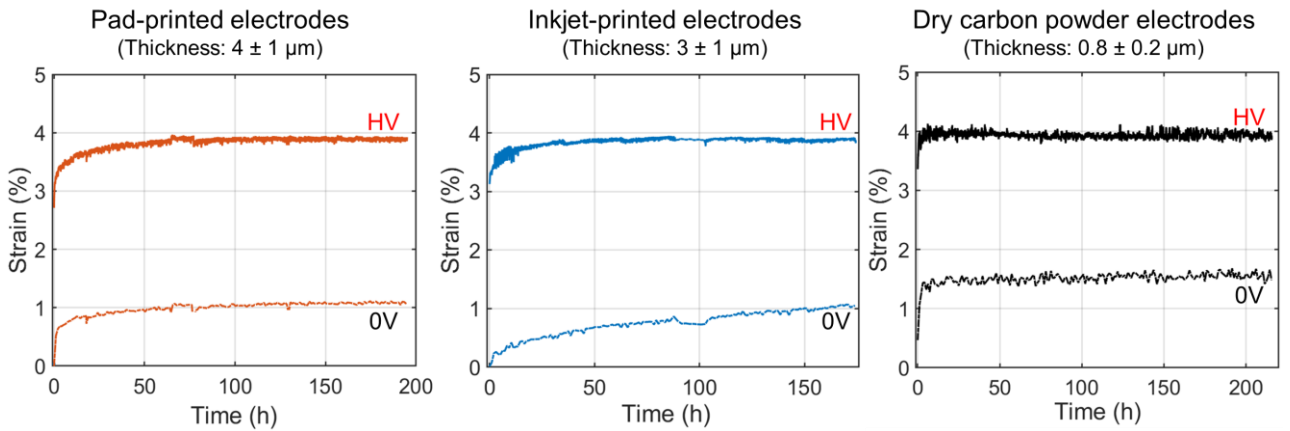


Figure 6.2: Evolution of strain at high voltage (HV, monitored every 10 seconds) and at no voltage (0 V, monitored every hour) for individual Elastosil 2030/20 DEAs made with pad-printed, inkjet-printed and dry carbon powder electrodes. DEAs with pad-printed and inkjet-printed electrodes are actuated at 1100 V ($90 \text{ V}/\mu\text{m}$) and DEAs with dry carbon powder electrodes are actuated at 600 V ($50 \text{ V}/\mu\text{m}$), in order to have the same strain for all material systems. The DEAs are operated at $20^\circ\text{C} - 30\% \text{ RH}$.

All DEAs failed by a sudden dielectric breakdown, and no significant change in strain was observed just before the breakdown events, i.e. I do not see any warning that failure is about to occur.

Dielectric breakdown of silicone-based DEAs systematically yields a pinhole of 100-300 μm diameter which can be observed by naked eye (Figure 6.3a), and with an optical microscope (Figure 6.3b).

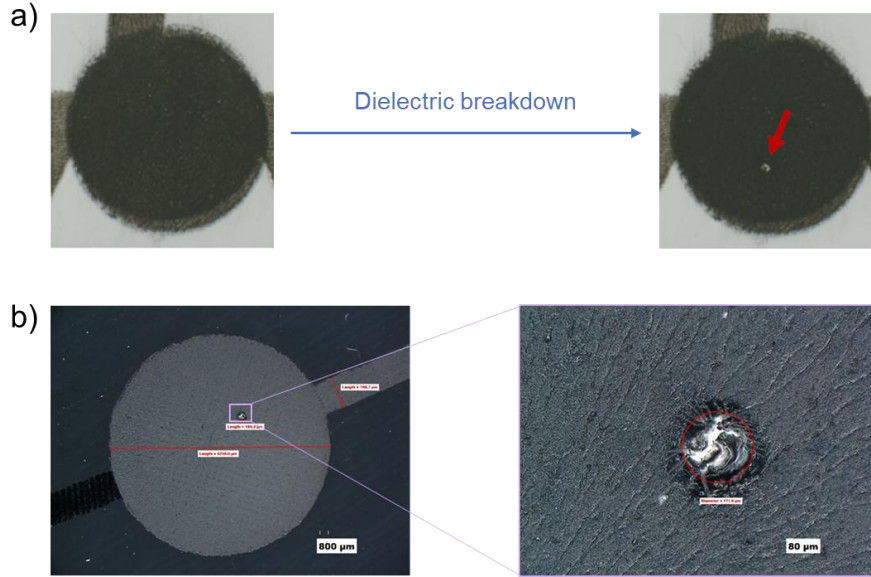


Figure 6.3: a) Upon dielectric breakdown of silicone-based DEAs with 5 mm diameter carbon black-PDMS pad-printed electrodes, a pinhole bridging the opposite electrodes is systematically observed within the electrode surface area. b) Optical microscope view of a pinhole site in DEA.

The pinhole is systematically found in the surface where the electrodes are sandwiching the silicone membrane. The exact location of the pinhole is stochastic, and can be either at the edges of the electrodes, or anywhere within the electrode. I have not conducted any detailed investigation to evaluate whether there is a preferential site for dielectric breakdown pinhole to occur (e.g. around defects or regions of thinner membrane thickness). Right after dielectric breakdown (approximately ms-s after breakdown), tearing is likely to occur in around 20% of the DEAs, and the ratio does not seem to be dependent on environmental conditions, although a rigorous study has not been conducted to quantitatively confirm that. Mechanical tearing right before dielectric breakdown did not occur in any DEAs tested, implying that the tearing is the result of the crack induced by the dielectric breakdown, which then propagates because of the membrane prestretch.

Figure 6.4 presents strain – voltage (Figure 6.4a) and strain – electric field (Figure 6.4b) plots for Elastosil 2030/20 DEAs under different environmental conditions. I observe that neither humidity nor temperature significantly affect DEA strain at constant voltage or field. Therefore, Elastosil 2030/20 DEAs exhibit a reproducible and reliable strain performance regardless of the operational humidity and temperature conditions.

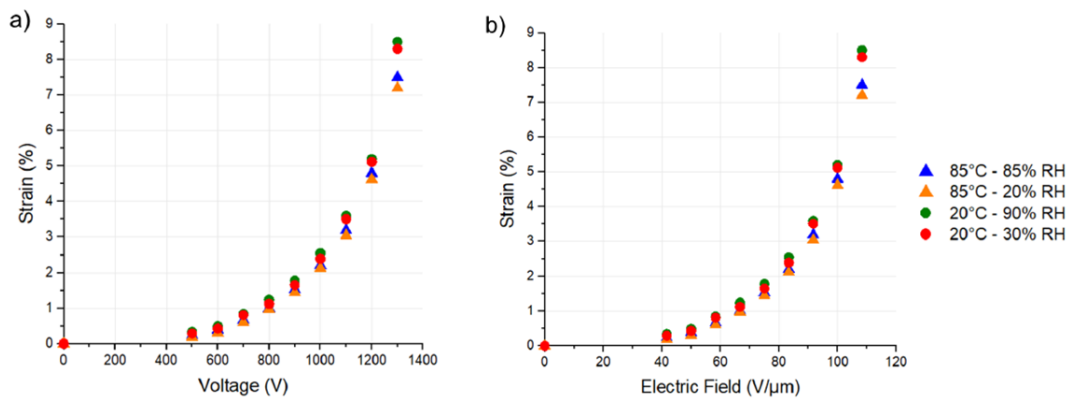


Figure 6.4: a) Strain vs. voltage and b) strain vs. field plots for Elastosil 2030/20 DEAs with pad-printed electrodes up to 1300 V (i.e. 110 $\text{V}/\mu\text{m}$) under different environmental conditions. The strain values reported here correspond to average values on 6 DEAs, and are recorded during the initial ramp cycle, i.e. later cycles and permanent set are not considered. The strain – voltage and strain – field curves are independent of environmental conditions within the tested range. For readability considerations, error bars are not shown.

Figure 6.5 shows electrode resistance – voltage plots for Elastosil 2030/20 DEAs with pad-printed electrodes under different environmental conditions and over actuation time. I observe that the electrode resistance is around 20 – 40 k Ω , regardless of the environmental conditions and that it increases with increasing applied voltage, as higher strains elongate the average distance between the conductive carbon black particles of the carbon black – PDMS electrode, therefore leading to a decrease of conductivity. However, the increase of resistance is not significant. During the initial actuation hour (e.g. between ramp 1 at 0 h and ramp 2 at 1 h), electrode resistance is found to moderately increase. After the first hour, the resistance vs. voltage curve remains stable and relatively reproducible, indicating no significant electrode degradation.

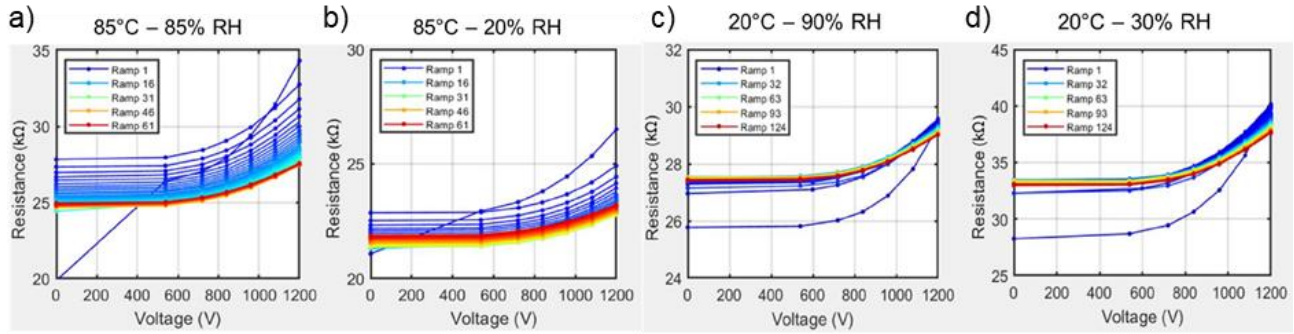


Figure 6.5: a) Resistance vs. voltage plots for Elastosil 2030/20 DEAs with pad-printed electrodes up to 1200 V (i.e. 100 V/ μ m) under different environmental conditions. The resistance values reported here correspond to 1 DEA, and are recorded during each ramp cycle (1 ramp cycle = 1 h of DC actuation at 100 V/ μ m). The resistance-voltage curves are relatively independent of environmental conditions within the tested range, and are relatively stable over actuation time after the initial first hour, where a moderate increase in resistance is witnessed between ramp 1 (0h) and ramp 2 (1h).

Figure 6.6a shows how electrode resistance evolves over time for Elastosil 2030/20 DEAs made with pad-printed, inkjet-printed and dry carbon powder electrodes. Figure 6.6b exhibits how the resistance evolves with voltage over time.

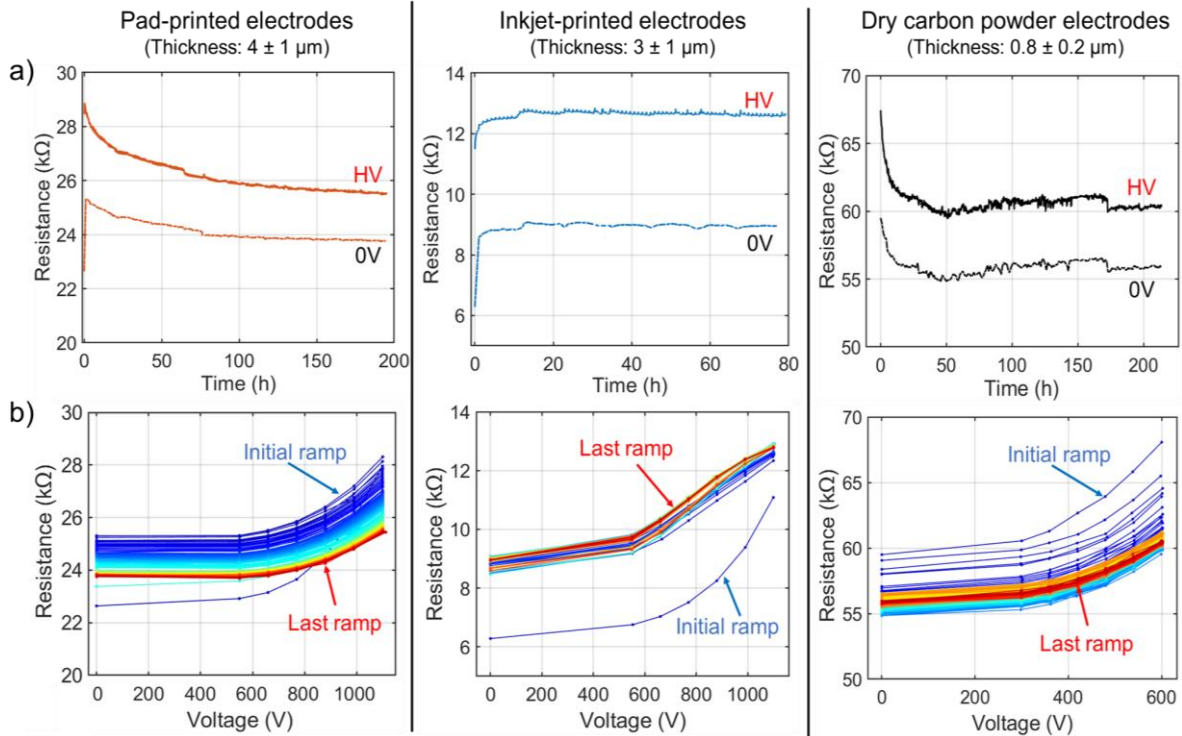


Figure 6.6: a) Evolution of four-point electrode resistance for Elastosil 2030/20 DEAs made with pad-printed, inkjet-printed and dry carbon powder electrodes. b) Evolution over time of the resistance vs voltage ramps for Elastosil 2030/20 DEAs made with pad-printed, inkjet-printed and dry carbon powder electrodes. DEAs with pad-printed and inkjet-printed electrodes are actuated at 1100 V (90 V/ μ m) and DEAs with dry carbon powder electrodes are actuated at 600 V (50 V/ μ m). The DEAs are operated at 20°C – 30% RH.

In Figure 6.6a, I observe that the DEAs with dry carbon powder electrodes exhibit the highest resistance (55 – 70 k Ω), whereas inkjet-printed electrodes have the lowest resistance (<15 k Ω). Pad-printed DEAs show intermediate resistances (20 – 30 k Ω). Both pad-printed and dry carbon powder electrodes exhibit a decrease of electrode resistance over the first hours of actuation and both show an initial resistance which is maximal over the range of DC actuation. This change in resistance was also seen in previous investigations under AC actuation on silicone-based DEAs carried out by Saint-Aubin et al.²⁵, where the resistance initially slightly decreases for the first thousands of AC cycles. However, the electrode resistance dramatically increased after several thousands of AC cycles (50 Hz)²⁵. Such a behavior is not seen here because the DEAs are actuated under DC and have not experienced numerous actuation cycles (200 hours = 200 cycles only).

Inkjet-printed electrodes show a slightly different aging behavior than the other two electrode materials, as the initial electrode resistance is small at the start of the test and that it slightly increases over the first hours of DC actuation. This different electrode resistance behavior cannot be explained. After the first few hours of DC actuation, the resistance of inkjet-printed electrodes becomes more stable over time, a characteristic also observed in pad-printed and dry carbon powder electrodes.

6.2 Effect of elastomer material on DC lifetime

In this section, I show how DC lifetime depends on the selection of the silicone elastomer material in order to identify the most reliable elastomer amongst those tested.

Figure 6.7. plots failure fraction vs. time for DEAs made from different silicone elastomer materials at 90 V/ μ m under humid (85%-90% RH) conditions at 20°C and at 85°C. Lifetimes, expressed as mean time to failure (MTTF - obtained from Weibull fits, c.f. Section 4.4) and actuation strains are shown in Table 6.2.

Electro 242-1 DEAs exhibits the highest lifetimes among the tested elastomer materials, with only few failures occurring below 200 h as shown in Figure 6.7. I compare here the lifetime of DEAs from the different elastomers with Elastosil 2030/20 DEAs as a reference, because it is a widely used commercially available elastomer that can be purchased as rolls of 20 μ m thick membranes.

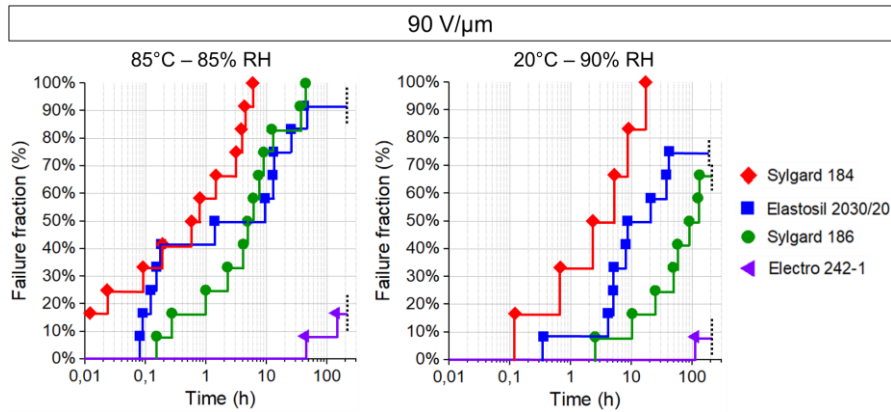


Figure 6.7: Effect of elastomer material on DC DEA lifetime at 90 V/ μ m at 85 °C – 85% RH and at 20 °C – 90% RH. Electro 242-1 based DEAs have the longest lifetime.

Table 6.2: MTTF of DEAs at high relative humidity, comparing different elastomer materials. Breakdown strengths (E_{DB}) are taken from Chapter 5. Lifetime is compared to Elastosil 2030/20 DEAs at 90 V/ μ m at 85°C and 85% RH.

Elastomer material	Thickness (μ m)	Young's modulus (MPa)	Condition	Field (V/ μ m)	E/E_{DB} (%)	Actuation strain (%)	MTTF (h)	Lifetime factor
Elastosil 2030	12.1 \pm 0.2	1.8 \pm 0.1	85°C 85% RH	90 V/ μ m	74 \pm 3	3.4 \pm 0.4	14	1x (ref)
Sylgard 186	13.2 \pm 0.4	1.8 \pm 0.1			74 \pm 3	4.2 \pm 0.3	12	0.86x
Sylgard 184	14.2 \pm 0.3	3.3 \pm 0.2			64 \pm 3	2.9 \pm 0.3	2	0.14x
Electro 242-1	15.1 \pm 0.4	1.5 \pm 0.1			81 \pm 2	3.1 \pm 0.4	> 200	> 15x
Elastosil 2030	12.0 \pm 0.2	1.3 \pm 0.1	20°C 90% RH	90 V/ μ m	73 \pm 2	3.6 \pm 0.3	36	2.6x
Sylgard 186	13.0 \pm 0.4	1.4 \pm 0.1			71 \pm 2	4.2 \pm 0.4	220	16x
Sylgard 184	14.0 \pm 0.3	3.9 \pm 0.1			53 \pm 3	3.0 \pm 0.4	9	0.64x
Electro 242-1	15.3 \pm 0.4	1.5 \pm 0.1			70 \pm 3	3.3 \pm 0.3	> 200	> 15x

At a constant electric field of $90 \text{ V}/\mu\text{m}$, Electro 242-1 DEAs have an MTTF higher than 200 h (> 8 days) at both $85^\circ\text{C} - 85\% \text{ RH}$ as well as $20^\circ\text{C} - 90\% \text{ RH}$. Compared to Elastosil 2030/20, the MTTF is increased by a factor of more than 15x at $85^\circ\text{C} - 85\% \text{ RH}$ and by a factor of more than 5x at $20^\circ\text{C} - 90\% \text{ RH}$. As observed in Table 6.2, the significant difference in lifetime observed between Electro 242-1 and Elastosil 2030/20 at constant fields is not likely to be due to differences in field to breakdown strength ratios. Both Electro 242-1 and Elastosil 2030/20 exhibit similar Young's moduli. I suspect that elastomer materials with increased chain length yield higher DC lifetime performance, but further investigations are needed to confirm that trend.

At $90 \text{ V}/\mu\text{m}$, Sylgard 186 achieves slightly higher actuation strains and exhibits 6x higher MTTF than Elastosil 2030/20 at $20^\circ\text{C} - 90\% \text{ RH}$, but 1.1x lower MTTF at $85^\circ\text{C} - 85\% \text{ RH}$.

The lowest DC lifetimes are achieved with Sylgard 184, with a MTTF of a factor 0.14x compared to Elastosil 2030/20 at $85^\circ\text{C} - 85\% \text{ RH}$ and of a factor 0.25x at $20^\circ\text{C} - 90\% \text{ RH}$.

There is no obvious correlation between actuation strain at failure and time to failure of individual DEAs (as discussed later in Section 6.4), nor between the mechanical and electrical properties of the elastomer material and lifetime (MTTF).

Based on these results, I only show data for Electro 242-1 (highest lifetime performance) and for Elastosil 2030/20 (standard commercially available elastomer) in Sections 6.3, 6.4 and 6.5.

6.3 Effect of electric field on DC lifetime

Figure 6.8 plots failure fraction vs. time for Elastosil 2030/20 DEAs under different applied electric fields (from $80 \text{ V}/\mu\text{m}$ to $110 \text{ V}/\mu\text{m}$) at constant environmental conditions. Figure 6.9 plots the mean DC lifetimes (MTTF) vs. the ratio of applied electric field to breakdown strength for Elastosil 2030/20 and Electro 242-1 DEAs. MTTF (obtained from Weibull plots) and actuation strains for each condition are presented in Table 6.3.

Increasing the electric field significantly reduces the MTTF of DEAs, with an approximately exponential decrease in MTTF with electric field. At $85^\circ\text{C} - 85\% \text{ RH}$, I observe that the MTTF of Elastosil 2030/20 DEAs decreases by a factor 7x from $80 \text{ V}/\mu\text{m}$ DC operation to $90 \text{ V}/\mu\text{m}$ DC operation, by a factor 62x from $80 \text{ V}/\mu\text{m}$ to $100 \text{ V}/\mu\text{m}$, and by a factor 990x from $80 \text{ V}/\mu\text{m}$ to $110 \text{ V}/\mu\text{m}$. I observe a similar trend for Electro 242-1 DEAs, where for example at $85^\circ\text{C} - 85\% \text{ RH}$, the MTTF decreases by a 7.5x factor from $100 \text{ V}/\mu\text{m}$ to $110 \text{ V}/\mu\text{m}$.

At $20^\circ\text{C} - 90\% \text{ RH}$, I observe a similar trend with the MTTF of Elastosil 2030/20 DEAs decreasing by a factor over 5.5x from $80 \text{ V}/\mu\text{m}$ to $90 \text{ V}/\mu\text{m}$, by a factor over 20x from $80 \text{ V}/\mu\text{m}$ to $100 \text{ V}/\mu\text{m}$, and by a factor over 83x from $80 \text{ V}/\mu\text{m}$ to $110 \text{ V}/\mu\text{m}$.

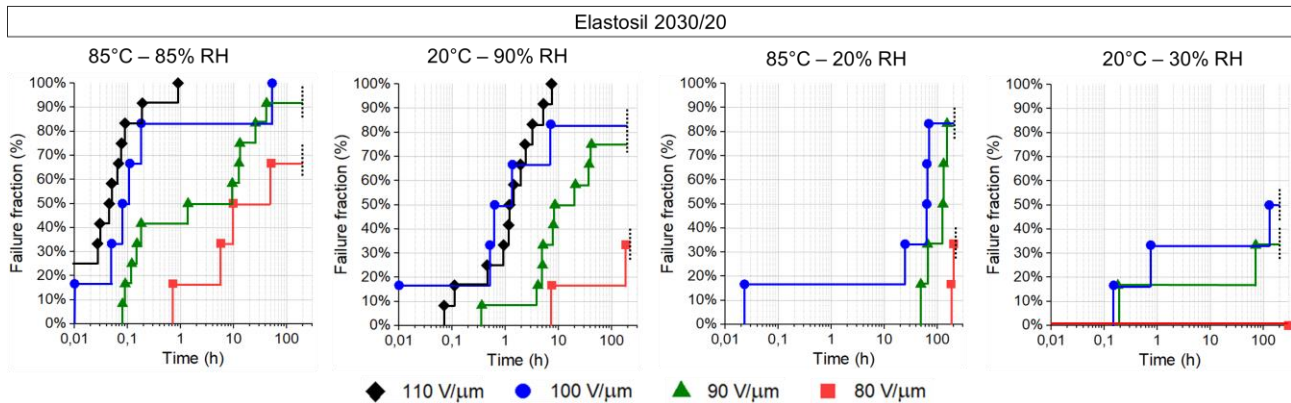


Figure 6.8: Effect of electric field on DC DEA lifetime under different environmental conditions for Elastosil 2030/20. Mean times to failure (MTTF) for each set are reported in Table 6.3. Higher electric fields lead to much shorter lifetimes under all environment conditions. High humidity strongly reduces lifetime.

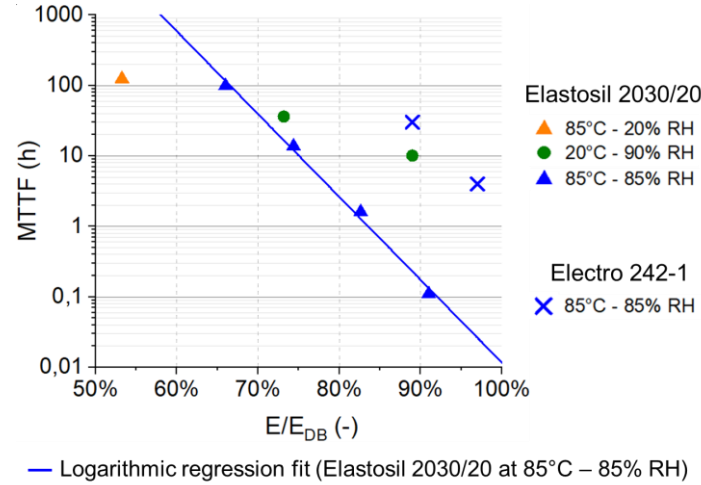


Figure 6.9: MTTF of Elastosil 2030/20 and Electro 242-1 DEAs vs. the ratio of applied electric field to breakdown strength (E/E_{DB}) under different environmental conditions. The logarithmic regression fit (in blue) is for Elastosil 2030/20 at 85°C – 85% RH. Conditions with MTTF longer than the maximum experiment duration (i.e. > 200 h) are not displayed. Lifetime decreases with increasing field to breakdown strength ratio at 85°C – 85% RH. The fit equation is $MTTF = A \cdot 10^{-(B \cdot E/E_{DB})}$, with $A = (6.9 \pm 0.3) \cdot 10^9$ h and $B = 11.8 \pm 0.6$ for unpassivated Elastosil 2030/20 at 85°C – 85% RH. For readability considerations, error bars are not shown.

Table 6.3: DC lifetime for Elastosil 2030/20 and Electro 242-1 DEAs under different electric fields and environmental conditions. N.D. stands for not determined. Lifetime is compared to Elastosil 2030 at 90 V/ μ m at 85°C – 85% RH.

Elastomer material	Thickness (μ m)	Environmental condition (T, RH)	Water vapor content (g/cm ³)	Field E (V/ μ m)	E/E_{DB} (%)	Actuation strain (%)	MTTF (h)	Lifetime factor
Elastosil 2030/20	12.1 \pm 0.2	85°C – 85% RH	297.6	80	66 \pm 2	2.1 \pm 0.3	99	7x
	12.1 \pm 0.2	85°C – 20% RH	70.0		47 \pm 2	2.1 \pm 0.4	> 200	> 14x
	12.0 \pm 0.2	20°C – 90% RH	15.6		65 \pm 1	2.3 \pm 0.3	> 200	> 14x
	12.2 \pm 0.2	20°C – 30% RH	5.2		50 \pm 2	2.3 \pm 0.3	> 200	> 14x
	12.1 \pm 0.2	85°C – 85% RH	297.6		74 \pm 3	3.4 \pm 0.4	14	1x (ref)
	12.2 \pm 0.2	85°C – 50% RH	175.1	90	N.D.	3.5 \pm 0.4	> 200	> 14x
	12.0 \pm 0.2	85°C – 20% RH	70.0		53 \pm 2	3.6 \pm 0.3	124	9x
	12.1 \pm 0.2	50°C – 90% RH	74.6		N.D.	3.4 \pm 0.4	> 200	> 14x
	12.0 \pm 0.2	50°C – 50% RH	41.4		N.D.	3.6 \pm 0.4	> 200	> 14x
	12.1 \pm 0.2	50°C – 20% RH	16.6		N.D.	3.5 \pm 0.4	> 200	> 14x
	12.0 \pm 0.2	20°C – 90% RH	15.6		73 \pm 2	3.7 \pm 0.3	36	2.6x
	12.3 \pm 0.2	20°C – 50% RH	8.6		N.D.	3.6 \pm 0.4	> 200	> 14x
	12.0 \pm 0.2	20°C – 30% RH	5.2		56 \pm 2	3.5 \pm 0.5	> 200	> 14x
	12.1 \pm 0.2	85°C – 85% RH	297.6		83 \pm 2	4.6 \pm 0.5	1.6	0.11x
	12.0 \pm 0.2	85°C – 20% RH	70.0		59 \pm 2	4.7 \pm 0.4	> 200	> 14x
	12.1 \pm 0.2	20°C – 90% RH	15.6	100	81 \pm 1	4.8 \pm 0.6	10	0.71x
	12.1 \pm 0.2	20°C – 30% RH	5.2		62 \pm 3	4.7 \pm 0.4	> 200	> 14x
	12.0 \pm 0.2	85°C – 85% RH	297.6		91 \pm 2	7.3 \pm 0.6	0.1	0.01x
	12.1 \pm 0.2	60°C – 90% RH	70.0		N.D.	7.1 \pm 0.6	0.5	0.04x
	12.1 \pm 0.2	40°C – 90% RH	15.6		N.D.	6.9 \pm 0.5	1.4	0.1x
Electro 242-1	12.0 \pm 0.2	20°C – 90% RH	15.6	110	89 \pm 1	7.5 \pm 0.5	2.4	0.17x
	15.5 \pm 0.4	85°C – 85% RH	297.6		89 \pm 2	4.8 \pm 0.3	30	2.1x
	15.1 \pm 0.4	85°C – 20% RH	70.0		72 \pm 3	4.9 \pm 0.4	> 200	> 14x
	15.4 \pm 0.4	20°C – 90% RH	15.6		78 \pm 2	5.7 \pm 0.4	138	10x
	15.3 \pm 0.4	20°C – 30% RH	5.2		67 \pm 4	4.7 \pm 0.4	> 200	> 14x
	15.2 \pm 0.4	85°C – 85% RH	297.6	110	97 \pm 2	7.0 \pm 0.8	4	0.29x
	15.1 \pm 0.3	20°C – 90% RH	15.6		86 \pm 2	7.3 \pm 0.5	25	1.8x

From the fit in Figure 6.9 ($MTTF = A \cdot 10^{-(B \cdot E/E_{DB})}$ with $A = (6.9 \pm 0.3) \cdot 10^9$ h and $B = 11.8 \pm 0.6$), I predict Elastosil 2030 DEA lifetimes of over 1 month (i.e. 730 hours) at 85°C – 85% RH for DC operation at electric fields below 60% of breakdown strength. However, lowering the electric field reduces actuation strains (c.f. Table 6.3). Using Electro 242-1 instead of Elastosil 2030/20 enables higher lifetimes to be achieved for a given E/E_{DB} ratio.

Figure 6.10 shows the time to failure of individual DEAs vs. electric to breakdown strength (E/E_{DB}) ratio under different environmental conditions.

The times to failure of individual DEAs made of Elastosil 2030/20 and Electro 242-1 span over wide timescales, with a general trend that lower times to failure are reached as electric field increases toward the dielectric breakdown strengths.

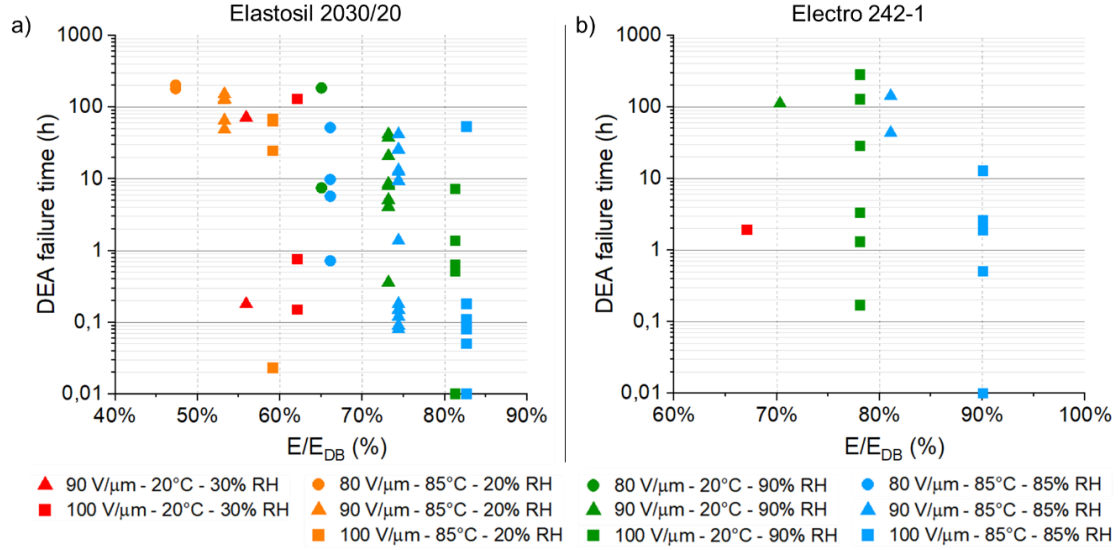


Figure 6.10: Time to failure for individual DEAs as a function of the ratio of electric field to breakdown strength (E/E_{DB}) for Elastosil 2030/20 (a) and Electro 242-1 (b) DEAs under different environmental conditions. Only failed DEAs are displayed, and each datapoint represents an individual DEA failure. For readability considerations, error bars are not shown.

6.4 Effect of temperature and humidity on DC lifetime

Figure 6.11 presents DEA failure fraction vs. time for Elastosil 2030/20 and for Electro 242-1 DEAs under different temperature and humidity conditions, and for different applied electric fields. MTTF and actuation strains are presented in Table 6.3. I observe that humidity is a major accelerating factor for the dielectric breakdown of DEAs.

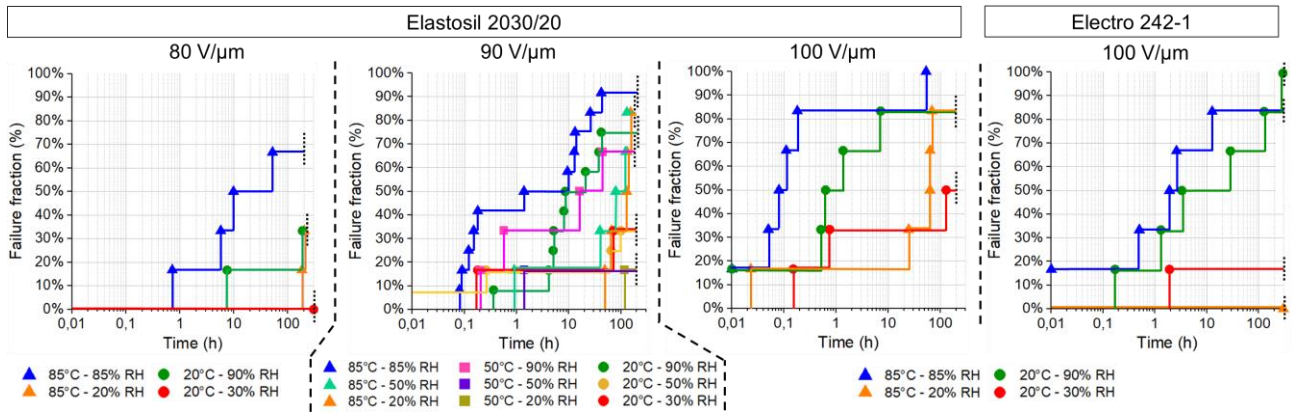


Figure 6.11: Effect of temperature and humidity on DC DEA lifetime under different electric fields from 80 $V/\mu m$ to 100 $V/\mu m$ for Elastosil 2030/20 DEAs, and at 100 $V/\mu m$ for Electro 242-1. Mean times to failure (MTTF) for each set are reported in Table 6.3. Increasing humidity significantly reduces DEA lifetime.

For Elastosil 2030/20 DEAs, at 100 $V/\mu m$ and 85°C, the MTTF decreases by more than 125 x from 20% RH to 85% RH. At 100 $V/\mu m$ and at 20°C, the MTTF decreases by more than 20 x from 30% RH to 90% RH. For Electro 242-1 DEAs at 100 $V/\mu m$ and 85°C, the MTTF decreases by more than 6x from 20% RH to 85% RH.

At 90 $V/\mu m$ and 85°C, the MTTF of Elastosil 2030/20 DEAs decreases by a factor 9x from 20% RH to 85% RH. At 90 $V/\mu m$ and 20°C, the lifetime of Elastosil 2030/20 DEAs decreases by more than 5x from 30% RH to 90% RH.

Temperature also accelerates dielectric breakdown failure of DEAs, but to a lesser extent than humidity. At 90 V/ μm and 90% RH, the MTTF of Elastosil 2030/20 DEAs decreases by a 2.6x factor from 20°C to 85°C. At 90 V/ μm and 20% RH, the lifetime of Elastosil 2030/20 DEAs decreases by a 1.6x factor from 50°C to 85°C. For Electro 242-1 DEAs at 100 V/ μm and 90% RH, lifetime decreases by a 4.6x factor from 20°C to 85°C.

The combination of humidity and high electric fields significantly accelerates the dielectric breakdown failure of silicone-based DEAs. Degradation mechanisms of polymer materials for high voltage applications include charge injection, partial discharges in voids, and electrical treeing^{118,210,223,309}. Humidity is a known accelerating factor for most of these degradation pathways¹¹⁸.

Data from sections 6.3 and 6.4 clearly show that DEA lifetime is affected by temperature, humidity, and electric field. However, the time to failure of individual DEAs can occur over wide timescales for each investigated set of environmental conditions, and there is no correlation between higher actuation strains at failure and lower times to failure, as shown in Figure 6.12. Furthermore, the strains at failure are not significantly influenced by temperature and humidity.

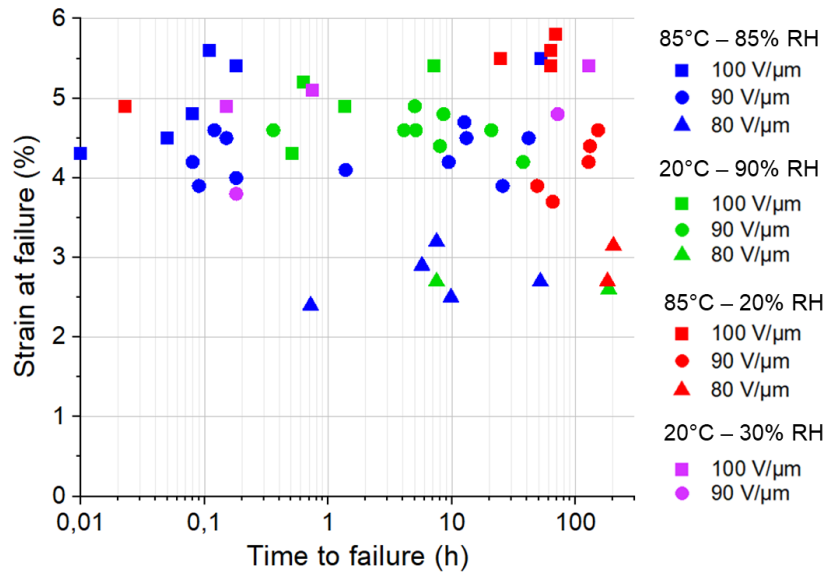


Figure 6.12: Strain at failure under different electric fields and environmental conditions for individual Elastosil 2030/20 DEAs.

6.5 Effect of encapsulation layer on DC lifetime

In this section, I investigate the effect of thin encapsulation layers on the DC lifetime for Elastosil 2030/20 and Momentive 242-1 DEAs. I select three materials as encapsulation layers: LSR 4305 (PDMS) for its low Young's modulus (0.2 MPa) and its strong adhesion to the DEA surface, Sylgard 186 (PDMS) for its Young's modulus (1.8 MPa) that matches the DEA and its strong adhesion to DEA surface, and SEBS (Hexpol Dryflex 500040) for its low water permeation³⁵⁵. Details on the encapsulation process are given in Section 4.1.1. I compared different thicknesses of the encapsulation layers and compared passivating both sides or only one side of the DEA. I demonstrate that encapsulation layers are effective in increasing DC lifetime of silicone-based DEAs under both humid and dry conditions for little decrease in actuation strain. From the results presented in this section, a US patent application has been filed³⁵⁶.

Figure 6.13 plots the failure fraction of DEAs vs. time, for 4 different environmental conditions, at 100 V/ μm . Figure 6.14 presents the DEA failure fraction vs. time at 85°C – 85% RH for DEAs with different encapsulation materials and thicknesses. Table 6.4 shows the MTTF and actuation strain of DEAs with and without SEBS or PDMS encapsulation layers.

As seen in Figures 6.13, 6.14, and in Table 6.4, the addition of LSR 4305 (PDMS) encapsulation layers increases the lifetime of Elastosil 2030/20 and Electro 242-1 DEAs under all investigated environmental conditions by factors between 2.2x and 75x, while only slightly reducing the actuation strain. The lifetime is improved in both low and high humidity conditions, and so may not be directly related to water permeation of the passivation layer.

The type of encapsulation material strongly impacts the lifetime and to a lesser extent the actuation strain of DEAs. At 85 °C – 85% RH and 100 V/ μm , the MTTF of Elastosil 2030/20 DEAs improves by a factor 1.5x with SEBS (3 μm) encapsulation, by a factor 7x with LSR 4305 (4 μm) encapsulation, and by a factor 23x with Sylgard 186 (4 μm) encapsulation. The actuation strain decreases owing to stiffening, by factors of 0.96x, 0.96x, and 0.81x with the addition of SEBS (3 μm), LSR 4305 (4 μm), and Sylgard 186 (4 μm) encapsulation layers. Selecting an encapsulation layer with high adhesion to the DEA substrate and with a low Young's modulus allows maximizing lifetime with a negligible reduction in actuation strain. At 85 °C – 85% RH and 100 V/ μm , the MTTF of Electro 242-1 DEAs

improves by a factor 1.2x with SEBS encapsulation at a 0.96x strain reduction factor, and by a factor of more than 10x with LSR 4305 (4 μm) encapsulation at a 0.94x strain reduction factor.

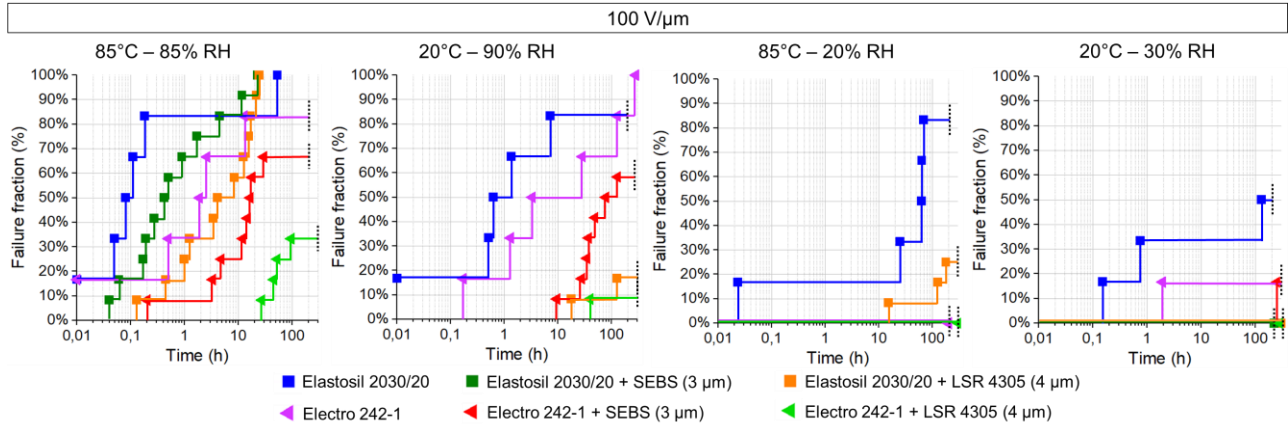


Figure 6.13: Effect of different double-sided encapsulation layers on DC DEA lifetime at 100 V/ μm under different temperature and relative humidity conditions for Elastosil 2030 and Momentive 242-1 membranes. Encapsulation with LSR 4305 provides longer lifetime than with SEBS.

The origin of the difference in MTTF between SEBS and PDMS encapsulation requires further investigation. I note that LSR 4305 and Sylgard 186 have excellent adhesion on the tested DEAs, whereas the adhesion of SEBS is less strong: it adheres to the DEAs under normal DEA operation, but can be manually peeled off with tweezers.

Encapsulating both sides is important to maximize lifetime, as shown in Figure 6.14a, and in Table 6.4. At 85 °C – 85% RH and 90 V/ μm , encapsulating Elastosil 2030/20 DEAs with LSR 4305 only on the ground (GND) or only on the high voltage (HV) electrode sides yields a 1.4x increase in DEA lifetime with an actuation strain factor of 0.94x, while encapsulating both sides yields a 19x increase in DEA lifetime with an actuation strain factor of 0.79x.

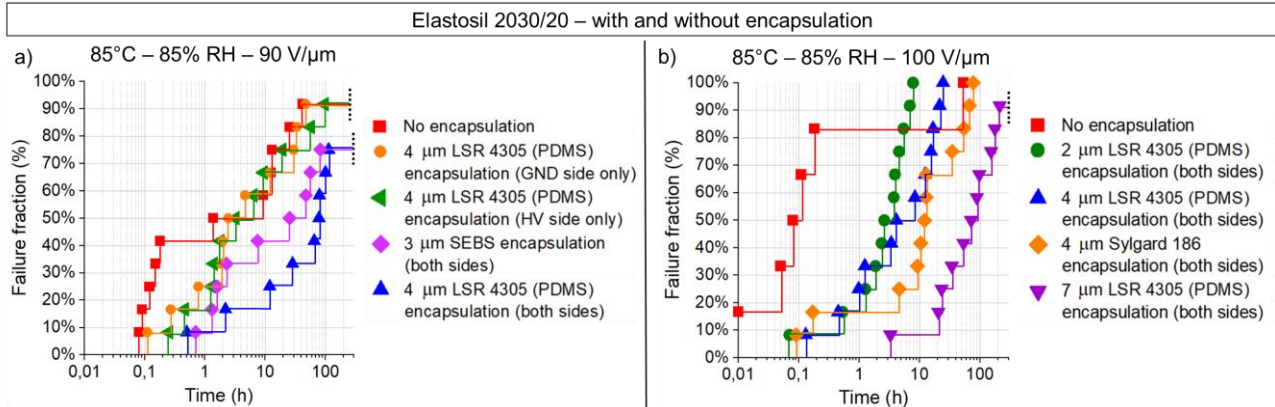


Figure 6.14: Effect of encapsulation layer coverage and type on DC lifetime of Elastosil 2030/20 DEAs at 85°C – 85% RH at: a) 90 V/ μm , b) 100 V/ μm . Covering both electrode sides with LSR 4305 encapsulation layers, and increasing the layer thickness maximize DEA lifetime.

Finally, I observe that higher encapsulation layer thickness yields increased lifetime of DEAs, as shown in Figure 6.14b. At 85°C – 85% RH and 100 V/ μm , adding 2 μm , 4 μm , and 7 μm thick LSR 4305 encapsulation layers increases MTTF by factors 2.6x, 7x, and 75x, with actuation strains factors of 0.98x, 0.96x, and 0.83x, showing a clear lifetime vs. strain trade-off owing to membrane stiffening.

Figure 6.15 presents mean DC lifetime (MTTF) vs. electric field for Elastosil 2030/20 and Electro 242-1 with and without encapsulation layers. As observed in Figure 6.15, the addition of a LSR 4305 (PDMS) encapsulation layer increases the lifetime of Elastosil 2030/20 and Electro 242-1 DEAs at constant electric field at 85°C – 85% RH by factors between 2.2x and 75x, while only slightly reducing the actuation strain.

From the fit to MTTF vs. electric field (Figure 6.15a), DEA lifetime can be predicted at any electric field (and hence strain) at 85°C – 85% RH for Elastosil 2030/20 DEAs. I predict a 1000 h (i.e. 1.4 months) lifetime at 70 V/ μm (i.e. \approx 1.5% strain) for non-encapsulated Elastosil 2030/20 DEAs, and at 85 V/ μm (i.e. \approx 2.5% strain) for LSR 4305 encapsulated (4 μm) Elastosil 2030/20 DEAs.

Table 6.4: Effect of encapsulation layer type and thickness on DC DEA lifetime. Lifetime is compared to Elastosil 2030 at 90 V/ μm at 85°C – 85% RH with no encapsulation. Adding encapsulation layers on both electrode sides significantly increases DEA lifetime. LSR 4305 (PDMS) encapsulation yields higher lifetimes than SEBS encapsulation, and thicker LSR 4305 encapsulation leads to increased lifetimes.

Elastomer material	Encapsulation layer	Membrane thick- ness (μm)	Field (V/μm)	Environmental condition (T, RH)	Actuation strain (%)	MTTF (h)	Lifetime factor	
Elastosil 2030/20	None	12.1 ± 0.2	90	85°C – 85% RH	3.4 ± 0.4	14	1x (ref)	
	SEBS (3 ± 1 μm)	12.2 ± 0.2			2.7 ± 0.5	70	5x	
	LSR 4305 (4 ± 1 μm)	12.2 ± 0.2			2.7 ± 0.4	264	19x	
	LSR 4305 (4 ± 1 μm) – HV electrode only	12.1 ± 0.2			3.2 ± 0.4	20	1.4x	
	LSR 4305 (4 ± 1 μm) – GND electrode only	12.1 ± 0.2			3.2 ± 0.5	20	1.4x	
	None	12.1 ± 0.2	100		4.7 ± 0.5	1.6	0.11x	
	SEBS (3 ± 1 μm)	12.1 ± 0.2			4.5 ± 0.4	2.4	0.17x	
	LSR 4305 (2 ± 1 μm)	12.0 ± 0.2			4.6 ± 0.4	4	0.3x	
	LSR 4305 (4 ± 1 μm)	12.2 ± 0.2			4.5 ± 0.4	11	0.8x	
	LSR 4305 (7 ± 1 μm)	12.1 ± 0.2			3.9 ± 0.5	121	8.6x	
	Sylgard 186 (4 ± 1 μm)	12.0 ± 0.2	3.8 ± 0.4		37	2.6x		
	None	12.2 ± 0.2	110		7.3 ± 0.6	0.1	0.01x	
	LSR 4305 (4 ± 1 μm)	12.1 ± 0.2			5.9 ± 0.5	2.8	0.2x	
Electro 242-1	None	15.5 ± 0.4	100	4.8 ± 0.3	30	2.1x		
	SEBS (3 ± 1 μm)	15.1 ± 0.4		4.6 ± 0.5	35	2.5x		
	LSR 4305 (4 ± 1 μm)	15.4 ± 0.4		4.5 ± 0.5	> 300	> 21x		
		None	15.2 ± 0.4	110	7.0 ± 0.8	4	0.3x	
		LSR 4305 (4 ± 1 μm)	15.2 ± 0.4		5.7 ± 0.6	104	7.4x	
Elastosil 2030/20	None	12.0 ± 0.2	100	85°C – 20% RH	4.7 ± 0.4	> 200	> 14x	
	LSR 4305 (4 ± 1 μm)	12.0 ± 0.2			4.6 ± 0.4	> 300	> 21x	
Electro 242-1	None	15.1 ± 0.4			4.9 ± 0.4	> 200	> 14x	
	LSR 4305 (4 ± 1 μm)	15.3 ± 0.3	4.4 ± 0.4		> 300	> 21x		
Elastosil 2030/20	None	12.1 ± 0.2	110		60°C – 90% RH	7.1 ± 0.6	0.5	0.04x
	LSR 4305 (4 ± 1 μm)	12.0 ± 0.2		6.0 ± 0.4		6.4	0.5x	
	None	12.1 ± 0.2		40°C – 90% RH	6.9 ± 0.5	1.4	0.1x	
	LSR 4305 (4 ± 1 μm)	12.2 ± 0.2			5.8 ± 0.5	28	2x	
Elastosil 2030/20	None	12.1 ± 0.2	100	20°C – 90% RH	4.8 ± 0.6	10	0.7x	
	LSR 4305 (4 ± 1 μm)	12.2 ± 0.2			4.5 ± 0.4	> 300	> 21x	
	None	12.0 ± 0.2	110		7.5 ± 0.6	2.4	0.17x	
	LSR 4305 (4 ± 1 μm)	12.1 ± 0.2			6.0 ± 0.6	70	5x	
Electro 242-1	None	15.3 ± 0.4	100		5.7 ± 0.4	138	10x	
	SEBS (3 ± 1 μm)	14.9 ± 0.4			5.1 ± 0.4	115	8x	
	LSR 4305 (4 ± 1 μm)	15.0 ± 0.4			5.2 ± 0.5	> 300	> 21x	
		None	15.1 ± 0.3		110	7.5 ± 0.5	25	1.8x
		LSR 4305 (4 ± 1 μm)	15.0 ± 0.3			6.1 ± 0.4	> 300	> 21x
Elastosil 2030/20	None	12.1 ± 0.2	100	20°C – 30% RH	4.7 ± 0.4	> 200	> 14x	
	SEBS (3 ± 1 μm)	12.2 ± 0.2			4.5 ± 0.3	> 300	> 21x	
	LSR 4305 (4 ± 1 μm)	12.0 ± 0.2			4.3 ± 0.3	> 300	> 21x	
Electro 242-1	None	15.3 ± 0.4			4.7 ± 0.4	> 200	> 14x	
	SEBS (3 ± 1 μm)	15.2 ± 0.4			4.6 ± 0.4	> 300	> 21x	
	LSR 4305 (4 ± 1 μm)	15.0 ± 0.4			4.5 ± 0.3	> 300	> 21x	

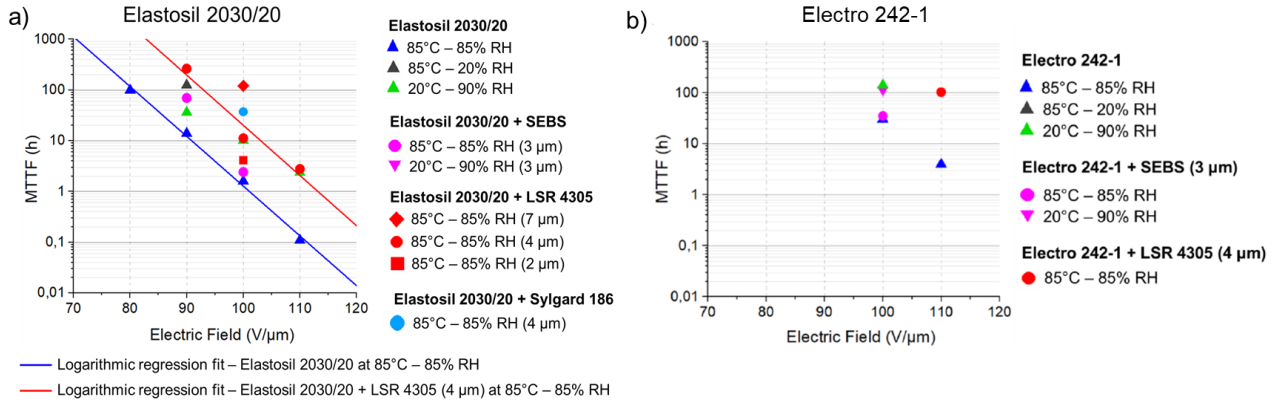


Figure 6.15: a) MTTF of a) Elastosil 2030 and b) Electro 242-1 DEAs under different environmental conditions. The fit equation is $MTTF = A * 10^{-B * E}$, with $A = (8.1 \pm 0.4) * 10^9$ h and $B = 0.098 \pm 0.005 \mu m * V^{-1}$ for unpassivated Elastosil 2030/20 at 85°C – 85% RH, and with $A = (155 \pm 31) * 10^9$ h and $B = 0.099 \pm 0.022 \mu m * V^{-1}$ for Elastosil 2030/20 + LSR 4305 (4 μm) at 85°C – 85% RH. Encapsulation with LSR 4305 (4 μm) shifts MTTF of Elastosil 2030/20 DEAs at constant electric field. At constant field and environmental conditions, Electro 242-1 DEAs show higher MTTF vs. Elastosil 2030/20 DEAs. Electro 242-1 DEAs with LSR 4305 (4 μm) encapsulation show the highest MTTF at 110 V/μm at 85°C – 85% RH. For readability considerations, error bars are not shown.

Figure 6.16 plots MTTF vs. actuation strain for Elastosil 2030/20 and Electro 242-1 DEAs at 85°C – 85% RH. As shown in Figure 6.16, adding LSR 4305 (4 μm thick) encapsulation layers on both sides is an effective strategy to increase the MTTF of Elastosil 2030/20 DEAs at a given strain by a factor 3x to 10x, or to achieve higher actuation strains (between 0.8% to 2% in actuation strain increase) for a given lifetime expectancy. At constant actuation strain, selecting Electro 242-1 over Elastosil 2030/20 as a dielectric yields over 10x higher lifetimes.

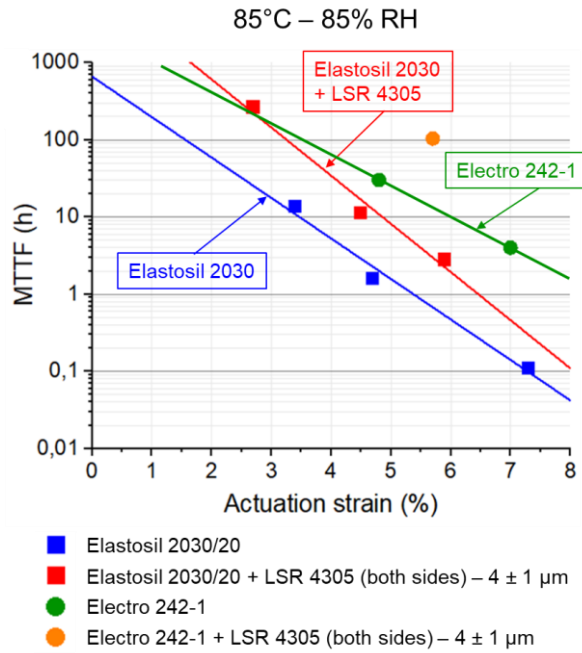


Figure 6.16: MTTF vs. actuation strain (ϵ_{act}) for Elastosil 2030/20 and Electro 242-1 DEAs at 85°C – 85% RH. The fit is to $MTTF = A * 10^{-B * \epsilon_{act}}$, with $A = (10.7 \pm 1.1) * 10^3$ h and $B = 0.624 \pm 0.094$ for Elastosil 2030/20 + LSR 4305 (4 μm, in red), and with $A = (6.6 \pm 0.8) * 10^2$ h and $B = 0.524 \pm 0.067$ for Elastosil 2030/20 (in blue). There is a significant tradeoff between actuation strain and DC lifetime. At constant actuation strain, Electro 242-1 DEAs yield over 10x higher MTTF vs. Elastosil 2030/20 DEAs. At constant actuation strain, adding LSR 4305 encapsulation layers (4 μm) on both electrodes yields a 3x to 10x increase in MTTF. For readability considerations, error bars are not shown.

Figure 6.17 plots MTTF vs. temperature for Elastosil 2030/20 DEAs at 110 V/μm. From the fit in Figure 6.17 ($MTTF = A * \exp^{B/k_B T}$), I find B is 0.47 ± 0.04 eV for encapsulated (LSR 4305, 4 μm) and 0.43 ± 0.07 eV for non-encapsulated Elastosil 2030 DEAs. The addition of the LSR 4305 (4 μm) encapsulation layer does not affect the B factor (i.e. slope), and increases the A factor, leading to a 18x to 25x lifetime increase at constant temperature.

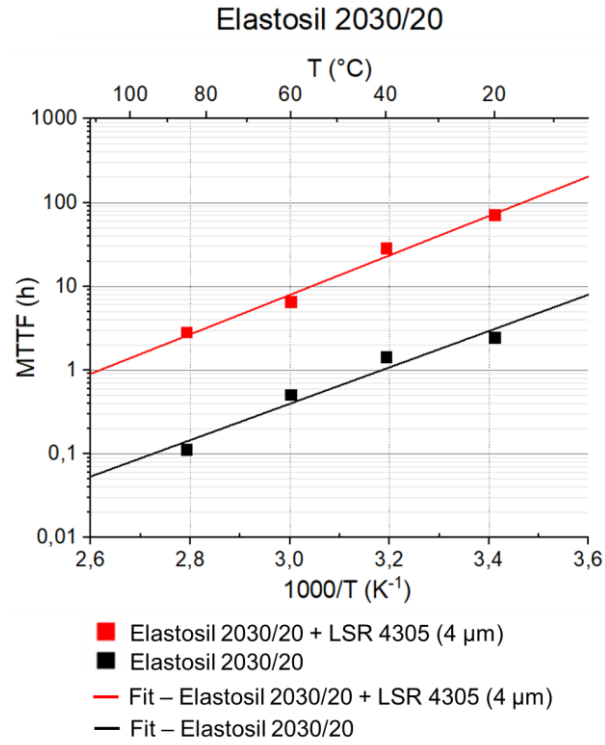


Figure 6.17: Temperature dependence of MTTF for Elastosil 2030/20 DEAs at 110 V/μm and 85% RH. The fit is to $MTTF = A * \exp^{B/k_B T}$, with $A = (1.2 \pm 0.2) * 10^{-7}$ h and $B = 0.43 \pm 0.07$ eV ($B/k_B = 4999 \pm 788$ K) for Elastosil 2030/20 (in black), and with $A = (6.8 \pm 0.7) * 10^{-7}$ h and $B = 0.47 \pm 0.04$ eV ($B/k_B = 5424 \pm 497$ K) for Elastosil 2030/20 + LSR 4305 (4 μm, in red) at 85% RH. The addition of an encapsulation layer does not significantly affect the B constant, but shifts MTTF of Elastosil 2030/20 DEAs at constant temperature. For readability considerations, error bars are not shown.

6.6 Effect of electrode material on DC lifetime

In this section, I show how the choice of the electrode composition and patterning method influences the lifetime of silicone-based DEAs under constant DC actuation and under different environmental conditions. Three types of electrodes are compared, shown in Figure 6.18a:

- 1) pad-printed carbon powder - PDMS composite consisting of Ketjenblack EC-600JD carbon black powder, Silbione LSR 4305 as a silicone matrix, and isopropanol and isooctane as solvents, following the recipe of Rosset et al.¹⁵³.
- 2) inkjet-printed carbon black suspension, composed of Ketjenblack EC-300J carbon powder, Wacker Belsil SPG 128 VP dispersant and OS2 as silicone solvent, according to the recipe of Schlatter et al.³³².
- 3) carbon black powder (grinded Ketjenblack EC-600JD), applied by hand with a paint brush over a mask.

Figure 6.18 shows how strain evolves vs. voltage (6.18b) and vs. electric field (6.18c) for silicone-based DEAs made with pad-printed, inkjet-printed, and dry carbon powder electrodes (shown in 6.18a).

Dry carbon powder (thickness: 0.8 ± 0.2 μm) leads to significantly higher strains at constant voltage and/or constant electric field in comparison to inkjet-printed (thickness: 3 ± 1 μm) and pad-printed (thickness: 4 ± 1 μm) electrodes. This behavior can be explained by the reduced stiffening effect of the dry carbon powder electrodes compared to the pad-printed and inkjet-printed electrodes. Inkjet-printed and pad-printed electrodes exhibit very similar strain behavior, because their similar thickness leads to comparable stiffening of the silicone membrane.

Figure 6.19 shows the DEA failure profile for each electrode material under the four investigated environmental conditions. The electric fields have been chosen to yield similar actuation strains for the three electrode materials. All DEAs failed through dielectric breakdown, and it is visually confirmed by the presence of a pinhole after failure (c.f. Section 6.1).

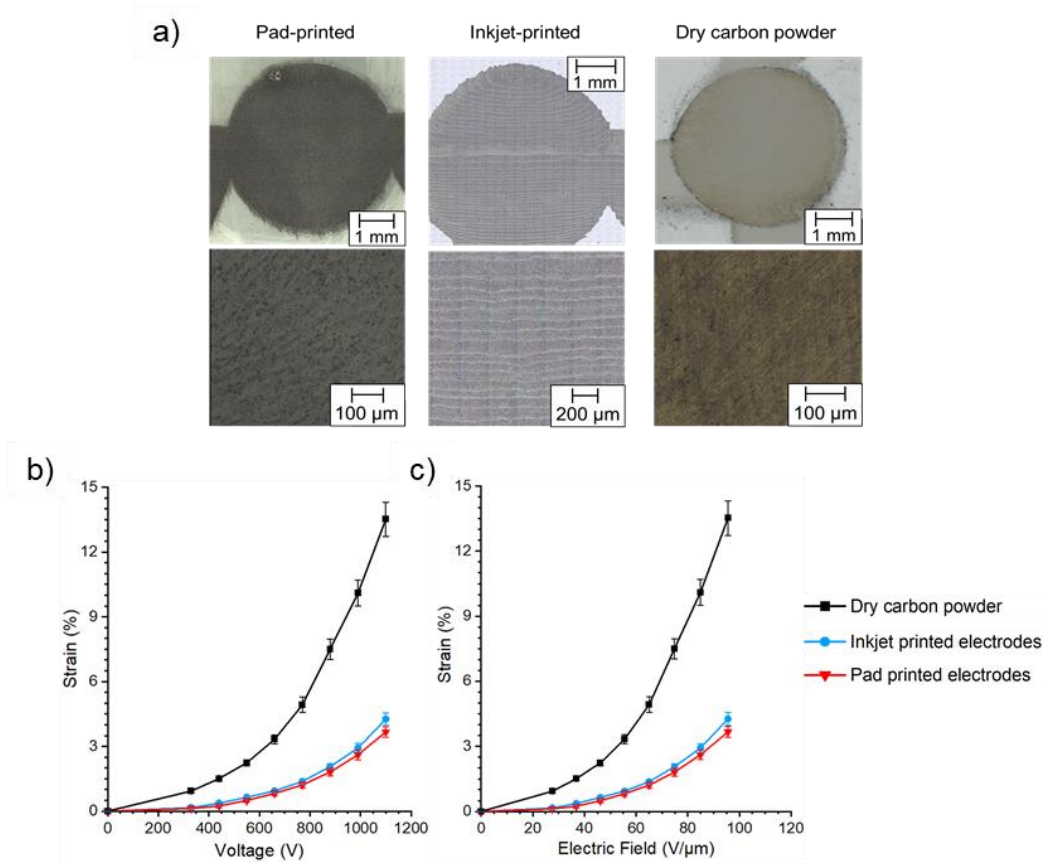


Figure 6.18: a) Optical micrograph of pad-printed carbon black-PDMS composite, inkjet-printed carbon black-PDMS composite and dry carbon black electrodes. b) Strain vs. voltage plots for the investigated electrode materials. c) Strain vs. electric field plot for the investigated electrode materials. The data is the initial voltage ramp, averaged over 6 DEAs. The DEAs are operated at 20°C and 90% RH. The error bars are standard deviation.

Figure 6.19 shows that DEAs with inkjet-printed electrodes have lower lifetimes than DEAs with pad-printed electrodes at constant electric fields under humid conditions ($85^\circ\text{C} - 85\% \text{ RH}$ and $20^\circ\text{C} - 90\% \text{ RH}$).

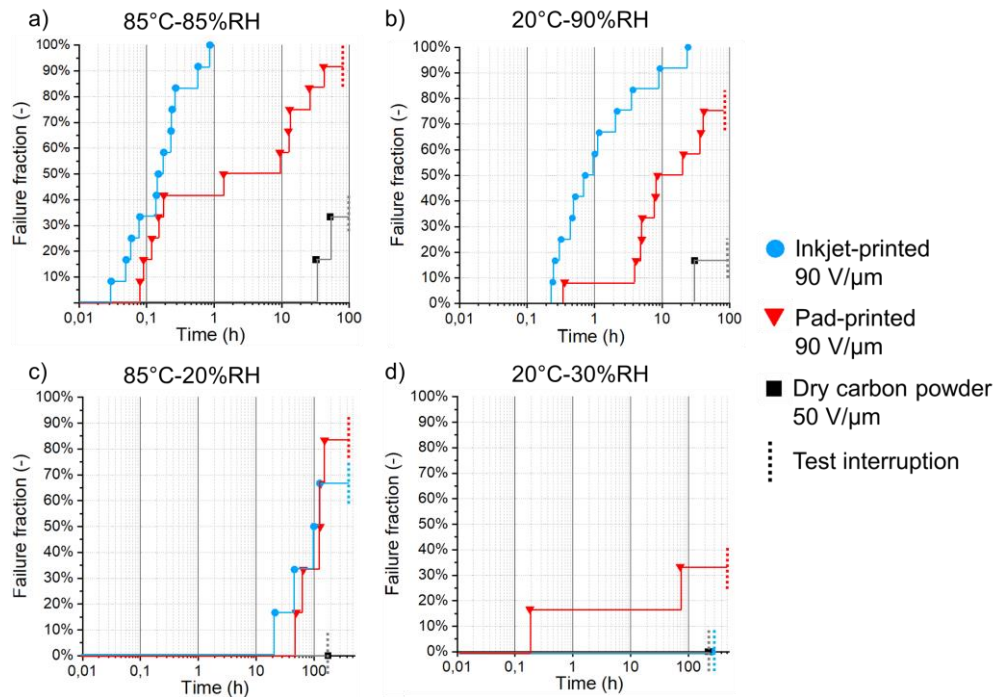


Figure 6.19: Failure fraction vs. time for DEAs tested at a) $85^\circ\text{C} - 85\% \text{ RH}$, b) $20^\circ\text{C} - 90\% \text{ RH}$, c) $85^\circ\text{C} - 20\% \text{ RH}$ and at d) $20^\circ\text{C} - 30\% \text{ RH}$, for the three different electrode materials.

The lifetime of pad-printed DEAs is more than 10x higher than for inkjet-printed electrodes at 85% RH and 90% RH. As shown in Table 6.5, the MTTF of DEAs with inkjet-printed electrodes are 0.2 h at 85°C – 85% RH and 2.4 h at 20°C – 90% RH, whereas the MTTF of DEAs with pad-printed electrodes reaches 14 h at 85°C – 85% RH and 36 h at 20°C – 90% RH. However, under dry conditions (85°C – 20% RH and 20°C – 30% RH), DEAs with inkjet-printed electrodes show similar or superior lifetimes to pad-printed electrodes.

For a given actuation strain, dry carbon black electrodes demonstrate higher lifetimes compared to inkjet-printed and pad-printed electrodes under both dry and wet conditions. This is due to the significantly lower fields used to achieve the actuation strain, as dry carbon black powder electrodes induce less membrane stiffening (c.f. Figure 6.18). Dry carbon black powder can be an interesting material to enhance the lifetime of DEAs, and its low stiffening is of interest for thin low-voltage DEAs. However, dry carbon black powder is challenging to use, as there is no matrix to keep the powder attached to the silicone elastomer material, making it messy to manufacture and a possible source of contamination.

Table 6.5: MTTF and actuation strain range for the investigated electrode materials under different environmental conditions. Lifetime is compared to pad-printed DEAs at 90 V/ μ m at 85°C – 85% RH.

Electrode	Electric field (V/ μ m)	% of break-down strength	Condition	Water vapor content (g/cm ³)	Actuation strain (%)	MTTF (h)	Lifetime factor
Pad-printed	90	75%	85°C – 85%RH	297	3.4 \pm 0.4	14	1 x (ref.)
Inkjet-printed					3.7 \pm 0.4	0.2	0.014 x
Dry carbon powder					3.1 \pm 0.3	> 100	> 7 x
Pad-printed	90	75%	20 °C – 90%RH	16	3.7 \pm 0.3	36	2.6 x
Inkjet-printed					3.9 \pm 0.5	2.4	0.17 x
Dry carbon powder					2.8 \pm 0.3	> 100	> 7 x
Pad-printed	90	53%	85°C – 20%RH	70	3.6 \pm 0.3	124	8.9 x
Inkjet-printed					3.2 \pm 0.4	146	10.4 x
Dry carbon powder					2.9 \pm 0.3	> 200	> 14 x
Pad-printed	90	56%	20°C – 30%RH	5	3.5 \pm 0.5	> 200	> 14 x
Inkjet-printed					3.1 \pm 0.3	> 200	> 14 x
Dry carbon powder					2.7 \pm 0.3	> 200	> 14 x

Figure 6.20 shows Weibull plots of failure probability vs. time for inkjet-printed and pad-printed DEAs.

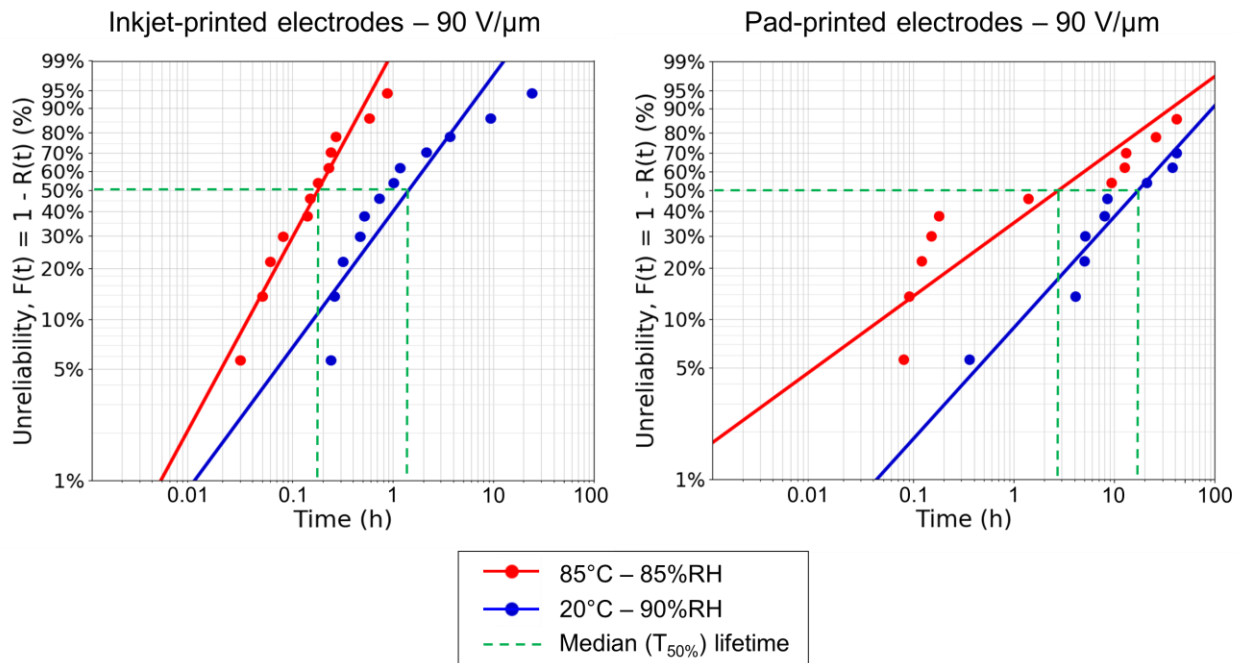


Figure 6.20: Weibull plots of failure probability vs. time for inkjet-printed and pad-printed DEAs under humid conditions. Median lifetimes are shown by green dashed lines. Only the datasets with enough datapoints from Figure 6.19 are shown here.

Figure 6.21 plots the strain at failure vs time for each of the DEAs presented in Figure 6.20. The same nominal electric field is applied to each DEA, but variations in thickness and in fabrication lead to a range of measured strains. As shown in Figure 6.21, higher strains are not correlated to shorter lifetimes for each given electrode material and environmental condition. Furthermore, for each individual electrode material, the strain at failure is not significantly affected by changes in environmental conditions, i.e. environmental conditions are not found to yield major changes in the strain at failure of the DEAs under constant electric fields.

DEAs exhibit a stable strain after the initial first hours of actuation, regardless of the electrode material used, as shown in the Figure 6.2 in Section 6.1. During the first hours of actuation, the increase of the strain at high voltage (HV) is tightly correlated to the increase in strain at 0 V (permanent set), which ranges between 0.5% to 1.7%. I do not see any dependence of permanent set on the type of electrode material.

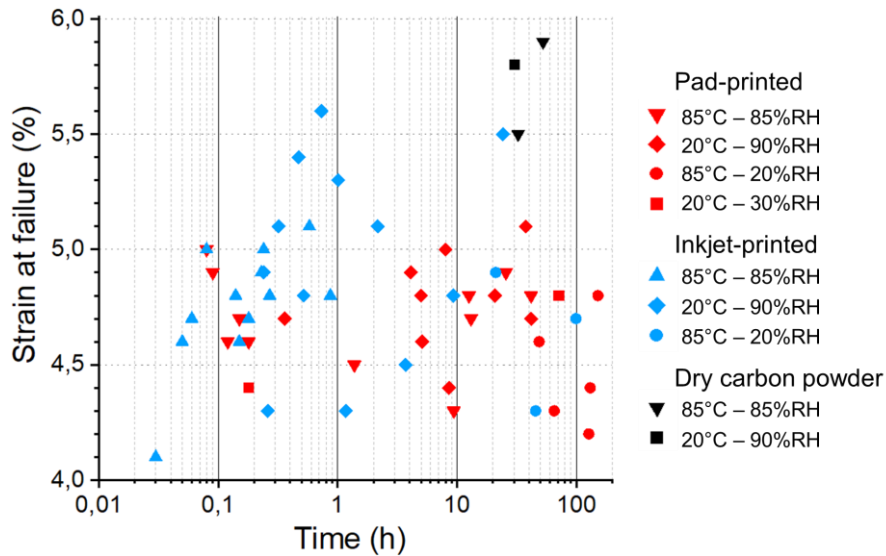


Figure 6.21: Strain at failure for the investigated electrode materials under the four environmental conditions. Dry carbon black powder electrodes are actuated at 50 V/ μm , whereas DEAs with other electrode materials are actuated at 90 V/ μm . Only the failed DEAs of our tests are shown in this figure. All DEAs failed by dielectric breakdown. For readability considerations, error bars are not shown.

Figure 6.6 (in Section 6.1) shows that the DEAs with dry carbon powder electrodes exhibit the highest resistance (55 – 70 k Ω), whereas inkjet-printed electrodes have the lowest resistance (<15 k Ω). Pad-printed DEAs show intermediate resistances (20 – 30 k Ω). Both pad-printed and dry carbon powder electrodes exhibit a decrease of electrode resistance over the first hours of actuation and both show an initial resistance which is maximal over the range of DC actuation.

6.7 Effect of polarity reversal

Figure 6.22 shows how alternating DC polarity influences the lifetime of Elastosil 2030/20 DEAs, to investigate whether higher lifetimes can be achieved by periodically reversing the polarity of the electrodes. If charge migration and space charge accumulation are significant factors that accelerate the breakdown failure of DEAs, then alternating the polarity of the electrodes could yield higher lifetimes.

I observe in Figure 6.22 and in Table 6.6 that the DC lifetime of Elastosil 2030/20 DEAs decreases by polarity reversal, at least for polarity reversal frequencies up to 0.3 Hz. By alternating the polarity, the MTTF decreases by a factor 0.16x (from 14 h to 2.2 h) at 0.01 Hz, by a factor 0.05x (from 14 h to 0.7 h) at 0.1 Hz, and by a factor 0.6x (from 14 h to 8.3 h) at 0.3 Hz. It is unclear why alternating the polarity leads to DC lifetime decrease vs. without any polarity reversal.

Lifetime which does not increase with polarity reversal up to 0.3 Hz could potentially indicate that large-scale charge accumulation would occur in timescales faster than 3 seconds. Further investigations are needed to investigate the relationship between space charges and DC lifetime in thin elastomer films, as well as how fast space charges accumulate in silicone elastomers. According to Iannarelli et al., silicone elastomers do display interface polarization which saturates within seconds³⁵⁷, which may explain why polarity reversal (up to 0.3 Hz) does not affect the lifetime of silicone-based DEAs.

Experiments at higher frequencies of polarity reversal are required to investigate whether fast (> 1 Hz) polarity reversal can lead to improved DC lifetimes. However, for practical applications where power consumption is important, reversing the polarity at fast rates is not ideal as it requires significant energy consumption, because the DEA needs to be charged and discharged in each reversal cycle.

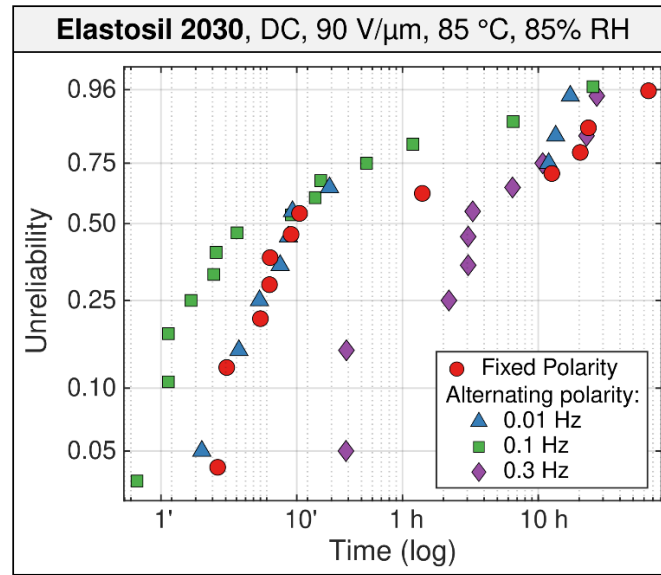


Figure 6.22: Weibull probability plot for Elastosil 2030/20 DEA lifetime: comparison between fixed DC polarity and alternating DC polarity at 0.01 Hz, 0.1 Hz, and 0.3 Hz. Despite subtle differences at 0.3 Hz, there is no significant increase in DC lifetime of DEAs with alternating polarity.

Table 6.6: MTTF and actuation strain range for the investigated DEAs with varying frequencies of polarity reversal at $90 \text{ V}/\mu\text{m}$ at $85^\circ\text{C} - 85\% \text{ RH}$. Lifetime is compared to DEAs at fixed polarity.

Condition	Electric field ($\text{V}/\mu\text{m}$)	% of break-down strength	Condition	Water vapor content (g/cm^3)	Actuation strain (%)	MTTF (h)	Lifetime factor
Fixed polarity	90	75%	$85^\circ\text{C} - 85\% \text{ RH}$	297	3.4 ± 0.4	14	1 x (ref.)
0.01 Hz alternating					3.8 ± 0.3	2.2	0.16 x
0.1 Hz alternating					3.8 ± 0.4	0.7	0.05 x
0.3 Hz alternating					3.7 ± 0.4	8.3	0.6 x

6.8 Conclusion

This chapter reports how the lifetime of equibiaxially prestretched single-layer silicone-based dielectric elastomer actuators (DEAs) is affected by the choice of dielectric elastomer and electrode material, by electric field and by environmental conditions under constant DC actuation, using an automated (MAPLE) lifetime setup presented in Section 4.3.

I demonstrate that silicone-based DEAs failed exclusively by dielectric breakdown. The onset of breakdown failure could not be predicted from changes in strain or changes in electrode resistance prior to breakdown.

Electric field and humidity are the key accelerating factors for dielectric breakdown failure of silicone-based equibiaxially prestretched DEAs, yielding a significant DC lifetime decrease. At $85^\circ\text{C} - 85\% \text{ RH}$, the lifetime of Elastosil 2030/20 decreases by a factor 7x from $80 \text{ V}/\mu\text{m}$ DC operation to $90 \text{ V}/\mu\text{m}$ DC operation, by a factor 62x from $80 \text{ V}/\mu\text{m}$ to $100 \text{ V}/\mu\text{m}$, and by a factor 990x from $80 \text{ V}/\mu\text{m}$ to $110 \text{ V}/\mu\text{m}$. At 85°C , the lifetime of Elastosil 2030/20 DEAs with pad-printed electrodes is reduced by a factor of 43x from 20% RH to 85% RH.

Higher temperatures also decrease DC lifetime, but to a lesser extent. From $20^\circ\text{C} - 90\% \text{ RH}$ to $85^\circ\text{C} - 85\% \text{ RH}$, a 6x lifetime decrease is observed for Elastosil 2030/20 DEAs.

I show that selecting Electro 242-1 as dielectric membrane yields the highest DC lifetimes among the investigated silicone elastomers. Its higher chain lengths could be responsible for its increased lifetime performance. At 85°C – 85% RH and 90 V/ μ m, Electro 242-1 DEAs show over 15x higher lifetimes (> 200 h vs. 14 h) vs. Elastosil 2030/20 DEAs for similar strains (3 % actuation strain). The DC lifetime performance of the investigated silicone-based DEAs cannot be straightforwardly correlated to mechanical properties, water vapor permeability or dielectric breakdown strength data shown in Chapter 5.

I find that pad-printed DEAs have more than 10x higher DC lifetimes than for inkjet-printed electrodes under humid conditions at constant DC fields (90 V/ μ m). DEAs with dry carbon powder electrodes exhibit the highest lifetimes of the investigated electrodes under 4% actuation strain because of their lower operational electric fields (50 V/ μ m) compared to pad-printed and inkjet-printed DEAs (90 V/ μ m). DEAs with dry carbon powder electrodes (operated at 50 V/ μ m) exhibit 35x higher lifetimes at 85°C - 85% RH and more than 5x higher lifetimes at 20°C - 90% RH in comparison to DEAs with pad-printed electrodes (operated at 90 V/ μ m). However, carbon powder electrodes have practical drawbacks compared to cured carbon-PDMS composites.

At constant electric field, encapsulating DEAs with a soft (0.1-0.2 MPa) and thin (4 μ m) silicone (LSR 4305) layer on both electrode sides (2-side) increases DC DEA lifetime by factors of 2.2x to 75x with little impact on actuation strain (5% to 15% reduction in actuation strain), under both humid and dry environments. Encapsulating only 1 side is not as effective as 2-side encapsulation for enhancing lifetime. Thicker encapsulation layers lead to increased lifetimes, but at lower actuation strains (up to 20% reduction in actuation strain).

At 85°C – 85% RH, 1000 h (i.e. 41.7 days) lifetime can be reached at 70 V/ μ m (i.e. \approx 1.5% strain) for non-encapsulated Elastosil 2030/20 DEAs, and at 85 V/ μ m (i.e. \approx 2.5% strain) for silicone LSR 4305 (4 μ m – 2 sides) encapsulated Elastosil 2030/20 DEAs.

The type of encapsulation layer material is important for increasing the lifetime of DEAs. Selecting silicone LSR 4305 (4 μ m – 2 sides) encapsulation layer yields higher lifetime increase than SEBS (3 μ m – 2 sides) encapsulation, despite the high hydrophobicity of SEBS. Silicone LSR 4305 shows excellent adhesion to the silicone-based DEAs, whereas SEBS can be peeled off. At 85°C – 85% RH under 100 V/ μ m, a stiffer encapsulation (silicone Sylgard 186, \approx 1.5 MPa) yields 2.3x higher DC lifetimes than silicone LSR 4305 (\approx 0.2 MPa) encapsulation for a reduced actuation strain (3.8% vs. 4.5%) at constant thickness (4 μ m).

In Chapter 7, I show how the DC lifetime of uniaxially prestretched strip DEAs is influenced by electric field, elastomer material, electrode surface area, the addition of encapsulation layers, and the number of layers (single-layer vs. multilayer).

Chapter 7 DC Lifetime of uniaxially pre-stretched strip single-layer and multilayer silicone-based DEAs

In this chapter, I show how electric field, electrode surface area, the choice of dielectric material, the addition of PDMS (LSR 4305) encapsulation layers, and the number of layers (single-layer vs. multilayer) influences the lifetime of uniaxially prestretched rectangular strip DEAs, shown in Chapter 4. All DEAs are uniaxially prestretched to 1.7 (equivalent to equibiaxial prestretch of 1.3) using linear springs. Section 7.1 presents an overview of the evolution of strain over time and voltage (in Elastosil 2030/20 DEAs). Section 7.2 shows the effect of electric field on DC DEA lifetime. Section 7.3 shows the influence of electrode surface area on DC DEA lifetime. Section 7.4 presents the effect of elastomer material and encapsulation layer on DC DEA lifetime. Section 7.5 presents the effect of number of layers on DC DEA lifetime of multilayer strip DEAs. The data, text and figures from Sections 7.1, 7.2, 7.3, and 7.4 were published in ³³⁰ ⁽⁶⁾.

7.1 Actuation behavior of uniaxially prestretched silicone-based DEAs

7.1.1 Actuation strain vs. time

This section presents the actuation strain behavior of uniaxially prestretched strip silicone-based DEAs prestretched with linear spring bias (c.f. Figure 7.1a). As shown in Figure 7.1b, the actuation strain of strip DEAs (which are uniaxially prestretched with linear spring bias) is dependent on the mechanical properties of the DEA (i.e. force – stretch curve at 0 V and under high voltage) and on the total spring constant (i.e. the slope of the green curve).

When a voltage is applied on the strip DEA at prestretch 1.7 (equivalent to equibiaxial prestretch of 1.3 in Chapter 6), the DEA yields a displacement from the blue circle to the purple circles shown in Figure 7.1b owing to Maxwell force (which reduces the DEA force magnitude at constant stretch from the black curve at 0V to the red curve under high voltage), along the slope of the total spring constant (in green). A decrease in the total spring constant yields a slight increase in strain, as further shown in Figure 7.3, Figure 7.6 and Table 7.2. The loading force – stretch curves can be described using a Gent model (dotted lines), as discussed in Section 7.1.2.

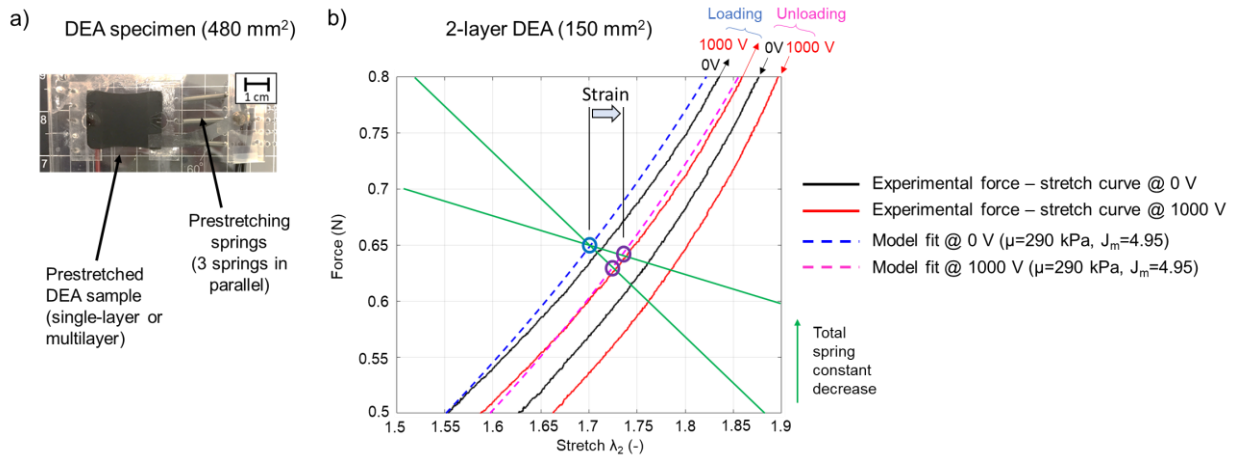


Figure 7.1: a) DEA strips are uniaxially prestretched using linear springs of a total spring constant in an adapted MAPLE lifetime setup (c.f. Chapter 4). b) The actuation strain of strip DEAs which are uniaxially prestretched by a linear spring constant is dependent on the force-stretch curve of DEAs (at 0 V in black, and at high voltage in red) and on the total spring constant (in green). Loading force-stretch curves can be described with a Gent model (dotted lines) both in absence of actuation (blue dotted) and under actuation (pink dotted). Lowering the total spring constant yields higher strains at constant voltage.

⁽⁶⁾ Beco Albuquerque, F. and Shea, H., "Factors influencing the mean-time-to-failure of single-layer uniaxially prestretched silicone-based DEAs," *Proc. SPIE In Press* (2022).

Figure 7.2 plots the strain and the permanent set (i.e. strain at 0V) vs. time for individual 150 mm² single-layer Elastosil 2030/20 DEAs (in black without any encapsulation layers and in red with 4 μ m thick LSR 4305 encapsulation layers) at constant environmental conditions prestretched at a total spring constant of 30 mN/mm.

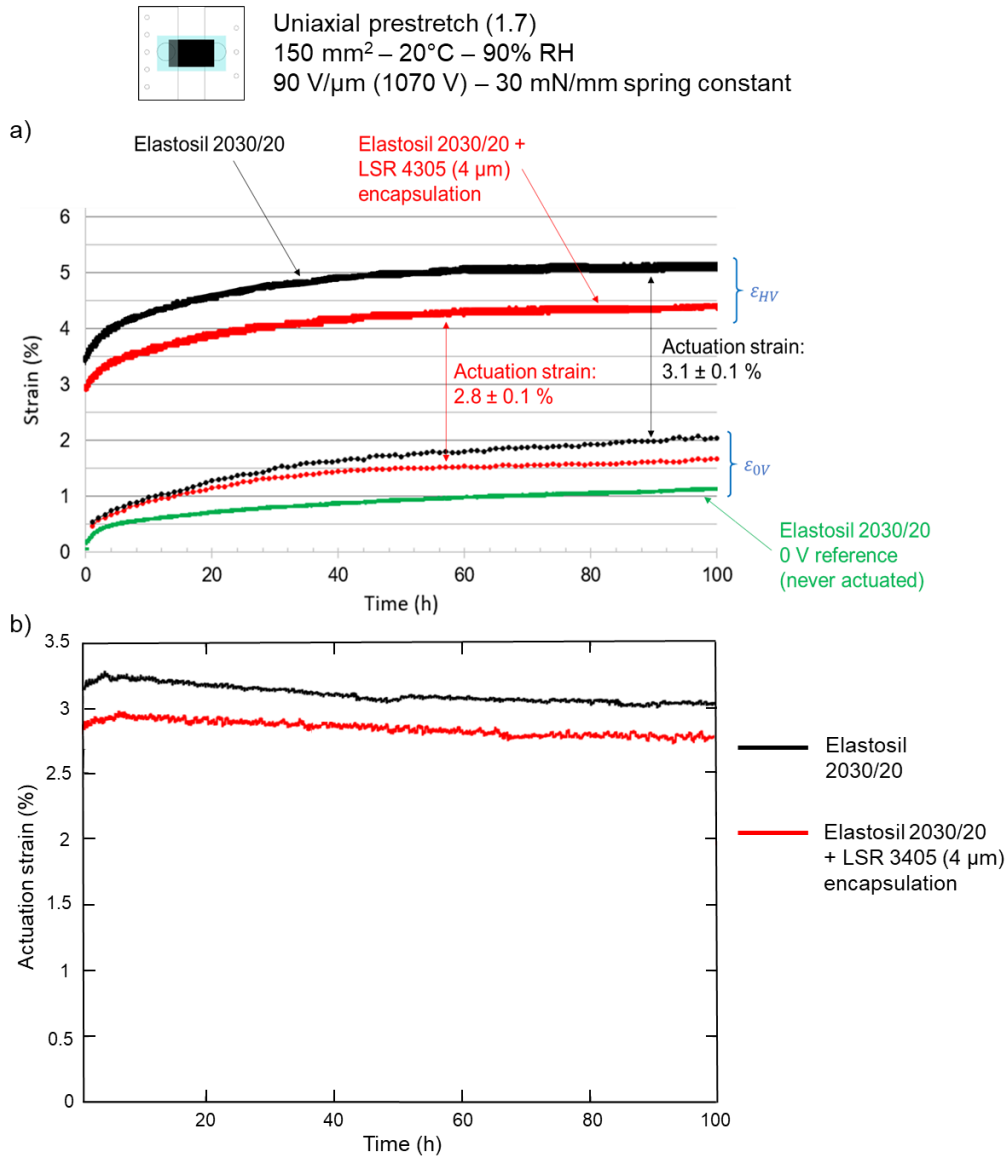


Figure 7.2: a) Strain and b) actuation strain vs. time plot for uniaxially prestretched single-layer strip DEAs of 150 mm² surface area (12 mm x 12 mm active surface area) made of Elastosil 2030/20 actuated at 1070 V at 20°C – 90% RH (red curves corresponding to DEAs encapsulated with LSR 4305, and black curves corresponding to DEAs without encapsulation) and a reference never actuated (green). DEAs show a stable actuation strain over time, but with a growing permanent set owing to actuation and to the spring bias.

As shown in Figure 7.2, the actuation strain ($\epsilon_{HV} - \epsilon_{0V}$) of uniaxially prestretched strip DEAs (red and black curves) is stable over time, and I observe no significant changes in actuation strain just prior to the breakdown event. The linear strain at high voltage ϵ_{HV} (1070 V) is steadily increasing in the first hours of DC actuation before stabilizing. The steady increase in strain at high voltage ϵ_{HV} matches the increase of permanent set (i.e. the strain at 0 V: ϵ_{0V}). Adding LSR 4305 encapsulation layers to DEAs reduces the magnitude of actuation strain from $3.1 \pm 0.1\%$ to $2.8 \pm 0.1\%$, because of the additional stiffening.

Figure 6.1a from section 6.1 also similarly demonstrated that equibiaxially prestretched silicone-based DEAs show a permanent set of around 1% to 2%, which builds up over the first hours of actuation and then gets stable over the remaining lifetime of the DEAs. Additionally, actuation strain (i.e. $\epsilon_{HV} - \epsilon_{0V}$) is relatively stable over time for equibiaxial DEAs.

A fraction of the observed gradual increase in permanent set is due to the prestretching method that uses linear springs which induces a gradual increase in permanent set even in the absence of voltage (green curve in Figure 7.2). Overprestretching the DEAs for 1 hour

at 1.9 uniaxial prestretch allows to slightly reduce the gradual increase in permanent set at 0 V (green curve). As a result, lifetime tests of DEAs carried out in this Chapter are conducted on DEAs after overprestretching them to 1.9 uniaxial prestretch for one hour before actuating them under 1.7 uniaxial prestretch.

Figure 7.3 plots the strain and the permanent set (i.e. strain at 0V) vs. time for individual multilayer 150 mm² Elastosil 2030/20 DEAs prestretched with different total spring constants at 20°C – 90% RH.

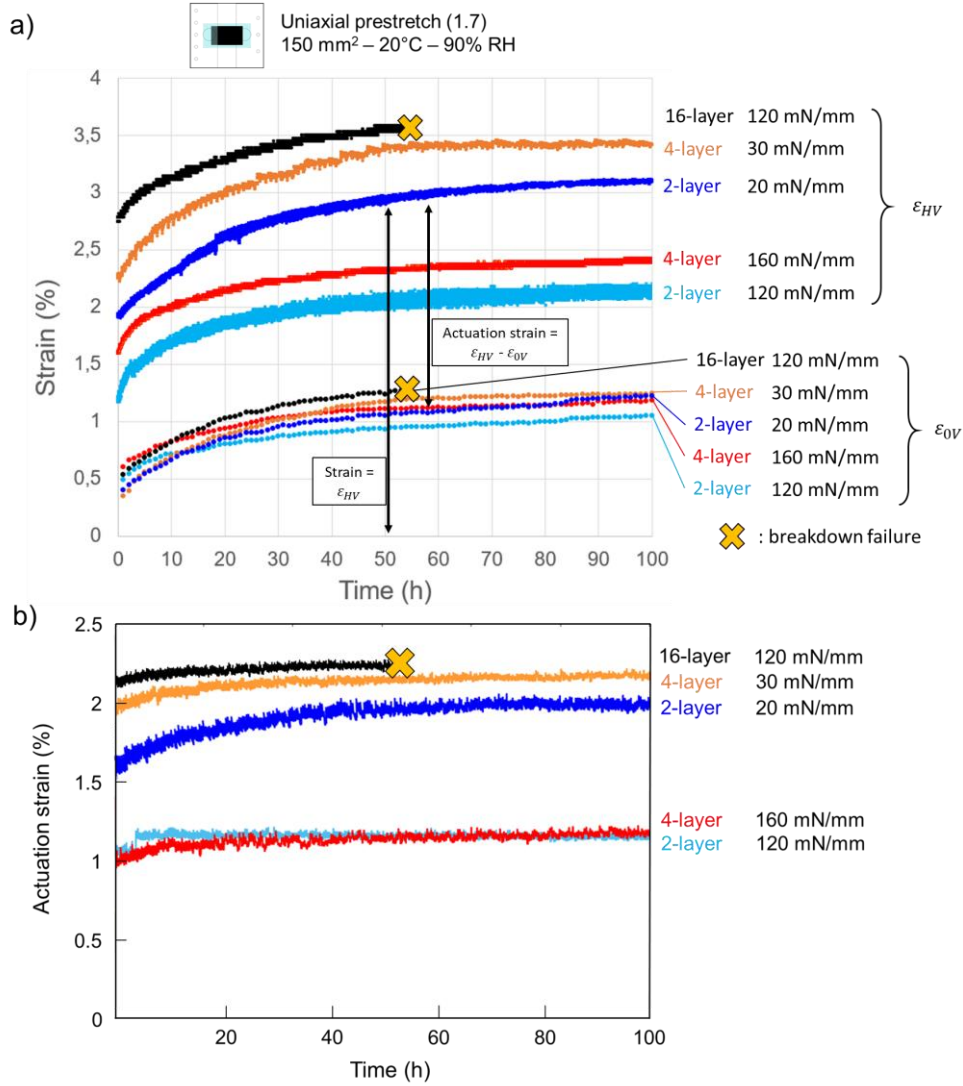


Figure 7.3: a) Strain and b) actuation strain vs. time plot for uniaxially prestretched multilayer strip DEAs of 150 mm² surface area (12 mm x 12 mm active surface area) made of Elastosil 2030/20 actuated at 90 V/ μ m, with varying number of layers and varying total spring constants. DEAs show a stable actuation strain over time, with a growing permanent set. Lower total spring constant for prestretch increases strain at constant electric field.

As shown in Figure 7.3, the actuation strain ($\epsilon_{HV} - \epsilon_{0V}$) of uniaxially prestretched multilayer strip DEAs is stable over time, as for single-layer DEAs in Figure 7.2. There is also no significant changes in actuation strain just prior to the breakdown event, and the linear strain at high voltage ϵ_{HV} (90 V/ μ m) increases progressively in the first hours of DC actuation before stabilizing, matching the increase of permanent set (i.e. the strain at 0 V: ϵ_{0V}).

Selecting a lower total spring constant increases the strain at high voltage ϵ_{HV} without a significant increase in permanent set. In Section 7.5, two sets of experiments are conducted in multilayer DEAs: one set of experiments where DEAs are prestretched with total spring constants matching the stiffness of the DEAs, and one set of experiments where DEAs are prestretched with reduced spring constants to achieve higher strains, and to conduct a lifetime study at constant strains for DEAs with varying number of layers.

The stiffness of the DEAs (for 150 mm² DEAs) is calculated by Eq.24 and presented in Table 7.1:

$$k_{DEA} = \frac{Y_{DE} w \delta}{L} \quad (Eq. 24)$$

where Y_{DE} is the Young's modulus of the dielectric membrane (1.2 MPa for Elastosil 2030/20), w is the DEA sample width (14 mm), δ is the thickness of the dielectric membrane (20 μ m), and L is the DEA sample length (12 mm).

Table 7.1: DEA stiffness calculated with Equation Eq.24.

Number of layers	DEA stiffness (mN/mm)
1 (no encapsulation)	30
1 (+2 encapsulation layers)	80
2 (+2 encapsulation layers)	120
4 (+2 encapsulation layers)	160
16 (+2 encapsulation layers)	500

Figure 7.4 presents linear strain vs. voltage (Figure 7.4a) and linear strain vs. electric field (Figure 7.4b) plots for single-layer uniaxially-prestretched Elastosil 2030/20 DEAs with pad-printed carbon black-PDMS electrodes with (in red) and without (in black) LSR 4305 encapsulation layers (4 μ m thick, on both electrodes).

I observe on Figure 7.4a that the linear strain vs. voltage curve of 150 mm² uniaxially prestretched Elastosil 2030/20 DEAs is slightly affected by the addition of LSR 4305 (4 μ m thick) encapsulation layers. At 1000 V, I observe that adding LSR 4305 (4 μ m thick) encapsulation layers reduces the linear strain by 0.6% (from 4.4% to 3.8% linear strain) because of the increased stiffening. On Figure 7.4b, I observe a similar linear strain decrease at constant electric field.

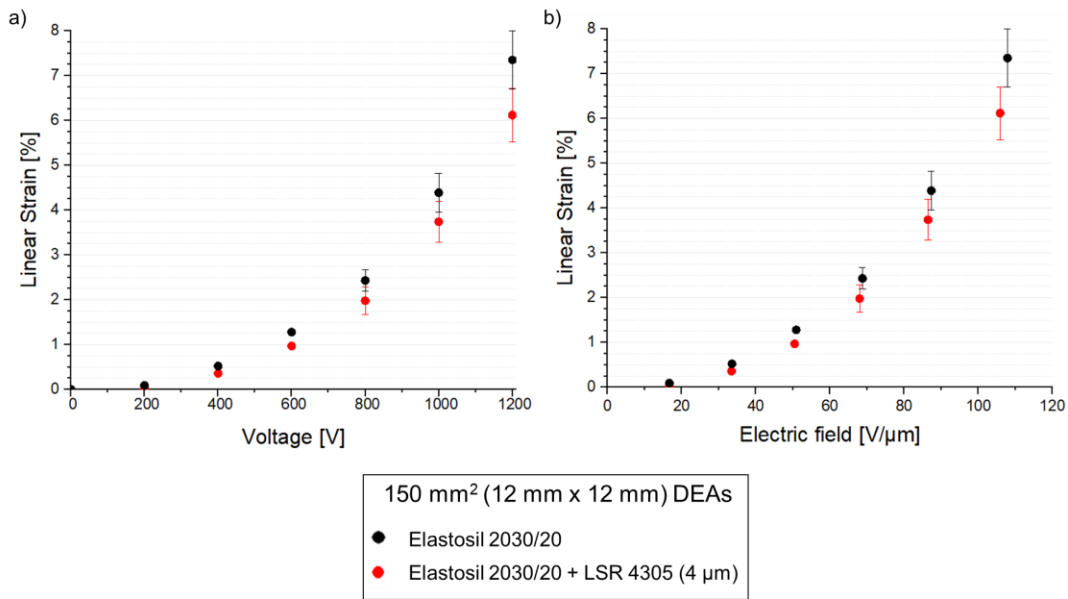


Figure 7.4: a) Strain vs. voltage and b) strain vs. field plots for uniaxially prestretched single-layer 150 mm² Elastosil 2030/20 DEAs with (red dots) and without (black dots) 4 μ m thick LSR 4305 encapsulation layers. Error bars correspond to standard error.

Figure 7.5 presents linear strain vs. voltage (Figure 7.5a) and linear strain vs. electric field (Figure 7.5b) plots for uniaxially-prestretched single-layer and multilayer Elastosil 2030/20 DEAs, prestretched with total spring constant matching DEA stiffness.

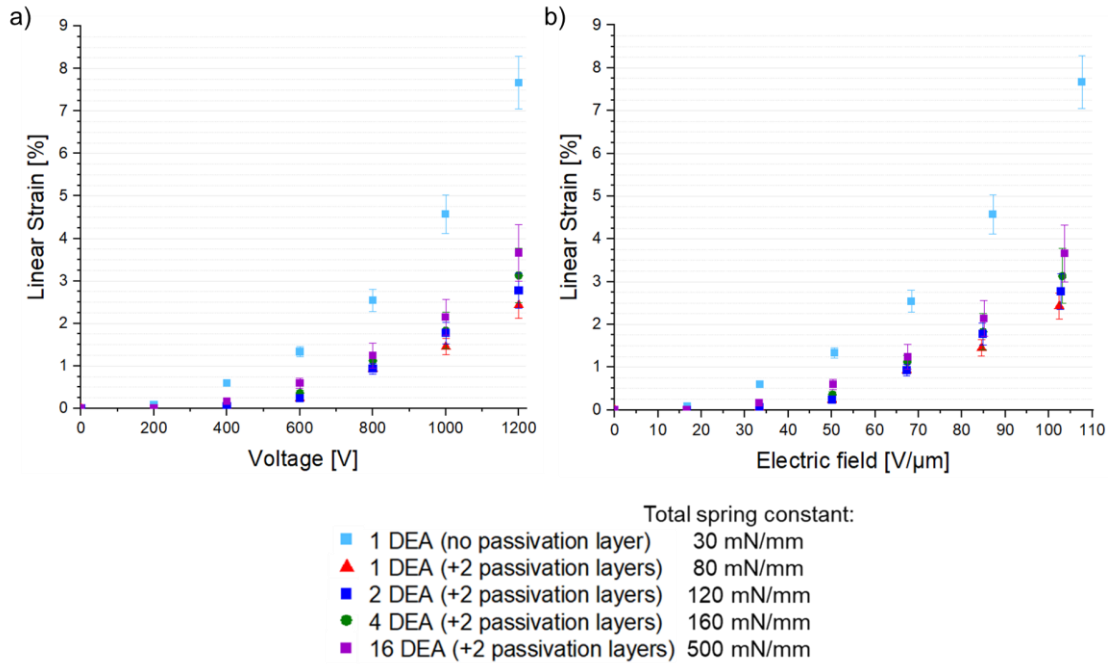


Figure 7.5: a) Strain vs. voltage and b) strain vs. field plots for uniaxially prestretched single-layer and multilayer 150 mm² Elastosil 2030/20 DEAs. The selected total spring constant matches the stiffness of DEAs (c.f. Table 7.1). Error bars correspond to standard error.

The strain at constant voltage and constant field of monolayer DEAs is significantly reduced by the stiffening of the added encapsulation layers. By adding extra DEA layers, strain at constant voltage and at constant field of multilayer DEAs only slightly increases. This absence of significant strain increase with higher number of layers is further discussed in Section 7.1.2.

For the DEAs in Figure 7.5, the selected total spring constant to prestretch the DEAs matches the stiffness of the DEAs, calculated in Table 7.1 using equation Eq.24. As shown in Figures 7.1 and 7.3, lowering the total spring constant at constant prestretch (i.e. by varying spring distance) yields higher achievable DEA strain ranges at constant field.

Figure 7.6 and Table 7.2 present how decreasing the total spring constant (at constant uniaxial prestretch of 1.7) increases the achievable strain at constant voltage for multilayer DEA stacks.

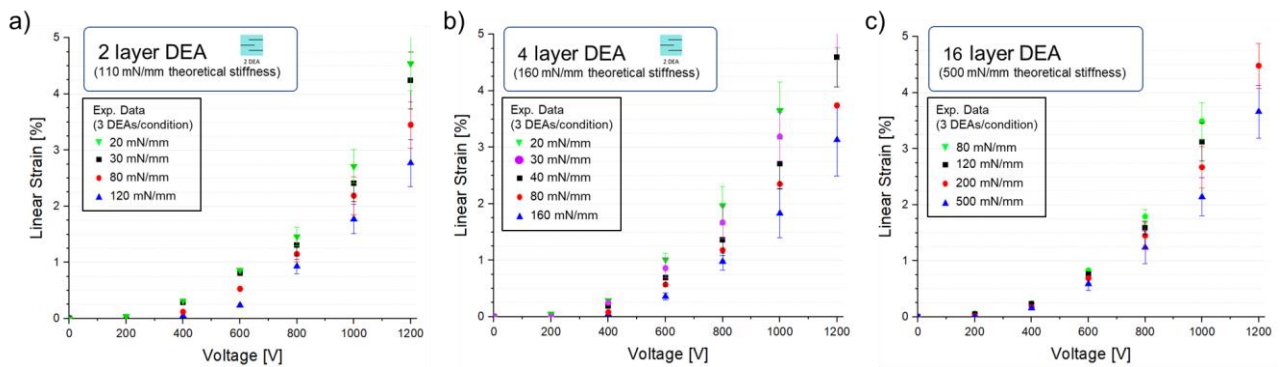


Figure 7.6: a) Strain vs. voltage plots for a) 2-layer, b) 4-layer, and c) 16-layer DEAs uniaxially prestretched to 1.7 with varying total spring constant (average of 3 DEAs per condition). Decreasing the total spring constant yields slightly higher strains at constant voltage. Error bars correspond to standard error (measured on 3 DEAs per condition).

Table 7.2: Strain and actuation strain range for the investigated multilayer DEAs with varying total spring constant under constant prestretch (uniaxial prestretch 1.7) at 1000 V and at 20°C – 90% RH. Reducing the spring constant slightly increases actuation strain at constant voltage.

Number of layers	DEA stiffness (mN/mm)	Total spring constant (mN/mm)	Voltage (V)	Condition	Strain (%) @ 1000 V	Actuation strain (%) @ 1000 V
2	110	120	1000 V	20°C – 90%RH	2.0 ± 0.3 %	1.2 ± 0.3 %
		80			2.2 ± 0.3 %	1.4 ± 0.3 %
		30			2.4 ± 0.3 %	1.9 ± 0.4 %
		20			2.8 ± 0.3 %	2.0 ± 0.3 %
4	160	160			1.8 ± 0.3 %	1.1 ± 0.3 %
		80			2.2 ± 0.3 %	1.4 ± 0.3 %
		40			2.7 ± 0.3 %	1.6 ± 0.3 %
		30			3.2 ± 0.3 %	2.0 ± 0.4 %
		20			3.6 ± 0.3 %	2.2 ± 0.3 %
16	500	500			2.2 ± 0.3 %	1.4 ± 0.3 %
		200			2.7 ± 0.3 %	1.8 ± 0.3 %
		120			3.1 ± 0.3 %	2.1 ± 0.4 %
		80			3.5 ± 0.3 %	2.3 ± 0.3 %

In Section 7.5, I conduct two sets of DC lifetime experiments on multilayer DEAs: one experimental set prestretched with a total spring constant matching the DEA stiffness, and one experimental set where the total spring constant is tuned to achieve DC lifetime studies at constant actuation strain (20 mN/mm for 2-layer DEAs, 30 mN/mm for 4-layer DEAs, and 120 mN/mm for 16-layer DEAs).

In Section 7.1.2, I investigate whether a theoretical model can be used to predict experimental strain vs. voltage plots of a N-layer DEA with varying total spring constants and number of layers N from a fit of the experimental nonlinear force – strain curves.

7.1.2 Actuation strain of single-layer and multilayer strip DEAs: data vs. model

I hereby present a model inspired from Rizzello et al.³⁵⁸ and Hodgins et al.³⁵⁹ that would allow to have a predictive tool for strain in single-layer and multilayer strip DEAs prestretched with spring bias, for any given spring constant, and any prestretch value for a N-layered DEA. I compare the strain results with experimental data to evaluate whether the model is suitable for predicting strain in multilayer DEAs.

For the model, I consider a DEA system prestretched with a linear spring bias. Two forces need to be considered: the DEA force and the spring force. The model presented here assumes that the DEAs are incompressible in volume (e.g. no mechanical losses), assuming no necking (i.e. constant DEA width w over strain λ_2), no stiffening from electrodes, no hysteresis, creep, permanent set and Mullins effect, no dependence of relative permittivity on strain (λ_2), no passive regions (i.e. entire surface area of each layer participates in actuation, e.g. no trapped air bubbles between DEA layers) and flat perfectly-adhering N layers.

There are three different states for the DEA force: state 1 where the DEA is at rest ($F_{DEA} = 0$), state 2 where the DEA is prestretched (i.e. total DEA force is purely mechanical), and state 3 where the prestretched DEA is actuated (i.e. total DEA force is mechanical and electromechanical), as presented in Figure 7.7.

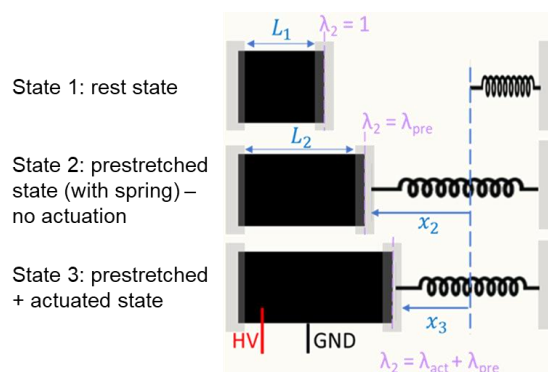


Figure 7.7: DEA model schematic. An ideal DEA of length L_1 in an initial state 1 is prestretched to a state 2 by a factor λ_{pre} to a length L_2 , assuming no necking. The DEA is then actuated to a state 3 for a total stretch factor of $\lambda_{pre} + \lambda_{act}$.

In state 2 (prestretched state of $\lambda_2 = \lambda_{pre}$ at no actuation), the force of a N -layer DEA of cross-sectional area A , width w and of dielectric thickness δ_0 (thickness of 1 DE layer) encapsulated by 2 outer layers only has a mechanical contribution, yielding the following stretch (λ_2) dependent equation:

$$F_{DEA, tot, 2} = F_{mech, 2} = \sigma_2 * (N + 2) * A = \sigma_2 * (N + 2) * \frac{w * \delta_0}{\lambda_2} \quad (Eq. 25)$$

Owing to the nonlinear mechanical properties of elastomers, I use a Gent hyperelastic model for the mechanical stress term σ :

$$\sigma = \sigma_{GENT} = \mu \frac{\lambda_2^2 - \lambda_1^{-2} \lambda_2^{-2}}{1 - (\lambda_1^2 + \lambda_2^2 + \lambda_1^{-2} \lambda_2^{-2} - 3)/J_m} \quad (Eq. 26)$$

with $\lambda_2 = \lambda_{pre}$ in state 2. For the computation of the model, necking is neglected, i.e. $\lambda_1 = 1$. μ [MPa] is the shear modulus and J_m [—] is the limiting stretch. Both μ and J_m parameters are determined by fitting (MATLAB's curve fitting tool) with the experimental force-strain loading curves (3rd loading stretch cycle, averaged over 3 DEAs and measured at a rate of 0.033 mm/s using the mechanical test bench presented in Chapter 4) of each N -layer DEA under no actuation (i.e. at 0 V).

Values for μ and J_m parameters are given in Table 7.3, and show that there is a significant stiffening with the addition of DEA layers from 2-layer ($\mu = 290$ kPa) to 4-layer ($\mu = 375$ kPa) and to 16-layer ($\mu = 410$ kPa) DEAs. This stiffening could be due to the plasma treatment process that is used to adhere each additional layer to the DEA stack, but further experiments are needed to confirm whether the plasma treatment is the major root cause of the observed stiffening.

Table 7.3: Gent model fit parameters of shear modulus and limiting stretch (obtained by minimizing root mean square error using MATLAB's curve fitting tool). The fit (Equation 25 with Equation 26) is carried out on the average (of 3 different DEAs) experimental loading force-stretch curve (using only the 3rd stretching cycle of each DEA). Higher number of layers leads to increased stiffening (i.e. higher shear modulus).

Number of layers	Shear modulus μ (kPa)	Limiting stretch J_m (—)
1 (no encapsulation)	345	5.15
1	280	5.2
2	290	4.95
4	375	9.4
16	410	9.2

In state 3 (prestretched + actuated state of $\lambda_2 = \lambda_{pre} + \lambda_{act}$), a voltage V is applied on the DEAs, leading to an additional electromechanical force (Maxwell force) which decreases the total DEA force at constant stretch proportionally with the number of DEA layers N . The Maxwell force is given by:

$$F_{Maxwell} = N * \sigma_{Maxwell} * A = N * \sigma_{Maxwell} * \frac{w * \delta_0}{\lambda_2} = -N * \epsilon_0 \epsilon_r \frac{V^2}{\delta_0} \lambda_2 * w \quad (Eq. 27)$$

The total DEA force (from Eq. 25) at actuated state 3 hence becomes:

$$F_{DEA, tot, 3} = F_{mech, 3} + F_{Maxwell} = (N + 2) * \sigma_{GENT, 3} * \frac{w * \delta_0}{\lambda_2} - N * \epsilon_0 \epsilon_r \frac{V^2}{\delta_0} \lambda_2 * w \quad (Eq. 28)$$

with $\sigma_{GENT, 3}$ is the Gent mechanical stress from Equation Eq.26 with $\lambda_3 = \lambda_{pre} + \lambda_{pre}$.

Equation 25 (with Gent model of fitted shear modulus μ and of limiting stretch J_m) yields the blue dotted curve on Figure 7.8, whereas Equation 28 (at $V = 1000$ V) yields the pink dotted curve on Figure 7.8.

In the DEA-spring system shown in Figure 7.7, there is also a contribution of the spring force for states 2 and 3. The spring force with a total spring constant of k (shown as green dotted line in Figure 7.8) in a state i is given by:

$$F_{spring, i} = -kx_i \quad (Eq. 29)$$

As shown in Figure 7.7, the distance between rest and equilibrium state of DEA after prestretch is x_2 for state 2 ($i=2$), and the position distance between rest and equilibrium state of DEA after prestretch and after actuation is x_3 for state 3 ($i=3$).

Figure 7.8 shows a significant hysteresis between the loading and the unloading force - strain curves in Elastosil 2030/20 DEA samples. This hysteresis is not present in the circular membrane DEAs (without any passive regions) of Hodgins et al.³⁵⁹ or in Rizzello et al.³⁵⁸, even though the model shifts from the experimental force curve at high pre-deflection³⁵⁹. Additionally, the samples do not reach a zero strain state after the loading and unloading process, indicating a potential slipping owing to clamping issues.

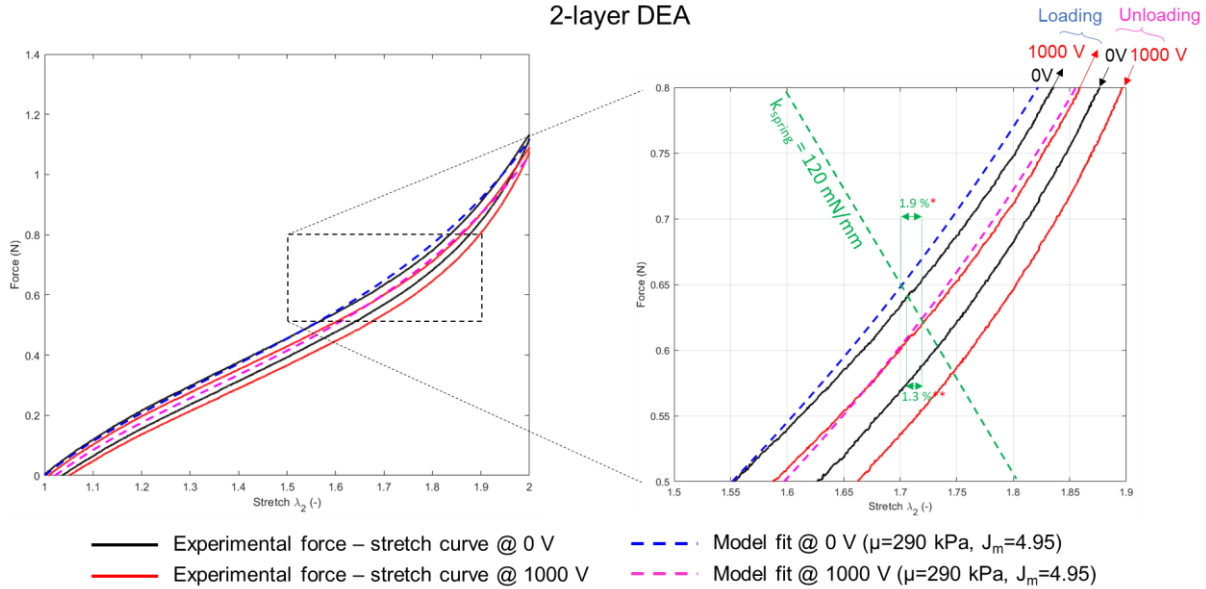


Figure 7.8: Force vs. stretch plots of 2-layer Elastosil 2030/20 DEAs: experimental curves (in black at 0 V, and in red at 1000 V) vs. theoretical (Gent) model (dotted blue lines at 0 V and dotted pink lines at 1000 V) fitted on the respective loading experimental curves. The theoretical model cannot be used to accurately predict actuation strain of linear-spring biased DEA stacks because of significant hysteresis of the experimental force – strain curves. At a total spring constant prestretch of 120 mN/mm matching DEA stiffness (green dotted line), the model strain(*) predicts 1.9 % actuation strain, whereas the difference in strain (**) between the experimental loading curves (in black and red) is of 1.3%, closer to the experimental actuation strain value of 1.2 ± 0.3 % obtained during DC lifetime tests.

The observed hysteresis from Figure 7.8 is significant vs. the difference in model curves between 0 V (dotted blue lines) and 1000 V (dotted pink lines), therefore compromising the accuracy in the predicted strain values vs. the experimentally obtained strain values. As shown in Figure 7.9, the experimental strain vs. voltage data and the theoretical model do not match for multilayer DEAs, and the mismatch increases with number of layers.

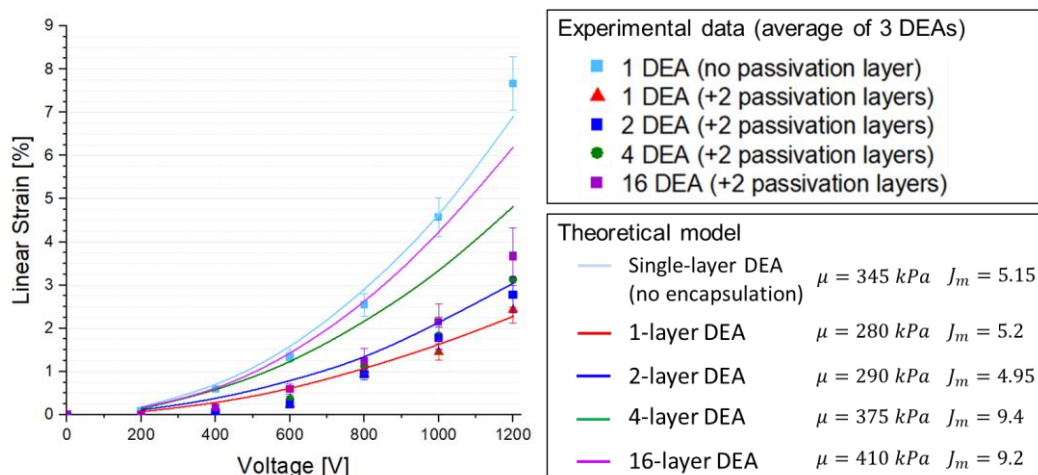


Figure 7.9: a) Strain vs. voltage plots of single-layer and multilayer DEAs: experimental data (represented as datapoints) vs. theoretical (Gent) model (represented as lines). Error bars are standard errors. The theoretical model does not accurately predict strain vs. voltage behaviour of multilayer DEAs.

Beyond the hysteresis in the force-strain curves and the clamping issues demonstrated in Figure 7.8, the mismatch between the strains achieved by the theoretical model and the experimental strain values obtained shown in Figure 7.9 could be due to other factors such as the manufacturing of the DEAs and sample necking, which is neglected within the model.

Figure 7.10 shows how the experimental Maxwell force, calculated by subtracting the loading force-stretch curve at 0 V by the loading force-stretch curve at high voltage at constant stretch (as shown in Figure 7.10a), evolves over stretch, and how it compares with the theoretical Maxwell force that is calculated with Equation Eq. 27, as shown in Figure 7.10b.

Figure 7.10b shows that the experimental Maxwell force is lower than the theoretical values for 1, 2, 4, and 16-layer DEAs. At a uniaxial stretch of 1.7, the gap between the experimental and theoretical values is of 29% for 1-layer DEAs, 12% for 2-layer DEAs, 18% for 4-layer DEAs, and of 11% for 16-layer DEAs. The gap increases with higher stretch, except at high stretch where the gap can slightly decrease, possibly owing to necking plateauing (i.e. width reduction significantly decreases at high stretch).

This observed decrease in Maxwell force can be due to sample necking (neglected in the calculation of theoretical Maxwell force), or to differences in thickness and dielectric permittivity with increasing stretch which are not considered in the calculation of the theoretical Maxwell force and which have not been monitored during the test.

The gaps in Maxwell stress observed in Figure 7.10 are relatively small compared to the strain gap observed in Figure 7.9 for multilayer DEAs, and therefore cannot explain why the tested multilayer DEAs exhibit lower strains than expected by the theoretical model.

Capacitance vs. stretch has also been investigated in Figure 7.11, where I observe that multilayer DEAs exhibit lower capacitance than calculated by theory. The theoretical capacitance (represented as solid lines in Figure 7.11) of a DEA of surface A ($w \times L_0$ initial width \times length), of initial thickness δ_0 , over stretch λ_2 is calculated with:

$$C = \frac{\epsilon_0 \epsilon_r A}{\delta_0} \lambda_2 = \frac{\epsilon_0 \epsilon_r w L_0}{\delta_0} \lambda_2^2 \quad (\text{Eq. 30})$$

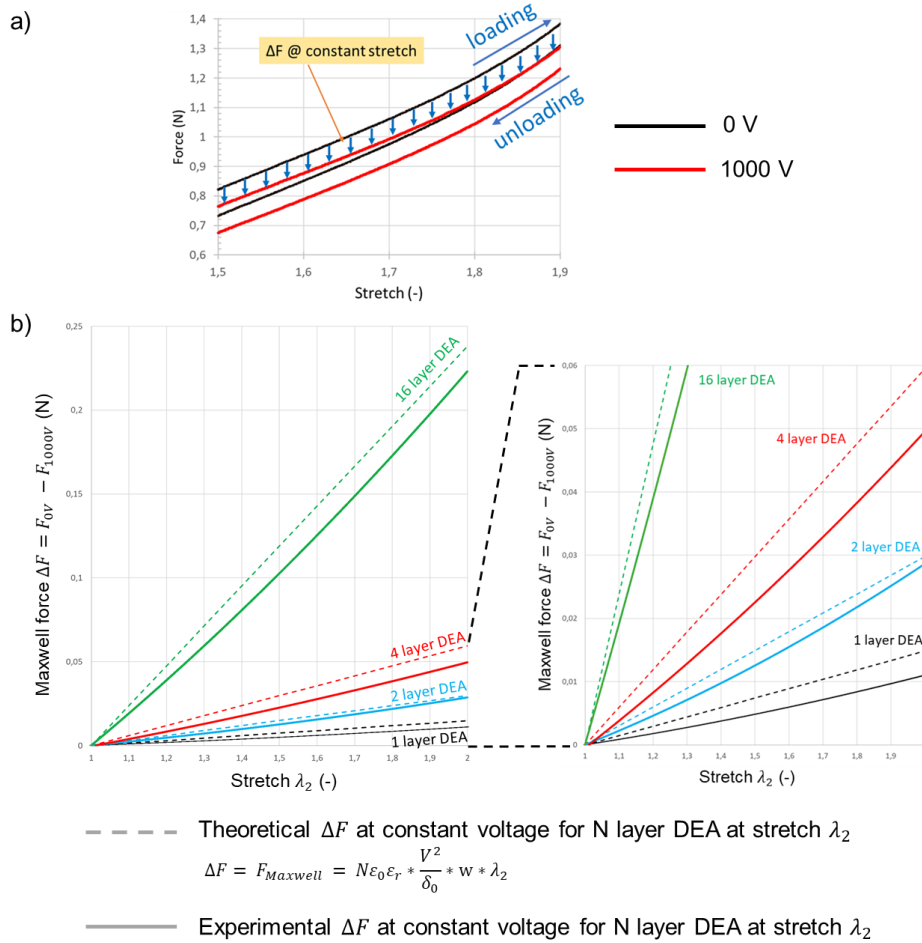


Figure 7.10: a) Example of Maxwell force (ΔF) calculated from the experimental force-stretch curves (averaged over 3 samples and obtained at 0.033 mm/s using the mechanical test bench from Chapter 4 at 20°C – 90% RH) of 4-layer DEAs. The Maxwell force is the difference between the loading force-stretch curve at 0 V and the loading force-stretch curve at high voltage (in red) at constant strain. b) Maxwell force vs. stretch plot for 1,2,4, and 16-layer DEAs calculated by the experimental force-stretch curves (solid lines), and theoretical values calculated with Equation 27 (dashed lines). There is a decrease in Maxwell force vs. theoretical value at constant stretch, regardless of the number of DEA stacks.

The decrease in capacitance is not significant (between -10% and -20%) vs. theoretical value (at constant stretch), and it does not explain why the achieved experimental strain is significantly lower than the theoretical model. The decrease in experimental capacitance in Figure 7.11 is potentially due to sample necking (which is not considered in Equation Eq.30) and to other sources such as manufacturing (e.g. with the presence of tiny air bubbles or possible local delaminations within the DEA stack which could decrease the active surface area and hence the capacitance of the DEA stack. Further studies are required to investigate those potential issues.

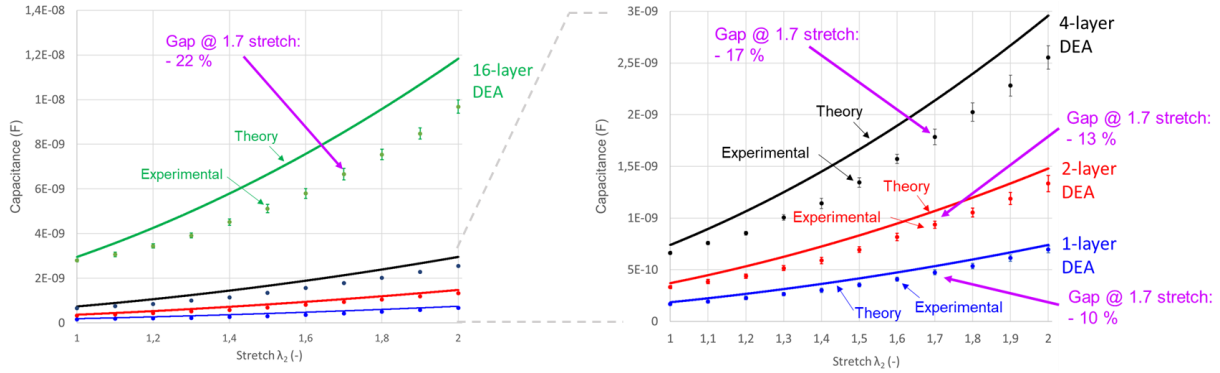


Figure 7.11: Capacitance vs. stretch for multilayer Elastosil 2030/20 DEAs. Multilayer DEAs show slightly lower capacitance (datapoints) than the calculated theoretical values (solid lines) using Equation Eq.30. Capacitance is measured using a Keithley DAQ6510 multimeter system on 3 DEAs per condition. Error bars correspond to standard error accounting for sample variability and calculated error of the capacitance measurement (calculated on 100 pF capacitor: ± 5 pF error).

Therefore, the model cannot be used to accurately predict and describe what strains can be reached, especially if the number of layers increases (to 4-layer and 16-layer DEAs). However, it is a useful tool to get an estimate for the order of magnitude of strain that can be achieved, and to describe how the selection of spring constant influences strain.

7.2 Effect of electric field on single-layer strip DEAs

Figure 7.12 plots failure fraction vs. time for uniaxially prestretched (1.7) Elastosil 2030/20 DEAs of 480 mm² surface area under humid (85%-90% RH) conditions at 85°C and at 20°C.

Higher electric fields yield lower DC DEA lifetimes. I observe that the MTTF decreases at 85°C – 85% RH by a factor 7x from 75 V/μm to 90 V/μm (from 4 h to 0.6 h), and by a factor 15x from 60 V/μm to 90 V/μm (from 9.1 h to 0.6 h).

Uniaxially prestretched (1.7) Elastosil 2030/20 DEAs (480 mm² active area)

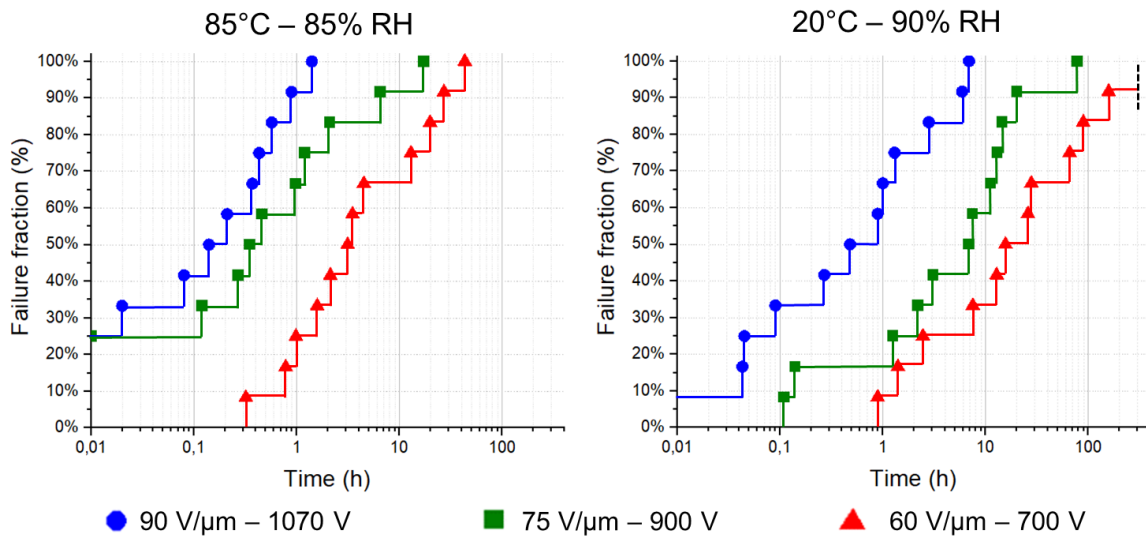


Figure 7.12: Effect of electric field on lifetime of 480 mm² uniaxially prestretched (1.7) Elastosil 2030/20 DEAs at a) 85°C – 85% RH, and at b) 20°C – 90% RH. DEAs are prestretched at a total spring constant of 30 mN/mm (i.e. 3x10 mN/mm springs in parallel). Mean times to failure (MTTF) for each set are reported in Table 7.4. Increasing electric field yields a significant decrease in DC lifetime.

At 20°C – 90% RH, the MTTF decreases by a factor 6x from 75 V/ μ m to 90 V/ μ m (from 15 h to 2.7 h), and by a factor 20x from 60 V/ μ m to 90 V/ μ m (from 54 h to 2.7 h).

Table 7.4: MTTF and actuation strains for 480 mm² uniaxially prestretched (1.7) Elastosil 2030/20 DEAs under different electric fields at 85°C – 85% RH and at 20°C – 90%RH.

Electric field (V/ μ m)	Thickness before prestretch (μ m)	Environmental condition (T, RH)	Water vapor content (g/cm ³)	E/E _{DB} (%)	Strain (%)	Actuation strain (%)	MTTF (h)	Lifetime factor
90	20.1 \pm 0.2	85°C – 85% RH	297.6	74 \pm 3	5.0 \pm 0.5	3.5 \pm 0.5	0.6	1 x (ref.)
75				62 \pm 2	3.6 \pm 0.5	1.8 \pm 0.5	4.0	7 x
60				49 \pm 2	2.1 \pm 0.6	0.9 \pm 0.3	9.1	15 x
90		20°C – 90% RH	15.6	73 \pm 2	4.9 \pm 0.6	3.2 \pm 0.6	2.7	4.5 x
75				61 \pm 2	3.6 \pm 0.5	2.0 \pm 0.5	15	25 x
60				49 \pm 2	2.6 \pm 0.3	1.1 \pm 0.4	54	90 x

By comparing the lifetime performance of uniaxial DEAs with equibiaxial DEAs vs. electric field in Figure 7.13a, I observe that the DC lifetime of uniaxial prestretched DEAs (480 mm²) is orders of magnitude lower than equibiaxial DEAs (20 mm²) at constant field for electric fields below 110 V/ μ m, possibly because of the difference in electrode surface area between equibiaxially prestretched DEAs (20 mm² expanding circle) and uniaxially prestretched DEAs (480 mm², i.e. 30 mm x 16 mm rectangular).

I find that the MTTF follows a logarithmic regression fit of $\log(\text{MTTF}) = \log(A) - BE$ with $B = 0.039 \pm 0.009 \mu\text{m/V}$ and $A = (2.5 \pm 0.5) \cdot 10^3$ h. Compared to equibiaxial DEAs (in blue, data from Chapter 6), the slope for MTTF vs. field plot is over 2x lower ($0.039 \mu\text{m/V}$ vs. $0.099 \mu\text{m/V}$) for uniaxially prestretched DEAs.

Besides, there is a significant trade-off between MTTF and actuation strain on uniaxially prestretched Elastosil 2030/20 DEAs, with a similar trend than for equibiaxially prestretched Elastosil 2030/20 DEAs (from Chapter 6). I find that the MTTF of uniaxially prestretched DEAs follows a logarithmic regression fit vs. actuation strain (c.f. Figure 7.13b): $\log(\text{MTTF}) = \log(A) - B\epsilon_{\text{act}}$ with $B = 0.458 \pm 0.022$ and $A = 25 \pm 1$ h.

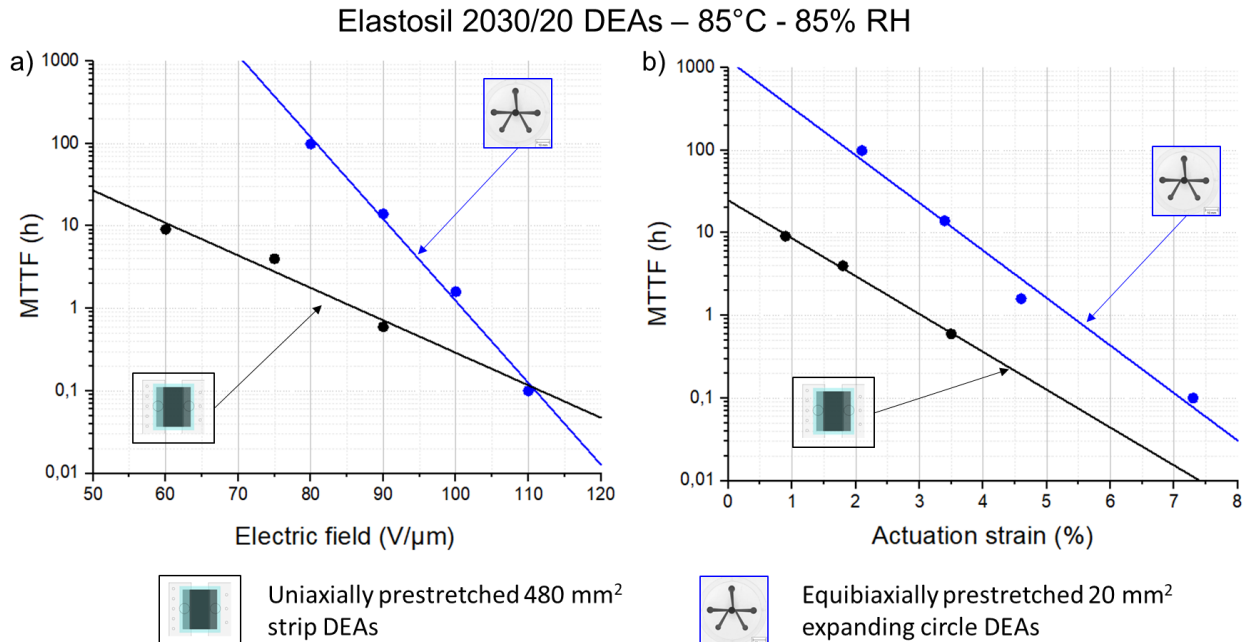


Figure 7.13: MTTF vs. electric field and b) MTTF vs. actuation strain for 480 mm² uniaxially prestretched (PR=1.7, equivalent to PR=1.3 equibiaxial prestretch) Elastosil 2030/20 single-layer strip DEAs at 85°C – 85% RH. DEAs are prestretched at a total spring constant of 30 mN/mm. Data in blue correspond to equibiaxially prestretched (PR=1.3) Elastosil 2030/20 DEAs at 85°C – 85% RH from Chapter 6. Increasing electric field yields a significant decrease in DC lifetime. The fit equation on mean time to failure (MTTF) in Figure 7.13a) is $\log(\text{MTTF}) = \log(A) - BE$ with $B = 0.039 \pm 0.009 \mu\text{m/V}$ and $A = (2.5 \pm 0.5) \cdot 10^3$ h for uniaxially prestretched (1.7) 480 mm² DEAs (in black), and with $B = 0.099 \pm 0.006 \mu\text{m/V}$ and $A = (10.4 \pm 0.6) \cdot 10^3$ h for equibiaxially prestretched (1.3) 20 mm² DEAs (in blue). The fit equation on MTTF in Figure 7.13b) is $\log(\text{MTTF}) = \log(A) - B\epsilon_{\text{act}}$ with $B = 0.458 \pm 0.022$ and $A = 25 \pm 1$ h for uniaxially prestretched (1.7) 480 mm² DEAs (in black), and with $B = 0.576 \pm 0.053$ and $A = 1230 \pm 100$ h for equibiaxially prestretched (1.3) 20 mm² DEAs (in blue). At constant electric field and at constant actuation strain, equibiaxial DEAs (square 20 mm²) show significantly higher DC lifetimes compared to uniaxial DEAs (rectangular 480 mm²). For readability considerations, error bars are not shown.

In Figure 7.13b, increasing actuation strain comes at the expense of significantly lower lifetimes, for both equibiaxially prestretched and uniaxially prestretched DEAs. However, the lifetime at constant actuation strain is significantly lower for uniaxial DEAs vs. equibiaxial DEAs.

7.3 Effect of electrode surface area on single-layer strip DEAs

Figure 7.14 plots failure fraction vs. time for uniaxially prestretched (1.7) Elastosil 2030/20 DEAs of varying surface area at 90 V/ μm under 85°C – 85% RH and 20°C – 90% RH. Table 7.5 shows the actuation strains and MTTF for each tested condition.

Higher electrode surface area yields significantly lower DC DEA lifetimes. The MTTF decreases at 85°C – 85% RH – 90 V/ μm by a factor 13x from 60 mm² to 480 mm² (from 7.9 h to 0.6 h), and by a factor 10x from 150 mm² to 480 mm² (from 6 h to 0.6 h). At 20°C – 90% RH – 90 V/ μm , the MTTF decreases by a factor 9x from 60 mm² to 480 mm² (from 24 h to 2.7 h), and by a factor 6x from 150 mm² to 480 mm² (from 16 h to 2.7 h). Actuation strain does not significantly vary between the tested conditions.

Table 7.5: MTTF and actuation strains for uniaxially prestretched (1.7) Elastosil 2030/20 DEAs with different electrode surface areas at 90 V/ μm at 85°C – 85% RH and at 20°C – 90%RH.

Electrode surface area	Thickness before prestretch (μm)	Environmental condition (T, RH)	Water vapor content (g/cm^3)	Strain (%)	Actuation strain (%)	MTTF (h)	Lifetime factor
480 mm ²	20.0 \pm 0.2	85°C – 85% RH	297.6	5.0 \pm 0.5	3.5 \pm 0.5	0.6	1 x (ref.)
150 mm ²				4.7 \pm 0.4	3.1 \pm 0.4	6.0	10 x
60 mm ²				4.7 \pm 0.4	3.3 \pm 0.5	7.9	13 x
480 mm ²		20°C – 90% RH	15.6	4.9 \pm 0.6	3.2 \pm 0.6	2.7	4.5 x
150 mm ²				4.8 \pm 0.5	3.2 \pm 0.5	16	27 x
60 mm ²				4.8 \pm 0.4	3.1 \pm 0.4	24	40 x

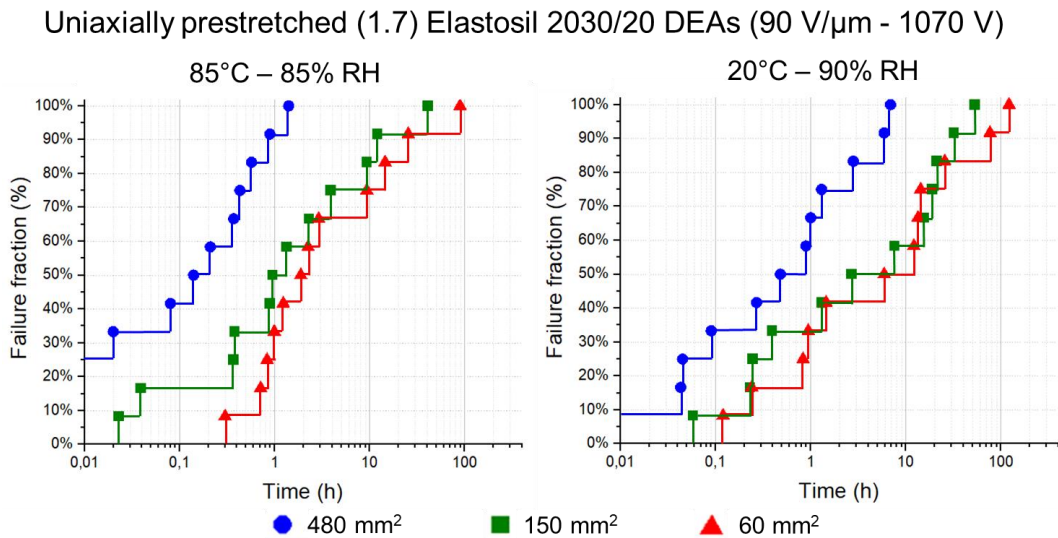


Figure 7.14: Effect of electrode surface area on lifetime of uniaxially prestretched (1.7) DEAs at 90 V/ μm at 85°C – 85% RH and 20°C – 90% RH. DEAs are prestretched at a total spring constant of 30 mN/mm (i.e. 3x10 mN/mm springs in parallel). Mean times to failure (MTTF) for each set are reported in Table 7.5. Increasing electrode surface area yields a significant decrease in DC lifetime.

7.4 Effect of elastomer material and of encapsulation layer on single-layer strip DEAs

Figure 7.15 plots failure fraction vs. time for uniaxially prestretched (1.7) DEAs of 150 mm² surface area at 90 V/ μm at 85°C – 85% RH and at 20°C – 90% RH, presenting how the choice of dielectric elastomer material (Elastosil 2030/20 and Electro 242-1) influences the DC lifetime. Table 7.6 shows the actuation strains and MTTF for each tested condition.

Selecting Electro 242-1 over Elastosil 2030/20 yields a 6x lifetime increase (39 h vs. 6 h) at 85°C – 85% RH and a 4x lifetime increase (59 h vs. 16 h) at 20°C – 90% RH. Both Electro 242-1 and Elastosil 2030/20 exhibit similar strain and actuation strain ranges.

Table 7.6: MTTF and actuation strains for 150 mm² uniaxially prestretched (1.7) Elastosil 2030/20 and Electro 242-1 DEAs at 90 V/ μ m under 85°C – 85 % RH and 20°C – 90% RH.

Elastomer material	Thickness before prestretch (μ m)	Environmental condition (T, RH)	Water vapor content (g/cm ³)	E/E _{DB} (%)	Strain (%)	Actuation strain (%)	MTTF (h)	Lifetime factor
Elastosil 2030/20	20.0 \pm 0.2	85°C – 85% RH	297.6	74 \pm 3	4.7 \pm 0.4	3.1 \pm 0.4	6	1x (ref.)
		20°C – 90% RH	15.6	73 \pm 2	4.8 \pm 0.5	3.2 \pm 0.5	16	2.7x
Electro 242-1	25.8 \pm 0.3	85°C – 85% RH	297.6	80 \pm 2	4.8 \pm 0.5	3.3 \pm 0.5	39	6x
		20°C – 90% RH	15.6	70 \pm 3	4.8 \pm 0.5	3.3 \pm 0.5	59	10x

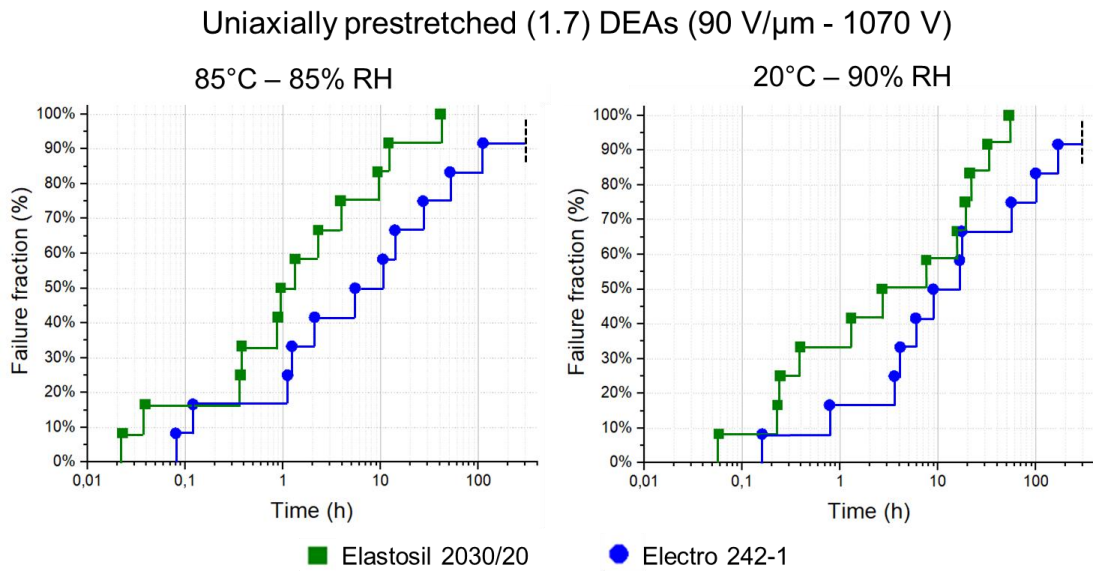


Figure 7.15: Effect of elastomer material (Elastosil 2030/20 and Electro 242-1) on lifetime of 150 mm² uniaxially prestretched (1.7) DEAs at 90 V/ μ m at 85°C – 85% RH and 20°C – 90% RH. DEAs are prestretched at a total spring constant of 30 mN/mm (i.e. 3x10 mN/mm springs in parallel). Mean times to failure (MTTF) for each set are reported in Table 7.6. Replacing Elastosil 2030/20 by Electro 242-1 as dielectric is an effective strategy to increase DC lifetime without changing the actuation strain.

Figure 7.16 plots failure fraction vs. time for uniaxially prestretched (1.7) 150 mm² Elastosil 2030/20 DEAs at 90 V/ μ m under 85°C – 85% RH and 20°C – 90% RH, where I compare Elastosil 2030/20 DEAs with LSR 4305 (4 μ m) encapsulated Elastosil 2030/20 DEAs. Adding soft 4 μ m LSR 4305 encapsulation layers on both electrodes is an effective strategy to increase the lifetime of uniaxially prestretched DEAs at constant fields, similar to equibiaxially prestretched DEAs in Chapter 6.

As shown in Figure 7.16 and in Table 7.7, the MTTF increases at 85°C – 85% RH by a factor 6x by adding a LSR encapsulation on Elastosil 2030/20 (from 6 h to 38 h), while actuation strain decreases from 3.1% to 2.7%. At 20°C – 90% RH, the MTTF increases by a factor 13x by adding a LSR encapsulation on Elastosil 2030/20 (from 16 h to 205 h), while actuation strain decreases from 3.2% to 2.9%.

Uniaxially prestretched (1.7) Elastosil 2030/20 DEAs (90 V/ μm - 1070 V)

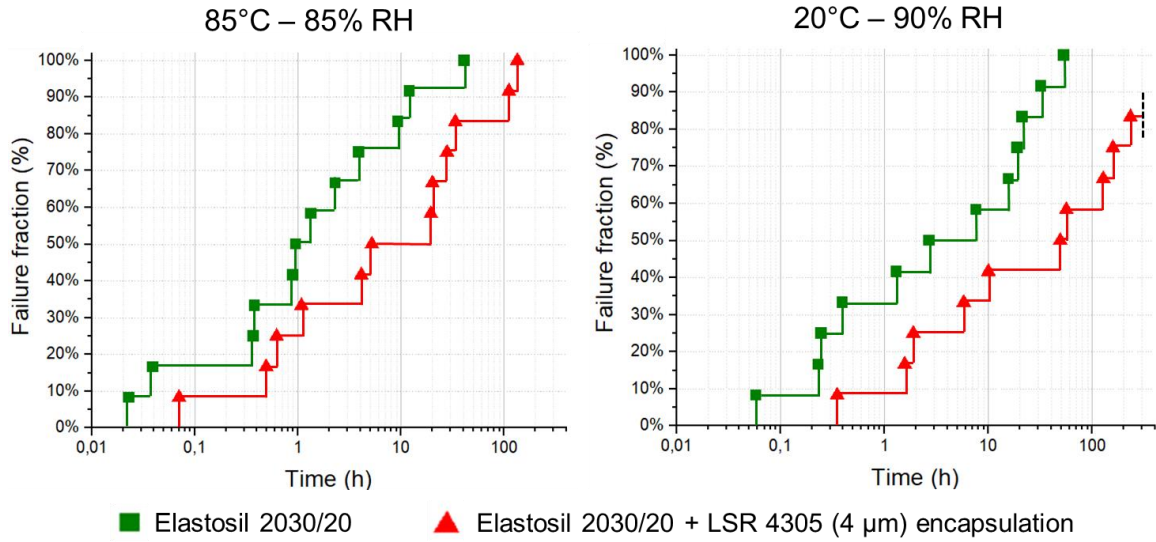


Figure 7.16: Effect of the addition of LSR 4305 (4 μm – both sides, in red) encapsulation layers to Elastosil 2030/20 DEAs (in green) on lifetime of 150 mm² uniaxially prestretched (1.7) DEAs at 90 V/ μm at 85°C – 85% RH and 20°C – 90% RH. DEAs are prestretched at a total spring constant of 30 mN/mm. Mean times to failure (MTTF) for each set are reported in Table 7.7. Adding LSR 4305 encapsulation layers is an effective strategy to increase DC lifetime.

Table 7.7: MTTF and actuation strains for 150 mm² uniaxially prestretched (1.7) Elastosil 2030/20 DEAs without encapsulation, and with LSR 4305 (4 μm – both electrodes) encapsulation at 90 V/ μm at 85°C – 85% RH and at 20°C – 90% RH.

Encapsulation layer	Thickness before prestretch (μm)	Environmental condition (T, RH)	Water vapor content (g/cm ³)	Strain (%)	Actuation strain (%)	MTTF (h)	Lifetime factor
None	20.0 \pm 0.2	85°C – 85% RH	297.6	4.7 \pm 0.4	3.1 \pm 0.4	6	1x (ref)
LSR 4305 (4 μm)				4.3 \pm 0.5	2.7 \pm 0.5	38	6 x
None		20°C – 90% RH	15.6	4.9 \pm 0.6	3.2 \pm 0.6	16	3 x
LSR 4305 (4 μm)				4.5 \pm 0.5	2.9 \pm 0.5	205	34 x

7.5 Effect of number of layers in multilayer DEAs

Increasing the number of DEA layers leads to increased output force, an important characteristic for applications such as e.g. valves. In this section, I investigate the lifetime of multilayer DEAs, prestretched with total spring constant matching the stiffness of DEAs (Figure 7.17 and Table 7.8), and prestretched with reduced total spring constant yielding studies at constant strain (Figure 7.19 and Table 7.9).

Figure 7.17 plots failure fraction vs. time for uniaxially prestretched (1.7) 150 mm² Elastosil 2030/20 DEAs with varying number of layers at 90 V/ μm under 85°C – 85% RH and 20°C – 90% RH. The DEAs are prestretched with total spring constants matching the stiffness of DEAs (c.f. Table 7.1).

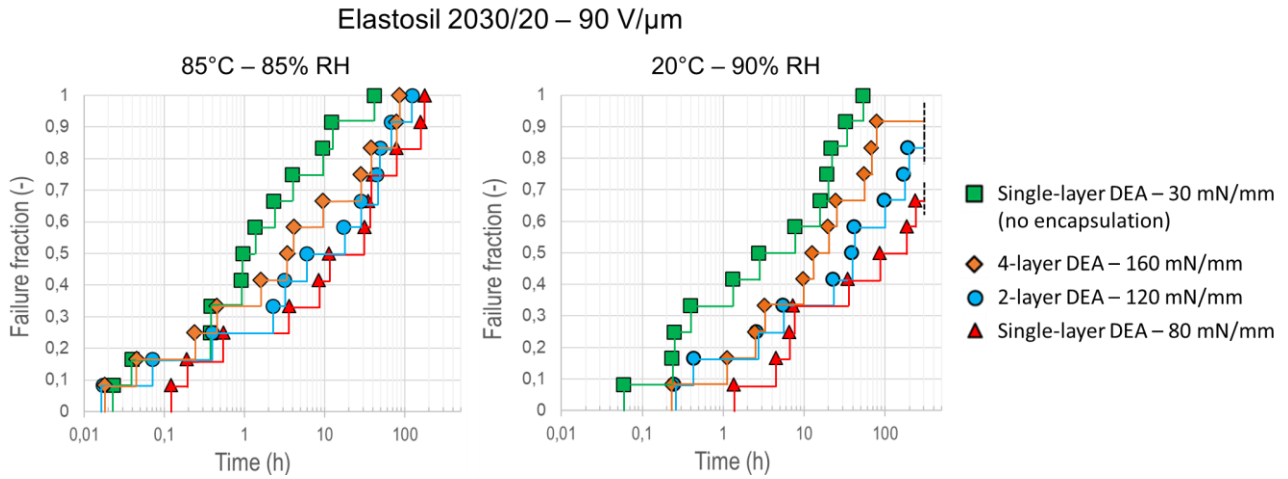


Figure 7.17: Effect of number of layers on DC DEA lifetime of uniaxially prestretched Elastosil 2030/20 DEAs at 85°C – 85% RH and at 20°C – 90% RH, with total spring constant matching DEA stiffness. Additional layers in multilayer DEAs lead to decreased lifetimes. Mean times to failure (MTTF) for each set are reported in Table 7.8. DEAs are prestretched at a total spring constants shown on the right legend.

Encapsulating single-layer Elastosil 2030/20 DEAs with two 20 μ m thick Elastosil 2030/20 encapsulation layers (single-layer DEA) significantly increases DEA lifetime by a factor 11x (from 6 h to 69 h) at 85°C – 85% RH and by a factor 19x (from 16.1 h to 308 h) at 20°C – 90% RH. However, because of the significant stiffening induced by the encapsulation layers, the actuation strain decreases by a factor 0.3x from 3.1 % to 1% at 85°C – 85% RH, and from 3.2% to 0.9% at 20°C – 90% RH.

Compared to encapsulation with soft (≈ 0.2 MPa) thin (4 μ m) LSR 4305 layers (c.f. Section 7.4), encapsulation with 20 μ m thick Elastosil 2030/20 (≈ 1 MPa) layers (described as 1-layer Elastosil 2030/20 DEA here) yields higher lifetimes, but at a significant trade-off owing to increased stiffening. At 20°C – 90% RH, 1-layer Elastosil 2030/20 DEAs exhibits 1.5x higher lifetimes (308 h vs. 205 h) than Elastosil 2030/20 with LSR 4305 (4 μ m) encapsulation, but with a 70% decrease in actuation strain (0.9% vs. 2.9%) at 90 V/ μ m. At 85°C – 85% RH, 1-layer Elastosil 2030/20 DEAs exhibits 1.8x higher lifetimes encapsulation (69 h vs. 38 h) than Elastosil 2030/20 with LSR 4305 (4 μ m), but with a 60% decrease in actuation strain (1.0% vs. 2.7%) at 90 V/ μ m.

Adding additional DEA layers yields a reduction in DC lifetime with increasing number of layers at constant environmental conditions and electric field (90 V/ μ m). As shown in Figure 7.17 and in Table 7.8, the DC lifetime decreases by a factor 0.85x (from 69 h to 59 h) at 85°C – 85% RH, and by a factor 0.75x (from 308 h to 231 h) at 20°C – 90% RH from 1-layer to 2-layer DEAs. The actuation strain only slightly increases from 1 % to 1.3 % at 85°C – 85% RH and from 0.9 % to 1.2 % at 20°C – 90% RH from 1-layer to 2-layer DEAs.

The DC lifetime further decreases by a factor 0.54x (from 59 h to 32 h) at 85°C – 85% RH, and by a factor 0.2x (from 231 h to 46 h) at 20°C – 90% RH from 2-layer to 4-layer DEAs. The actuation strain only slightly increases from 1.3 % to 1.6 % at 85°C – 85% RH and from 1.2 % to 1.5 % at 20°C – 90% RH from 2-layer to 4-layer DEAs.

Table 7.8: MTTF and actuation strain range for the investigated multilayer DEAs with varying number of layers. DEAs are prestretched with total spring constants matching DEA stiffness.

Number of DEA layers	Electric field (V/ μ m)	% of break-down strength	Condition	Water vapor content (g/cm ³)	Actuation strain (%)	MTTF (h)	Lifetime factor
1 (no encapsulation)	90	75 %	85°C – 85% RH	297	3.1 \pm 0.4 %	6.0	1 x (ref.)
1					1.0 \pm 0.5 %	69	11 x
2					1.3 \pm 0.4 %	59	10 x
4					1.6 \pm 0.4 %	32	5 x
1 (no encapsulation)	90	73 %	20°C – 90% RH	15.6	3.2 \pm 0.5 %	16.1	2.7 x
1					0.9 \pm 0.4 %	308	51 x
2					1.2 \pm 0.3 %	231	38 x
4					1.5 \pm 0.4 %	46	8 x

As shown in Figure 7.18, I systematically calculate the capacitance (at 0 prestretch) of unfailed multilayer DEAs at the start of test, after 1 day, 2 days, 3 days, and after 7 days, using the Keithley DAQ 6510 multimeter with a measured error of ± 5 pF.

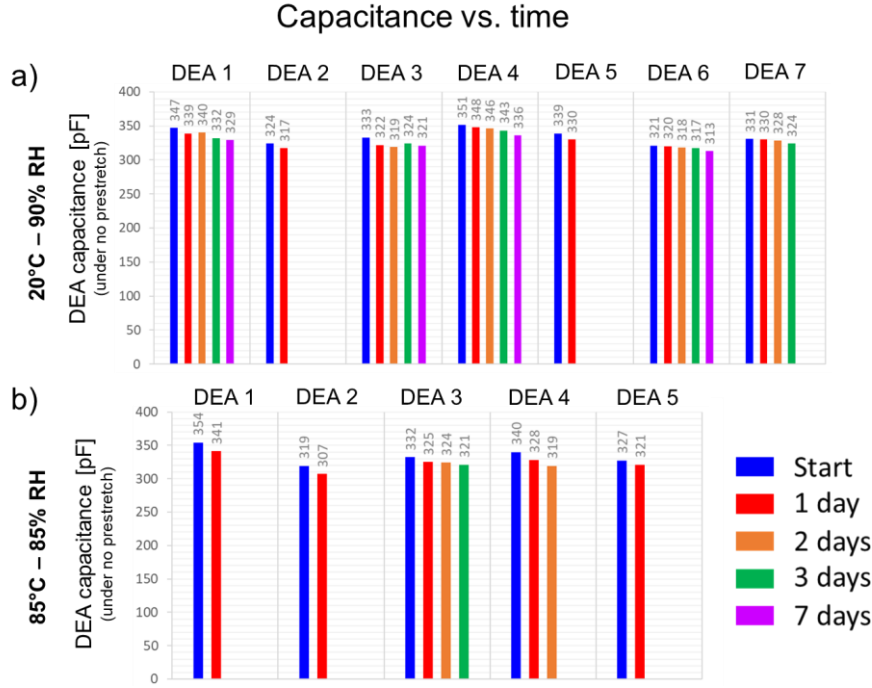


Figure 7.18: Monitoring of individual 2-layer DEA capacitance (at zero prestretch) vs. time at a) 20°C – 90% RH and b) at 85°C – 85% RH. The capacitance is measured initially before the test, after 24 h, 48 h, 72 h, and 1 week of DC actuation if the individual DEA has not failed in the meantime. Only the capacitance of DEAs surviving at least 24 hours of actuation at 90 V/ μ m are shown. There is no significant capacitance decrease over time.

Measuring the initial capacitance of multilayer DEAs allows to check the quality of the electrical connections of the DEA stack and to select only DEA samples that have a sufficiently high capacitance. The theoretical capacitance of a N-layer DEA of surface area A and of layer thickness δ_0 under no prestretch is given by Equation 31:

$$C = N * \frac{\epsilon_0 \epsilon_r A}{\delta_0} \quad (Eq. 31)$$

Assuming a relative permittivity of $\epsilon_r = 2.8$ and considering a DEA geometry of 150 mm² (i.e. 12 mm x 12 mm) and a dielectric elastomer layer thickness of 20 μ m, the theoretical DEA capacitance at zero prestretch is 180 pF for 1-layer DEAs, 360 pF for 2-layer DEAs, 720 pF for 4-layer DEAs, and 3.1 nF for 16-layer DEAs. For the DC lifetime tests, DEAs with insufficient capacitance before the test (e.g. < 160 pF for 1-layer DEAs, < 320 pF for 2-layer DEAs, < 650 pF for 4-layer DEAs, and < 2.8 nF for 16-layer DEAs) are discarded.

Monitoring the capacitance over time allows to see if there is any loss of electrical connections conductivity or decrease in active surface area (e.g. by delamination between layers or trapped air bubbles) occurring during actuation. As shown in Figure 7.18 for 2-layer DEAs, there is no significant decrease in capacitance over time. Similar findings are observed in 4-layer and in 16-layer DEAs.

The failure of multilayer DEAs occurs exclusively by dielectric breakdown within one of the layers and could not be anticipated by changes in strain right before breakdown. I have not conducted any experiment to evaluate if a significant change in capacitance occurs right before breakdown.

In contrast to equibiaxially prestretched expanding circle DEAs (c.f. Chapter 6), mechanical tearing and layer delamination can occur when uniaxially prestretching the DEAs. I systematically overprestretched each single-layer or multilayer DEA presented in Chapter 7 to uniaxial prestretch 1.9 for 1 hour before actuating the DEAs at uniaxial prestretch 1.7. This preconditioning step allows to reduce permanent set (as discussed in section 7.1.1) but also to exclude any DEAs that fails by tearing or by layer delamination at prestretch 1.9. None of the tested DEAs that survive the preconditioning step fail by mechanical tearing.

Figure 7.19 shows how the number of layers influences the DC lifetime of DEA stacks at constant strain, using reduced spring constants vs. the datasets in Figure 7.18. The total spring constant is selected such that an actuation strain of 2 % (i.e. 3% strain) is

achieved in 2, 4, and 16-layer DEAs. As shown in Table 7.2 and in Figure 7.6, the selected total spring constants are 20 mN/mm for 2-layer DEAs, 30 mN/mm for 4-layer DEAs, and 120 mN/mm for 16-layer DEAs.

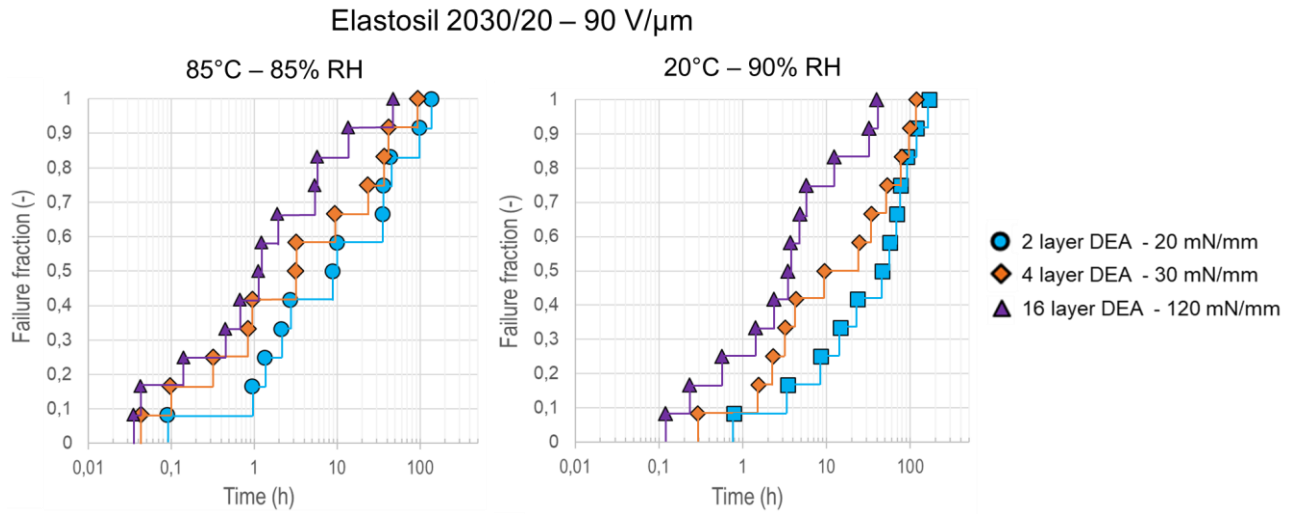


Figure 7.19: Effect of number of layers on DC DEA lifetime of multilayer uniaxially prestretched Elastosil 2030/20 DEAs at 85°C – 85% RH and at 20°C – 90% RH with reduced spring constant for constant strain operation. Additional layers in multilayer DEAs lead to decreased lifetimes. Mean times to failure (MTTF) for each set are reported in Table 7.9. DEAs are prestretched at a total spring constants shown on the right legend.

As observed in Figure 7.19 and in Table 7.9, the DC lifetime decreases by a factor 0.55x (from 38 h to 21 h) at 85°C – 85% RH, and by a factor 0.6x (from 72 h to 43 h) at 20°C – 90% RH from 2-layer to 4-layer DEAs.

The DC lifetime further decreases by a factor 0.27x (from 21 h to 5.6 h) at 85°C – 85% RH, and by a factor 0.21x (from 43 h to 9 h) at 20°C – 90% RH from 4-layer to 16-layer DEAs.

Table 7.9: MTTF and actuation strain range for the investigated multilayer DEAs with varying number of layers. DEAs are prestretched using reduced total spring constants for constant actuation strain tests.

Number of DEA layers	Electric field (V/ μ m)	% of break-down strength	Condition	Water vapor content (g/cm ³)	Actuation strain (%)	MTTF (h)	Lifetime factor
2	90	75 %	85°C – 85% RH	297	2.1 \pm 0.4 %	38	1 x (ref.)
4					2.3 \pm 0.3 %	21	0.55 x
16					2.4 \pm 0.5 %	5.6	0.15 x
2		73 %	20°C – 90% RH	15.6	2.1 \pm 0.3 %	72	1.9 x
4					2.4 \pm 0.4 %	43	1.1 x
16					2.4 \pm 0.4 %	9.0	0.24 x

7.6 Conclusion

This chapter reports how the choice of dielectric material, the addition of an encapsulation layer, the applied electric field, the electrode surface area, and the addition of number of layers influence the lifetime of uniaxially prestretched single-layer and multilayer silicone strip DEAs under DC actuation, using a characterization setup adapted from the automated (MAPLE) lifetime setup presented in Section 4.3.

I show that uniaxially prestretched silicone-based DEAs fail exclusively by dielectric breakdown, similar to the expanding circle DEAs in Chapter 6. Breakdown cannot be predicted by changes in strain. Capacitance of multilayer DEAs does not significantly decrease over time.

I demonstrate that selecting Electro 242-1 over Elastosil 2030/20 as dielectric increases the mean time to failure (MTTF) by a 6x factor at 85°C – 85% RH (39 h vs. 6 h) and by a 4x factor (59 h vs. 16 h) at 20°C – 90% RH.

Higher fields yield significantly lower lifetimes in single-layer DEAs. Increasing the electric field decreases MTTF of single-layer Elastosil 2030/20 DEAs by 2x (9.1 h vs. 4 h) from 60 V/ μ m to 75 V/ μ m with actuation strain increasing from 0.9% to 1.8%, and by 15x (9.1 h vs. 0.6 h) from 60 V/ μ m to 90 V/ μ m with actuation strain increasing from 0.9% to 3.5% at 85°C – 85% RH. At 20°C – 90% RH, MTTF decreases by 4x (54 h vs. 15 h) from 60 V/ μ m to 75 V/ μ m with actuation strain increasing from 1.1% to 2.0%, and by 20x (54 h vs. 2.7 h) from 60 V/ μ m to 90 V/ μ m with actuation strain increasing from 1.1% to 3.2%. There is a trade-off between actuation strain and DC lifetime.

Increasing the electrode surface area decreases the MTTF of Elastosil 2030/20 DEAs without significant changes in actuation strain. Increasing the electrode area from 60 mm² to 150 mm² decreases MTTF by factors 1.3x-1.5x, and by factors 9x-13x from 60 mm² to 480 mm².

At constant field (90 V/ μ m), adding soft (0.2 MPa) thin (4 μ m) LSR 4305 encapsulation layers on both electrodes increases the MTTF of Elastosil 2030/20 DEAs by a 6x factor (38 h vs. 6 h) at 85°C – 85% RH and by a 13x factor (205 h vs. 16 h) at 20°C – 90% RH, with little impact on actuation strain (4.4% vs. 4.8% without encapsulation).

Encapsulating Elastosil 2030/20 DEAs with two 20 μ m thick Elastosil 2030/20 encapsulation layers significantly increases DEA lifetime by a factor 11x (from 6 h to 69 h) at 85°C – 85% RH and by a factor 19x (from 16.1 h to 308 h) at 20°C – 90% RH. However, because of the significant stiffening induced by the encapsulation layers, the actuation strain decreases by a factor 0.3x from 3.1 % to 1% at 85°C – 85% RH, and from 3.2% to 0.9% at 20°C – 90% RH.

Adding additional DEA layers yields a reduction in DC lifetime with increasing number of layers at constant environmental conditions, and at constant electric field (90 V/ μ m). At constant actuation strain of 2% (i.e. 3% strain), the DC lifetime decreases by a factor 0.55x (from 38 h to 21 h) at 85°C – 85% RH, and by a factor 0.6x (from 72 h to 43 h) at 20°C – 90% RH from 2-layer DEAs to 4-layer DEAs. From 4-layer DEAs to 16-layer DEAs, the DC lifetime further decreases by a factor 0.27x (from 21 h to 5.6 h) at 85°C – 85% RH, and by a factor 0.21x (from 43 h to 9 h) at 20°C – 90% RH. The actuation strains of multilayer DEAs are significantly lower than expected vs. a theoretical model. Actuation strains can be increased at constant electric fields and at constant prestretch by decreasing the total spring constant used for prestretch.

Chapter 8 Conclusion

8.1 Achieved results

I demonstrated how the lifetime of silicone-based DEAs is influenced by environmental conditions (T, % RH), by operational conditions (electric field), and by the selection of electrode and dielectric material. The objectives are to find out the main failure mechanism of DEAs under high DC fields, and to find effective solutions to increase DC lifetime under ambient and harsh environmental conditions. I measure the DC lifetime of equibiaxially prestretched expanding circle DEAs and uniaxially prestretched strip DEAs using an automated test setup (MAPLE) which monitors strain and electrode resistance.

The key achieved findings of this thesis are listed here:

Failure mechanism of DEAs:

- Both equibiaxially and uniaxially prestretched silicone-based DEAs fail exclusively by dielectric breakdown, under DC fields. Dielectric breakdown cannot be predicted from changes in strain or in electrode resistance right before breakdown. Over the lifetime of DEAs, I observe stable actuation strain and electrode resistance.

Properties of dielectric membranes:

- The investigated silicone elastomer films (20-25 μm thick) show dielectric breakdown strengths in the range of $110 \text{ V } \mu\text{m}^{-1}$ to $210 \text{ V } \mu\text{m}^{-1}$, except LSR 4305 with values from $50 \text{ V } \mu\text{m}^{-1}$ to $80 \text{ V } \mu\text{m}^{-1}$.
- Thin (30-60 μm) silicone elastomers show similar water vapor transmission rates (between 200 and $310 \text{ g day}^{-1} \text{ m}^{-2}$) and similar water vapor permeability (7 to $11 \cdot 10^{-3} \text{ g mm Pa}^{-1} \text{ day}^{-1} \text{ m}^{-2}$).
- At uniaxial stretch of 69% (equivalent to equibiaxial prestretch of 1.3), the investigated silicone elastomer films exhibit Young's moduli between 1.2 to 1.8 MPa , except LSR 4305 with Young's moduli around 0.2 MPa , and Sylgard 184 with Young's moduli between 3.1 and 3.9 MPa .

Investigations on dielectric breakdown strength of silicone membranes:

- Increasing the prestretch of the silicone membrane is an effective strategy to increase the breakdown strength and the stress figure of merit of silicone elastomers under dry conditions, but leads to lower strain figure of merit due to higher Young's moduli.
- The DEA stress figure of merit falls by 10% - 30% when enhancing temperature from 20°C to 80°C and by 20% - 70% when enhancing relative humidity from 10% RH to 90% RH. The DEA strain figure of merit falls by 10% - 60% when enhancing temperature from 20°C to 80°C and by 20% - 70% when enhancing relative humidity from 10% RH to 90% RH. For silicone elastomers, Sylgard 184 shows the highest stress figures of merit and LSR 4305 the highest strain figures of merit under all investigated conditions.
- Humidity has a larger influence than temperature on lowering the breakdown strength of the investigated prestretched silicone elastomers. Increasing the temperature from 20°C to 80°C leads up to 30% lower breakdown strengths for pre-stretched silicone membranes. Higher relative humidity (from 10% RH to 90% RH) yields up to 43% reductions in breakdown strength under moderate (PR 1.3) and larger (PR 1.5) prestretch, and limited (2% - 10%) reductions in breakdown strength under lower prestretch (PR 1.1).

Investigations on DC lifetime of equibiaxially-prestretched silicone-based DEAs:

- The DC lifetime performance of the investigated silicone-based DEAs cannot be correlated to mechanical properties, water vapor permeability or dielectric breakdown strength of the selected elastomer material. Selecting Electro 242-1 as dielectric membrane yields the highest DC lifetimes among the investigated silicone elastomers. At 85°C - 85% RH and $90 \text{ V}/\mu\text{m}$ electric field, Electro 242-1 DEAs show over 15x higher lifetimes ($> 200 \text{ h}$ vs. 14 h) vs. Elastosil 2030/20 DEAs for similar strains (3 % actuation strain). This could be due to the higher chain lengths in Electro 242-1.

- The combination of high humidity with high electric fields significantly decreases the DC lifetime of equibiaxially pre-stretched silicone-based (Elastosil 2030) DEAs by accelerating dielectric breakdown failure. For equibiaxially prestretched Elastosil 2030/20 DEAs at 85°C – 85% RH, the mean DC lifetime decreases by a factor of 62x when increasing the electric field from 80 V/μm (2% actuation strain) to 100 V/μm (5% actuation strain), and by a factor of 1000x from 80 V/μm (2% actuation strain) to 110 V/μm (7% actuation strain). At 100 V/μm (4 - 5% actuation strain), the DC lifetime decreases by a factor of >125x from 20% RH to 85% RH at 85°C, and by a factor >20x from 30% RH to 90% RH at 20°C.
- The selection of the electrode material influences the lifetime of equibiaxially prestretched DEAs at constant electric field. Elastosil 2030/20 DEAs with pad-printed electrodes have more than 10x higher DC lifetimes than with inkjet-printed electrodes under humid conditions at 90 V/μm. DEAs with dry carbon powder electrodes exhibit 35x higher DC lifetimes at 85°C - 85% RH vs. DEAs with pad-printed electrodes (operated at 90 V/μm) at 4% actuation strain because of their lower operational electric fields (50 V/μm) compared to pad-printed and inkjet-printed DEAs (90 V/μm).
- Significantly higher lifetimes (by factors up to 75x) at constant electric field can be reached by adding a soft (0.2 MPa) and thin (4 μm) PDMS (LSR 4305) encapsulation layer on both electrodes, with low impact on actuation strain (e.g. -5% to -15% reduction in actuation strain). Encapsulation works under both humid and dry environments, and is significantly more effective if both electrode sides are encapsulated vs. only one side. I predict 1000 h DC lifetime at 70 V/μm (1.5% strain) for Elastosil 2030 DEAs, and at 85 V/μm (2.5% strain) for LSR4305 encapsulated Elastosil 2030 DEAs at 85°C – 85% RH using an exponential model fit. Adding encapsulation layers is effective to increase DC lifetime for both equibiaxially prestretched DEAs and uniaxially prestretched strip DEAs.

Investigations on DC lifetime of uniaxially-prestretched silicone-based DEAs:

- Higher electric fields also negatively impact DC lifetime of uniaxially prestretched strip DEAs. Increasing the electric field decreases DC lifetime of single-layer uniaxially prestretched Elastosil 2030/20 strip DEAs by 2x (9.1 h vs. 4 h) from 60 V/μm to 75 V/μm with actuation strain increasing from 0.9% to 1.8%, and by 15x (9.1 h vs. 0.6 h) from 60 V/μm to 90 V/μm with actuation strain increasing from 0.9% to 3.5% at 85°C – 85% RH. There is a trade-off between actuation strain and DC lifetime.
- Decreasing the electrode surface area, replacing Elastosil 2030/20 by Electro 242-1 as dielectric, and adding thin (4 μm) and soft (0.2 MPa) PDMS (LSR 4305) encapsulation layers on both electrodes are effective approaches to significantly increase the DC lifetime of uniaxially prestretched DEAs. Selecting Electro 242-1 silicone instead of Elastosil 2030/20 silicone as dielectric elastomer increases the lifetime of uniaxially prestretched strip DEAs by factors 4x – 6x. Increasing the electrode surface area decreases the DC lifetime of uniaxially prestretched Elastosil 2030/20 strip DEAs without significant changes in actuation strain. Increasing the electrode area from 60 mm² to 150 mm² decreases MTTF by factors 1.3x-1.5x, and by factors 9x-13x from 60 mm² to 480 mm².
- For multilayer uniaxially prestretched strip DEAs, increasing the number of DEA layers yields a reduction in DC lifetime at constant environmental conditions, and at constant electric field (90 V/μm). At constant actuation strain of 2%, the DC lifetime decreases by a factor 0.55x (from 38 h to 21 h) at 85°C – 85% RH, and by a factor 0.6x (from 72 h to 43 h) at 20°C – 90% RH from 2-layer DEAs to 4-layer DEAs. From 4-layer DEAs to 16-layer DEAs, the DC lifetime further decreases by a factor 0.27x (from 21 h to 5.6 h) at 85°C – 85% RH, and by a factor 0.21x (from 43 h to 9 h) at 20°C – 90% RH. Actuation strains can be increased at constant electric fields and at constant prestretch by decreasing the total spring constant used for prestretch.

Figure 8.1 below summarizes the impact of each factor on DC lifetime on DEAs.

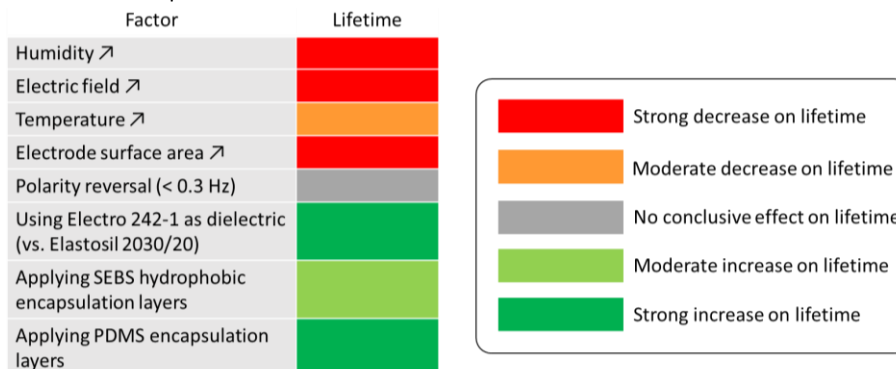


Figure 8.1: Summarized overview of the dependence of DC lifetime of silicone-based DEAs on material and external factors.

8.2 Future development

Our work revealed how the DC lifetime of DEAs is influenced by electric field, environmental conditions, and encapsulation. There is little progress on understanding the fundamental failure mechanisms and phenomena preceding the dielectric breakdown of DEAs. In the future, I suggest the following investigations and developments:

- Developing a leakage current measurement setup

Monitoring leakage current would be interesting to assess the degradation of the dielectric membrane, and to evaluate if it can predict the imminent dielectric breakdown of DEAs. The MAPLE setup has the functionality to measure the total leakage current on 6 DEAs in parallel. However, it did not yield reliable results, notably because of e.g. capacitive coupling between wires. A measurement setup that can reliably monitor pA to nA leakage currents on individual DEAs at a very high-speed frequency (e.g. MHz) constitutes an interesting improvement from our current setup.

- Assessing the importance of space charges on breakdown failure of silicones

A PEA (e.g. pulsed electro acoustic method ³¹²) setup for assessing and comparing how space charge accumulation evolves over time for the different investigated silicone elastomer materials under different environmental conditions, electric fields (with or without polarity reversal) would be an interesting experiment. I speculate that higher densities of space charge and faster space charge accumulation within the dielectric elastomer lead to faster dielectric breakdown failure. However, the limitation is that PEA can only be used with samples with significantly higher thickness ($> 500 \mu\text{m}$, ideally $> 1 \text{ mm}$) than the elastomer membranes used for DEAs in this work, as the spatial resolution of PEA is $> 100 \mu\text{m}$. Therefore, extrapolating results from thick (0.5 - 1 mm) membranes to the DEA membrane thickness ($\approx 12 \mu\text{m}$) used in this work can be complicated.

- Investigating self-clearing electrodes

The section 6.6 shows that the choice of electrode material is also an important contributor to DC lifetime. In the future, further thin and stretchable electrode materials could be explored, such as silver nanowires (AgNW), single-walled carbon nanotubes (SWCNT), and multi-walled carbon nanotubes (MWCNT). Single-walled carbon nanotubes (SWCNT) electrodes can self-clear upon dielectric breakdown, hence extending the DC lifetime beyond breakdown, albeit at lower strains ^{174,191}. Using silver nanowires or carbon nanotube electrodes would also enable DEA lifetime studies at higher strains ($> 5 \%$ actuation strain) owing to its lower stiffening.

- Investigating why encapsulation layers yield significantly higher DC lifetimes

I propose two hypotheses that may explain the observed lifetime increase with the addition of encapsulation layers for both dry and humid conditions.

1. The encapsulation layer is not only a barrier for water vapor, but also for oxygen molecules from the atmosphere as the encapsulation works under both humid and dry conditions. Therefore, I can expect that the diffusion of oxygen molecules toward the DEA is slowed if dielectric breakdown is dominated by oxidation (chemical degradation) processes.
2. The encapsulation layer also mechanically limits the actuation strain of DEAs. If electromechanical breakdown is a dominant mechanism, then the encapsulation layer could participate in delaying the mechanical tearing at the micro-scale prior to dielectric breakdown and hence increase DEA lifetime under both humid and dry conditions.

I also recommend to further investigate how different encapsulation materials (with different known water vapor and oxygen permeability) influence the lifetime of DEAs to evaluate hypothesis 1. For hypothesis 2, evaluating whether electromechanical breakdown is a dominant mechanism would require transparent electrodes (e.g. thin transparent SWCNT or AgNW electrodes) and the use of high-speed cameras to monitor whether any local deformations of the membrane would occur in the milliseconds preceding dielectric breakdown. Yet, it could still be challenging to observe any significant differences. Future investigations on encapsulation shall focus on screening the lifetime performance of encapsulation layers made of elastomer materials of low Young's modulus ($\approx 0.1 \text{ MPa}$) and of low water vapor transmission rate, which adhere extremely well to silicone and the electrode material, as such materials would be excellent candidates as encapsulation layers.

Finally, I observe that Sylgard 186 ($\approx 1.5 \text{ MPa}$) encapsulation yields 2.3x higher DC lifetimes than LSR 4305 ($\approx 0.2 \text{ MPa}$) encapsulation for a 15% reduced actuation strain (3.8% vs. 4.5%) at constant thickness ($4 \mu\text{m}$) and environmental conditions @ $85^\circ\text{C} - 85\% \text{ RH} - 100 \text{ V}/\mu\text{m}$. It is unclear whether the lifetime increase is due to a reduction in strain (i.e. failure owing to electromechanical breakdown), or owing to the intrinsic properties (e.g. Young's modulus, etc.) of the encapsulation layer material. I recommend to screen

several elastomer materials with different mechanical and electrical properties to find out how lifetime is dependent on these properties and hence select an encapsulation layer material that yields the highest lifetimes for a minimal strain tradeoff.

- Investigating the relationship between molecular structure and DC lifetimes

The higher DC lifetimes observed for Electro 242-1 vs. other investigated silicone elastomers in Section 6.2 hint that the structure of the elastomer (i.e. chain length) might lead to significant differences in DC lifetimes. I hence recommend in the future to investigate how the average elastomer chain length correlates with DC DEA lifetime. Furthermore, as the structure of the polymer chain seems to be an important factor for enhancing lifetime, I also recommend investigating how other parameters such as the crosslink density, type of crosslinking chemistry (addition curing vs. condensation curing), catalyst type and concentration affect the molecular structure and hence DC lifetime. Those experiments are however time-consuming, complex and challenging, as the modification of one property or parameter directly influences other intrinsic mechanical or electrical properties, but it has the potential to enhance our understanding of the relationship between the molecular structure of the dielectric elastomer and the lifetime of DEAs under DC fields, and hence pave the way for solutions to further maximize DEA lifetime.

- Investigating DC lifetimes of DEAs with modified dielectric elastomer properties

Beyond the silicone elastomer materials tested in this thesis, the automated (MAPLE) lifetime setup can be used with different elastomer materials, such as slide-ring materials ²⁶ or tailored silicone elastomers ³⁶⁰. In the future, other dielectric elastomer membranes with varying mechanical, chemical or electrical properties could be investigated to further understand how lifetime is correlated with intrinsic properties of elastomers to further increase DC lifetime at constant strains.

- Conduct larger-scale studies for industrial applications

Our study uses up to 12 DEAs per condition. For more reliable lifetime estimations, I recommend conducting DC lifetimes studies using a population above 50 (ideally 100) samples for each environmental condition of interest.

References

- [1] Pelrine, R., Kornbluh, R., Pei, Q. and Joseph, J., "High-speed electrically actuated elastomers with strain greater than 100%," *Science* (80-.). **287**(5454), 836–839 (2000).
- [2] Anderson, I. A., Gisby, T. A., McKay, T. G., O'Brien, B. M. and Calius, E. P., "Multi-functional dielectric elastomer artificial muscles for soft and smart machines," *J. Appl. Phys.* **112**(4), 041101 (2012).
- [3] Rosset, S. and Shea, H. R., "Small, fast, and tough: Shrinking down integrated elastomer transducers," *Appl. Phys. Rev.* **3**(3), 031105 (2016).
- [4] Brochu, P. and Pei, Q., "Advances in Dielectric Elastomers for Actuators and Artificial Muscles," *Macromol. Rapid Commun.* **31**, 10–36 (2010).
- [5] Qiu, Y., Zhang, E., Plamthottam, R. and Pei, Q., "Dielectric Elastomer Artificial Muscle: Materials Innovations and Device Explorations," *Acc. Chem. Res.* **52**, 316–325 (2019).
- [6] Hill, M., Rizzello, G. and Seelecke, S., "Development and experimental characterization of a pneumatic valve actuated by a dielectric elastomer membrane," *Smart Mater. Struct.* **26**(8), 085023 (2017).
- [7] Pelrine, R. E., Kornbluh, R. D. and Joseph, J. P., "Electrostriction of polymer dielectrics with compliant electrodes as a means of actuation," *Sensors Actuators, A Phys.* **64**(1), 77–85 (1998).
- [8] Shian, S., Diebold, R. M. and Clarke, D. R., "Tunable lenses using transparent dielectric elastomer actuators," *Opt. Express* **21**(7), 8669–8676 (2013).
- [9] Maffli, L., Rosset, S., Ghilardi, M., Carpi, F. and Shea, H., "Ultrafast all-polymer electrically tunable silicone lenses," *Adv. Funct. Mater.* **25**(11), 1656–1665 (2015).
- [10] Shintake, J., Rosset, S., Schubert, B., Floreano, D. and Shea, H., "Versatile Soft Grippers with Intrinsic Electrodeposition Based on Multifunctional Polymer Actuators," *Adv. Mater.* **28**(2), 231–238 (2016).
- [11] Shian, S., Bertoldi, K. and Clarke, D. R., "Dielectric Elastomer Based 'grippers' for Soft Robotics," *Adv. Mater.* **27**(43), 6814–6819 (2015).
- [12] Shintake, J., Caccuciolo, V., Floreano, D. and Shea, H., "Soft Robotic Grippers," *Adv. Mater.* **30**(29), 1–33 (2018).
- [13] Linnebach, P., Rizzello, G. and Seelecke, S., "Design and validation of a dielectric elastomer membrane actuator driven pneumatic pump," *Smart Mater. Struct.* **29**(7), 075021 (2020).
- [14] Petralia, M. T. and Wood, R. J., "Fabrication and analysis of dielectric-elastomer minimum-energy structures for highly-deformable soft robotic systems," *IEEE/RSJ 2010 Int. Conf. Intell. Robot. Syst. IROS 2010 - Conf. Proc.*, 2357–2363 (2010).
- [15] Duduta, M., Hajiesmaili, E., Zhao, H., Wood, R. J. and Clarke, D. R., "Realizing the potential of dielectric elastomer artificial muscles," *Proc. Natl. Acad. Sci. U. S. A.* **116**(7), 2476–2481 (2019).
- [16] P. Heydt, R., Kornbluh, R., Eckerle, J. and Pelrine, R., "Dielectric elastomer loudspeakers," [Dielectric Elastomers as Electromechanical Transducers], F. Carpi, D. De Rossi, R. Kornbluh, R. Pelrine, and P. Sommer-Larsen, Eds., Elsevier, 313–320 (2008).
- [17] Matysek, M., Lotz, P. and Schlaak, H. F., "Tactile display with dielectric multilayer elastomer actuators," *Electroact. Polym. Actuators Devices 2009* **7287**(April 2009), 72871D (2009).
- [18] Boys, H., Frediani, G., Poslad, S., Busfield, J. and Carpi, F., "A dielectric elastomer actuator-based tactile display for multiple fingertip interaction with virtual soft bodies," *Electroact. Polym. Actuators Devices 2017* **10163**(April 2017), 101632D (2017).
- [19] Giousouf, M. and Kovacs, G., "Dielectric elastomer actuators used for pneumatic valve technology," *Smart Mater. Struct.* **22**(10), 104010 (2013).
- [20] Rosset, S. and Shea, H. R., "Small, fast, and tough: Shrinking down integrated elastomer transducers," *Appl. Phys. Rev.* **3**(3), 031105 (2016).
- [21] CTsystems AG., "Polymer Actuator CT25.2," <https://www.ct-systems.ch/index.php/products/polymer-actuator-ct25-2>, Last visited on the 5th of August 2020.
- [22] Biggs, S. J. and Hitchcock, R. N., "Artificial muscle actuators for haptic displays: system design to match the dynamics and tactile sensitivity of the human fingerpad," *Electroact. Polym. Actuators Devices 2010* **7642**(April 2010), 76420I (2010).
- [23] www.toyoda-gosei.com/e-rubber - Last consulted on 06.02.2022., "Toyoda Gosei e-Rubber," Toyoda Gosei Co., Ltd.
- [24] Madsen, F. B., Dugaard, A. E., Hvilsted, S. and Skov, A. L., "The Current State of Silicone-Based Dielectric Elastomer Transducers," *Macromol. Rapid Commun.* **37**(5), 378–413 (2016).
- [25] De Saint-Aubin, C. A., Rosset, S., Schlatter, S. and Shea, H., "High-cycle electromechanical aging of dielectric elastomer actuators with carbon-based electrodes," *Smart Mater. Struct.* **27**(7), 074002 (2018).
- [26] Kühnel, D., B. Albuquerque, F., Py, V. and Shea, H., "Automated test setup to quantify the lifetime of dielectric elastomer actuators under a wide range of operating conditions," *Smart Mater. Struct.* **30**(6), 065020 (2021).

- [27] Röntgen, W. C., "Über die durch Electricität bewirkten Form- und Volumenänderungen von dielectricischen Körpern," *Ann. Phys. Chem.* **11**, 771–786 (1880).
- [28] Huang, J., Li, T., Chiang Foo, C., Zhu, J., Clarke, D. R. and Suo, Z., "Giant, voltage-actuated deformation of a dielectric elastomer under dead load," *Appl. Phys. Lett.* **100**(4) 041911 (2012).
- [29] Li, T., Keplinger, C., Baumgartner, R., Bauer, S., Yang, W. and Suo, Z., "Giant voltage-induced deformation in dielectric elastomers near the verge of snap-through instability," *J. Mech. Phys. Solids* **61**(2), 611–628 (2013).
- [30] Keplinger, C., Li, T., Baumgartner, R., Suo, Z. and Bauer, S., "Harnessing snap-through instability in soft dielectrics to achieve giant voltage-triggered deformation," *Soft Matter* **8**(2), 285–288 (2012).
- [31] Suo, Z., "Theory of dielectric elastomers," *Acta Mech. Solida Sin.* **23**(6), 549–578 (2010).
- [32] Koh, S. J. A., Li, T., Zhou, J., Zhao, X., Hong, W., Zhu, J. and Suo, Z., "Mechanisms of large actuation strain in dielectric elastomers," *J. Polym. Sci. Part B Polym. Phys.* **49**(7), 504–515 (2011).
- [33] Gu, G. Y., Zhu, J., Zhu, L. M. and Zhu, X., "A survey on dielectric elastomer actuators for soft robots," *Bioinspiration and Biomimetics* **12**(1), 011003 (2017).
- [34] Lu, T., Ma, C. and Wang, T., "Mechanics of dielectric elastomer structures: A review," *Extrem. Mech. Lett.* **38**, 100752 (2020).
- [35] Zhang, R., Lochmatter, P., Kunz, A. and Kovacs, G., "Spring roll dielectric elastomer actuators for a portable force feedback glove," *Smart Struct. Mater. 2006 Electroact. Polym. Actuators Devices* **6168**(May), 61681T (2006).
- [36] F. Carpi, D. De Rossi, R. Kornbluh, R. Pelrine, P. S.-L., [Dielectric elastomers as Electromechanical Transducers - Fundamentals, Materials, Devices, Models and Applications of an Emerging Electroactive Polymer Technology], Elsevier B.V. (Amsterdam, NL) (2008).
- [37] Kovacs, G., Düring, L., Michel, S. and Terrasi, G., "Stacked dielectric elastomer actuator for tensile force transmission," *Sensors Actuators, A Phys.* **155**(2), 299–307 (2009).
- [38] Lotz, P., Matysek, M. and Schlaak, H. F., "Fabrication and application of miniaturized dielectric elastomer stack actuators," *IEEE/ASME Trans. Mechatronics* **16**(1), 58–66 (2011).
- [39] Randazzo, M., Buzio, R., Metta, G., Sandini, G. and Valbusa, U., "Architecture for the semi-automatic fabrication and assembly of thin-film based dielectric elastomer actuators," *Electroact. Polym. Actuators Devices 2008* **6927**(April 2008), 69272D (2008).
- [40] McKay, T. G., Rosset, S., Anderson, I. A. and Shea, H., "Dielectric elastomer generators that stack up," *Smart Mater. Struct.* **24**(1), 15014 (2015).
- [41] Duduta, M., Wood, R. J. and Clarke, D. R., "Multilayer Dielectric Elastomers for Fast, Programmable Actuation without Prestretch," *Adv. Mater.* **28**(36), 8058–8063 (2016).
- [42] Schlaak, H. F., Jungmann, M., Matysek, M. and Lotz, P., "Novel multilayer electrostatic solid state actuators with elastic dielectric," *Smart Struct. Mater. 2005 Electroact. Polym. Actuators Devices* **5759**(May 2005), 121 (2005).
- [43] Carpi, F., Salaris, C. and De Rossi, D., "Folded dielectric elastomer actuators," *Smart Mater. Struct.* **16**(2) S300 (2007).
- [44] Zhao, H., Hussain, A. M., Duduta, M., Vogt, D. M., Wood, R. J. and Clarke, D. R., "Compact Dielectric Elastomer Linear Actuators," *Adv. Funct. Mater.* **28**(42), 1804328 (2018).
- [45] Klug, F., Solano-Arana, S., Hoffmann, N. J. and Schlaak, H. F., "Multilayer dielectric elastomer tubular transducers for soft robotic applications," *Smart Mater. Struct.* **28**(10) 104004 (2019).
- [46] Hau, S., Rizzello, G. and Seelecke, S., "A novel dielectric elastomer membrane actuator concept for high-force applications," *Extrem. Mech. Lett.* **23**(July), 24–28 (2018).
- [47] Maas, J., Tepel, D. and Hoffstadt, T., "Actuator design and automated manufacturing process for DEAP-based multilayer stack-actuators," *Meccanica* **50**(11), 2839–2854 (2015).
- [48] Araromi, O. A., Conn, A. T., Ling, C. S., Rossiter, J. M., Vaidyanathan, R. and Burgess, S. C., "Spray deposited multilayered dielectric elastomer actuators," *Sensors Actuators, A Phys.* **167**(2), 459–467 (2011).
- [49] Hau, S., Bruch, D., Rizzello, G., Motzki, P. and Seelecke, S., "Silicone based dielectric elastomer strip actuators coupled with nonlinear biasing elements for large actuation strains," *Smart Mater. Struct.* **27**(7) 074003 (2018).
- [50] Rizzello, G., Loew, P., Agostini, L., Fontana, M. and Seelecke, S., "A lumped parameter model for strip-shaped dielectric elastomer membrane transducers with arbitrary aspect ratio," *Smart Mater. Struct.* **29**(11), 115030 (2020).
- [51] Hodgins, M. and Seelecke, S., "Systematic experimental study of pure shear type dielectric elastomer membranes with different electrode and film thicknesses," *Smart Mater. Struct.* **25**(9), 095001 (2016).
- [52] Fasolt, B., Hodgins, M., Rizzello, G. and Seelecke, S., "Effect of screen printing parameters on sensor and actuator performance of dielectric elastomer (DE) membranes," *Sensors Actuators, A Phys.* **265**, 10–19 (2017).
- [53] Hill, M., Rizzello, G. and Seelecke, S., "Development and validation of a fatigue testing setup for dielectric elastomer membrane actuators," *Smart Mater. Struct.* **28**(5), 055029 (2019).

- [54] Bruch, D., Nalbach, S., Rizzello, G., Motzki, P. and Seelecke, S., "Multifunctional fatigue testing setup for in-plane operating DEAs," *Proc. SPIE* **11380**, 113800S (2020).
- [55] Hodgins, M., Rizzello, G., York, A., Naso, D. and Seelecke, S., "A smart experimental technique for the optimization of dielectric elastomer actuator (DEA) systems," *Smart Mater. Struct.* **24**(9) 094002 (2015).
- [56] Hodgins, M., York, A. and Seelecke, S., "Experimental comparison of bias elements for out-of-plane DEAP actuator system," *Smart Mater. Struct.* **22**(9) 094016 (2013).
- [57] Chen, Y., Agostini, L., Moretti, G., Fontana, M., Chen, Y., Agostini, L., Moretti, G. and Berselli, G., "Fatigue life performances of silicone elastomer membranes for dielectric elastomer transducers : preliminary results," *Electroact. Polym. Actuators Devices* **10966**(March), 1096616 (2019).
- [58] Bruch, D., Nalbach, S., Rizzello, G., Motzki, P. and Seelecke, S., "Multifunctional fatigue testing setup for in-plane operating DEAs," *Proc. SPIE* **11380**, 113800S (2020).
- [59] Kofod, G., Paajanen, M. and Bauer, S., "New design concept for dielectric elastomer actuators," *Smart Struct. Mater. 2006 Electroact. Polym. Actuators Devices* **6168**(March 2006), 61682J (2006).
- [60] Kofod, G., Wirges, W., Paajanen, M. and Bauer, S., "Energy minimization for self-organized structure formation and actuation," *Appl. Phys. Lett.* **90**(8), 1–4 (2007).
- [61] O'Brien, B., Calius, E., Xie, S. and Anderson, I., "An experimentally validated model of a dielectric elastomer bending actuator," *Electroact. Polym. Actuators Devices 2008* **6927**(April 2008), 69270T (2008).
- [62] Rosset, S., Araromi, O. A., Shintake, J. and Shea, H. R., "Model and design of dielectric elastomer minimum energy structures," *Smart Mater. Struct.* **23**(8), 085021 (2014).
- [63] Pei, Q., Rosenthal, M., Stanford, S., Prahlad, H. and Pelrine, R., "Multiple-degrees-of-freedom electroelastomer roll actuators," *Smart Mater. Struct.* **13**(5), N86–N92 (2004).
- [64] Hosoya, N., Masuda, H. and Maeda, S., "Balloon dielectric elastomer actuator speaker," *Appl. Acoust.* **148**, 238–245 (2019).
- [65] Kornbluh, R. D., Pelrine, R., Pei, Q., Heydt, R., Stanford, S., Oh, S. and Eckerle, J., "Electroelastomers: applications of dielectric elastomer transducers for actuation, generation, and smart structures," *Smart Struct. Mater. 2002 Ind. Commer. Appl. Smart Struct. Technol.* **4698**(July 2002), 254–270 (2002).
- [66] Rosset, S., Niklaus, M., Dubois, P. and Shea, H. R., "Large-stroke dielectric elastomer actuators with ion-implanted electrodes," *J. Microelectromechanical Syst.* **18**(6), 1300–1308 (2009).
- [67] Verthey, R., Frisoli, A., Bergamasco, M., Carpi, F., Frediani, G. and De Rossi, D., "Modeling and experimental validation of buckling dielectric elastomer actuators," *Smart Mater. Struct.* **21**(9) 094005 (2012).
- [68] Carpi, F., Fantoni, G., Guerrini, P. and De Rossi, D., "Buckling dielectric elastomer actuators and their use as motors for the eyeballs of an android face," *Smart Struct. Mater. 2006 Electroact. Polym. Actuators Devices* **6168**(March 2006), 61681A (2006).
- [69] Zhu, R., Wallrabe, U., Woias, P., Wapler, M. and Mescheder, U., "Semi-rigid ring-shaped electrode dielectric electroactive polymer membrane as buckling actuator," *J. Micromechanics Microengineering* **29**(5) 055001 (2019).
- [70] Gerratt, A. P., Balakrishnan, B., Penskiy, I. and Bergbreiter, S., "Dielectric elastomer actuators fabricated using a micro-molding process," *Smart Mater. Struct.* **23**(5), 055004 (2014).
- [71] Ji, X., Liu, X., Cacucciolo, V., Civet, Y., El Haitami, A., Cantin, S., Perriard, Y. and Shea, H., "Untethered Feel-Through Haptics Using 18- μ m Thick Dielectric Elastomer Actuators," *Adv. Funct. Mater.* **2006639**, 1–10 (2020).
- [72] Mun, S., Yun, S., Nam, S., Park, S. K., Park, S., Park, B. J., Lim, J. M. and Kyung, K. U., "Electro-Active Polymer Based Soft Tactile Interface for Wearable Devices," *IEEE Trans. Haptics* **11**(1), 15–21 (2018).
- [73] Ji, X., "Low voltage fast dielectric elastomer actuators - Thèse N° 9533," PhD Thesis **EPFL** (2019).
- [74] Shintake, J., Cacucciolo, V., Floreano, D. and Shea, H., "Soft Robotic Grippers," *Adv. Mater.* **30**(29), 1707035 (2018).
- [75] Araromi, O. A., Gavrilovich, I., Shintake, J., Rosset, S. and Shea, H. R., "Towards a deployable satellite gripper based on multisegment dielectric elastomer minimum energy structures," *Electroact. Polym. Actuators Devices 2014* **9056**(March 2014), 90562G (2014).
- [76] Zaidi, S., Maselli, M., Laschi, C. and Cianchetti, M., "Actuation Technologies for Soft Robot Grippers and Manipulators : A Review," *Curr. Robot. Reports* **2**, 355–369 (2021).
- [77] Rich, S. I., Wood, R. J. and Majidi, C., "Untethered soft robotics," *Nat. Electron.* **1**(2), 102–112 (2018).
- [78] Gu, G. Y., Zhu, J., Zhu, L. M. and Zhu, X., "A survey on dielectric elastomer actuators for soft robots," *Bioinspiration and Biomimetics* **12**(1), 011003 (2017).
- [79] Ji, X., Liu, X., Cacucciolo, V., Imboden, M., Civet, Y., Haitami, A. El, Cantin, S., Perriard, Y. and Shea, H., "An autonomous untethered fast soft robotic insect driven by low-voltage dielectric elastomer actuators," *Sci. Robot.* **4**(37), eaaz6451 (2019).
- [80] Chen, Y., Zhao, H., Mao, J., Chirarattananon, P., Helbling, E. F., Hyun, N. seung P., Clarke, D. R. and Wood, R. J., "Controlled

- flight of a microrobot powered by soft artificial muscles," *Nature* **575**(7782), 324–329 (2019).
- [81] Chen, L., Ghilardi, M., Busfield, J. C. and Carpi, F., "Electrically Tunable Lenses : A Review," *Front. Robot. AI* **8**(June), 678046 (2021).
- [82] Imboden, M., de Coulon, E., Poulin, A., Dellenbach, C., Rosset, S., Shea, H. and Rohr, S., "High-speed mechano-active multielectrode array for investigating rapid stretch effects on cardiac tissue," *Nat. Commun.* **10**(834), 1–10 (2019).
- [83] Poulin, A., Imboden, M., Sorba, F., Grazioli, S., Martin-Olmos, C., Rosset, S. and Shea, H., "An ultra-fast mechanically active cell culture substrate," *Sci. Rep.* **8**(1), 1–10 (2018).
- [84] Heydt, R., Kornbluh, R., Eckerle, J. and Pelrine, R., "Sound radiation properties of dielectric elastomer electroactive polymer loudspeakers," *Electroact. Polym. Actuators Devices* **6168**(March 2006), 61681M (2006).
- [85] O'Halloran, A., O'Malley, F. and McHugh, P., "A review on dielectric elastomer actuators, technology, applications, and challenges," *J. Appl. Phys.* **104**(7), 071101 (2008).
- [86] Guo, Y., Liu, L., Liu, Y. and Leng, J., "Review of Dielectric Elastomer Actuators and Their Applications in Soft Robots," *Adv. Intell. Syst.* **3**(10), 2000282 (2021).
- [87] Pei, Q., Hu, W., McCoul, D., Biggs, S. J., Stadler, D. and Carpi, F., "Dielectric elastomers as EAPs: Applications," [Electromechanically Active Polymers], F. Carpi, Ed., Springer Switzerland, Cham(CH), 739–766 (2016).
- [88] CT Systems AG., "CT Stack - The transducer technology," 2021, <<https://ct-systems.ch/technology/ctstack-the-transducer-technology/>> (18 March 2022).
- [89] Romasanta, L. J., Lopez-Manchado, M. A. and Verdejo, R., "Increasing the performance of dielectric elastomer actuators: A review from the materials perspective," *Prog. Polym. Sci.* **51**, 188–211 (2015).
- [90] Hao, M., Wang, Y., Zhu, Z., He, Q., Zhu, D. and Luo, M., "A Compact Review of IPMC as Soft Actuator and Sensor: Current Trends, Challenges, and Potential Solutions From Our Recent Work," *Front. Robot. AI* **6**(December), 1–7 (2019).
- [91] Zhang, Q. M., Bharti, V. and Zhao, X., "Giant electrostriction and relaxor ferroelectric behavior in electron-irradiated poly (vinylidene fluoride-trifluoroethylene) copolymer," *Science* (80-.). **280**, 2101–2104 (1998).
- [92] Lehmann, W., Skupin, H., Tolksdorf, C., Gebhard, E., Zentel, R. and Kremer, F., "Giant lateral electrostriction in ferroelectric liquid-crystalline elastomers," *Nature* **410**, 447–450 (2001).
- [93] Wang, Y., Sun, C., Zhou, E. and Su, J., "Deformation mechanisms of electrostrictive graft elastomer," *Smart Mater. Struct.* **13**(6), 1407–1413 (2004).
- [94] Su, J., Harrison, J. S., Clair, T. L., Bar-cohen, Y. and Leary, S., "Electrostrictive graft elastomers and applications," *MRS Symp. FF Electroact. Polym.*, 1–6 (1999).
- [95] Shankar, R., Ghosh, T. K. and Spontak, R. J., "Dielectric elastomers as next-generation polymeric actuators," *Soft Matter* **3**(9), 1116–1129 (2007).
- [96] Hines, L., Petersen, K., Lum, G. Z. and Sitti, M., "Soft Actuators for Small-Scale Robotics," *Adv. Mater.* **29**(1603483), 1–43 (2017).
- [97] Michel, S., Zhang, X. Q., Wissler, M., Löwe, C. and Kovacs, G., "A comparison between silicone and acrylic elastomers as dielectric materials in electroactive polymer actuators," *Polym. Int.* **59**(3), 391–399 (2010).
- [98] Molberg, M., Leterrier, Y., Plummer, C. J. G., Walder, C., Löwe, C., Opris, D. M., Nüesch, F. A., Bauer, S. and Mnson, J. A. E., "Frequency dependent dielectric and mechanical behavior of elastomers for actuator applications," *J. Appl. Phys.* **106**(5), 1–7 (2009).
- [99] Alici, G., "Softer is harder: What differentiates soft robotics from hard robotics?," *MRS Adv.* **3**(28), 1557–1568 (2018).
- [100] Liu, C., Qin, H. and Mather, P. T., "Review of progress in shape-memory polymers," *J. Mater. Chem.* **17**(16), 1543–1558 (2007).
- [101] Miriyev, A., Stack, K. and Lipson, H., "Soft material for soft actuators," *Nat. Commun.* **8**(1), 1–8 (2017).
- [102] Huber, J. E., Fleck, N. A. and Ashby, M. F., "The selection of mechanical actuators," *Proc. R. Soc. London. Ser. A Math. Phys. Eng. Sci.* **453**(1965), 2185–2205 (1997).
- [103] Youn, J. H., Jeong, S. M., Hwang, G., Kim, H., Hyeon, K., Park, J. and Kyung, K. U., "Dielectric elastomer actuator for soft robotics applications and challenges," *Appl. Sci.* **10**(640), 1–32 (2020).
- [104] Mohd Jani, J., Leary, M., Subic, A. and Gibson, M. A., "A review of shape memory alloy research, applications and opportunities," *Mater. Des.* **56**(April), 1078–1113 (2014).
- [105] Kim, J., Kim, J. W., Kim, H. C., Zhai, L., Ko, H. U. and Muthoka, R. M., "Review of Soft Actuator Materials," *Int. J. Precis. Eng. Manuf.* **20**(12), 2221–2241 (2019).
- [106] Hollerbach, J. M., Hunter, I. M. and Ballentyne, J., "A comparative analysis of actuator technologies for robotics," *Robot. Rev.* **2**, 299–342 (1992).
- [107] Poulin, A., Rosset, S. and Shea, H. R., "Printing low-voltage dielectric elastomer actuators," *Appl. Phys. Lett.* **107**(244104)

- (2015).
- [108] Poulin, A., Rosset, S. and Shea, H., "Fully printed 3 microns thick dielectric elastomer actuator," *Electroact. Polym. Actuators Devices* 2016 **9798**(April 2016), 97980L (2016).
 - [109] Sheima, Y., Caspari, P. and Opris, D. M., "Artificial Muscles : Dielectric Elastomers Responsive to Low Voltages," *Macromol. Rapid Commun.* **40**, 1900205 (2019).
 - [110] Madsen, F. B., Yu, L., Hvilsted, S. and Skov, A. L., "Super soft silicone elastomers with high dielectric permittivity," *Electroact. Polym. Actuators Devices* 2015 **9430**, 94301D (2015).
 - [111] Mateiu, R. V., Yu, L. and Skov, A. L., "Electrical breakdown phenomena of dielectric elastomers," *Electroact. Polym. Actuators Devices* 2017 **10163**, 1016328 (2017).
 - [112] Ghilardi, M., Busfield, J. J. C. and Carpi, F., "Electrical breakdown detection system for dielectric elastomer actuators," *Electroact. Polym. Actuators Devices* 2017 **10163**(May), 101632B (2017).
 - [113] De Saint-Aubin, C. A., Rosset, S., Schlatter, S. and Shea, H., "High-cycle electromechanical aging of dielectric elastomer actuators with carbon-based electrodes," *Smart Mater. Struct.* **27**(7), 074002 (2018).
 - [114] Lotz, P., Matysek, M. and Schlaak, H. F., "Lifetime of dielectric elastomer stack actuators," *Electroact. Polym. Actuators Devices* 2011 **7976**(May), 79760P (2011).
 - [115] Matysek, M., Lotz, P. and Schlaak, H. F., "Lifetime investigation of dielectric elastomer stack actuators," *IEEE Trans. Dielectr. Electr. Insul.* **18**(1), 89–96 (2011).
 - [116] Iannarelli, A., Niasar, M. G. and Ross, R., "The effects of static pre-stretching on the short and long-term reliability of dielectric elastomer actuators," *Smart Mater. Struct.* **28**(12), 125014 (2019).
 - [117] Kornbluh, R., Wong-Foy, A., Pelrine, R., Prahlad, H. and McCoy, B., "Long-lifetime all-polymer artificial muscle transducers," *Mater. Res. Soc. Symp. Proc.* **1271**, 1271-JJ03-01 (2010).
 - [118] Dissado, L. A. and Fothergill, J. C., [Electrical Degradation and Breakdown in Polymers], Peter Peregrinus Ltd (London, UK) (1992).
 - [119] Pelrine, R. and Kornbluh, R., "Dielectric Elastomers as Electroactive Polymers (EAPs): Fundamentals," [Electromechanically Active Polymers], 671–686 (2016).
 - [120] Biggs, J., Danielmeier, K., Hitzbleck, J., Krause, J., Kridl, T., Nowak, S., Orselli, E., Quan, X., Schapeler, D., Sutherland, W. and Wagner, J., "Electroactive polymers: Developments of and perspectives for dielectric elastomers," *Angew. Chemie - Int. Ed.* **52**(36), 9409–9421 (2013).
 - [121] Shankar, R., Krishnan, A. K., Ghosh, T. K. and Spontak, R. J., "Triblock copolymer organogels as high-performance dielectric elastomers," *Macromolecules* **41**(16), 6100–6109 (2008).
 - [122] Mok Ha, S., Yuan, W., Pei, Q., Pelrine, R. and Stanford, S., [Interpenetrating polymer networks as high performance dielectric elastomers], Elsevier Ltd. (2008).
 - [123] Ha, S. M., Wissler, M., Pelrine, R., Stanford, S., Kovacs, G. and Pei, Q., "Characterization of electroelastomers based on interpenetrating polymer networks," *Proc. SPIE* **6524**, 652408 (2007).
 - [124] Niu, X., Yang, X., Brochu, P., Stoyanov, H., Yun, S. and Yu, Z., "Bistable Large-Strain Actuation of Interpenetrating Polymer Networks," *Adv. Mater.* **24**, 6513–6519 (2012).
 - [125] Zhang, H., Düring, L., Kovacs, G., Yuan, W., Niu, X. and Pei, Q., "Interpenetrating polymer networks based on acrylic elastomers and plasticizers with improved actuation temperature range," *Polym. Int.* **59**, 384–390 (2010).
 - [126] Pelrine, R., Kornbluh, R., Joseph, J., Heydt, R., Pei, Q. and Chiba, S., "High-field deformation of elastomeric dielectrics for actuators," *Mater. Sci. Eng. C* **11**(2), 89–100 (2000).
 - [127] Chen, Z., Xiao, Y., Fang, J., He, J., Gao, Y., Zhao, J., Gao, X. and Luo, Y., "Ultrasoft-yet-strong pentablock copolymer as dielectric elastomer highly responsive to low voltages," *Chem. Eng. J.* **405**, 126634 (2021).
 - [128] Zhang, L., Wang, D., Hu, P., Zha, J., You, F., Li, S. and Dang, Z., "Highly improved electro-actuation of dielectric elastomers by molecular grafting of azobenzenes to silicon rubber," *J. Mater. Chem. C* **3**, 4883–4889 (2015).
 - [129] Caspari, P., Dünki, S. J., Nüesch, F. A. and Opris, D. M., "Dielectric elastomer actuators with increased dielectric permittivity and low leakage current capable of suppressing electromechanical instability," *J. Mater. Chem. C* **6**(8), 2043–2053 (2018).
 - [130] Perju, E., Shova, S. and Opris, D. M., "Electrically Driven Artificial Muscles Using Novel Polysiloxane Elastomers Modified with Nitroaniline Push–Pull Moieties," *ACS Appl. Mater. Interfaces* **12**, 23432–23442 (2020).
 - [131] Sheima, Y., Caspari, P. and Opris, D. M., "Artificial Muscles: Dielectric Elastomers Responsive to Low Voltages," *Macromol. Rapid Commun.* **40**(16), 1–8 (2019).
 - [132] Razak, A. H. A. and Skov, A. L., "Silicone elastomers with covalently incorporated aromatic voltage stabilisers," *RSC Adv.* **7**(1), 468–477 (2017).
 - [133] Yin, L. J., Zhao, Y., Zhu, J., Yang, M., Zhao, H., Pei, J. Y., Zhong, S. L. and Dang, Z. M., "Soft, tough, and fast polyacrylate

- dielectric elastomer for non-magnetic motor," *Nat. Commun.* **12**(4517), 1–10 (2021).
- [134] Skov, A. L. and Yu, L., "Optimization Techniques for Improving the Performance of Silicone-Based Dielectric Elastomers," *Adv. Eng. Mater.* **20**(5), 1–21 (2018).
- [135] Opris, D. M., "Polar Elastomers as Novel Materials for Electromechanical Actuator Applications," *Adv. Mater.* **30**(5), 1703678 (2018).
- [136] Banet, P., Zeggai, N., Chavanne, J., Nguyen, G. T. M., Chikh, L., Plesse, C., Almanza, M., Martinez, T., Civet, Y., Perriard, Y. and Fichet, O., "Evaluation of dielectric elastomers to develop materials suitable for actuation," *Soft Matter* **17**(48), 10786–10805 (2021).
- [137] Vogan, J. D., "Development of dielectric elastomer actuators for MRI devices," MIT, MSc Thesis, Massachusetts Institute of Technology (2004).
- [138] Pelrine, R., Kornbluh, R. and Kofod, G., "High-strain actuator materials based on dielectric elastomers," *Adv. Mater.* **12**(16), 1223–1225 (2000).
- [139] Rosset, S. and Shea, H. R., "Towards fast, reliable, and manufacturable DEAs: miniaturized motor and Rupert the rolling robot," *Proc. SPIE* **9430**, 943009 (2015).
- [140] Kaltseis, R., Keplinger, C., Adrian Koh, S. J., Baumgartner, R., Goh, Y. F., Ng, W. H., Kogler, A., Tröls, A., Foo, C. C., Suo, Z. and Bauer, S., "Natural rubber for sustainable high-power electrical energy generation," *RSC Adv.* **4**(53), 27905–27913 (2014).
- [141] Chen, Y., Agostini, L., Moretti, G., Fontana, M. and Versteck, R., "Dielectric elastomer materials for large-strain actuation and energy harvesting: A comparison between styrenic rubber, natural rubber and acrylic elastomer," *Smart Mater. Struct.* **28**(11), 114001 (2019).
- [142] Zhao, X. and Suo, Z., "Theory of dielectric elastomers capable of giant deformation of actuation," *Phys. Rev. Lett.* **104**(17), 178302 (2010).
- [143] Plante, J. S. and Dubowsky, S., "Large-scale failure modes of dielectric elastomer actuators," *Int. J. Solids Struct.* **43**(25–26), 7727–7751 (2006).
- [144] Akbari, S., Rosset, S. and Shea, H. R., "Improved electromechanical behavior in castable dielectric elastomer actuators," *Appl. Phys. Lett.* **102**(7), 071906 (2013).
- [145] Zhu, J., Kolloosche, M., Lu, T., Kofod, G. and Suo, Z., "Two types of transitions to wrinkles in dielectric elastomers," *Soft Matter* **8**(34), 8840–8846 (2012).
- [146] Iannarelli, A., Niasar, M. G. and Ross, R., "The effects of static pre-stretching on the short and long-term reliability of dielectric elastomer actuators," *Smart Mater. Struct.* **28**(12), 125014 (2019).
- [147] Fasolt, B., Welsch, F., Jank, M. and Seelecke, S., "Effect of actuation parameters and environment on the breakdown voltage of silicone dielectric elastomer films," *Smart Mater. Struct.* **28**(9), 094002 (2019).
- [148] Gatti, D., Haus, H., Matysek, M., Frohnapfel, B., Tropea, C. and Schlaak, H. F., "The dielectric breakdown limit of silicone dielectric elastomer actuators," *Appl. Phys. Lett.* **104**(5), 052905 (2014).
- [149] Förster-Zügel, F., Solano-Arana, S., Klug, F. and Schlaak, H. F., "Dielectric breakdown strength measurements with silicone-based single-layer dielectric elastomer transducers," *Smart Mater. Struct.* **28**(7), 075042 (2019).
- [150] Zakaria, S., Yu, L., Kofod, G. and Skov, A. L., "The influence of static pre-stretching on the mechanical ageing of filled silicone rubbers for dielectric elastomer applications," *Mater. Today Commun.* **4**, 204–213 (2015).
- [151] Zakaria, S., Morshuis, P. H. F., Benslimane, M. Y., Yu, L. and Skov, A. L., "The electrical breakdown strength of pre-stretched elastomers, with and without sample volume conservation," *Smart Mater. Struct.* **24**(5), 055009 (2015).
- [152] Palakodeti, R. and Kessler, M. R., "Influence of frequency and prestrain on the mechanical efficiency of dielectric electroactive polymer actuators," *Mater. Lett.* **60**, 3437–3440 (2006).
- [153] Rosset, S., Araromi, O. A., Schlatter, S. and Shea, H. R., "Fabrication process of silicone-based dielectric elastomer actuators," *J. Vis. Exp.* **108**, e53423 (2016).
- [154] Boonstra, B. B., "Role of particulate fillers in elastomer reinforcement: a review," *Polymer (Guildf)*. **20**(6), 691–704 (1979).
- [155] Paul, D. R. and Mark, J. E., "Fillers for polysiloxane ('silicone') elastomers," *Prog. Polym. Sci.* **35**(7), 893–901 (2010).
- [156] Kopylov, V. M., Kostyleva, E. I., Kostylev, I. M. and Koviazin, A. V., "Silica fillers for silicone rubber," *Kauchuk i Rezina* **5**, 32–43 (2010).
- [157] Mazurek, P., Vudayagiri, S. and Skov, A. L., "How to tailor flexible silicone elastomers with mechanical integrity: A tutorial review," *Chem. Soc. Rev.* **48**(6), 1448–1464 (2019).
- [158] Diani, J., Fayolle, B., Gilormini, P., Diani, J., Fayolle, B. and Gilormini, P., "A review on the Mullins effect," *Eur. Polym. J.* **45**, 601–612 (2009).
- [159] Krpovic, S., Dam-Johansen, K. and Skov, A. L., "Importance of Mullins effect in commercial silicone elastomer formulations for soft robotics," *J. Appl. Polym. Sci.* **138**(19), e50380 (2020).

- [160] Carpi, F., Gallone, G., Galantini, F. and De Rossi, D., "Enhancing the dielectric permittivity of elastomers," [Dielectric Elastomers as Electromechanical Transducers], Elsevier Ltd., 51–68 (2008).
- [161] Gallone, G., Galantini, F. and Carpi, F., "Perspectives for new dielectric elastomers with improved electromechanical actuation performance: Composites versus blends," *Polym. Int.* **59**(3), 400–406 (2010).
- [162] Rosset, S. and Shea, H. R., "Flexible and stretchable electrodes for dielectric elastomer actuators," *Appl. Phys. A Mater. Sci. Process.* **110**(2), 281–307 (2013).
- [163] Töpfer, T., Weiss, F., Osmani, B., Bippes, C., Leung, V. and Müller, B., "Siloxane-based thin films for biomimetic low-voltage dielectric actuators," *Sensors Actuators, A Phys.* **233**, 32–41 (2015).
- [164] Yu, L. and Skov, A. L., "Silicone rubbers for dielectric elastomers with improved dielectric and mechanical properties as a result of substituting silica with titanium dioxide," *Int. J. Smart Nano Mater.* **6**(4), 268–289 (2015).
- [165] McCoul, D., Hu, W., Gao, M., Mehta, V. and Pei, Q., "Recent Advances in Stretchable and Transparent Electronic Materials," *Adv. Electron. Mater.* **2**(5), 1500407 (2016).
- [166] Cacucciolo, V., Shintake, J., Kuwajima, Y., Maeda, S., Floreano, D. and Shea, H., "Stretchable pumps for soft machines," *Nature* **572**(7770), 516–519 (2019).
- [167] Ji, X., El Haitami, A., Sorba, F., Rosset, S., Nguyen, G. T. M., Plesse, C., Vidal, F., Shea, H. R. and Cantin, S., "Stretchable composite monolayer electrodes for low voltage dielectric elastomer actuators," *Sensors Actuators, B Chem.* **261**, 135–143 (2018).
- [168] Campbell, D. S. and Chapman, A. V., "Relationships between structure and performance of vulcanisates," *J. Nat. Rubber Res.* **5**(4), 246–258 (1990).
- [169] Andriot, M., Degroot, J. V., Meeks, R., Gerlach, E., Jungk, M., Wolf, a. T., Cray, S., Easton, T., Mountney, A., Leadley, S., Chao, S. H., Colas, A., de Buyl, F., Dupont, A., Garaud, J. L., Gubbels, F., Lecomte, J. P., Lenoble, B., Stassen, S., et al., "Silicones in Industrial Applications," Dow Corning, 1–106 (2007).
- [170] Dargazany, R. and Itskov, M., "Constitutive modeling of the Mullins effect and cyclic stress softening in filled elastomers," *Phys. Rev. E - Stat. Nonlinear, Soft Matter Phys.* **88**(1), 012602 (2013).
- [171] Yu, L., Madsen, F. B. and Skov, A. L., "Degradation patterns of silicone-based dielectric elastomers in electrical fields," *Int. J. Smart Nano Mater.* **9**(4), 217–232 (2018).
- [172] Rosset, S., De Saint-Aubin, C., Poulin, A. and Shea, H. R., "Assessing the degradation of compliant electrodes for soft actuators," *Rev. Sci. Instrum.* **88**(10), 105002 (2017).
- [173] Rosset, S., Poulin, A., de Saint-Aubin, C., Shea, H. and Schlatter, S., "The NERD setup: assessing the life time of electrodes for dielectric elastomer transducers," *Electroact. Polym. Actuators Devices* **10594**, 105940N (2018).
- [174] Stoyanov, H., Brochu, P., Niu, X., Lai, C., Yun, S. and Pei, Q., "Long lifetime, fault-tolerant freestanding actuators based on a silicone dielectric elastomer and self-clearing carbon nanotube compliant electrodes," *RSC Adv.* **3**(7), 2272–2278 (2013).
- [175] Yuan, W., Brochu, P., Zhang, H., Jan, A. and Pei, Q., "Long lifetime dielectric elastomer actuators under continuous high strain actuation," *Electroact. Polym. Actuators Devices* 2009 **7287**(April 2009), 728700 (2009).
- [176] Yun, S., Niu, X., Yu, Z., Hu, W., Brochu, P. and Pei, Q., "Compliant silver nanowire-polymer composite electrodes for bistable large strain actuation," *Adv. Mater.* **24**(10), 1321–1327 (2012).
- [177] Zhang, M., Denes, I., Xue, Y. and Buchmeiser, M. R., "Ageing of Silicone-Based Dielectric Elastomers Prepared with Varying Stoichiometric Imbalance: Changes in Network Structure, Mechanical, and Electrical Properties," *Macromol. Chem. Phys.* **217**(15), 1729–1736 (2016).
- [178] Pan, C., Markvicka, E. J., Malakooti, M. H., Yan, J., Hu, L., Matyjaszewski, K. and Majidi, C., "A Liquid-Metal-Elastomer Nanocomposite for Stretchable Dielectric Materials," *Adv. Mater.* **31**(23), 1–10 (2019).
- [179] Xiao, P., Kim, J. H. and Seo, S., "Flexible and stretchable liquid metal electrodes working at sub-zero temperature and their applications," *Materials (Basel)*. **14**(15), 4313 (2021).
- [180] Keplinger, C., Sun, J., Foo, C. C., Rothmund, P., Whitesides, G. M. and Suo, Z., "Stretchable, Transparent, Ionic Conductors," *Science (80-.)*. **341**(6149), 984–987 (2013).
- [181] Benslimane, M. Y., Kiil, H. E. and Tryson, M. J., "Dielectric electro-active polymer push actuators: Performance and challenges," *Polym. Int.* **59**(3), 415–421 (2010).
- [182] Finkenauer, L. R. and Majidi, C., "Complaint liquid metal electrodes for dielectric elastomer actuators," *Electroact. Polym. Actuators Devices* 2014 **9056**(March 2014), 905631 (2014).
- [183] Benslimane, M., Gravesen, P. and Sommer-Larsen, P., "Mechanical properties of dielectric elastomer actuators with smart metallic compliant electrodes," *Smart Struct. Mater.* 2002 *Electroact. Polym. Actuators Devices* **4695**(July 2002), 150–157 (2002).
- [184] Jones, R. W. and Sarban, R., "Inverse grey-box model-based control of a dielectric elastomer actuator," *Smart Mater. Struct.* **21**(7), 075019 (2012).

- [185] Rosset, S., Niklaus, M., Dubois, P. and Shea, H. R., "Metal ion implantation for the fabrication of stretchable electrodes on elastomers," *Adv. Funct. Mater.* **19**(3), 470–478 (2009).
- [186] Corbelli, G., Ghisleri, C., Marelli, M., Milani, P. and Ravagnan, L., "Highly deformable nanostructured elastomeric electrodes with improving conductivity upon cyclical stretching," *Adv. Mater.* **23**(39), 4504–4508 (2011).
- [187] Lee, Y. R., Kwon, H., Lee, D. H. and Lee, B. Y., "Highly flexible and transparent dielectric elastomer actuators using silver nanowire and carbon nanotube hybrid electrodes," *Soft Matter* **13**(37), 6390–6395 (2017).
- [188] Xu, F. and Zhu, Y., "Highly conductive and stretchable silver nanowire conductors," *Adv. Mater.* **24**(37), 5117–5122 (2012).
- [189] Shian, S., Diebold, R. M., Mcnamara, A. and Clarke, D. R., "Highly compliant transparent electrodes," *Appl. Phys. Lett.* **101**, 061101 (2012).
- [190] Duduta, M., Hajiesmaili, E., Zhao, H., Wood, R. J. and Clarke, D. R., "Realizing the potential of dielectric elastomer artificial muscles," *PNAS* **116**(7), 2476–2481 (2019).
- [191] Yuan, W., Li, H., Brochu, P., Niu, X. and Pei, Q., "Fault-tolerant silicone dielectric elastomers," *Int. J. Smart Nano Mater.* **1**(1), 40–52 (2010).
- [192] Peng, Z., Shi, Y., Chen, N., Li, Y. and Pei, Q., "Stable and High-Strain Dielectric Elastomer Actuators Based on a Carbon Nanotube-Polymer Bilayer Electrode," *Adv. Funct. Mater.* **2008321**, 1–8 (2020).
- [193] Peng, Z., Shi, Y., Xie, Z., Li, Y., Chen, N. and Pei, Q., "Self-clearable bilayer electrode for dielectric elastomer actuators," *Proc. SPIE* **11587**, 115871Y (2021).
- [194] Zhu, F. bo, Zhang, C. li, Qian, J. and Chen, W. qiu., "Mechanics of dielectric elastomers: materials, structures, and devices," *J. Zhejiang Univ. Sci. A* **17**(1), 1–21 (2016).
- [195] Suo, Z., "Theory of dielectric elastomers," *Acta Mech. Solida Sin.* **23**(6), 549–578 (2010).
- [196] Jiang, L., Zhou, Y., Chen, S., Ma, J., Betts, A. and Jerrams, S., "Electromechanical instability in silicone- and acrylate-based dielectric elastomers," *J. Appl. Polym. Sci.* **135**(9), 45733 (2018).
- [197] Niu, X., Stoyanov, H., Hu, W., Leo, R., Brochu, P. and Pei, Q., "Synthesizing a New Dielectric Elastomer Exhibiting Large Actuation Strain and Suppressed Electromechanical Instability without Prestretching," *J. Polym. Sci. Part B Polym. Phys.* **51**, 197–206 (2013).
- [198] Shankar, R., Ghosh, T. K. and Spontak, R. J., "Electromechanical Response of Nanostructured Polymer Systems with no Mechanical Pre-Strain," *Macromol. Rapid Commun.* **28**, 1142–1147 (2007).
- [199] Zhao, X. and Suo, Z., "Method to analyze electromechanical stability of dielectric elastomers," *Appl. Phys. Lett.* **91**(6), 2–4 (2007).
- [200] Gisby, T. A., Xie, S. Q., Calius, E. P. and Anderson, I. A., "Leakage current as a predictor of failure in dielectric elastomer actuators," *Electroact. Polym. Actuators Devices 2010* **7642**(April 2010), 764213 (2010).
- [201] Muffoletto, D. P., Burke, K. M. and Zirnheld, J. L., "Anticipating electrical breakdown in dielectric elastomer actuators," *Electroact. Polym. Actuators Devices 2013* **8687**(May), 86870U (2013).
- [202] Zhang, M., Denes, I., Xue, Y. and Buchmeiser, M. R., "Ageing of Silicone-Based Dielectric Elastomers Prepared with Varying Stoichiometric Imbalance: Changes in Network Structure, Mechanical, and Electrical Properties," *Macromol. Chem. Phys.* **217**(15), 1729–1736 (2016).
- [203] Yu, L. and Skov, A. L., "Molecular Strategies for Improved Dielectric Elastomer Electrical Breakdown Strengths," *Macromol. Rapid Commun.* **39**(16), 1–6 (2018).
- [204] Förster-Zuegel, F., Grotepaß, T. and Schlaak, H. F., "Characterization of the dielectric breakdown field strength of PDMS thin films: thickness dependence and electrode shape," *Electroact. Polym. Actuators Devices 2015* **9430**(April 2015), 94300D (2015).
- [205] Zakaria, S., Morshuis, P. H. F., Benslimane, M. Y., Gernaey, K. V. and Skov, A. L., "The electrical breakdown of thin dielectric elastomers: thermal effects," *Electroact. Polym. Actuators Devices 2014* **9056**, 90562V (2014).
- [206] K.C.Kao., [Dielectric phenomena in solids], Elsevier, London, UK (2004).
- [207] Zeller, H. R., "Breakdown and prebreakdown phenomena in solid dielectrics," *IEEE Trans. Electr. Insul.* **EI-22**(2), 115–122 (1987).
- [208] Dissado, L. A., Mazzanti, G. and Montanari, G. C., "The role of trapped space charges in the electrical aging of insulating materials," *IEEE Trans. Dielectr. Electr. Insul.* **4**(5), 496–506 (1997).
- [209] Ieda, M., "Dielectric breakdown process of polymers," *IEEE Trans. Electr. Insul.* **EI-15**(3), 206–224 (1980).
- [210] Mazzanti, G., Montanari, G. C. and Dissado, L. A., "Electrical aging and life models: The role of space charge," *IEEE Trans. Dielectr. Electr. Insul.* **12**(5), 876–890 (2005).
- [211] Tommasini, D., "Dielectric insulation and high-voltage issues," CAS 2009 - Cern(Accessed in <https://cas.web.cern.ch/sites/default/files/lectures/bruges-2009/tommasini.pdf>), 335–355 (2010).

- [212] Ohring, M., [Reliability and failure of electronic materials and devices], Academic Press Ltd, London, UK (1998).
- [213] Gallagher, T. J. and Pearmain, A. J., [High voltage — measurement, testing and design], Wiley (1984).
- [214] Skvarenina, T. L., "An introduction to electrical breakdown in dielectrics," Rep. Number 85-2470(Air Command and Staff College Air University, Maxwell Air Force Base (Alabama)), United States Army Air Force (1985).
- [215] Wang, H. and Zeng, Z., "Electric Breakdown Model for Super-Thin Polyester Foil," [Polyester], Intechopen, London, UK (2012).
- [216] Li, S., Yin, G., Chen, G., Li, J., Bai, S., Zhong, L., Zhang, Y. and Lei, Q., "Short-term breakdown and long-term failure in nanodielectrics: A review," IEEE Trans. Dielectr. Electr. Insul. **17**(5), 1523–1535 (2010).
- [217] Ieda, M., Nagao, M. and Hikita, M., "High-field conduction and breakdown in insulating polymers - present situation and future prospects," IEEE Trans. Dielectr. Electr. Insul. **1**(5), 934–945 (1994).
- [218] Fothergill, J. C., "Ageing, space charge and nanodielectrics: ten things we don't know about dielectrics," 2007 Int. Conf. Solid Diel., 1–10 (2007).
- [219] Baudoin, F., Laurent, C., Le Roy, S. and Teyssedre, G., "Conduction Mechanisms and Numerical Modeling of Transport in Organic Insulators: Trends and Perspectives," [Dielectric Materials for Electrical Engineering], J. Martinez-Vega, Ed., Wiley, Hoboken(NJ), 37–78 (2013).
- [220] Chiu, F., "A review on conduction mechanisms in dielectric films," Adv. Mater. Sci. Eng. **2014**, 578168 (2014).
- [221] Watson, P. K., "Transport and trapping of electrons in polymers," Conf. Electr. Insul. Dielectr. Phenom. (CEIDP), Annu. Rep. **2**(5), 21–27 (1995).
- [222] Chiang, T. H. and Wager, J. F., "Electronic conduction mechanisms in insulators," IEEE Trans. Electron Devices **65**(1), 223–230 (2018).
- [223] Laurent, C. and Teyssedre, G., "Hot electron and partial-discharge induced ageing of polymers," Nucl. Instruments Methods Phys. Res. Sect. B Beam Interact. with Mater. Atoms **208**(1–4), 442–447 (2003).
- [224] Gerratt, A. P. and Bergbreiter, S., "Dielectric breakdown of PDMS thin films," J. Micromechanics Microengineering **23**(6), 067001 (2013).
- [225] Danikas, M. G., "On the breakdown strength of silicone rubber," IEEE Trans. Dielectr. Electr. Insul. **1**(6), 1196–1200 (1994).
- [226] Yamada, M., Murakami, Y., Kawashima, T. and Nagao, M., "Electrical breakdown of dielectric elastomer and its lamination effect," 2014 IEEE Conf. Electr. Insul. Dielectr. Phenomena, CEIDP 2014, 126–129 (2014).
- [227] Förster-Zugel, F., Braisz, L. and Schlaak, H. F., "Characterization of the dielectric breakdown strength of thin elastic films in various ambient media," Proc. 2016 IEEE Int. Conf. Dielectr. ICD 2016 **1**, 569–572 (2016).
- [228] Silau, H., Stabell, N. B., Petersen, F. R., Pham, M., Yu, L. and Skov, A. L., "Weibull Analysis of Electrical Breakdown Strength as an Effective Means of Evaluating Elastomer Thin Film Quality," Adv. Eng. Mater. **20**(9), 1800241 (2018).
- [229] Mojsiewicz-Pieńkowska, K., "Review of Current Pharmaceutical Applications of Polysiloxanes (Silicones)," [Handbook of Polymers for Pharmaceutical Technologies: Volume 2 Processing and Applications], V. K. Thakur and M. K. Thakur, Eds., Scrivener Publishing LLC, 363–382 (2015).
- [230] Yuan, W., Hu, L., Ha, S., Lam, T., Grüner, G. and Pei, Q., "Self-clearable carbon nanotube electrodes for improved performance of dielectric elastomer actuators," Proc. SPIE **6927**(April 2008), 69270P (2008).
- [231] Vaicekauskaitė, J., Yu, L. and Skov, A. L., "Insights into the Complex Prebreakdown Actuation of Silicone Elastomers and its Influence on Breakdown Behavior," ACS Omega **5**(30), 18584–18593 (2020).
- [232] Tanaka, T., "Aging of polymeric and composite insulating materials: aspects of interfacial performance in aging," IEEE Trans. Dielectr. Electr. Insul. **9**(5), 704–716 (2002).
- [233] Ghosh, D. and Khastgir, D., "Degradation and Stability of Polymeric High-Voltage Insulators and Prediction of Their Service Life through Environmental and Accelerated Aging Processes," ACS Omega **3**(9), 11317–11330 (2018).
- [234] Papailiou, K. O. and Schmuck, F., [Silicone Composite Insulators: Materials, Design, Applications.], Springer Berlin Heidelberg, Luxembourg (LU) (2013).
- [235] Tomer, N. S., Delor-Jestin, F., Frezet, L. and Lacoste, J., "Oxidation, Chain Scission and Cross-Linking Studies of Polysiloxanes upon Ageings," Open J. Org. Polym. Mater. **02**, 13–22 (2012).
- [236] Bleszynski, M. and Kumosa, M., "Silicone rubber aging in electrolyzed aqueous salt environments," Polym. Degrad. Stab. **146**, 61–68 (2017).
- [237] Kobayashi, S., Matsuzaki, Y., Arashitani, Y. and Kimata, R., "Development of composite insulators for overhead lines (Part 2)," Furukawa Rev.(21), 56–61 (2002).
- [238] Montanari, G. C., Seri, P. and Dissado, L. A., "Aging mechanisms of polymeric materials under DC electrical stress: A new approach and similarities to mechanical aging," IEEE Trans. Dielectr. Electr. Insul. **26**(2), 634–641 (2019).
- [239] Zakrevskii, V. A. and Sudar', N. T., "Electrical breakdown of thin polymer films," Phys. Solid State **47**(5), 961–967 (2005).

- [240] Mazzanti, G., "The combination of electro-thermal stress, load cycling and thermal transients and its effects on the life of high voltage ac cables," *IEEE Trans. Dielectr. Electr. Insul.* **16**(4), 1168–1179 (2009).
- [241] Crine, J.-P., "A molecular model to evaluate the impact of aging on space charges in polymer dielectrics," *IEEE Trans. Dielectr. Electr. Insul.* **4**(5), 487–495 (1997).
- [242] Zhurkov, S. N., "Kinetic concept of the strength of solids," *Int. J. Fract.* **26**(4), 295–307 (1984).
- [243] Zhurkov, S. N. and Korsukov, V. E., "Atomic mechanism of fracture of solid polymers," *J. Polym. Sci. Polym. Phys. Ed.* **12**, 385–398 (1974).
- [244] Bulinski, A. T., Crine, J. P., Noirhomme, B., Densley, R. J. and Bamji, S., "Polymer oxidation and water treeing," *IEEE Trans. Dielectr. Electr. Insul.* **5**(4), 558–570 (1998).
- [245] Ross, R., Geurts, W. S. M., Smit, J. J., van der Maas, J. H. and Lutz, B. T. G., "The hydrophilic nature of water trees (in polyethylene)," *IEEE Int. Symp. Electr. Insul.*, 169–172 (1990).
- [246] Zakrevskii, V. A., Sudar, N. T., Zaopo, A. and Dubitsky, Y. A., "Mechanism of electrical degradation and breakdown of insulating polymers," *J. Appl. Phys.* **93**(4), 2135–2139 (2003).
- [247] Zeller, H. R. and Schneider, W. R., "Electrofracture Mechanics of Dielectric Aging," *J. Appl. Phys.* **56**(2), 455–459 (1984).
- [248] Parpal, J.-L., Crine, J.-P. and Dang, C., "Electrical Aging of Extruded Dielectric Cables - A physical model," *IEEE Trans. Dielectr. Electr. Insul.* **4**(2), 197–209 (1997).
- [249] Swanson, J. W. and Dall, F. C., "On the dielectric strength of synthetic electrical insulating materials," *IEEE Trans. Electr. Insul.* **EI-12**(2), 142–146 (1977).
- [250] Harley, S. J., Glascoe, E. A., Lewicki, J. P. and Maxwell, R. S., "Advances in modeling sorption and diffusion of moisture in porous reactive materials," *ChemPhysChem* **15**(9), 1809–1820 (2014).
- [251] Owen, M. J., "Why silicones behave funny.," *Chim. Nouv.* **85**(27), (Revised and reprinted from Owen, M. J. *Chemtech.* (2004).
- [252] Brook, M. A., Saier, H. U., Schnabel, J., Town, K. and Maloney, M., "Pretreatment of liquid silicone rubbers to remove volatile siloxanes," *Ind. Eng. Chem. Res.* **46**(25), 8796–8805 (2007).
- [253] Nelson, W., [Accelerated testing - Statistical models, test plans, and data analysis, 2nd Editio], Wiley-Interscience, Hoboken (NJ) (2004).
- [254] Dakin, T. W., "Electrical insulation deterioration treated as a chemical rate phenomenon," *Trans. Am. Inst. Electr. Eng.* **67**(1), 113–122 (1948).
- [255] Chen, G., "The missing link - The role of space charge in polymeric insulation lifetime," *Proc. Int. Symp. Electr. Insul. Mater.*, 12–16 (2014).
- [256] Dakin, T. W. and Studniarz, S. A., "The voltage endurance of cast and molded resins," *EIC 13th Electr. Insul. Conf.*, 216–221 (1977).
- [257] Peck, D. S., "Comprehensive Model For Humidity Testing Correlation," *Proc. IEEE Int. Reliab. Phys. Symp.*, 44–50 (1986).
- [258] Lewis, T. J., "Charge transport, charge injection and breakdown in polymeric insulators," *J. Phys. D. Appl. Phys.* **23**(12), 1469–1478 (1990).
- [259] Lewis, T. J., "Ageing — A Perspective," *IEEE Electr. Insul. Mag.* **17**, 6–16 (2001).
- [260] Huang, J., Shian, S., Diebold, R. M., Suo, Z. and Clarke, D. R., "The thickness and stretch dependence of the electrical breakdown strength of an acrylic dielectric elastomer," *Appl. Phys. Lett.* **101**(12), 122905 (2012).
- [261] Kofod, G., Sommer-Larsen, P., Kornbluh, R. and Pelrine, R., "Actuation response of polyacrylate dielectric elastomers," *J. Intell. Mater. Syst. Struct.* **14**(12), 787–793 (2003).
- [262] Tröls, A., Kogler, A., Baumgartner, R., Kaltseis, R., Keplinger, C., Schwödiauer, R., Graz, I. and Bauer, S., "Stretch dependence of the electrical breakdown strength and dielectric constant of dielectric elastomers," *Smart Mater. Struct.* **22**(10), 104012 (2013).
- [263] Vertechy, R. and Fontana, M., "Electromechanical characterization of a new synthetic rubber membrane for dielectric elastomer transducers," *Electroact. Polym. Actuators Devices 2015* **9430**(April 2015), 94300K (2015).
- [264] Vaicekauskaitė, J., Mazurek, P., Vudayagiri, S. and Skov, A. L., "Mapping the mechanical and electrical properties of commercial silicone elastomer formulations for stretchable transducers," *J. Mater. Chem. C* **8**(4), 1273–1279 (2020).
- [265] Kollosche, M., Stoyanov, H., Ragusch, H., Risse, S., Becker, A. and Kofod, G., "Electrical breakdown in soft elastomers: Stiffness dependence in un-pre-stretched elastomers," *Proc. 2010 IEEE Int. Conf. Solid Dielectr. ICSD 2010*(3), 1–4 (2010).
- [266] Madsen, F. B., Yu, L., Daugaard, A. E., Hvilsted, S. and Skov, A. L., "Silicone elastomers with high dielectric permittivity and high dielectric breakdown strength based on tunable functionalized copolymers," *Electroact. Polym. Actuators Devices 2015* **9430**(April 2015), 943012 (2015).
- [267] Liu, Y., Liu, L., Zhang, Z. and Leng, J., "Dielectric elastomer film actuators: Characterization, experiment and analysis," *Smart Mater. Struct.* **18**(9), 095024 (2009).

- [268] Lotz, P., Matysek, M., Lechner, P., Hamann, M. and Schlaak, H. F., "Dielectric elastomer actuators using improved thin film processing and nanosized particles," *Electroact. Polym. Actuators Devices* 2008 **6927**(April 2008), 692723 (2008).
- [269] Li, Z., Okamoto, K., Ohki, Y. and Tanaka, T., "Effects of nano-filler addition on partial discharge resistance and dielectric breakdown strength of Micro-Al₂O₃/epoxy composite," *IEEE Trans. Dielectr. Electr. Insul.* **17**(3), 653–661 (2010).
- [270] Kochetov, R., Tsekmes, I. A. and Morshuis, P. H. F., "Short-term and long-term breakdown analysis of electroactive polymer with and without nanofillers," *Polym. Test.* **59**, 136–141 (2017).
- [271] Jain, P. and Rymaszewski, E. J., "Embedded thin film capacitors - Theoretical limits," *IEEE Trans. Adv. Packag.* **25**(3), 454–458 (2002).
- [272] Hinchet, R. and Shea, H., "High Force Density Textile Electrostatic Clutch," *Adv. Mater. Technol.* **5**(4), 1–7 (2020).
- [273] Vudayagiri, S., Zakaria, S., Yu, L., Hassoun, S. S., Benslimane, M. and Skov, A. L., "High breakdown-strength composites from liquid silicone rubbers," *Smart Mater. Struct.* **23**(10), 105017 (2014).
- [274] Szabo, J. P., Hiltz, J. A., Cameron, C. G., Underhill, R. S., Massey, J., White, B. and Leidner, J., "Elastomeric composites with high dielectric constant for use in Maxwell stress actuators," *Smart Struct. Mater.* 2003 *Electroact. Polym. Actuators Devices* **5051**(July 2003), 180 (2003).
- [275] Huang, X., Xie, L., Hu, Z. and Jiang, P., "Influence of BaTiO₃ Nanoparticles on Dielectric, Thermophysical and Mechanical Properties of Ethylene- Vinyl Acetate Elastomer / BaTiO₃ Microcomposites," *IEEE Trans. Dielectr. Electr. Insul.* **18**(2), 375–383 (2011).
- [276] Böse, H., Uhl, D., Flittner, K. and Schlaak, H., "Dielectric elastomer actuators with enhanced permittivity and strain," *Electroact. Polym. Actuators Devices* 2011 **7976**(March 2011), 79762J (2011).
- [277] Hu, W., Zhang, S. N., Niu, X., Liu, C. and Pei, Q., "An aluminium nanoparticle-acrylate copolymer nanocomposite as a dielectric elastomer with a high dielectric constant," *J. Mater. Chem. C* **2**, 1658–1666 (2014).
- [278] Yao, Y., Ning, N., Zhang, L., Nishi, T. and Tian, M., "Largely improved electromechanical properties of thermoplastic polyurethane dielectric elastomer by carbon nanospheres," *RSC Adv.* **5**(30), 23719–23726 (2015).
- [279] Opris, D. M., Molberg, M., Walder, C., Ko, Y. S., Fischer, B. and Nüesch, F. A., "New silicone composites for dielectric elastomer actuator applications in competition with acrylic foil," *Adv. Funct. Mater.* **21**(18), 3531–3539 (2011).
- [280] Tian, M., Wei, Z., Zan, X., Zhang, L., Zhang, J., Ma, Q., Ning, N. and Nishi, T., "Thermally expanded graphene nanoplates/polydimethylsiloxane composites with high dielectric constant, low dielectric loss and improved actuated strain," *Compos. Sci. Technol.* **99**, 37–44 (2014).
- [281] Meunier, L., Chagnon, G., Favier, D., Orgéas, L. and Vacher, P., "Mechanical experimental characterisation and numerical modelling of an unfilled silicone rubber," *Polym. Test.* **27**(6), 765–777 (2008).
- [282] Carpi, F., Gallone, G., Galantini, F. and Rossi, D. De., "Silicone-Poly (hexylthiophene) Blends as Elastomers with Enhanced Electromechanical Transduction Properties," *Adv. Funct. Mater.* **18**, 235–241 (2008).
- [283] Kollosche, M. and Kofod, G., "Electrical failure in blends of chemically identical, soft thermoplastic elastomers with different elastic stiffness," *Appl. Phys. Lett.* **96**, 071904 (2010).
- [284] Stanford, S., "Biomimetic robots (Chapter 24)," [Dielectric Elastomers as Electromechanical Transducers], F. Carpi, D. De Rossi, R. Kornbluh, R. Pelrine, and P. Sommer-Larsen, Eds., Elsevier Ltd., 251–258 (2008).
- [285] Madsen, F. B., Yu, L., Dagaard, A. E., Hvilsted, S. and Skov, A. L., "A new soft dielectric silicone elastomer matrix with high mechanical integrity and low losses," *RSC Adv.* **5**(14), 10254–10259 (2015).
- [286] Madsen, P. J., Yu, L., Boucher, S. and Skov, A. L., "Enhancing the electro-mechanical properties of polydimethylsiloxane elastomers through blending with poly(dimethylsiloxane-co-methylphenylsiloxane) copolymers," *RSC Adv.* **8**(41), 23077–23088 (2018).
- [287] Madsen, F. B., Yu, L., Mazurek, P. and Skov, A. L., "A simple method for reducing inevitable dielectric loss in high-permittivity dielectric elastomers," *Smart Mater. Struct.* **25**(7), 075018 (2016).
- [288] Madsen, F. B., Zakaria, S., Yu, L. and Skov, A. L., "Mechanical and Electrical Ageing Effects on the Long-Term Stretching of Silicone Dielectric Elastomers with Soft Fillers," *Adv. Eng. Mater.* **18**(7), 1154–1165 (2016).
- [289] Stoyanov, H., Kollosche, M., McCarthy, D. N. and Kofod, G., "Molecular composites with enhanced energy density for electroactive polymers," *J. Mater. Chem.* **20**(35), 7558–7564 (2010).
- [290] Kussmaul, B., Risse, S., Kofod, G., Waché, R., Wegener, M., McCarthy, D. N., Krüger, H. and Gerhard, R., "Enhancement of dielectric permittivity and electromechanical response in silicone elastomers: Molecular grafting of organic dipoles to the macromolecular network," *Adv. Funct. Mater.* **21**(23), 4589–4594 (2011).
- [291] Perju, E., Song Ko, Y., Dünki, S. J. and Opris, D. M., "Increased electromechanical sensitivity of polysiloxane elastomers by chemical modification with thioacetic groups," *Mater. Des.* **186**, 108319 (2020).
- [292] Böse, H., Uhl, D. and Rabindranath, R., "Novel DEA with organically modified silicone elastomer for permittivity enhancement," *Electroact. Polym. Actuators Devices* 2012 **8340**(April 2012), 83402E (2012).

- [293] Racles, C., Bele, A., Dascalu, M., Musteata, V. E., Varganici, C. D., Ionita, D., Vlad, S., Cazacu, M., Dünki, S. J. and Opris, D. M., "Polar – nonpolar interconnected elastic networks with increased permittivity and high breakdown fields for dielectric elastomer transducers," *RSC Adv.* **5**, 58428–58438 (2015).
- [294] Sun, H., Liu, X., Yu, B., Feng, Z., Ning, N., Hu, G., Tian, M. and Zhang, L., "Simultaneously improved dielectric and mechanical properties of silicone elastomer by designing a dual crosslinking network," *Polym. Chem.* **10**, 633–645 (2019).
- [295] Yu, L., Madsen, F. B., Hvilsted, S. and Skov, A. L., "Dielectric elastomers, with very high dielectric permittivity, based on silicone and ionic interpenetrating networks," *RSC Adv.* **5**(61), 49739–49747 (2015).
- [296] Madsen, F. B., Yu, L. and Skov, A. L., "Self-Healing, High-Permittivity Silicone Dielectric Elastomer," *ACS Macro Lett.* **5**, 1196–1200 (2016).
- [297] Dünki, S. J., Ko, Y. S., Nüesch, F. A. and Opris, D. M., "Self-repairable, high permittivity dielectric elastomers with large actuation strains at low electric fields," *Adv. Funct. Mater.* **25**(16), 2467–2475 (2015).
- [298] Zhang, Y., Ellingford, C., Zhang, R., Roscow, J., Hopkins, M., Keogh, P., McNally, T., Bowen, C. and Wan, C., "Electrical and Mechanical Self-Healing in High-Performance Dielectric Elastomer Actuator Materials," *Adv. Funct. Mater.* **29**, 1808431 (2019).
- [299] Ellingford, C., Zhang, R., Wemyss, A. M., Zhang, Y., Brown, O. B., Zhou, H., Keogh, P., Bowen, C. and Wan, C., "Self-Healing Dielectric Elastomers for Damage-Tolerant Actuation and Energy Harvesting," *ACS Appl. Mater. Interfaces* **12**, 7595–7604 (2020).
- [300] Tan, M. W. M., Thangavel, G. and Lee, P. S., "Enhancing dynamic actuation performance of dielectric elastomer actuators by tuning viscoelastic effects with polar crosslinking," *NPG Asia Mater.* **11**(62), 1–10 (2019).
- [301] Kleo, M., Förster-Zügel, F., Schlaak, H. F. and Wallmersperger, T., "Thermo-electro-mechanical behavior of dielectric elastomer actuators : experimental investigations , modeling and simulation," *Smart Mater. Struct.* **29**, 085001 (2020).
- [302] Christensen, L. R., Hassager, O. and Skov, A. L., "Electro-Thermal Model of Thermal Breakdown in Multilayered Dielectric Elastomers," *AIChE J.* **65**(2), 859–864 (2019).
- [303] Chen, B., Kollosche, M., Stewart, M., Busfield, J. and Carpi, F., "Electrical breakdown of dielectric elastomers: influence of compression, electrode's curvature and environmental humidity," *Electroact. Polym. Actuators Devices 2016* **9798**(April 2016), 97980Q (2016).
- [304] Liu, X., Zhang, J. and Chen, H., "Ambient humidity altering electromechanical actuation of dielectric elastomers," *Appl. Phys. Lett.* **115**(18), 184101 (2019).
- [305] Chen, B., Kollosche, M., Stewart, M., Busfield, J. and Carpi, F., "Electrical breakdown of an acrylic dielectric elastomer: Effects of hemispherical probing electrodes size and force," *Int. J. Smart Nano Mater.* **6**(4), 290–303 (2015).
- [306] Kochetov, R., Ospino, A. H. S., Andritsch, T., Morshuis, P. H. F., Smit, J. J., Feller, T. and Wagner, J., "DC breakdown investigation on polyurethane elastomeric films with and without deposited electrodes," *Proc. IEEE Int. Conf. Solid Dielectr. ICSD*, 37–40 (2013).
- [307] Iannarelli, A., Niasar, M. G. and Ross, R., "Assessing Partial Discharge Activity in Dielectric Elastomer under Cyclic Tensile Stress," *2018 IEEE Electr. Insul. Conf. EIC 2018*(June), 562–565 (2018).
- [308] Muffoletto, D. P., Burke, K. M. and Zirnheld, J. L., "Partial discharge analysis of prestretched and unstretched acrylic elastomers for Dielectric Elastomer Actuators (DEA)," *Electroact. Polym. Actuators Devices 2012* **8340**(May), 834021 (2012).
- [309] Montanari, G. C., "Bringing an insulation to failure: The role of space charge," *IEEE Trans. Dielectr. Electr. Insul.* **18**(2), 339–364 (2011).
- [310] Li, S., Zhu, Y., Min, D. and Chen, G., "Space Charge Modulated Electrical Breakdown," *Sci. Rep.* **6**(August), 20–23 (2016).
- [311] Francis, A., Martinez, A., Thompson, K., Burke, K. and Zirnheld, J., "Space charge accumulation as a contributor to partial discharge activity in dielectric elastomer actuators under high voltage DC," *2016 IEEE Int. Power Modul. High Volt. Conf. IPMHVC 2016*, 330–335 (2017).
- [312] Rizzo, G., Romano, P., Imburgia, A. and Ala, G., "Review of the PEA method for space charge measurements on HVDC cables and mini-cables," *Energies* **12**(3512), 1–23 (2019).
- [313] Kochetov, R., Tsekmes, I. A. and Morshuis, P. H. F., "Electrical conductivity, dielectric response and space charge dynamics of an electroactive polymer with and without nanofiller reinforcement," *Smart Mater. Struct.* **24**(7), 075019 (2015).
- [314] Moiz, S. A., Khan, I. A., Younis, W. A. and Karimov, K. S., "Space Charge–Limited Current Model for Polymers," [Conducting Polymers], F. Yilmaz, Ed., Intechopen, London, UK, 91–118 (2016).
- [315] Montanari, G. C. and Morshuis, P. H. F., "Space charge phenomenology in polymeric insulating materials," *IEEE Trans. Dielectr. Electr. Insul.* **12**(4), 754–767 (2005).
- [316] Teyssedre, G. and Laurent, C., "Charge transport modeling in insulating polymers: From molecular to macroscopic scale," *IEEE Trans. Dielectr. Electr. Insul.* **12**(5), 857–874 (2005).
- [317] Teyssedre, G., Zheng, F., Boudou, L. and Laurent, C., "Charge trap spectroscopy in polymer dielectrics: A critical review," *J.*

- Phys. D. Appl. Phys. **54**(26), 263001 (2021).
- [318] Rose, A., "Space-charge-limited currents in solids," Phys. Rev. **97**(6), 1538–1544 (1955).
- [319] Chen, G., Zhao, J., Li, S. and Zhong, L., "Origin of thickness dependent dc electrical breakdown in dielectrics," Appl. Phys. Lett. **100**(22), 222904 (2012).
- [320] Zurlo, G., Destrade, M., DeTommasi, D. and Puglisi, G., "Catastrophic Thinning of Dielectric Elastomers," Phys. Rev. Lett. **118**(7), 078001 (2017).
- [321] Moscardo, M., Zhao, X., Suo, Z. and Lapusta, Y., "On designing dielectric elastomer actuators," J. Appl. Phys. **104**(9), 093503 (2008).
- [322] Lotz, P., Matysek, M. and Schlaak, H. F., "Lifetime of dielectric elastomer stack actuators," Electroact. Polym. Actuators Devices 2011 **7976**(March 2011), 79760P (2011).
- [323] Iannarelli, A. and Niasar, M. G., "Mechanical stretch influence on lifetime of dielectric elastomer films," Electroact. Polym. Actuators Devices 2017 **10163**(April 2017), 1016326 (2017).
- [324] Yuan, W., Hu, L., Yu, Z., Lam, T., Biggs, J., Ha, S. M., Xi, D., Chen, B., Senesky, M. K., Grüner, G. and Pei, Q., "Fault-Tolerant Dielectric Elastomer Actuators using Single-Walled Carbon Nanotube Electrodes," Adv. Mater. **20**, 621–625 (2008).
- [325] Lau, G.-K., Shiau, L.-L. and Chua, S.-L., "Effects of Thinner Compliant Electrodes on Self-Clearability of Dielectric Elastomer Actuators," Actuators **9**(4), 121 (2020).
- [326] Zhang, M., Denes, I. and Buchmeiser, M. R., "An Investigation of Structure-Property Relationships in Silicone-Based Dielectric Electroactive Elastomers by Varying Stoichiometric Imbalance of the Network," Macromol. Mater. Eng. **301**(3), 337–347 (2016).
- [327] Albuquerque, F. B. and Shea, H., "Influence of humidity, temperature and prestretch on the dielectric breakdown strength of silicone elastomer membranes for DEAs," Smart Mater. Struct. **29**(10), 105024 (2020).
- [328] Beco Albuquerque, F. and Shea, H., "Influence of electric field, temperature, humidity, elastomer material, and encapsulation on the lifetime of dielectric elastomer actuators (DEAs) under DC actuation," Smart Mater. Struct. **30**, 125022 (2021).
- [329] Beco Albuquerque, F. and Shea, H. R., "Effect of electrode composition and patterning method on the lifetime of silicone-based dielectric elastomer actuators (DEA) under different environmental conditions," Electroact. Polym. Actuators Devices XXIII **11587**(115871B), 115871B (2021).
- [330] Beco Albuquerque, F. and Shea, H., "Factors influencing the mean-time-to-failure of single-layer uniaxially prestretched silicone-based DEAs," Proc. SPIE **In Press** (2022).
- [331] Chen, Y., Agostini, L., Moretti, G., Berselli, G., Fontana, M. and Verthey, R., "Fatigue life performances of silicone elastomer membranes for dielectric elastomer transducers: preliminary results," Proc. SPIE **10966**(March 2019), 1096616 (2019).
- [332] Schlatter, S., Grasso, G., Rosset, S. and Shea, H., "Inkjet Printing of Complex Soft Machines with Densely Integrated Electrostatic Actuators," Adv. Intell. Syst. **2**(11), 2000136 (2020).
- [333] Vaicekauskaitė, J., Mazurek, P., Vudayagiri, S. and Skov, A. L., "Silicone elastomer map: design the ideal elastomer," Electroact. Polym. Actuators Devices XXI **10966**(March), 1096625 (2019).
- [334] Hodgins, M., York, A. and Seelecke, S., "Systematic experimental characterization of dielectric elastomer membranes using a custom-built tensile test rig," J. Intell. Mater. Syst. Struct. **28**(15), 2117–2128 (2017).
- [335] Carpi, F., Anderson, I., Bauer, S., Frediani, G., Gallone, G., Gei, M., Graaf, C., Jean-Mistral, C., Kaal, W., Kofod, G., Kollosche, M., Kornbluh, R., Lassen, B., Matysek, M., Michel, S., Nowak, S., O'Brien, B., Pei, Q., Pelrine, R., et al., "Standards for dielectric elastomer transducers," Smart Mater. Struct. **24**(10), 105025 (2015).
- [336] ASTM Standard E96/E96M-16 Standard Test Methods for Water Vapor Transmission of Materials., ASTM International, West Conshohocken (PA), United States (2016).
- [337] Trifol, J., Plackett, D., Sillard, C., Hassager, O., Dagaard, A. E., Bras, J. and Szabo, P., "A comparison of partially acetylated nanocellulose, nanocrystalline cellulose, and nanoclay as fillers for high-performance polylactide nanocomposites," J. Appl. Polym. Sci. **133**, 43257 (2016).
- [338] Kämpfer, N., [Monitoring Atmospheric Water Vapour: ground-based remote sensing and in-situ methods], Springer, New York (USA) (2013).
- [339] Crank, J., [The Mathematics of Diffusion, 2nd Ed.], Oxford University Press, London, UK (1975).
- [340] Wang, Z., Zhao, L. H., Jia, Z. D. and Guan, Z. C., "Water and moisture permeability of high-temperature vulcanized silicone rubber," IEEE Trans. Dielectr. Electr. Insul. **24**(4), 2440–2448 (2017).
- [341] Schlatter, S., Illenberger, P. and Rosset, S., "Peta-pico-Voltron: An open-source high voltage power supply," HardwareX **4**, e00039 (2018).
- [342] McPherson, J. W. and Ogawa, E. T., [Reliability physics and engineering: Time-to-failure modeling], Springer, Cham(CH) (2013).

- [343] Jones, J. R., "<https://github.com/slightlynybbled/weibull>," 2017.
- [344] Kapur, K. C. and Pecht, M., [Reliability engineering], John Wiley & Sons, Hoboken(NJ) (2014).
- [345] Benard, A. and Bos-Levenbach, E. C., "'Het uitzetten van waarnemingen op waarschijnlijkheids-papier' (The Plotting of Observations on Probability Paper)," Stat. Neerl. **7**, 163–173 (1953).
- [346] Stull, R., [Meteorology for Scientists & Engineers, 3rd Edition.], Brooks/Cole, Pacific Grove (USA) (2007).
- [347] Liu, L., Chen, H., Sheng, J., Zhang, J., Wang, Y. and Jia, S., "Effect of temperature on the electric breakdown strength of dielectric elastomer," Electroact. Polym. Actuators Devices 2014 **9056**(March 2014), 905634 (2014).
- [348] Lutz, B., Guan, Z., Wang, L., Zhang, F. and Lu, Z., "Water absorption and water vapor permeation characteristics of HTV silicone rubber material," IEEE Int. Symp. Electr. Insul., 478–482 (2012).
- [349] Huang, Y. and Schadler, L. S., "On the nature of high field charge transport in reinforced silicone dielectrics: Experiment and simulation," J. Appl. Phys. **120**(5), 055101 (2016).
- [350] Kumagai, S. and Yoshimura, N., "Influence of single and multiple environmental stresses on tracking and erosion of RTV silicone rubber," IEEE Trans. Dielectr. Electr. Insul. **6**(2), 211–225 (1999).
- [351] Khan, H., Amin, M. and Ahmad, A., "Characteristics of silicone composites for high voltage insulations," Rev. Adv. Mater. Sci. **56**(1), 91–123 (2018).
- [352] Dai, J., Yao, X., Yeh, H. Y. and Liang, X., "Moisture absorption of filled silicone rubber under electrolyte," J. Appl. Polym. Sci. **99**(5), 2253–2257 (2006).
- [353] Sommer-Larsen, P. and Larsen, A. L., "Materials for dielectric elastomer actuators," Electroact. Polym. Actuators Devices 2004 **5385**(July 2004), 68–77 (2004).
- [354] Mazurek, P., Vudayagiri, S. and Ladegaard Skov, A., "Design of reliable silicone elastomers for dielectric elastomers and stretchable electronics," Proc. SPIE **10966**, 109660M (2019).
- [355] Domansky, K., Sliz, J. D., Wen, N., Hinojosa, C., Thompson, G., Fraser, J. P., Hamkins-Indik, T., Hamilton, G. A., Levner, D. and Ingber, D. E., "SEBS elastomers for fabrication of microfluidic devices with reduced drug absorption by injection molding and extrusion," Microfluid. Nanofluidics **21**(107), 1–12 (2017).
- [356] Beco Albuquerque, F. and Shea, H. R., "Actuator, Valve Actuator Unit and Valve," filed on April 30, 2021, United States Patent Application n°17/245304 (2021).
- [357] Iannarelli, A., Ghaffarian Niasar, M. and Ross, R., "Electrode interface polarization formation in dielectric elastomer actuators," Sensors Actuators, A Phys. **312**, 111992 (2020).
- [358] Rizzello, G., Hodgins, M., Naso, D., York, A. and Seelecke, S., "Modeling of the effects of the electrical dynamics on the electromechanical response of a DEAP circular actuator with a mass-spring load," Smart Mater. Struct. **24**(9), 094003 (2015).
- [359] Hodgins, M., Rizzello, G., Naso, D., York, A. and Seelecke, S., "An electro-mechanically coupled model for the dynamic behavior of a dielectric electro-active polymer actuator," Smart Mater. Struct. **23**(10), 104006 (2014).
- [360] Hu, P., Beco Albuquerque, F., Madsen, J. and Skov, A. L., "Highly Stretchable Silicone Elastomer Applied in Soft Actuators," Macromol. Rapid Commun. **2100732**, 1–9 (2022).

Curriculum Vitae

FABIO BECO ALBUQUERQUE



PERSONAL INFORMATION

Born in Montreux, Switzerland in 1994
 fabio.becoalbuquerque@gmail.com
 Rue de la Maladière 4 – CH-2000 Neuchâtel

EMPLOYMENT HISTORY

- **Chemical Management Assistant for HSEQ – Maersk Supply Service – Kongens Lyngby (DK)** 08/16 – 12/16
 - Acquisition of material safety data sheets (MSDS), and risk assessment of 5000+ chemicals in offshore vessels for compliance towards international laws and audits. Update and design of an online inventory for chemicals and assisting of an internal asset management (Sharepoint) platform for HSEQ department.
- **Research Assistant in Swiss Federal Research Projects (Swiss Civil Service Scheme)** 08/15 – 07/16
 - **Agroscope (Swiss Federal Institute for Agricultural Research) – Nyon (CH)**
 - Studies of allelopathic effects of a crop on its environment for potential herbicide effect.
 - Preparation, sampling and output data analysis of wine and musts samples for HPLC analysis of the constituent amino acids and their chemical profile.
 - **HEIA-FR (Applied Engineering School of Fribourg) – Fribourg (CH)**
 - Synthesis of reduced graphene oxide for high-performance graphene-based batteries at lab scale.

EDUCATION

- **Ecole Polytechnique Fédérale de Lausanne (EPFL) – Neuchâtel (CH)** 2019 – 2022
 - PhD in Microengineering
 - Thesis title: Lifetime of dielectric elastomer actuators under DC electric fields
- **Technical University of Denmark – (DTU)** 2016 – 2018
 - MSc in Applied Chemistry – Polymer Engineering
- **Ecole Polytechnique Fédérale de Lausanne (EPFL)** 2012 – 2015
 - BSc in Chemistry and Chemical Engineering (Overall grade: 5.2/6)
- **Gymnase de Burier (Lycée)** 2009 – 2012
 - Specialization in Biology and Chemistry

SKILLS

- Preparation of elastomer materials / Chemical synthesis of polymers
- Characterization of polymer/elastomer materials
- Accelerated ageing tests and reliability
- Software: Microsoft Office + Sharepoint, Origin, MATLAB, Python (basic)

PUBLICATIONS

- Journal articles (first author):
1. Fabio Beco Albuquerque and Herbert Shea, Influence of humidity, temperature and prestretch on the dielectric breakdown strength of silicone elastomer membranes for DEAs, Smart Materials and Structures **29** (10) 105024 (2020)
<https://doi.org/10.1088/1361-665X/aba5e3>

2. Fabio Beco Albuquerque and Herbert Shea, Influence of electric field, temperature, humidity, elastomer material, and encapsulation on the lifetime of dielectric elastomer actuators (DEAs) under DC actuation, *Smart Materials and Structures* **30** (12) 125022 (2021) <https://doi.org/10.1088/1361-665X/ac3433>

- Journal articles (second author):

3. Djen Kühnel, Fabio Beco Albuquerque, Valentin Py and Herbert Shea, Automated test setup to quantify the lifetime of dielectric elastomer actuators under a wide range of operating conditions, *Smart Materials and Structures* **30** (6) 065020 (2021) <https://doi.org/10.1088/1361-665X/abfb85>
4. Pengpeng Hu, Fabio Beco Albuquerque, Jeppe Madsen, and Anne Ladegaard Skov, Highly stretchable silicone elastomer applied in soft actuators, *Macromolecular Rapid Communications* **In Press** 2100732 (2022) <https://doi.org/10.1002/marc.202100732>

- Conference presentations and proceedings:

5. Fabio Beco Albuquerque and Herbert Shea, The effect of humidity on the lifetime of silicone-based dielectric elastomer actuators under DC actuation, EuroEAP – International conference on Electromechanically Active Polymer (EAP) transducers and artificial muscles (Dresden, 2019) – Poster Presentation
6. Fabio Beco Albuquerque and Herbert Shea, Effect of humidity, temperature, and elastomer material on the lifetime of silicone-based dielectric elastomer actuators under a constant DC electric field, SPIE EAPAD XXII 11375 113751E (Online, 2020) – Presentation <https://doi.org/10.1117/12.2558428>
7. Fabio Beco Albuquerque and Herbert Shea, Effect of electrode composition and patterning method on the lifetime of silicone-based dielectric elastomer actuators (DEA) under different environmental conditions, SPIE EAPAD XXIII 11587 115871B (Online, 2021) – Presentation and Proceedings <https://doi.org/10.1117/12.2581071>
8. Fabio Beco Albuquerque and Herbert Shea, Lifetime of silicone-based dielectric elastomer actuators (DEAs) under DC actuation, EuroEAP – International conference on Electromechanically Active Polymer (EAP) transducers and artificial muscles (Online, 2021) – Poster Presentation
9. Fabio Beco Albuquerque and Herbert Shea, Factors influencing the mean-time-to-failure of single-layer uniaxially prestretched silicone-based DEAs, SPIE EAPAD XXIV (Online, 2022) – Presentation and Proceedings

- Patent applications:

10. Herbert Shea, Fabio Beco Albuquerque (2021) Actuator, valve actuator unit and valve, U.S. Provisional Patent Application No. 17/245304, filed on the 30th April 2021

LANGUAGES

- FRENCH: NATIVE
- ENGLISH: C1
- GERMAN: B2
- PORTUGUESE: B2
- DANISH: A1

INTERESTS

- HIKING / PARCOURS-VITA
- GEOGRAPHY, MAPS (GEOGUESSR) AND GEOPOLITICAL RISKS
- ECONOMICAL INTELLIGENCE, MONETARY POLICY AND INVESTMENTS
- CRYPTOCURRENCIES, ON-CHAIN METRICS & BLOCKCHAIN TECHNOLOGY
- METEOROLOGY AND EXTREME WEATHER EVENTS